Mechanisms of force generation for vesicle transport processes: identification and characterisation of the Spir actin nucleator - myosin V motor protein complex

DISSERTATION ZUR ERLANGUNG DES
DOKTORGRADES DER NATURWISSENSCHAFTEN (DR. RER. NAT.)
DER FAKULTÄT FÜR BIOLOGIE UND VORKLINISCHE MEDIZIN
DER UNIVERSITÄT REGENSBURG

vorgelegt von

Tobias Welz

aus

Leipzig

im Jahr

2016

Das Promotionsgesuch wurde eingereicht am:

05.12.2016

Die Arbeit wurde angeleitet von:

Prof. Dr. Eugen Kerkhoff

Unterschrift:

Selbstständigkeitserklärung

Ich, Tobias Welz, geboren am 23.07.1988 in Leipzig, erkläre hiermit, dass ich die vorliegende Arbeit ohne unzulässige Hilfe Dritter und ohne Benutzung anderer als der angegebenen Hilfsmittel angefertigt habe. Ergebnisse, Abbildungen und Beschreibungen, die im Rahmen einer Kollaboration entstanden sind, sind entsprechend gekennzeichnet.

Die aus anderen Quellen direkt oder indirekt übernommenen Daten und Konzepte sind unter Angabe der Quelle gekennzeichnet. Insbesondere habe ich nicht die entgeltliche Hilfe von Vermittlungs- bzw. Beratungsdiensten (Promotionsberater oder andere Personen) in Anspruch genommen.

Die Arbeit wurde bisher weder im In- noch im Ausland in gleicher oder ähnlicher Form einer anderen Prüfungsbehörde vorgelegt.

_____ _____

Ort, Datum Tobias Welz

Table of contents

Abstract

The establishment and maintenance of cell polarity constitutes the basis for the morphological and functional diversity of metazoan cells. Intracellular vesicle transport processes mediate the delivery of cell surface receptors, adhesion proteins and other components to the desired locales, in order to define the polarised higher eukaryotic nature of cells. Members of the Rab family of small GTPases thereby act as master regulators for the complex network of trafficking routes, as they specifically attach to intracellular membranes and recruit distinct effector proteins, including motor proteins, in order to facilitate directed transport along microtubule networks and actin tracks. The Rab11 GTPase is critical for exocytic and recycling pathways and has been shown before to recruit the processive actin motor protein myosin V (MyoV) to vesicle surfaces to drive specific cellular functions.

Furthermore, there is growing evidence for a coupling of actin assembly by actin nucleation and elongation factors, and myosin motor activity in eukaryotic cells. However, the mechanisms for recruitment of actin nucleators and motor proteins to specific membrane compartments remain unclear. By a set of protein interaction studies, this thesis unravelled a direct physical interaction of the Spir actin nucleators and myosin V motors. The interaction was shown to be mediated by the MyoV globular tail domain (GTD) and a newly identified highly conserved sequence motif (GTBM) in the central Spir linker region and the crystal structure of the Spir-2-GTBM:MyoVa-GTD complex was solved. By means of fluorescence microscopy and FLIM-FRET analysis, the Spir/MyoV interaction was observed in living cells at vesicle membranes as well, proving its biological significance. Further, a regulatory mechanism was revealed in which the Spir-2 protein is able to bind to the back-folded, auto-inhibited MyoV protein and targets it from a cytoplasmic state towards vesicle surfaces.

Spir proteins have been shown before to functionally overlap with Rab11 in exocytic and recycling pathways, although a direct Rab11/Spir interaction has never been revealed. The direct interaction of myosin V motors and Spir proteins identified here enables the formation of a tripartite Rab11:MyoV:Spir protein complex at vesicle surfaces in which the MyoV protein acts as a linker between Rab11 and Spir, as was shown by *in vitro* interaction studies and fluorescence microscopy. The ternary complex architecture would explain how Rab11 vesicles support coordinated F-actin nucleation and myosin force generation for vesicle transport and tethering. Considering the large diversity of MyoV cooperation with Rab family members, the coordinated recruitment of actin nucleators and actin motors to vesicle surfaces could provide a common mechanism to control force generation and motility of vesicles and organelles in different cellular processes.

Zusammenfassung

Zur Gewährleistung der ordentlichen Entwicklung einer Zelle und deren Funktionen, und um deren Überleben zu sichern, ist die Ausbildung und Aufrechterhaltung einer Zellpolarität entscheidend. Diese wird maßgeblich durch eine differentielle Zusammensetzung der Plasmamembran beeinflusst. Für die Bereitstellung bestimmter Zelloberflächen-Rezeptoren, Anheftungsproteine und weiterer Membranbestandteile an den jeweiligen Membranbereichen sind intrazelluläre, Membranvesikel-getriebene Transportprozesse verantwortlich. Die kleinen Rab GTPasen werden als Hauptregulatoren der diversen, miteinander verknüpften Transportwege angesehen. Diese binden spezifisch an intrazelluläre Membranen und rekrutieren anschließend bestimmte Effektorproteine, wie beispielsweise Motorproteine, welche daraufhin den gerichteten Transport entlang von Mikrotubuli-Netzwerken und Aktinfasern umsetzen. Das Rab11 Protein ist hierbei speziell für den nach außen gerichteten, exozytotischen, und den wieder verwendenden, rückführenden Transport wichtig. In vorherigen Studien wurde bereits gezeigt, dass das Rab11 Protein in der Lage ist, das kontinuierlich laufende Aktin-Motorprotein Myosin V (MyoV) an die Vesikeloberfläche zu ziehen um damit bestimmte Zellfunktionen zu regulieren.

Des Weiteren gibt es vermehrt Hinweise darauf, dass an bestimmten Membrankompartimenten der Aufbau von Aktinfasern mittels Aktin-Nukleations- und Aktin-Polymerisierungs-Proteinen mit der Funktion von Motorproteinen verknüpft ist, wobei der genaue Mechanismus bisher unbekannt ist. Mit Hilfe einer Reihe von Protein-Interaktions-Studien gelang es nun hier, eine direkte, unmittelbare Bindung des Aktin-Nukleations-Proteins Spir-2 an das Myosin V Motorprotein aufzudecken. An dieser direkten Bindung ist zum einen die kompakt gefaltete Endstruktur des MyoV Proteins (globular tail domain, GTD) und zum anderen ein hierbei neu entdecktes, hoch konserviertes Sequenzmotiv (globular tail domain binding motif, GTBM) in der Mitte des Spir Proteins beteiligt. Zudem wurde die Kristallstruktur für diesen Proteinkomplex gelöst. Mittels Fluoreszenz-Mikroskopie und FLIM-FRET Untersuchungen konnte die Interaktion von Spir und MyoV Proteinen auch an Membranvesikeln lebender Zellen beobachtet werden, wodurch letztendlich eine biologische Bedeutung dieser Komplexbildung abzuleiten ist. Außerdem wurde eine regulatorische Funktion des Spir-2 Proteins entdeckt, indem es in der Lage ist, an ein in sich gefaltetes und dadurch selbst-inaktiviertes MyoV-Dimer zu binden und es folglich aus dem Zytoplasma an die Oberfläche bestimmter Vesikel zu bringen.

Obwohl eine direkte Bindung von Spir Proteinen an Rab11 GTPasen nie gezeigt wurde, gibt es einen funktionellen Zusammenhang beider Proteine im exozytotischen und rückführenden Transport. Die im Rahmen dieser Arbeit identifizierte direkte Bindung von Myosin V Motorproteinen an Spir

Proteine ebnet allerdings den Weg für die Zusammensetzung eines aus drei Komponenten bestehenden Rab11:MyoV:Spir Proteinkomplex direkt an der Vesikeloberfläche. Wie mittels *in vitro* Interaktions-Studien und Fluoreszenz-Mikroskopie abgeleitet wurde, fungiert das MyoV Protein hierbei als ein verknüpfendes Protein, das die Funktionen von Rab11 und Spir miteinander verbindet. Der Aufbau dieses dreiteiligen Komplexes würde die koordinierte Bildung von Aktinfasern und Myosin-vermittelter Krafterzeugung erklären, die beide über das Rab11 Protein an die Vesikelmembran lokalisiert werden und die letztendlich den Vesikeltransport und die Vesikelanheftung steuern. Bedenkt man die Vielzahl möglicher Interaktionen von MyoV Proteinen und Rab GTPasen für unterschiedliche Zwecke in verschiedenen Bereichen der Zelle, könnte die genau koordinierte Verknüpfung von Aktin-Nukleatoren und Aktin-Motorproteinen an der Vesikeloberfläche einen möglichen generellen Mechanismus der Krafterzeugung an Vesikeln und anderen Zellorganellen darstellen, um folglich deren Bewegung während verschiedener zellulärer Prozesse zu steuern.

1 Introduction

1.1 Cell polarisation as a prerequisite for cellular and organismic function

A common feature of eukaryotic cells is their polarised morphological and functional organisation. The establishment of cellular polarity is indispensable for developmental processes, such as asymmetric oocyte division, formation of epithelial tissues and the development of the central nervous system. Highly polarised cells undergo complex cellular rearrangements during their development in order to generate cells in which different cellular regions with different properties mediate different functions. Neuronal cells, being one of the most polarised cell types in vertebrate organisms, require a proper formation of morphological and thus functional polarity during development in order to fulfil their purpose to propagate excitation signals from the environment to the central nervous system and back to executing organs for reflexes and fine-tuned reactions (*Figure 1A*). Epithelial cells, lining the cavities and inner surfaces of organs and vessels in higher order organisms, demand a strong apical to basal polarity in order to fulfil their functions in secretion, absorption and transcellular transport, protection and sensing. Other cell types, such as immune cells, fibroblasts and, although not desired, cancer cells require fast and rather short-lasting polarisation processes as the base for cell migration (*Figure 1B*).

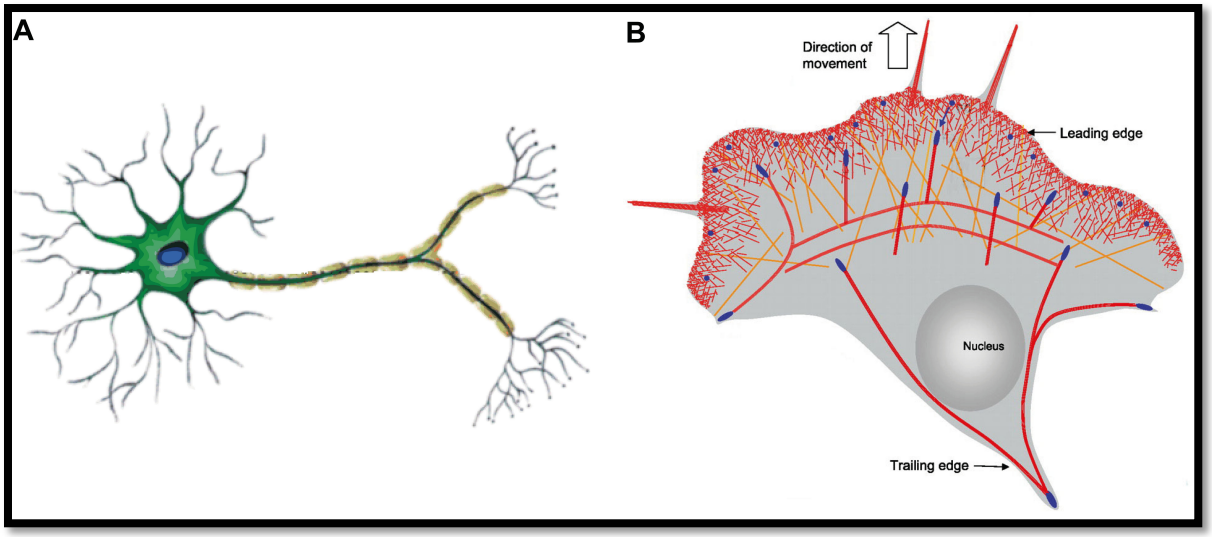

Figure 1 | Highly polarised eukaryotic cells. (*A*) Neuronal cells show a highly polarised morphology, forming branched dendrites for input and axons for output processing. The specified neuronal cell structure is required to enable efficient signal transduction within the nervous system. **(*B*)** Migrating cells adopt a highly polarised morphology, forming a leading edge with membrane protrusions and a retracting trailing edge. Both, persistent (*A*) and short-lasting or adaptive (*B*) cell polarisation, require the polarised expression of cell surface proteins mediated by intracellular transport. Images are adapted and modified from Chavarría and Cárdenas, 2013 (1) and Le Clainche and Carlier, 2008 (2).

The establishment of cell polarity is largely mediated by changes in the composition of the plasma membrane, therefore affecting how cells might act or react on their environment. Differential abundance of plasma membrane receptors, such as growth factor receptors, allows that one region of the cell is able to sense and respond to external signals in a different way than other regions of the cell do. The timely and spatially regulated presence (and absence) of cell adhesion proteins, such as integrin receptors, at the cell surface allows directed cell migration. Here, the adhesion receptors are constantly internalised at former adhesion sites and transported towards newly established adhesion sites. The insulin dependent insertion of glucose transporters provides the base for efficient glucose uptake from the intestinal tract and also other nutrients get internalised for breakdown and energy consumption. As another example, melanin, a natural pigment required for skin and hair colouration, needs to be transported from the centre towards the periphery of specialised cells, the melanocytes, to finally reach keratinocytes in the outer epidermal regions.

The cellular polarity is primarily mediated by intracellular transport processes in which highly sophisticated and highly regulated transport machineries deliver different cargoes, especially membrane vesicles, but also organelles, proteins, signalling peptides or RNAs to the demanding cellular regions. Different kinds of vesicle transport processes exist which are distinct in respect of contribution of specific proteins and co-factors, but which are also interconnected to generate a continuous flow of membrane trafficking inside the cell, thereby requiring complex regulatory mechanisms. Proteins considered for directed transport are newly synthesised at endoplasmatic reticulum (ER) associated ribosomes, delivered to the Golgi system where they undergo sorting for subsequent transport towards the desired target sites, for instance for exocytic transport through the trans-Golgi-network (TGN) towards the plasma membrane. Extracellular particles, nutrients, plasma membrane receptors but also other membrane components undergo endocytosis for sequential transport towards the cell interior and for subsequent degradation or reuse via recycling pathways. In this case, the endocytosed membrane components are sorted to specific membrane compartments, including the recycling endosome, from which they are transported back to the plasma membrane.

The aspects of intracellular vesicle transport are widely described by the so called *highways and local roads* model (*Figure 2*) (3–6), which includes a fast and long-range transport mediated by a complex and highly polarised microtubule network in order to quickly, but rather coarsely, transport cargo to distinct cellular regions. Arrived there, a more slowly, but also more flexible cargo trafficking system takes over which is mediated by the highly dynamic actin cytoskeleton that allows transport beyond the microtubule network to precisely reach outlying regions of the cell and to provide the delivery at the desired subcellular locales (7).

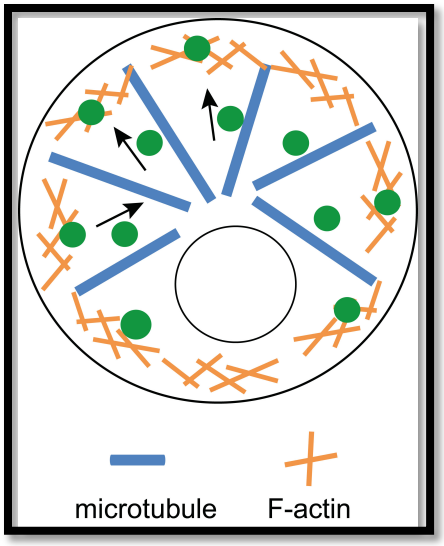

Figure 2 | Schematic overview on intracellular vesicle transport processes. Membrane vesicles (green) containing proteins, membrane components and other material, are transported along microtubules (blue) for fast and long-range transport towards the cell periphery (microtubule plus end) and also towards the cell centre (microtubule minus end), as indicated by arrows. F-actin tracks (orange) are located in more peripheral regions of the cell and mediate rather slow but more flexible transport due to the highly dynamic character of actin filaments, in order to reach more outlying subcellular regions.

1.2 Motor proteins as force generators for vesicle transport

Microtubule networks and actin filaments, spanning the cell with different characteristics, serve as tracks for specific motor proteins which act as molecular motors that produce the force necessary for cargo movement. Motor proteins are ATPases, i.e. they hydrolyse ATP to produce energy and force, and are thus commonly referred to as mechanoenzymes (8). There are three major groups of motor proteins. Kinesin motors move along microtubules towards their plus ends, whereas dynein motors move in the opposite direction towards the microtubule minus end. The third major group comprises the myosin motor proteins which generate forces on actin filaments.

1.2.1 Kinesins and dyneins transport cargo along microtubule networks

There two major groups of microtubule associated motor proteins which are responsible for cargo movement. The kinesin motors comprise a large group of motor proteins, devided into 14 classes so far identified, including ~40 human genes (9–12). Kinesin motors move unidirectionally towards the microtubule plus end (13) with few exceptions (kinesins-14, e.g. *Drosophila* Ncd (nonclaret disjunctional), move minus end directed and kinesins-13 might not move at all) (9, 12). Most kinesins are heavy chain dimers and function as processive motors, i.e. they move continuously along microtubules due to their two motor heads binding in a sequential fashion to the microtubule tracks, finally allowing efficient cargo transport. One of those processive kinesins is the family of classical kinesins (kinesins-1). Kinesin-1 family members are capable to move over long distances with a velocity of $\sim 0.8\ \mu m/s$. Considering a step size of 8 nm (distance between two consecutive tubulin dimers), the motor takes a step every 10 ms (14, 15).

Dyneins belong to the AAA family of ATPases (ATPases Associated with Diverse Activities) and have a distinct evolutionary origin compared to kinesin and myosin motors (16). There are two classes of

dyneins: the axonemal dynein and the cytoplasmic dynein (17). The axonemal dynein is important for the sliding of microtubules within the axonemes of cilia and flagella and thus for the beating movement of those. The cytoplasmic dynein motors transport diverse cargo towards the microtubule minus end and are thus involved in different cellular functions (18–21). Cytoplasmic dynein 1 transports cargo towards the cell centre and is essentially involved in mitosis, asymmetric cell division and developmental processes (22–31), whereas cytoplasmic dynein 2 has only transport functions within cilia (17). The cytoplasmic dynein comprises are large, 1.6 MDa motor complex formed by two heavy chains, including 6 AAA ATPase modules, and additional intermediate and light chains (16, 18). Not least owing their large size, dynein motor complexes are hard to handle in terms of recombinant expression and purification for subsequent analysis. In combination with the multiple ATPase domains within the heavy chain dimer the knowledge on the mechanism of dynein motors movement is limited compared to what is known for kinesin and myosin motors. Recent advances in the structural determination of dyneins allowed a better understanding of its motility mechanism, although it is still not completely clear how the specific minus end directed movement is mediated (17). A mechanism is proposed in which the two motor domains of the dynein dimer rather move in an inch-worm step manner, in which the leading head takes a step forward and is followed by the trailing head, in combination with other movement patterns, including eventual hand-over-hand steps, backward steps and steps with different step sizes (17, 32). By time-lapse fluorescence microscopy employing an intermediate chain-GFP fusion protein, the minus end directed movement velocities of cytoplasmic dynein have been measured ranging from ~ 1.4 to $2.8\ \mu m/s$ (33).

In many cell types the microtubule network is organised by the microtubule-organising centre (MTOC), located next to the nucleus, leading to a polarised microtubule network in that the minus ends are trapped within the MTOC in the cell centre and the plus ends protrude towards the cell periphery. Therefore, kinesins are generally considered as motors driving outward directed movement towards the cell cortex, whereas dyneins are inward-directed motors to transport cargo towards the cell centre (13, 18).

1.2.2 Myosin actin motor proteins

Myosin motor proteins are molecular motors that associate with actin filaments. Myosin motors are involved in a multitude of cellular and sub-cellular processes, including cell adhesion and migration, cell division and transport of cargo, including vesicles, to drive endocytic and exocytic trafficking events. Myosin motors are ATPases which hydrolyse ATP induced by actin filament binding in order to generate forces which are subsequently used to either modulate the actin cytoskeleton leading to morphological changes, or to move along actin tracks to transport cellular components.

The myosin superfamily consists of 35 classes (34) and 40 myosin genes have been identified in humans which are grouped into 13 classes. Myosin heavy chains are generally composed of three domains (35). A large *motor domain*, also referred to as *head*, is usually located at the N-terminus of the protein, harbours the ATPase activity and binds to F-actin. The motor is followed by a *neck* region containing a variable number of IQ motifs required for binding of calmodulin light chains or calmodulin related light chains. The neck region is also termed *lever arm* because of its structural rigidity that is utilized for the power stroke in consequence of conformational changes of the motor domain during the ATP hydrolysis cycle (see below) (36–39). The C-terminal part of myosin heavy chains comprises the *tail domain* which represents the highest diversity across different myosin classes in order to ensure the diversity of subcellular myosin functions.

The first myosin class discovered was the class II myosins, therefore named *conventional myosins* (40). All ensuing myosin classes discovered have been named accordingly *unconventional myosins*. The most prominent member of conventional myosins is the sarcomeric myosin II which is primarily expressed in the striated skeletal muscle and cardiac muscle (8). Additionally, non-muscle myosin II and smooth muscle myosin II are found in vertebrates (8, 41). All class II myosins share the ability to form bipolar filaments of varying length wherein their motor heads are oriented in opposite directions to mediate the movement of complementary actin filaments towards each other. These characteristics enable sarcomeric myosin II to generate forces for muscle contraction by forming large bipolar filaments (8). Non-muscle myosin II forms shorter bipolar filaments and also generates forces on actin filaments, and is involved in cell adhesion and migration, protrusion formation and cytokinesis (8, 41–45). Myosin II family members also work to crosslink actin filaments (8).

1.3 Class V myosin motor proteins

One member of the unconventional myosin motors comprises the class V myosins. In contrast to class II myosins which exert forces on actin to rather induce structural alterations, class V myosins work as molecular motors to transport a diversity of cargo along actin filaments (35, 46). The ability of class V myosins to function as a transporting motor is achieved by their specific structural organisation (*Figure 3*). Class V myosin proteins contain an N-terminal motor domain, an elongated neck with six IQ motifs and the C-terminal tail which is further subdivided into a *coiled-coil* region that mediates the dimerisation of two myosin V heavy chains and a *globular tail domain* (GTD) at the very C-terminus which serves as the cargo binding domain (8, 47). Myosin V motors move towards the actin filaments barbed end (plus end) and its gliding velocities are in the order of a magnitude slower than that of kinesins or dyneins and have been reported roughly between 0.2 and $0.8\ \mu m/sec$, although exceptions exist towards slower and faster movements (48–50).

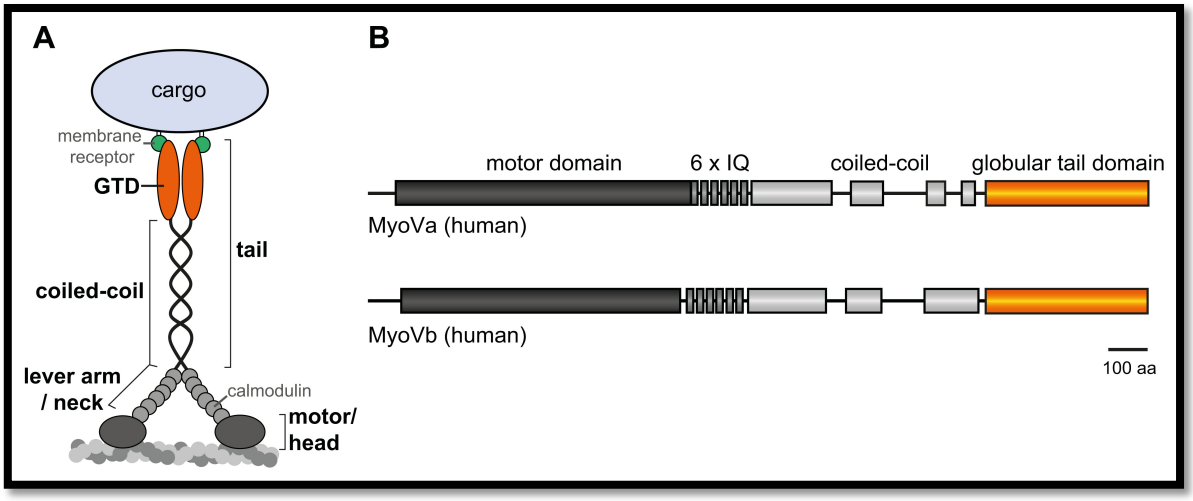

Figure 3 | Structural organisation of class V myosins exemplified by the vertebrate myosin V (MyoV). (*A*) MyoV proteins contain an N-terminal *motor domain* (also called *head*) which binds to actin filaments and mediates the actin dependent ATPase activity. Six *IQ motifs* each bind calmodulin light chains and are also referred to as *neck* and forming the *lever arm* required for forward movement. The C-terminal *tail* is divided into a *coiled-coil* region which is periodically interrupted and required for heavy chain dimerisation, and the very C-terminal *globular tail domain* (GTD) which is the cargo binding domain, e.g. by binding to specific membrane receptors, and a major protein interaction site. **(*B*)** Schematic overview of the myosin Va and myosin Vb domain organisation. *IQ*, isoleucine/glutamine; *GTD*, globular tail domain; *aa*, amino acids.

1.3.1 Vertebrate myosin V

Class V myosins are conserved across almost all eukaryotic species (34). Three myosin V genes can be found in humans: *MYO5A*, *MYO5B* and *MYO5C,* encoding the myosin Va (MyoVa), myosin Vb (MyoVb) and myosin Vc (MyoVc) proteins, respectively (51–54). MyoVa and MyoVb proteins are expressed throughout the body (55) and can also be found in the brain, in contrast to myosin Vc (8, 54, 56–59). In the brain, MyoVb is strongly expressed in the hippocampus (57), whereas MyoVa is more widely distributed to other brain regions (58). Within neuronal cells, both isoforms are localised to dendritic spines and the postsynaptic densities (57, 60–62). Myosin Vc is highly abundant in epithelial and glandular tissues, such as pancreas, prostate, mammary, stomach, colon and lung, and is mainly expressed in epithelial cells (54). Different splice variants of all three MyoV isoforms exist, which are differentially expressed and which mediate specific interactions and functions (see below) (53, 55, 63–67). The vertebrate myosin Va protein has been first described *in vitro* to processively move along actin filaments, i.e. it moves processively as an isolated dimer on actin tracks in a step-wise, hand-over-hand fashion (8, 48, 68, 69). This characteristic is suggested to be demanded for an efficient actin dependent transport of cargo in living cells (69, 70). The vertebrate MyoV feature of processive movement is in contrast to other myosin classes and is even not conserved within the myosin V family (myosin Vc and *Drosphila* myosin V; see below).

The base for efficient MyoVa movement along F-actin is provided by its specific structural organisation and adaptation. The myosin Va heavy chain dimer binds to actin filaments by its motor domains forming a leading and a trailing head each time (*Figure 4*). At the point the trailing head

detaches from the filament, the leading head undergoes a slight conformational change, referred to as the *power stroke*, bringing the trailing head in front to become the new leading head, i.e. the motor takes one step (35, 71). The *step size* of myosin motors largely depends on the length of the neck region/lever arm. The two heads of the MyoVa dimer bind to the actin filament within a distance (step size) of $36\,nm$ which is facilitated by the elongated neck region containing six IQ motifs (69). In comparison, the step size of the conventional myosin II is only about $7\,nm$ due to the shorter neck (72). The large step size of myosin Va perfectly fits to the double helical actin filament organisation with consecutive actin monomers every $36\,nm$ on the short pitch helix. Thus, MyoVa is able to walk along actin filaments in a linear, step-like fashion instead of spiralling around the filament by following the long pitch helix, which would strongly impede transport through the cytoplasm (71, 73–77). Another structural feature facilitating continuous transport of cargo along actin tracks is the flexibility of the tail domain induced by interruptions in between the coiled-coil regions (78, 79). Finally, myosin Va proteins adapted to intracellular transport in terms of binding to specific cargoes in distinct ways therefore allowing to specifically switch between different cargoes for different transport routes. Although the cargo binding is mainly mediated by the globular tail domain which interacts with specific membrane associated proteins, such as Rab GTPases or their respective adaptors (80–84), the ability to select between different cargoes is further supported by other parts of the protein, for instance the flexible regions within the coiled-coil domains, and cell type specific alternative splicing events (66, 67, 80). The elongated neck of MyoVa also enables the motor to switch from one actin filament to another one allowing transport of cargo across a complex network of actin filaments or along branched filaments (6, 85).

The kinetic properties of myosin Va motors are another rationale for its processive movement (*Figure 4*). In general, there are four kinetic states of the motor domain influencing the actin binding capacity and strength. The motor alone or the motor binding ADP shows high affinity for F-actin, whereas the motor binding ADP and inorganic phosphate (P_i) or the motor binding ATP shows low affinity for F-actin. As the hydrolysis of ATP to ADP and P_i and the subsequent release of P_i are rather fast processes, the dissociation of ADP from the motor domain is considered to be the rate-limiting step in the ATPase cycle of the myosin V motor domain (86, 87). Considerng that, the motor domain is most of the cycle time tightly bound to the actin filament (it has a high *duty ratio*), which is reported to be demanded for processive movement along actin tracks (8, 35, 68). As a final requirement for the continuous movement, the ATP hydrolysis cycles within the two motor domains of the dimer need to be tightly regulated in a way, that only one of the motors can detach from the filament at a given time (68, 88–91).

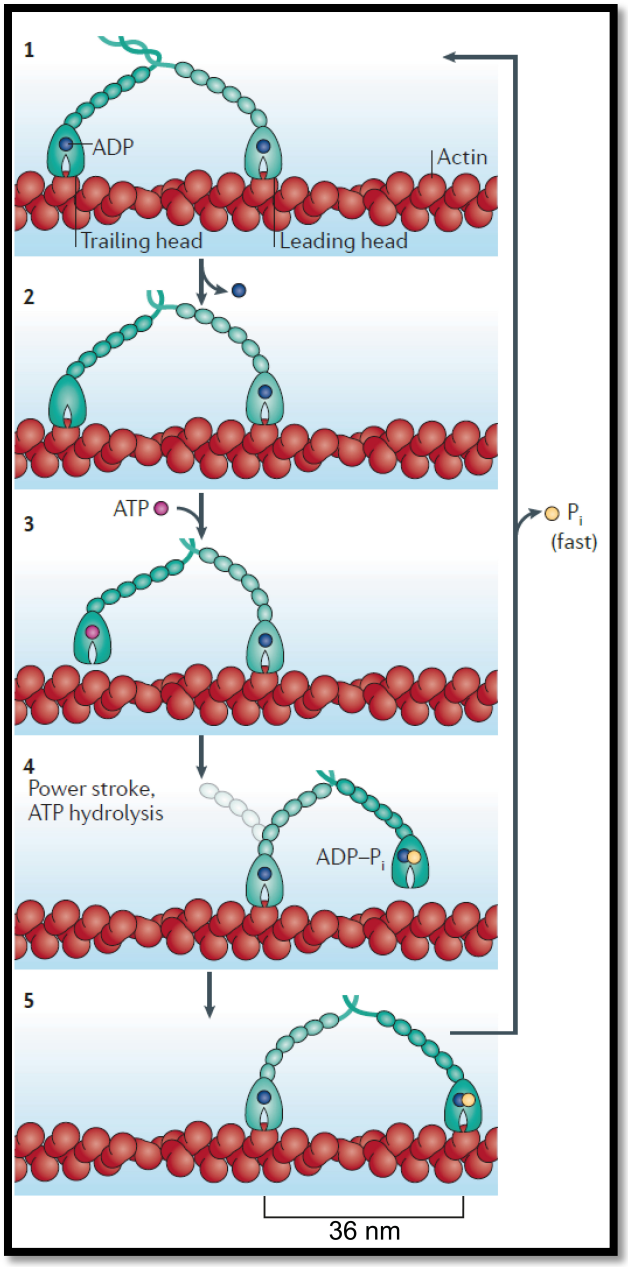

Figure 4 | Processive movement of MyoVa along actin filaments. (*1*) Both motor heads of the MyoVa dimer bind ADP and are strongly attached to the actin track. **(*2*)** Due to an intramolecular strain, ADP is released first from the trailing head. **(*3*)** The trailing head binds ATP and subsequently dissociates from the actin track. **(*4*)** The still attached leading head undergoes a conformational change (power stroke) to bring the former trailing head in front to become the new leading head. ATP bound to the new leading head gets hydrolysed to ADP and P_i and by a thermally driven search the new leading head finds a binding site. **(*5*)** The new leading head binds to actin inducing the fast release of P_i followed by strong binding of the head to the actin track. The cycle is completed and the MyoVa dimer moved 36 nm (step size) towards the F-actin barbed end. Adapted and modified from Hammer and Sellers, 2012 (35).

Among the vertebrate class V myosins, myosin Vb is very similar to myosin Va in terms of structure and kinetics and is also reported to be a processive actin motor at single dimer level (48). The third vertebrate MyoV isoform, myosin Vc, is also similar in terms of structure (~50% overall identity to both MyoVa and MyoVb) (54), but has not been considered to be a processive motor as a single dimer. That is reasoned by the ADP release being not the rate-limiting step within the ATP hydrolysis cycle of myosin Vc (92, 93). Nevertheless, specific conditions are discussed in which myosin Vc might act as processive motor or that multiple MyoVc proteins assemble to a large motor complex to efficiently transport cargo (94).

1.3.2 Insect and yeast class V myosin motors

The *Drosophila melanogaster* myosin V (Dm-MyoV) is a well-characterised example for class V myosin members significantly differing from vertebrate MyoVa and MyoVb (49). As it is true for vertebrate MyoVc, the structural organisation of Dm-MyoV is similar to that of vertebrate MyoV proteins, besides their distinct evolutionary origin. Although the velocity of Dm-MyoV is nearly identical to that of vertebrate MyoV processive motors, major alterations can be found in respect to the kinetic cycle. Dm-MyoV is considered to be a *low duty ratio* myosin, i.e. the motor is most of the time of the ATP hydrolysis cycle detached from F-actin (in contrast to vertebrate MyoV), which prevents its function as a processive motor at the single molecule level. To overcome these intrinsic deficits, multiple motor proteins cluster at the potential cargo to form a processive motor unit which ultimately drives the processive transport (49).

In line with that, the two class V myosin members found in yeast, Myo2p and Myo4p, also act differently compared to vertebrate MyoV (95–97). Myo2p is structurally similar to vertebrate MyoV but does not function as a processive motor as a single dimeric molecule (95). Myo4p is even more different as it has a distinct structural organisation by forming a heterodimeric complex with the Swi5-dependent HO expression 3 protein (She3). Thus, Myo4p is a single-headed motor which does not move processively along F-actin alone but only by clustering into motor units, similar to Dm-MyoV (95, 97).

1.3.3 Regulation of myosin V activity and function

The property of myosin V motor proteins being processive motors on actin tracks demand regulatory mechanisms that prevent its activity and movement on F-actin when not required, e.g. when not attached to cargo. The full-length myosin V motor exists in two distinct states. There is an auto-inhibited, inactive state in which the MyoV dimer is back-folded in a way that its globular tail domains (GTD) bind to its motor domains (*Figure 5*) (98–100). In this state, the ATPase activity is inhibited and the motor binds only weakly to actin filaments (101, 102). Furthermore, the auto-inhibited motor shows a cytoplasmic localisation and is therefore not attached to vesicles or other cargo (103). Activatory mechanisms release the inhibiting GTD/motor domain interactions and enable MyoV to adopt an open and extended conformation that resembles the active state at which it binds to cargo and F-actin. Increased concentrations of intracellular Ca^{2+} ions induce the MyoV dimer opening and activate the ATPase activity *in vitro* (104). At the same time, excessive Ca^{2+} concentrations ultimately lead to the dissociation of calmodulin light chains from the neck region thereby making it very flexible and thus not suited to drive the motor movement, which finally results in the inability of MyoVa to move on F-actin tracks (102, 105, 106). The binding of cargo to the globular tail domains might be ultimately the more physiologically relevant opening mechanism for

MyoV proteins. A perfect example in that respect is the melanophilin (MLPH or Slac-2a) protein (see below) which binds to the GTD of MyoVa, activates its ATPase activity and facilitates its movement on actin filaments *in vitro* (107, 108). Furthermore, it has been demonstrated very recently by means of electron microscopy, that MLPH is able to bind to the purified full-length back-folded MyoVa dimer and induces its opening into the extended conformation (109).

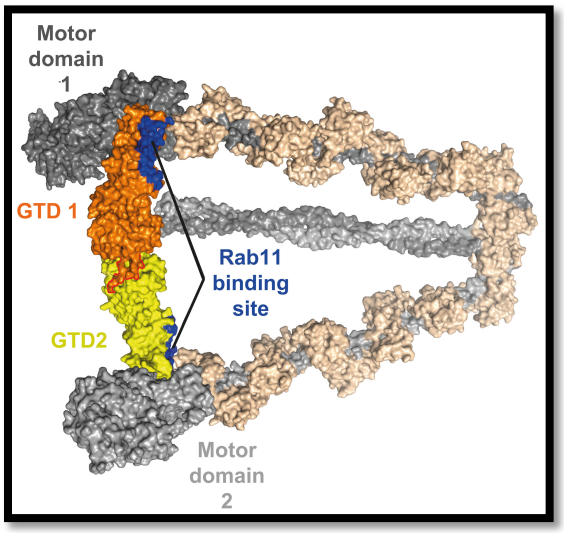

Figure 5 | Model of the back-folded auto-inhibited state of the full-length myosin V motor. The two globular tail domains (GTD 1, 2) of the heavy chain dimer interact with the two motor domains to adopt a back-folded state in which the ATPase activity of the motor is inhibited and only weak F-actin binding is obtained. Increased concentrations of Ca^{2+} ions induce MyoV opening and ATPase activity of the motor but do not promote efficient processive movement due to the release of calmodulin from the neck region. Cargo binding to the GTDs induces MyoV unfolding, activates ATPase activity and allows efficient MyoV driven cargo transport. The MyoVa-GTD Rab11 binding site is highlighted in blue. The model was generated from a partial electron microscopy model (PDB ID 2DFS) (99), mutational analysis data on residues participating in the GTD/motor interactions (109) and the crystal structures of the MyoVb GTD (210). Image provided by Olena Pylypenko.

Besides the regulated opening and activation mechanisms for myosin V dimers, myosin motors also undergo a fine-tuned regulation at their active state, at least in some cases. Although, generally, myosin V proteins (e.g. the mammalian MyoVa and MyoVb) are processive actin-based motors as dimeric molecules, it has been repeatedly observed that myosin V proteins cluster at the cargo surface to form motor units (110–112), in a similar way as was described for the *Drosophila* MyoV or mammalian MyoVc. This mechanistic behaviour increases the run length of the motors on actin tracks but also reduces their velocities compared to single dimeric molecules (113–120). This phenomenon might be explained by a hindrance due to asynchronous movement of the different motors (119) and by a load dependence of the motor kinetics, meaning that the cargo itself can influence the motors walking behaviour, at least to some extent (88, 121–123). Even the lipid composition of the vesicular cargo can influence the myosin movement (50). A more fluid vesicle nature thereby induces walking velocities higher than those at the single dimeric molecule level even measuring up to velocities of unloaded motors. Contrary, more gel-like vesicle compositions reduced the walking velocity. These findings are further supported by a mechanism in which the melanophilin protein has also been demonstrated to slow myosin Va movement (~4-fold), but, on the other hand, increases the length of processive walks (~2-fold) compared to the single dimeric motor. Altogether, the time the motor is attached to actin tracks is significantly increased, therefore facilitating melanosome trafficking in melanocytes (124). A suitable explanation for these observations might be

that electrostatic interactions between MLPH and actin filaments make MLPH to act as a tether for the myosin Va motor to stay longer attached to the actin tracks.

Furthermore, an interconnectivity has been revealed in which motor proteins of different families cooperate to influence each other's processivity (125). One example here is the cooperation of myosin V and kinesin family motors in the periphery-directed transport. In this process, myosin V performs a diffusional search along microtubules which in turn prolongs the run length of the kinesin motor attached to the same cargo. The same effects occur the other way around for myosin V motors on actin tracks. The proposed mechanism for a mutual run length enhancement might be explained (in similarity to the aforementioned MLPH effects on myosin Va processivity) by electrostatic interactions within the non-specific motor-cytoskeleton connections, which possibly have a tethering character that reduces the diffusion rate of the cytoskeleton specific motor.

1.4 The Ras superfamily of small GTPases

Kinesin, dynein and myosin motor proteins were introduced as the molecular motors that provide the forces required for movement of cargo on cytoskeletal tracks. The delivery of the highly diverse set of intracellular membrane vesicles to their respective destinations requires to be coordinated in a timely and spatially regulated manner. Members of the Rab family of small GTPases, being a family of the Ras superfamily of small GTPases, act here as master regulators as they control the membrane identity in order to provide the basis for a proper sequence of vesicle budding, movement and fusion by recruiting specific adaptor and effector proteins to intracellular membranes (126).

1.4.1 The Ras superfamily includes five families of small GTPases

The Ras superfamily comprises a very large and diverse set of small GTP binding proteins and is subdivided into five major families (127). The Rab (Ras-like in brain) family comprises the largest group of small GTPases (126, 127), next to the other four major families of Ras, Rho, Arf/Sar and Ran GTPases all of which serve different functions (127). Shortly, the Ras (Rat sarcoma) family members act as signalling molecules, integrating extracellular stimuli to activate intracellular signalling cascades (for instance the mitogen activated protein kinase cascade) to control gene transcription. The most prominent members of the Ras family might be the oncogenic Ras proteins. Members of the Rho (Ras homology) family are well known for their function in the regulation of actin dynamics (128, 129), cell polarity (130), cell cycle progression and gene expression (127). The Ran (Ras-like nuclear) family of small GTPases contains only one member in eukaryotic cells, except plants having multiple members, and are involved in nuclear transport across the nuclear envelop (127). The Arf

(ADP-ribosylation factor) family is the most divergent family of the Ras superfamily and is also involved in vesicle transport (131).

The structural organisation that is shared by Ras superfamily small GTPases includes a large (~170 amino acids) G domain which mediates the GTP binding and hydrolysis, and the interaction with different effectors (131, 132). The G domain itself contains five G-boxes (G1 to G5) with conserved residues. The switch I and switch II regions as part of the G domain are particularly involved in effector binding and undergo a conformational change upon GTP binding, especially Switch I located around G2 (133).

1.4.2 The Ras cycle

A common feature of most Ras superfamily small GTPases is their function as molecular switches by alternating between two distinct conformational states: the GTP bound active state and the GDP bound inactive state. The conversion between the two states is mediated by a Ras GDP-GTP cycle (*Figure 6*). GDP in the inactive Ras protein is exchanged by GTP under support of *guanine nucleotide exchange factors* (GEFs) which facilitate the release of GDP and favour fast GTP loading due to the high abundance of GTP in the cytoplasm (~1 mM) (126). *GTPase activating proteins* (GAPs) stimulate the hydrolysis of GTP to GDP and inorganic phosphate (P_i) within the GTPase which is necessary given the relatively poor intrinsic GTP hydrolysis activity of the GTPase itself (132, 134). This is also the reason for the term *GTPase* being not completely precise, as GTP hydrolysis needs the support by GAPs, and therefore the term *small G-protein* might be more suited for these kinds of proteins. However, to stay with the literature I will keep to the term *small GTPase* throughout this thesis. Generally, GEFs and GAPs are essential factors determining small GTPase activity in time and space as they integrate a wide range of cellular inputs coming from different signal sources, such as binding of signalling proteins, second messengers like cAMP, or structural proteins (134).

Most family members of the Ras superfamily of small GTPases are specifically targeted to distinct subcellular compartments, such as membrane vesicles or larger organelles, either by membrane-targeting protein sequences or by post-translational lipid modifications inserting into the membrane lipid bilayer (132). Members of the Ras, Rho and Rab families are typically modified via isoprenylation at the C-terminus. Farnesyl, geranylgeranyl or palmitoyl lipid groups are here covalently linked to cysteine residues of common sequence motifs, including the Caax (cysteine-aliphatic-aliphatic-arbitrary) motif (131, 132, 135). Within the large and diverse family of Rab GTPases isoprenylation motifs were found with C-terminal cysteine residues involving the motifs: xxxCC, xxCxC, xxCCx, xCCcc and CCxxx which are modified by geranylgeranylation (135, 136). To ensure efficient isoprenylation, members of the Rab family need the assistance of a helper protein, the *Rab escort protein* (REP)

(137). REP binds to newly synthesised Rab proteins and presents them to geranylgeranyl transferases, thus allowing efficient geranylgeranylation of both C-terminal cysteins (138–140). Arf family members are typically N-terminally myristoylated and Ran family members are not modified (131, 132, 141). In providing a strong and specific subcellular localisation of small GTPases to distinct vesicle pools and/or organelles, the post-translational modification is only one part of the truth; the target membrane composition, electrostatic properties of both membrane and protein, and the support by chaperones must act together in order to achieve selectivity and specificity in membrane targeting of Ras small GTPases (132).

The eventual presence of lipid modifications require a further regulatory feature for small GTPases involving the *guanine nucleotide dissociation inhibitors* (GDIs) (142). GDIs have a high affinity for the inactive, GDP bound and lipid modified GTPases and serve first, to prevent the release of GDP in order to stabilise the inactive form (143) and second, as a shield for the hydrophobic lipid modified part against the hydrophilic cytoplasm when being transported to destined locales (132, 144–149).

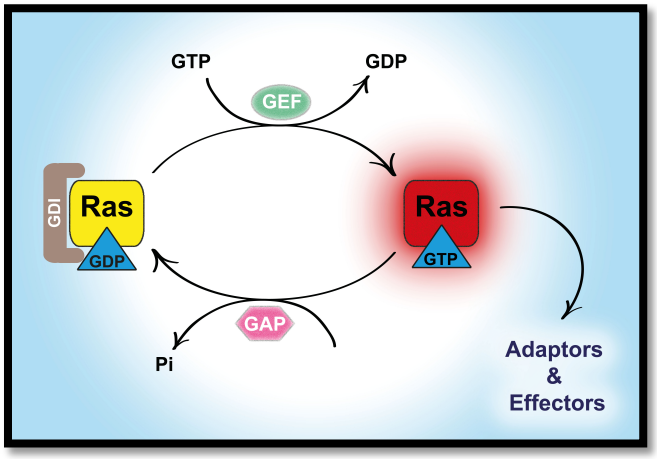

Figure 6 | Activity cycle of Ras superfamily small GTPases. Ras small GTPases exist in to distinct states: the GDP bound inactive state (*yellow*) and GTP bound active state (*red*). Ras-GDP is bound by guanine nucleotide dissociation inhibitors (GDI, *brown*) to prevent GDP dissociation and shielding lipid modifications. Guanine nucleotide exchange factors (GEF, *green*) mediate the exchange of GDP by GTP inducing Ras GTPase activation and enabling its interaction with a wide range of effector and adaptor proteins. GTPase activating proteins (GAP, *pink*) support the intrinsic GTP hydrolysis activity of Ras proteins to hydrolyse GTP to GDP and inorganic phosphate (P_i), and finally inactivate the GTPase to complete the activity cycle.

1.5 Rab family GTPases

The Rab family of small GTPases comprises the largest group within the Ras superfamily. Rab proteins are considered as being the master regulators of intracellular vesicle transport processes as they tightly coordinate all stages of a membrane vesicles lifecycle, including vesicle budding from the donor compartment, vesicle uncoating, vesicle transport, vesicle docking at the acceptor compartment and subsequent membrane fusion (*Figure 7*) (7, 126, 127). So far, 65 members of the Rab family have been identified in the human genome, which are divided into 9 functional groups. The large diversity of this family is mainly explained by gene duplications during evolution. Each member of the Rab family is localised to specific intracellular membrane compartments (126, 127, 150–153). Rab proteins decide on the membrane identity and mediate their functions in membrane

transport by recruiting specific adaptor and effector proteins towards the membrane surface. To do so, they interact with a wide range of membrane associated proteins, such as vesicle coat proteins, motor proteins, tethering factors, signalling proteins and SNARE (SNAP (Soluble NSF Attachment Protein) Receptor) complex proteins (126).

1.5.1 Regulation of Rab GTPase activity and its impact on intracellular membrane cycling

The aforementioned cycling between the active, GTP bound and inactive, GDP bound Rab GTPase states induces major conformational changes in the switch I and switch II regions (154). Rab GEFs specifically recognise distinct residues in these switch regions to induce GDP release and GTP binding. Following the GTP-binding induced conformational change, adaptor and effector proteins bind to both switch and interswitch regions of the active Rab-GTP (155). GTP hydrolysis of Rab proteins is supported by Rab GAPs. Rab GAPs contain a conserved catalytic TBC domain (Tre2/Bub2/Cdc16) (156–158) promoting GTP hydrolysis by a dual arginine-glutamine-finger mechanism (157, 159, 160). There are at least 40 Rab GAPs in humans, suggesting specific interactions of individual GAPs with their respective Rab proteins (161, 162).

A well-regulated interplay between Rab GEFs and Rab GAPs with specific Rab GDIs, the Rab escort protein REP, and membrane bound *GDI displacement factors* (GDFs), last of which recognise cytoplasmic Rab-GDI complexes and induce GDI release, is proposed to be the driving force for specific targeting of distinct geranylgeranylated Rab GTPases to their desired membrane compartments, finally enabling the directed transport from donor to acceptor compartments (*Figure 7*) (126, 163). The whole membrane transfer procedure can be divided into five major steps (126): vesicle budding and sorting of target proteins to the budding vesicle, potentially accompanied by vesicle coating with stabilising coat proteins (i), vesicle uncoating (ii), vesicle transport through the cytoplasm along cytoskeletal tracks (iii), vesicle tethering at target membrane compartments, supported by tethering factors and SNARE complex proteins (iv), and vesicle fusion with the destined compartment (v).

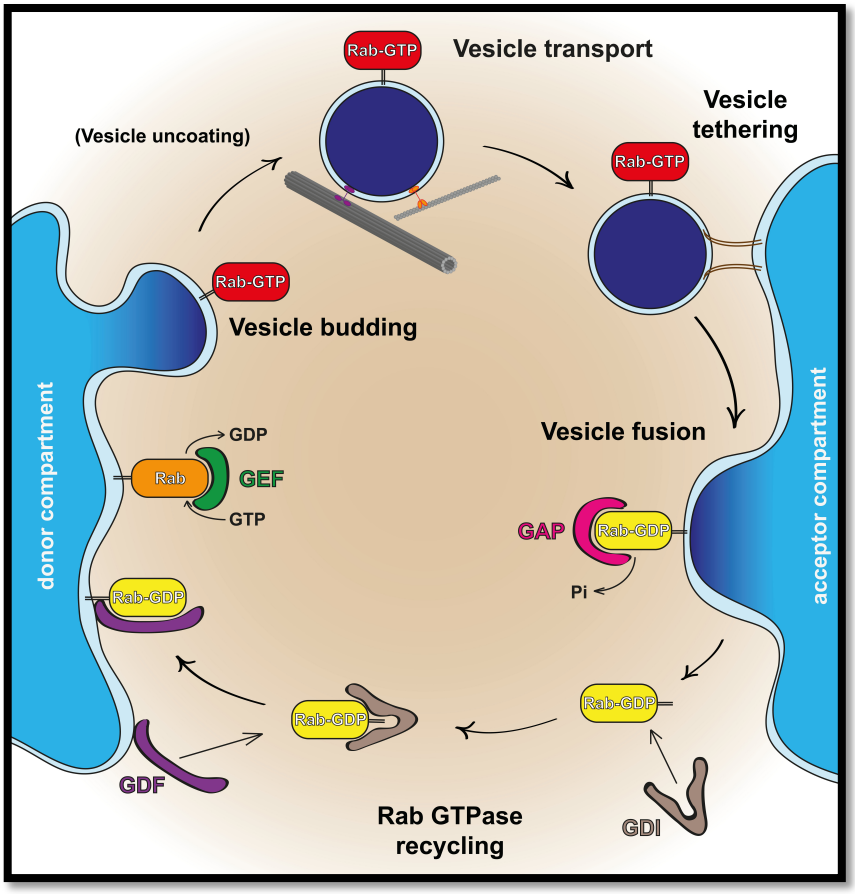

Figure 7 | Schematic overview on vesicle transport from a donor towards an acceptor membrane compartment and the involvement of Rab small GTPases. Vesicle budding starts from the donor membrane compartment. This step requires active, GTP bound Rab GTPases located at the future bud site and recruiting different adaptor and effector proteins. Cargo destined to undergo trafficking is sorted into the vesicle bud. Potentially, vesicle formation involves clathrin coating of the membrane for clathrin mediated endocytosis. Following contingent uncoating, membrane vesicles are transported in a Rab-GTP and motor protein dependent fashion along microtubule and actin tracks. When reaching the acceptor compartment, vesicle docking and subsequent vesicle fusion is facilitated by tethering factors located at the target membrane and SNARE proteins on both vesicle and target membrane. In succession of vesicle fusion with the target Rab GAPs bind to Rab-GTP and support GTP hydrolysis to GDP and the release of inorganic phosphate (P_i), leading to Rab GTPase inactivation and subsequent Rab-GDP liberation from the membrane. Rab-GDIs bind to cytosolic Rab-GDP to prevent GDP dissociation and to shield hydrophobic lipid tails. Rab-GDP is recycled and eventually returned to membrane compartments. Here, Rab-GDFs target cytosolic Rab-GDP:GDI complexes, facilitate GDI release from Rab-GDP thus retargeting Rab proteins to membranes. Rab-GEFs mediate the exchange of GDP by GTP therefore activating Rab GTPases and start the cycle from the beginning. *GAP*, GTPase activating protein; *GDI*, guanine nucleotide dissociation inhibitor; *GDF*, GDI displacement factor; *GEF*, guanine nucleotide exchange factor.

1.5.2 Rab GTPases as master regulators of intracellular transport

Intracellular membrane trafficking comprises a large array of different types of membrane vesicles, transported between different types of donor and acceptor compartments, organelles and other cargo. Specific Rab GTPases are associated with distinct membraneous compartments and are therefore involved in particular transport processes. These have been reviewed in detail by Harald Stenmark (*Figure 8*) (126) and are shortly summarised here. Rab1 is involved in trafficking from the endoplasmatic reticulum (ER) to the Golgi as it is localised to the ER and pre-Golgi intermediate compartment (IC). Rab2 might have similar functions. Trafficking within the Golgi system is mediated by Rab6, Rab33 and Rab40. Rab8 is a major regulator of exocytic transport from the *trans*-Golgi network (TGN) to the plasma membrane, e.g. it supports the transport of GLUT4 vesicles, together with Rab10 and Rab14. Different types of exocytic transport are further mediated by Rab3, Rab26, Rab27 and Rab37. Rab27a is particularly important for the periphery directed transport of melanosomes in melanocytes as an essential mechanism in skin and hair pigmentation, and Rab32 and Rab38 participate in the biogenesis of melanosomes, as do Rab7 and Rab8. Rab32 is furthermore

crucial for mitochondria fission. Rab22 is required for trafficking between the TGN and the early endosomes. Rab5 is potentially the most important regulator of endocytosis as it is localised to endocytic sites at the plasma membrane and to early endosomes and phagosomes as well. Rab5 functions in mediating endocytic events, for instance by inducing the formation of clathrin-coated pits and clathrin-mediated endocytosis, and macropinocytosis, and is also involved in subsequent endocytic pathways, such as the fusion of clathrin-coated vesicles with the early endosome and the maturation of early phagosomes, often together with other Rab proteins. Rab21, for instance, participates in integrin receptor re-uptake. Recycling pathways are used to return endocytosed receptors, signalling molecules and other membrane components back to the plasma membrane. Fast recycling only involves the early endosome and is mediated by Rab4. In contrast, a more slowly recycling traverses the recycling endosome and requires function of Rab11 and Rab35. In this process also Rab15 plays a role in trafficking from the early endosome towards the recycling endosome. Despite its role in exocytosis, Rab8 is also involved in endocytic and recycling events. Together with the Arf family member Arf6, Rab8 induces macropinosome formation, subsequent tubulation of those and final recycling of receptors, signalling molecules and membrane components (164). Rab7a and Rab7b are structurally very similar but contribute to different endosomal transport steps (165, 166). Rab7a is localised to the early endosome and mediates transport towards the late endosome and lysosome, therefore playing a role in protein degradation (165). In contrast, Rab7b is additionally localised to the TGN and Golgi and rather mediates retrograde trafficking from the late endosome towards the TGN (167). Similar functions are described for Rab9.

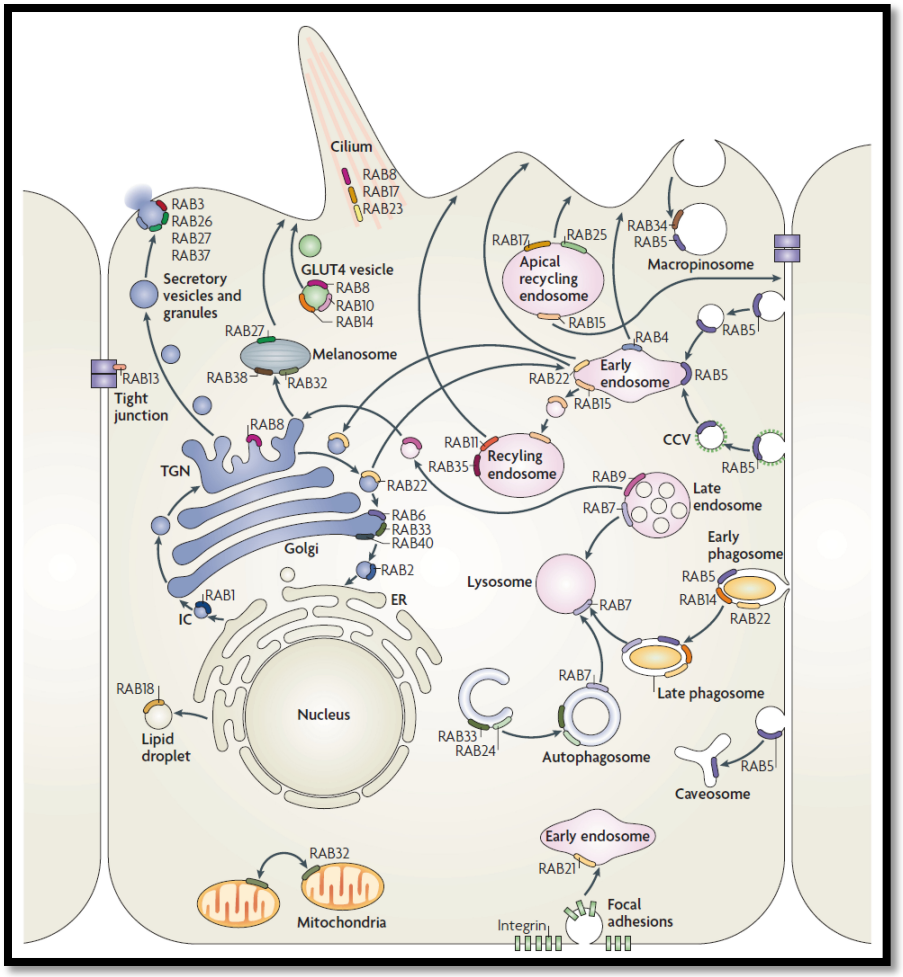

Figure 8 | Localisation and function of Rab GTPases at intracellular membranes. Members of the large family of Rab GTPases regulate different steps of intracellular trafficking, including exocytosis, endocytosis and recycling transport, pathways for degradation of cellular content, organelle transport and dynamics, and cell morphological alterations, such as cilia formation and cell adhesion. Adapted from Harald Stenmark, 2009 (126).

1.5.3 Rab GTPases form complexes with motor proteins

In order to achieve vesicle transport along cytoskeletal tracks, motor proteins need to associate with vesicle membranes in a highly specific and well-regulated fashion. Rab family GTPases specifically recruit motor proteins directly or indirectly to the respective vesicle surface. This mechanism is well described for class V myosin actin motors which have been shown to associate with Rab GTPases at vesicle membranes in both, in yeast and higher order eukaryotic cells. The yeast Rab GTPase Ypt11p has been shown to interact with the class V myosin member Myo2p in transporting the Golgi into a growing bud (168). Furthermore, a cooperation of Ypt11p and Myo2p has been implicated in the transport and inheritance of mitochondria (169, 170), and the yeast Rab GTPase Sec4p (the mammalian homolog is Rab8) has been demonstrated to recruit Myo2p to secretory vesicles (169, 171).

The well-studied role of Rab27a in melanosome transport in melanocytes is another example for the formation of Rab GTPase myosin V motor protein complexes (80, 124, 169, 172–174). Here, Rab27a forms a tripartite complex with myosin Va and the melanophilin protein (MLPH). MLPH functions to connect the myosin Va actin motor with the melanosome associated Rab27a small GTPase (83). The formation of this tripartite complex is essential for the transport of melanosomes to the periphery of

melanocytes for subsequent transfer to keratinocytes, an important process for skin and hair pigmentation (80, 175). Mutation of either of the complex partners underlies the manifestation of a disease called *Griscelli syndrome* (GS) (174, 176–180). There are three types of disease presentation all of which have in common a skin and hair hypopigmentation (176). Griscelli syndrome type 1 further includes severe neurological impairments and is caused by mutations in the MYO5A gene (176, 180). GS type 2 is based on mutations in the RAB27A gene and presents with misfunctions of the immune system and increased infection susceptibility (174, 176, 177). GS type 3 is related to mutations in the MLPH gene and here patients only show the phenotype of partial albinism (176, 178, 179).

The Myosin and Rab interacting protein (MyRIP or Slac-2c) is another Rab27a binding protein which has been shown to form a similar tripartite complex with myosin VIIa. The *Drosophila* myosin VIIa protein has been shown to function as a processive motor on actin filaments and the mammalian homolog is supposed to act in a similar way (181–183). Myosin VIIa plays a crucial role in the retina and in the inner ear as it is localised to photoreceptor cells and pigmented epithelial cells of the retina, and to the pericuticular necklace of sensory hair cells (181, 184–186), where it functions as a molecular transporter (187, 188). In particular, a Rab27a:MyRIP:myosin VIIa complex is required for melanosome motility in the retinal pigment epithelium (189). Mutations of the MYO7A gene have been shown to cause the human Usher syndrome type 1B (184). Usher syndrome type 1 is the most frequent cause for inherited deaf-blindness in humans (190), presenting sensorineural hearing loss, vestibular dysfunctions and early-onset retinis pigmentosa (184, 191), and underlies mutations in multiple loci leading to different disease subtypes (myosin VIIa is encoded by the *USH1B* locus) (184, 190).

This mechanism of differential targeting of distinct motor proteins to Rab27a vesicles by co-recruitment of specific adaptor proteins (MLPH vs. MyRIP) nicely shows the fine-tuned regulation of vesicle associated protein complex formation, depending on cell type and cargo. In accordance, Rab27a has been shown to functionally correlate with myosin Va in the transport of dense core secretory granules to the plasma membrane of pancreatic beta-cells (192). Here, Rab27a and myosin Va form a tripartite complex with the adaptors granuphilin-a, granuphilin-b and rabphilin-3A, respectively.

The small GTPase Rab3A, being the most abundant Rab family member in the brain (193), has been shown to directly interact with myosin Va at synaptic vesicles to facilitate the transport of these vesicles in neuronal cells (194), as has also been shown for Rab27b (195). Rab8a directly interacts with myosin Vb at the aforementioned tubular recycling network containing Eps-15-homology domain-containing proteins EHD1 and EHD3 (196). Rab8a, in conjunction with Rab11a, interacts with myosin Vb in the regulation of enterocyte polarity by driving apical transport processes, and regulate

enterocytic microvilli growth (197). Mis-regulation of these Rab motor complexes has a major impact on the pathogenesis of microvillus inclusion disease, in which impaired interactions of MyoVb and Rab8a induce microvilli loss and uncoupling of MyoVb and Rab11a lead to microvilli inclusions. Rab8a also interacts with myosin Va in the insulin triggered transport of GLUT4 (glucose transporter type 4) vesicles towards the plasma membrane of rat muscle cells (198–200). A similar mechanism has been proposed for the cooperation of Rab10 and MyoVa in adipocytes (201). These studies nicely show the interconnection of stimuli induced intracellular signalling (e.g. phosphorylation events following insulin receptor activation) and vesicle transport processes (Rab GTPase activity). Rab8a is furthermore suggested to interact with the epithelial-related myosin Vc in the transferrin receptor transport in epithelial cells (54). Rab10, which is related to Rab8a and localises to the same tubular network (196), has also been shown to interact with myosin Va, Vb and Vc *in vivo* and is thus proposed to be involved in similar recycling functions (55, 202–206). Vertebrate myosin Vc directly interacts with Rab38 and the closely related Rab32 to cooperate in the biogenesis and secretion of melanosomes (207). Here, the myosin Vc motor is required to transport distinct melanosome biogenesis factors, such as the tyrosinase-related proteins Tyrp1 and Tyrp2, and the SNARE protein Vamp7, from the early and recycling endosomes towards maturing melanosomes. Interestingly, Rab32 and Rab38 interact specifically with MyoVc, but neither with MyoVa nor with MyoVb. In the following melanosome maturation process, MyoVc also interacts with Rab7a and Rab8a.

Alternatively spliced exons within the C-terminal regions between the neck and the globular tail domain in myosin Va, myosin Vb and myosin Vc specifically determine the interaction of the motor proteins with distinct Rab GTPases (*Figure 9*) (55). Myosin Va has six alternatively spliced exons: exons A, B, C, D, E and F, whereas myosin Vb has only five as it misses exon F. Particularly, the three exons B, D and F undergo alternative splicing in myosin Va (53, 63, 64). Exon F supports the association of myosin Va with melanophilin to form a functional complex with Rab27a (80, 83, 208, 209). Exon B has been demonstrated to play a role in the interaction of myosin Va with dynein light chain 2 (DLC2), which, however, has not been resembled for the exon B of myosin Vb (66, 67). Exon D is required for MyoVa binding to Rab8a and Rab10. For MyoVb the exon D is also essential for Rab10 interaction, but, in contrast to MyoVa, inhibits binding to Rab8a (55). Rab11a interacts with both, myosin Va and myosin Vb, in an exon independent fashion (55, 210, 211). Myosin Vc also expresses an alternatively spliced exon F which determines its interaction with Rab32 and Rab38 (207).

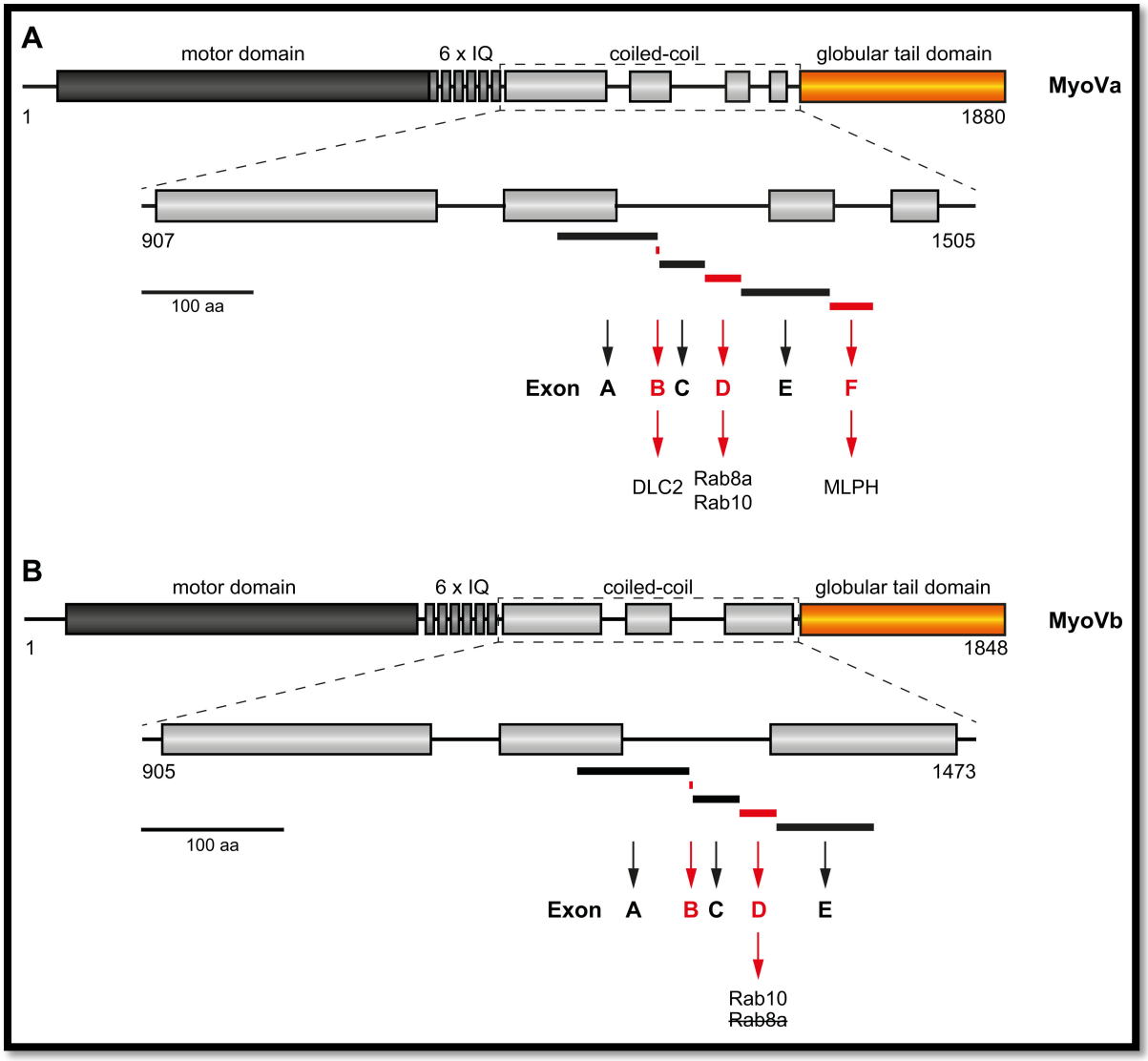

Figure 9 | Schematic representation of alternatively spliced exons of mammalian MyoVa and MyoVb proteins. Alternatively spliced exons are located within the coiled-coil regions of the MyoV-tail (exons A, B, C, D, E and F for MyoVa, and exons A, B, C, D and E for MyoVb). ***(A)*** Three exons are particularly subjected to alternative splicing in MyoVa: exons B, D and F (drawn in red). Exon B mediates interaction with dynein light chain 2 (DLC2). Exon D is essential for MyoVa interaction with Rab8a and Rab10. The melanocyte specific exon F is required for efficient interaction with melanophilin (MLPH). ***(B)*** Only two exons in particular undergo alternative splicing in MyoVb: exons B and D (drawn in red). A specific function for exon B has not been demonstrated so far. Exon D mediates MyoVb interaction with Rab10, similar to MyoVa, but, in contrast, inhibits its interaction with Rab8a, which binds to the same region in absence of exon D. There is no exon F present in MyoVb. Numbers on the protein domains indicate amino acids for mouse (Mm) MyoVa and human (Hs) MyoVb; *aa*, amino acids.

1.6 The Rab11 GTPase

Of special interest for this thesis is the Rab11 subfamily of Rab small GTPases. Rab11 proteins regulate exocytic and recycling processes following plasma membrane internalisation by clathrin-mediated endocytosis and subsequent recycling towards the cell surface (7, 196). Rab11 proteins localise to the trans-Golgi network (TGN) and post-Golgi vesicles to support secretory pathways (212), and to the pericentriolar recycling endosome, therefore participating in later recycling steps, but not in early endosomal recycling (*Figure 10*) (213, 214). As an example, Rab11 has been observed

to function in the establishment and maintenance of epithelial polarity being localised to the pericentriolar recycling compartments (215, 216). E-cadherin, a cell surface protein that mediates cell-cell contacts, continuously undergoes recycling, after internalisation from the cell surface, via recycling endosomes. The importance of Rab11 in the process of E-cadherin recycling has been described during all stages of epithelial polarity formation (217, 218). Furthermore, Rab11 has been implicated in the transport of several other cargoes, especially cell surface receptors and adhesion proteins, in different cell types. Some of those are the α-amino-3-hydroxy-5-methyl-4-isoxazolepropionic acid (AMPA) receptor in dendritic spines of neuronal cells, rhodopsin in photoreceptor cells, epidermal growth factor (EGF) receptor, Toll-like receptor 4 (TLR4), and other adhesion proteins besides cadherins, such as integrin receptors (219). Considering that, Rab11 is involved in multiple cellular functions depending on proper secretory vesicle transport which comprise, besides others, ciliogenesis, neuritogenesis, oogenesis, and the establishment and maintenance of epithelial polarity (*Figure 10*) (215, 217, 220–226). Furthermore, Rab11 drives endosomal membrane organisation, contributes to phagocytosis and is involved in cytokinesis (213, 227–229).

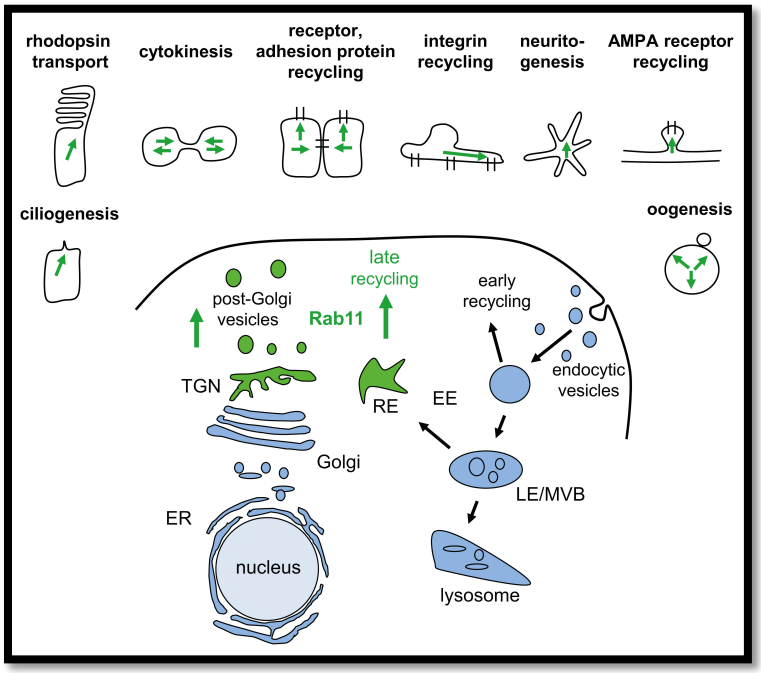

Figure 10 | Overview on Rab11 functions in intracellular transport and cellular processes. Rab11 small GTPases are localised to the trans-Golgi network, post-Golgi vesicles and the recycling endosome (green membrane compartments) to mediate secretory and recycling transport of diverse cargo towards the plasma membrane. A Rab11 function has been described for diverse cellular processes, including membrane receptor transport, such as rhodopsins in photoreceptor cells, adhesion proteins or AMPA receptor subunits in dendritic spines, ciliogenesis, cytokinesis, neuritogenesis and vesicle transport in metaphase oocytes required for proper oogenesis. Adapted from Welz, Wellbourne-Wood and Kerkhoff, 2014 (7).

In mammals, three Rab11 isoforms exist: Rab11a, Rab11b and Rab11c, which is also termed Rab25 (7). The overall sequence homology between the three isoforms is considerably high, but the tissue expression varies. Rab11a shows a wide expression pattern (7, 230), whereas the Rab11b expression is rather restricted to brain, testis and heart (231). Also the Rab11c expression shows a restricted pattern, with lung, kidney and gastric tract being the major expressing tissues (232). The Rab11

isoforms typically have two lipid modifications at their C-termini as they contain the CCxxx isoprenylation motif (see above). Both cysteine residues get geranylgeranylated to facilitate membrane association (135).

1.6.1 Regulation of Rab11 activity

Rab11 specific GTPase activating proteins (GAPs) belong to the TBC domain containing proteins. So far, three distinct Rab11 GAPs have been identified: TBC1D11, TBC1D15 and the ecotropic viral integration site 5 protein (Evi5) (233–235). Evi5 has been investigated in terms of *Drosophila* border cell migration during which the protein is critical to drive the Rab11 dependent localisation of receptor tyrosine kinases to the leading edge cell surface to initiate collective cell migration (236, 237). Furthermore, Evi5 negatively regulates the localisation of Rab11 to the centrosome (238). In contrast to Evi5, not much is known about the other two Rab11-GAPs, TBC1D11 and TBC1D15, and their role in regulating Rab11 dependent processes. Both GAPs are also not specific to Rab11 as they also regulate the activity of Rab7 and Rab4 (233, 235).

The knowledge about Rab11 specific guanine nucleotide exchange factors (GEFs) is by now very limited. In *Drosophila*, a Rab11-GEF has been identified recently: the calmodulin-binding protein related to a Rab3 GDP/GTP exchange protein (Crag) which interacts with Rab11 during light induced rhodopsin transport in photoreceptor cells (239). The Crag protein belongs to the DENN (differentially expressed in normal and neoplastic cells) domain proteins which have been shown to be able to activate human Rab proteins including Rab10 and Rab11, but not Rab5 (239, 240). Interestingly, the Rab-GEF activity of Crag is increased in presence of Ca^{2+} and calmodulin which opens the opportunity of Ca^{2+} regulated mechanisms for Rab11 activation and Rab11 dependent processes (239). Very recently, a novel Rab11-GEF has been identified in *Caenorhabditis elegans*, the RAB-11-interacting protein-1 (REI-1), which was proposed to regulate Rab11 activity in early *C. elegans* embryos (241). The human homolog of REI-1, SH3BP5, also showed a strong GEF activity for the human Rab11 protein. Before that, no mammalian Rab11-GEF has been undoubtedly identified. Intriguingly, the mammalian genome encodes for three homologs of the *Drosophila* Crag protein: DENND4A, DENND4B and DENND4C, which might point towards a conserved role for these proteins in Rab11 activation (7). The huntingtin protein has also been described to mediate Rab11 GEF activity (242, 243). Huntingtin colocalises with Rab11 at endosomal membranes and the Rab11 mediated recycling transport is impaired in cells from Huntington's disease patients and from Huntington's disease mouse models. A GEF activity for Rab11 has been demonstrated for co-precipitates from brain lysates, but a direct interaction of Rab11 and huntingtin has not been revealed. Thus, huntingtin might affect Rab11 activity rather as part of a protein complex containing a discrete Rab11-GEF than solely by itself.

1.6.2 Rab11 family-interacting proteins act as Rab11 specific adaptor proteins

Rab11 family-interacting proteins (Rab11-FIPs) resemble a well-characterised group of Rab11 interacting adaptor proteins (7, 244–247). Five members of Rab11-FIPs are known, Rab11-FIP1-5, separated into two classes, which all share a C-terminal Rab11-binding domain mediating a specific interaction with Rab11-GTP. Class I FIPs include Rab11-FIP1 (also termed *Rab coupling protein*; RCP), Rab11-FIP2 and Rab11-FIP5 (also termed *Rab11-interacting protein*; Rip11). Members of the class I FIPs contain an N-terminal C2 membrane binding motif which mediates phospholipid binding and potentially supports the membrane association of Rab11/effector protein complexes (244, 247). Class II FIPs include Rab11-FIP3 and Rab11-FIP4.

1.6.3 Rab11 motor protein complexes

Rab11 specifically recruits effector and adaptor proteins to vesicle surfaces to mediate their functionality. Motor proteins of the kinesin, dynein and myosin families have been repeatedly reported as being direct or indirect Rab11 effector proteins to mediate vesicle transport along microtubules (kinesins and dyneins) and F-actin tracks (myosins) and thus a number of Rab11 motor protein complexes have been described so far (*Figure 11*).

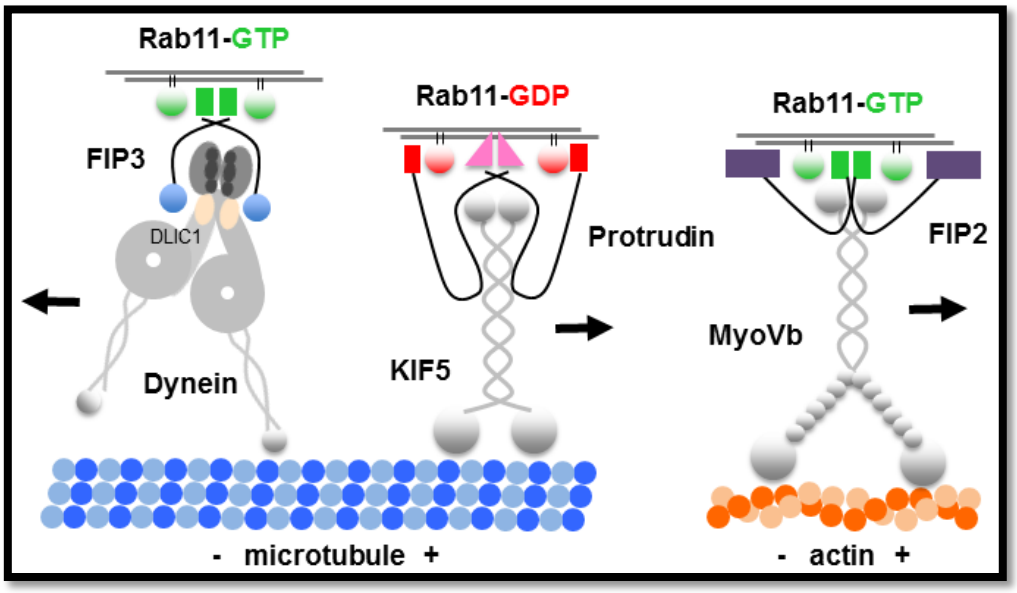

Figure 11 | Rab11 motor protein complexes. Rab11 directly and indirectly forms protein complexes with both microtubule and actin associated motor proteins depending on its activity state and distinct adaptor proteins. Rab11-GTP interacts via the Rab11 family-interacting protein Rab11-FIP3 with the microtubule minus end directed dynein motor. In contrast, Rab11-GDP interacts with the adaptor protein protrudin and the microtubule plus end directed kinesin motor KIF5 (kinesin-1). Interactions of Rab11-GTP with the actin motor protein myosin Vb (MyoVb) are either direct or indirect via the Rab11 family-interacting protein Rab11-FIP2 in order to drive plus end (barbed end) directed transport along F-actin tracks. Adapted and modified from Welz, Wellbourne-Wood and Kerkhoff, 2014 (7).

The first of those identified was the Rab11/myosin Vb complex (248) and also myosin Va has been described to interact directly with Rab11 (*Table 1*). By now, the crystal structures of both, the MyoVb-GTD:Rab11 complex (PDB ID: 4LX0) (210) and the MyoVa-GTD:Rab11 complex (PDB ID: 5JCZ) (211), have been solved. Long-term-potentiation (LTP) within neuronal networks is the activity dependent strengthening of synaptic connections, inducing synaptic plasticity important for learning and memory. As a molecular base for LTP establishment, GluA1 AMPA receptor subunits are delivered from the recycling endosome located at the spine base and dendritic shaft towards the plasma membrane and postsynaptic densities (249, 250). Rab11 and myosin Vb have been shown to interact in the transport of AMPA receptor subunit containing recycling endosomes towards the postsynaptic densities of hippocampal neurons (251). Myosin Vb is here actively recruited to the recycling endosome by Rab11 and the Rab11 family-interacting protein 2 (Rab11-FIP2). This complex is required to pull the recycling endosomal membranes from the spine base towards the postsynaptic densities along F-actin tracks, and thus for exocytic events within the dendritic spine. The whole process is strongly Ca^{2+} dependent. It has been suggested that increased Ca^{2+} concentrations following synaptic activity lead to the opening of the back-folded MyoVb motor and to a local reduction of the motors walking ability (see above) (252). This is thought to promote myosin Vb recruitment at the spine base, and the local rise in Ca^{2+} concentrations would subsequently allow myosin Vb to pull the recycling endosome into the spine heads. Myosin Va as well has been demonstrated to associate with Rab11 and GluA1 (55, 253). However, the existing data about the essential involvement and a potential underlying mechanism for myosin Va function in hippocampal synaptic plasticity diverges and needs to be further investigated (251, 253–255).

Rab11 and myosin Vb have been implicated in the transport of membrane vesicles towards the cortex of mouse metaphase oocytes by actin dependent long-range transport (222). These Rab11- and myosin Vb-positive vesicles directly modulate the density of the actin network which is crucial for the proper asymmetric spindle positioning in mouse oocytes (see below) (256).

As already mentioned, Rab11 is involved in the proper functioning of the *Drosophila* eye. Rab11 forms a tripartite complex with myosin V (Dm-MyoV) and the Rab11-interacting protein RIP11 to mediate the transport of rhodopsin containing post-Golgi secretory vesicles towards the developing rhabdomere membrane of photoreceptor cells (257).

The Rab11 and myosin Vb interaction is crucial for the apical constriction during *Xenopus* gastrulation. Furthermore, both proteins potentially mediate the trafficking of the planar cell polarity protein Vangl2 to the cell surface (258).

A complex formed by Rab11a, myosin Vb and Rab11-FIP2 at the endosomal recycling compartment and at vesicle docking and tethering sites participates in the transport of the C type lectin receptor

langerin being an important cell surface receptor of Langerhans cells within the epidermis, which undergoes continuous endocytosis and recycling (259).

By regulating the recycling transport of distinct kinases towards the apical surface of enterocytes, Rab11a and myosin Vb are crucial determinants for the proper development of microvilli required for the absorption of nutrients within the intestinal tract (260). Interference with either Rab11a or MyoVb, as it is the case in microvillus inclusion disease (already described earlier), leads to mis-regulated trafficking of kinases and reduced phosphorylation of ezrin, a member of the ezrin-radixin-moesin (ERM) family which are essential factors for the development and organisation of the apical plasma membrane and microvilli of epithelial cells (261–263).

MyoV protein (adaptor)	**Cell type**	**Function/Mechanism**
MyoVa	Hippocampal neurons	Hippocampal synaptic plasticity
MyoVb (FIP2)	Hippocampal neurons	Hippocampal synaptic plasticity; transport of AMPA receptor subunits from recycling endosomes to postsynaptic densities
MyoVb	Metaphase oocytes	Transport of vesicles towards oocyte cortex, asymmetric spindle positioning
MyoVb	*Xenopus* oocytes	Apical constriction; transport of Vangl2 towards the cell surface
MyoVb (FIP2)	Langerhans cells	Cell surface transport of langerin receptors
MyoVb	Intestinal tract (enterocytes)	Development of microvilli; apical transport of kinases, phosphorylation of ezrin
Dm-MyoV (RIP11)	*Drosophila* photoreceptor cells	Transport of rhodopsin containing secretory vesicles to rhabdomer membranes

Table 1 | Rab11 interactions with MyoV proteins.

Rab11 GTPases also functionally interact with microtubule associated motors of the dynein and kinesin families. Class II Rab11-FIP3 mediates the interaction between Rab11 and the microtubule minus end directed cytoplasmic dynein motors by forming a tripartite complex with the dynein light intermediate chains (DLIC-1 and DLIC-2) (264–266). A function of this complex has been proposed for transport processes from the peripheral sorting endosome to centrally located recycling endosome compartments (265), for instance for the transport of membrane containing vesicles towards the recycling endosome which are further delivered to the cleavage furrow during cytokinesis (267, 268). Rab11-FIP5 facilitates the formation of a complex containing Rab11 and the microtubule plus end directed kinesin family member kinesin-2 (also known as KIF3), which is involved in the regulation of

protein recycling at the perinuclear recycling endosome (269). Another Rab11-interacting protein, protrudin, mediates the interaction of Rab11 and kinesin-1a (also known as KIF5A) (13). This tripartite complex has been revealed to play a role in neuronal process formation (13, 270). Interestingly, and in contrast to what is found normally, the protrudin protein interacts with Rab11-GDP and not with Rab11-GTP. Its Rab11-GDP binding site is similar to that of the Rab11-GDP dissociation inhibitors Rab-GDIα and Rab-GDIβ and differs from other Rab11-binding domains (221, 271). This opens the possibility that the conversion of Rab11 from the GDP bound state to the GTP bound state could switch the direction of microtubule dependent transport (FIP3-dynein vs. protrudin-kinesin-1a) or between transport mechanism (microtubule vs. actin).

1.7 Myosin motors and actin nucleators and elongators cooperate at intracellular membranes

The actin cytoskeleton is involved in a wide range of cellular processes, such as the establishment and maintenance of cell shape and polarity, critical as the base for cell adhesion and cell motility, and intracellular transport, including endocytosis and exocytosis (272–275). Actin filaments, or filamentous actin (F-actin), comprise a right-handed double helical filament generated by the assembly of monomeric or globular actin (G-actin), which is polarised throughout the filament with a fast-growing *barbed end* (or *plus end*) and a *pointed end* (or *minus end*) (*Figure 12*) (276). Actin monomers bind and hydrolyse ATP. The ATPase activity of actin monomers mainly decides on the transition between G-actin and F-actin as ATP-actin preferably binds to the barbed end, ATP-hydrolysis occurs within the filament and ADP-actin is released from the pointed end. The depolymerisation from the filaments pointed end is enhanced by actin depolymerising factors (ADF)/cofilin proteins, which bind to ADP-actin rich regions of the filament and increase the actin monomer dissociation rate by filament severing (277–281). The whole process of actin polymerisation and depolymerisation is considered as the actin treadmilling.

The dynamics of actin networks needs to be tightly regulated. The well-controlled formation of new actin filaments from free actin monomers, filament stabilisation and crosslinking, but also the regulated capping and depolymerisation, as well as filament severing and actin monomer sequestering, is required to temporally and spatially coordinate actin network functions (276). The control of actin dynamics is thereby executed by a large and very diverse set of G- and F-actin binding proteins, as well as signalling and scaffolding proteins (272, 276).

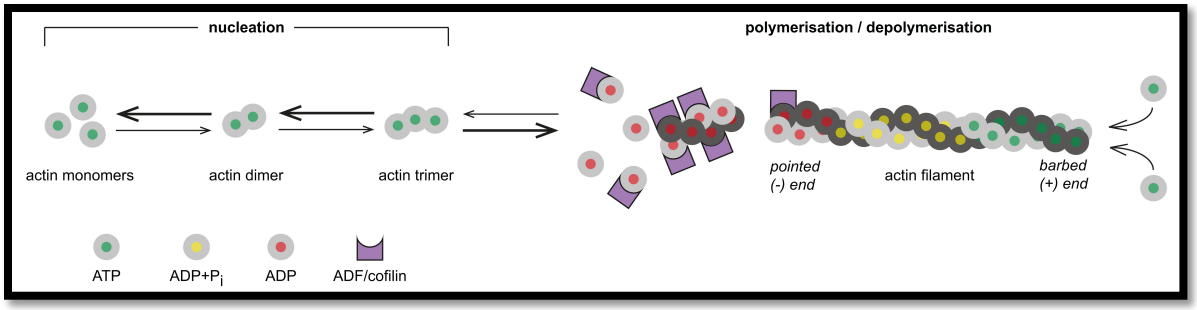

Figure 12 | Principles of actin nucleation, polymerisation and depolymerisation. Spontaneous actin polymerisation from free actin monomers is inhibited due to the high dissociation constants for small actin oligomers. After the formation of an actin nucleus, polymerisation of ATP-actin starts to form an actin-filament with barbed end (+) and pointed end (-). ATP hydrolysis takes place within the filament in a way that ATP-actin is found rather at the barbed end and ADP-actin at the pointed end. A treadmilling process occurs in which new ATP-actin binds to the barbed end and ADP-actin is released from the pointed end. ADF/cofilin binds to ADP-actin rich regions and induces filament severing to increase the depolymerisation rate.

1.7.1 Actin nucleation factors

Actin nucleation factors include proteins that bind actin monomers to form and stabilise an actin nucleus from which further actin polymerisation starts to generate new actin filaments. The cellular concentrations of actin monomers, being the most abundant proteins in most eukaryotic cells, range from 100-500 µM and are much higher than the critical concentrations for the addition of monomers to barbed end (0.1 µM) and pointed end (0.7 µM) (272, 276). In order to prevent exceeding spontaneous actin polymerisation, two mechanisms developed. First, a diverse set of actin monomer binding proteins exist, which reduce the pool of free actin monomers available for filament formation. Second, the formation of small actin oligomers, like dimers and trimers, required as a seed for filament elongation, is an energetically unfavourable process (276, 282). The function of actin nucleators warrants a very tight temporal and spatial regulation of F-actin generation as they help to overcome the kinetic barrier of oligomer formation when desired.

There are three major groups of actin nucleation factors (283). The Arp (actin-related protein) 2/3 complex is the best studied actin nucleator and is composed of seven subunits, including Arp2 and Arp3 and the Arp complex proteins ARPC1 to ARPC5 (284). The Arp2/3 complex binds to pre-existing filaments to generate branched actin networks, with an angle of 70° between two filaments, which have major contributions in determining cell shape and enabling cell migration (272, 285, 286). The complex by itself has only weak actin nucleation capacities (287). Thus, it requires the support by nucleation promoting factors (NPFs), including, besides others, the Wiskott-Aldrich syndrome protein (WASP) family and WASP-family verprolin homology (WAVE) family members (286, 288–291). NPFs are tightly regulated by diverse signalling mechanisms, for instance by the activity of Rho family GTPases, and act by recruiting one to three actin monomers to the Arp2/3 complex, and by inducing a conformational change of the complex (276, 292–296).

Formin proteins, as the second major group of actin nucleators, are large modular proteins which share the two formin-homology domains FH1 and FH2 (297). Formin proteins dimerise to form a dimeric ring of FH2 domains in which each FH2 binds two actin monomers to form the nucleus. The ring subsequently moves processively with the fast-growing barbed end to elongate the filament and prevent access of capping proteins (298–300). The FH1 domain is a proline rich region which is able to bind profilin-actin complexes, the main source of ATP-actin monomers in the cell (301). FH1 is suggested to enhance both, the nucleation and elongation activity of the FH2 domain by recruiting and pre-orienting the actin monomers towards the FH2 domains (299, 302–306).

The third major group of actin nucleation factors comprise the Wiskott-Aldrich syndrome protein homology 2 (WH2) domain containing actin nucleators. This group includes the Cordon-bleu protein (Cobl), Leiomodin (Lmod), the Junction-mediating and regulatory protein (JMY) and the Spir proteins which all have in common the presence of one or multiple WH2 domains used for actin binding and nucleation (307). Cobl is described as a vertebrate specific actin nucleator, with major expression in the brain, and contains three WH2 domains for highly efficient actin nucleation (307). A role for Cobl has been suggested in vertebrate axis formation (308) and midbrain neural tube closure (309), and proven in neuromorphogenesis by neurite induction and branching, related to Cobl mediated actin polymerisation and generation of unbranched actin filaments (310). Leiomodin is a heart, skeletal and smooth muscle related actin nucleator, with three so far identified isoforms that show strong actin nucleation activity to generate unbranched filaments (307, 311). JMY was added to that group recently and is considered as a transcriptional co-activator of the tumour suppressor p53. It is furthermore suggested to function both, as a NPF for the Arp2/3 complex and as an independent actin nucleator (312).

1.7.2 Spir actin nucleators

Spir proteins were first identified in *Drosophila* as the protein product of the *spire* gene and as a Jun N-terminal kinase (JNK)-interacting protein (313–315). Spir proteins have been identified only in metazoans (283, 316). Besides *Ciona savignyi* PEM-5 (posterior end mark-5) and *Drosophila* dSpir (p150-Spir), there are two *spir* genes in vertebrates: *spir-1* and *spir-2* (317). The respective gene products, Spir-1 and Spir-2 proteins, are highly similar with an identity of 37% and a similarity of 50% for the mouse proteins (283). It has been proposed first that Spir proteins act as nucleation promoting factors for the Arp2/3 complex due to their WH2 domains (314, 315). Subsequent experiments did not reveal any interaction of Spir proteins and Arp2/3, but rather showed that the WH2 domains of Spir are sufficient to nucleate actin polymerisation (318). It has been shown that Spir proteins not only function in actin nucleation but also in sequestering of actin monomers and severing of actin filaments (319–321).

Both, *spir-1* and *spir-2* genes are highly expressed in the central nervous system (322, 323). *In situ* hybridisations in mice demonstrated strong *spir-1* expression in the developing nervous system and in the adult brain (322) with highest expression levels observed in hippocampus, dentate gyrus and cerebellum, especially in Purkinje cells. The *spir-1* gene was also expressed in the thalamus, the lateral septal nucleus and the cerebral cortex (323). Similarly, *spir-2* is also strongly expressed in the murine central nervous system, both, during development and in adulthood (323). During embryogenesis, a high expression of *spir-2* was detected throughout the whole brain and in the spinal cord, as well as in the peripheral nervous system. Interesting to note is that the specific expression patterns of both *spir* genes during development indicate a high spatial regulation of *spir* gene expression. In early developmental stages both *spir* genes are differentially expressed and might therefore have distinct functions. However, in later stages of development a rather overlapping expression pattern was observed which indicates a redundant function of both genes during this developmental stage. In the adult mouse brain, *spir-2* expression was enriched in thalamus, inferior colliculus, cerebral cortex and in particular in the cerebellum (323). The *spir-2* gene is also expressed in the digestive tract within intestinal and colonic epithelial cells along villi and crypts, in the seminiferous tubules and spermatocytes of testis, and kidney (323).

The *spir* gene products are modular proteins containing multiple domains (*Figure 13*) (283). The N-terminal KIND (kinase non-catalytic C-lobe domain) resembles the organisation of a protein kinase C-lobe without catalytic kinase activity and developed into a protein interaction domain (316). KIND mediates the interaction with Formin (FMN) family formin proteins (324). A cluster of four WH2 domains binds actin monomers and is necessary and sufficient to nucleate actin polymerisation, potentially by forming a longitudinal tetrameric actin nucleus (318). At the C-terminal end of Spir proteins, the Spir-box and the FYVE-type zinc-finger are located. The specific function of the Spir-box is still not revealed. The short region is highly conserved across species and shares sequence homology to an α-helical region within the Rab3A effector protein rabphilin-3A mediating its interaction with Rab3A (325, 326). This opens the opportunity that the C-terminal Spir-box mediates the interaction of Spir proteins with Rab family GTPases, potentially Rab3A or the related Rab27a.
The FYVE-type zinc-finger (after Fab1, YOTB/ZK632.12, VAC1, EEA1; the proteins in which the domain was first discovered) at the very C-terminus mediates membrane targeting of Spir proteins to intracellular membranes (325, 327). The zinc-finger comprises eight cysteine residues which together bind two zinc ions (328, 329). Membrane association is enabled by the formation of a hydrophobic turret loop that penetrates the membrane (330, 331). In contrast to canonical FYVE domains, which can be found for instance in the Early Endosome Antigen 1 (EEA1) protein, the Spir FYVE-type zinc-finger binds rather non-specifically to negatively charged membranes in an phosphatidylinositol-3-

phosphate independent manner (327). Within the central Spir linker region, connecting the WH2 domains and the Spir-box, a highly conserved short sequence motif (globular tail domain binding motif, GTBM) was discovered, which will be of major interest in this thesis (see results).

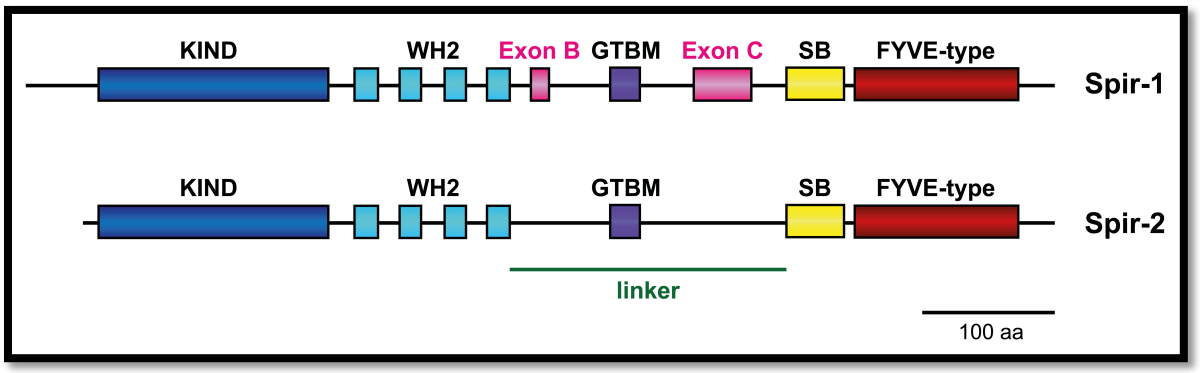

Figure 13 | Domain organisation of vertebrate Spir-1 and Spir-2 proteins. The N-terminal KIND (kinase non-catalytic C-lobe domain) mediates interaction with Formin (FMN) family formins and intramolecularly with the Spir-FYVE-type. A cluster of four Wiskott-Aldrich syndrome protein homology 2 (WH2) domains binds monomeric actin and serves actin filament nucleation. The central Spir linker region contains the newly identified globular tail domain binding motif (GTBM) for myosin V interaction (see results for more detail). Within the vertebrate Spir-1 proteins, two alternatively spliced exons, exon B and exon C, have been identified. The function of exon B is so far unknown and exon C mediates Spir-1 targeting to mitochondria membranes. The C-terminal Spir-box (SB) has yet unknown functions but is potentially involved in binding to distinct Rab GTPases. The FYVE-type zinc-finger (after Fab1, YOTB/ZK632.12, VAC1, EEA1) mediates targeting of Spir proteins to negatively charged intracellular membranes.

Although Spir proteins are capable to nucleate actin polymerisation *in vitro* due to their four WH2 domains, they are not able to bind and nucleate profilin-actin, the major source of monomeric actin in living cells, *in vivo* (285, 318, 332). The physical and functional interaction of Spir and FMN family formins is meanwhile well established, in which both proteins are suggested to form a heterotetrameric complex at intracellular membranes (317) and regulate each other's nucleation activity, thus being a highly efficient actin nucleator complex for profilin-actin (332, 333) (*Figure 14*). The Spir/FMN cooperativity has been demonstrated to be essential in oocyte development both, in mouse (FMN-2) (222, 334) and in *Drosophila* (335, 336). Spir and FMN-2 work together to generate a vesicle originating actin meshwork in metaphase mouse oocytes which is not formed by either of the two nucleators alone (222, 334). This mechanism is conserved as the *Drosophila* Spir protein (p150-Spir) also interacts with the *Drosophila* FMN family protein Cappuccino (Capu) to form an actin meshwork in fly oocytes (335, 336). Spir and FMN proteins interact directly by the Spir KIND domain and the evolutionary conserved formin/Spir interaction (FSI) sequence at the very C-terminus of FMN proteins which is stabilised by electrostatic interactions of a negatively charged acidic groove within the KIND domain and a positively charged basic cluster of the FMN-FSI sequence (324, 337, 338).

Very recently, an intramolecular interaction between the N-terminal KIND and the C-terminal FYVE domains was unravelled which prevents membrane association of Spir proteins. The KIND/FSI and KIND/FYVE interactions are competitive as FMN proteins can only interact with membrane bound

Spir proteins thereby releasing the KIND/FYVE interaction. Together with findings that Spir proteins are monomeric in the cytoplasm, a mechanism has been proposed in which Spir adopts an inactive, back-folded cytoplasmic state, next to an active, open and membrane bound state (*Figure 14*) (327).

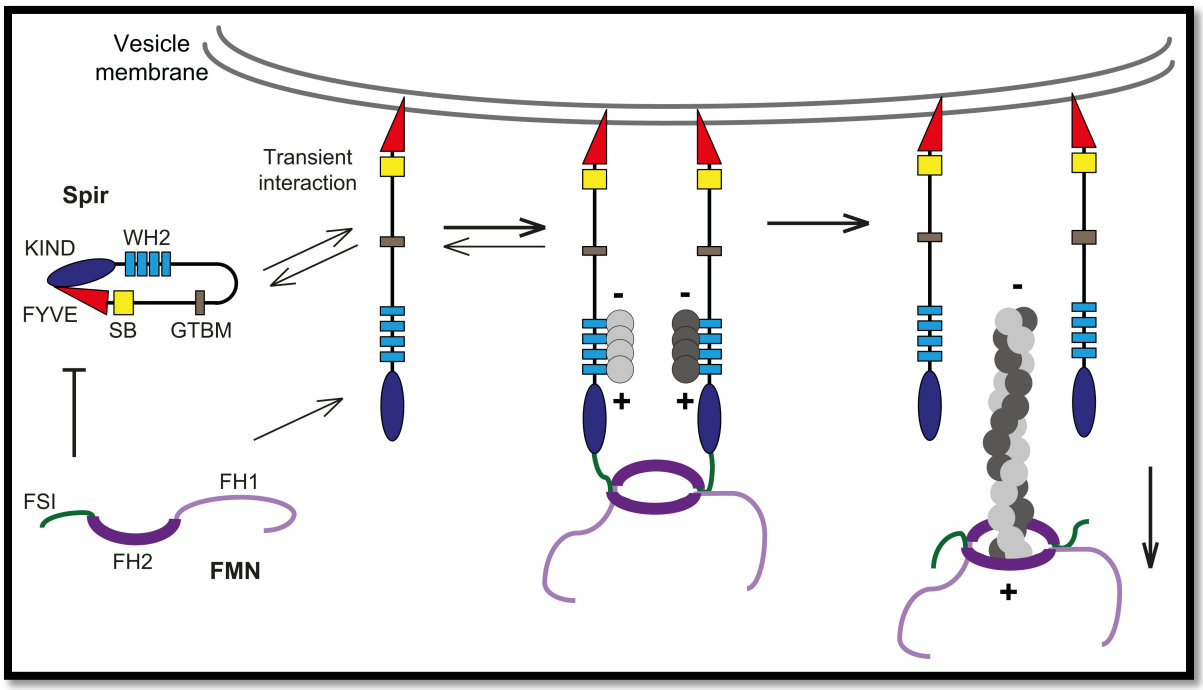

Figure 14 | Model for the Spir/FMN actin nucleator complex at vesicle membranes. Spir proteins are supposed to be back-folded in the cytoplasm via the recently discovered KIND/FYVE interaction. In this state, FMN family formins cannot bind to Spir proteins. Spir proteins transiently interact in a non-specific fashion with negatively charged intracellular membranes. At this state, FMN associates with Spir via the Spir-KIND/FMN-FSI interaction leading to the formation of a heterotetrameric Spir/FMN complex. The current model suggests that Spir nucleates actin monomers via its WH2 domains and passes over to FMN proteins which elongate the Spir nucleated filaments. FMN dissociates from Spir and processively moves with the growing barbed (+) end of actin filaments continuously inserting new actin monomers by its FH2 domains. *KIND*, kinase non-catalytic C-lobe domain; *WH2*, Wiskott-Aldrich syndrome protein homology 2; *GTBM*, globular tail domain binding motif; *SB*, Spir-box; *FYVE*, Fab1, YOTB/ZK632.12, VAC1, EEA1; *FSI*, formin/Spir interaction sequence; *FH*, formin homology. Only the C-terminal half of FMN proteins, including FH1, FH2 and FSI, is shown for better orientation.

Very recently, an alternatively spliced exon has been discovered in a more C-terminal part of the linker region of vertebrate Spir-1 proteins, which was termed e*xon C* (*Figure 13*) (339). This exon is 58 amino acids in length and highly conserved across vertebrates, although not present in zebrafish. Exon C mediates the association of Spire1C, as the protein was termed accordingly, to mitochondrial membranes. It has been observed that the mitochondrial Spire1C cooperates with the endoplasmatic reticulum (ER) localised inverted formin 2 (INF2) to polymerise actin filaments used to induce mitochondrial fission (*Figure 15*). Furthermore, the short alternatively spliced exon B has been identified close to the WH2 domains. So far, no specific functions could be related to that exon.

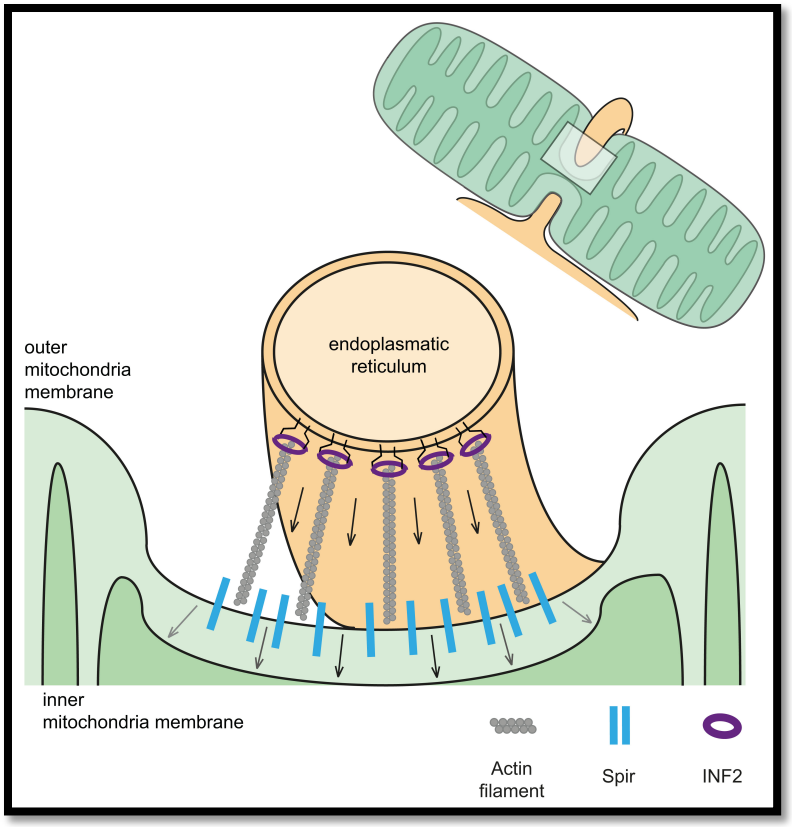

Figure 15 | Cooperation of Spire1C and INF2 in mitochondrial fission. Spire1C is located at the outer mitochondrial membrane, mediated by the alternatively spliced exon C, and physically interacts with the endoplasmatic reticulum associated inverted formin 2 (INF2) (339). The endoplasmatic reticulum wraps around the mitochondria and the Spire1C/INF2 mediated actin nucleation and polymerisation is suggested to generate pressure on the mitochondrial membranes in order to drive an initial membrane invagination (indicated by arrows). Subsequent recruitment of additional proteins is required to finally complete mitochondrial fission (339).

1.7.3 Cooperation of myosin motors and actin assembly factors in membrane trafficking

Within the last years growing evidence arose about the functional interconnection between intracellular cargo and their related receptors, motor proteins and actin assembly machineries to drive intracellular transport mechanisms (222, 334, 340–344).

A body of evidence exists, dealing with the interplay of actin nucleation and myosin motor activity in order to generate forces to drive membrane invagination during endocytic events (340–343). The mammalian class I myosin member myosin 1E (Myo1E) has been revealed to be recruited to sites of clathrin-mediated endocytosis in mammalian cells along with the Arp2/3 complex actin nucleator and its activators WIP/WIRE and N-WASP (340). This co-recruitment facilitates first, the internalisation of cargo as an actin dependent process and second, the subsequent transport of the internalised membrane vesicles to endosomal compartments. The whole process demands a very tightly regulated protein and co-factor recruitment in space and time, to efficiently drive membrane invagination, vesicle scission and trafficking towards target compartments. Similar mechanisms have been demonstrated before in single cell organisms including fission yeast (341), budding yeast (342) and *Dictyostelium* (343) in which class I myosins cooperate with the Arp2/3 complex in actin polymerisation to subsequently induce endocytic events. In fission yeast, the classical Arp2/3 complex activators Wsp1p and Vrp1p work together with Myo1p to activate Arp2/3 in order to generate branched actin filaments at sites of actin patch assembly as a prerequisite for endocytosis

(341). In budding yeast, the sequential recruitment of Las17p, Vrp1p, syndapin Bzz1p and class I myosin Myo5p to endocytic sites induces actin polymerisation, and motor activity of Myo5p is essential for the following endocytic internalisation (342). A study on *Dictyostelium* actin assembly mechanisms has shown the formation of a multimeric protein complex by the p116 protein which links the Arp2/3 complex to the class I myosins myosin IB (myoB) and myosin IC (myoC) (343). In the proposed model myosin I moves the Arp2/3 complex nucleator machinery along F-actin to reach specific locales.

Work in mouse metaphase oocytes provided insight into the cooperativity of actin nucleators, myosin motors and Rab GTPases (222, 334). As already described above, myosin Vb and Rab11 cooperate to transport membrane vesicles towards the oocyte cortex in a completely actin dependent fashion (222). More intriguingly, the actin filaments serving as transport tracks are generated directly at the vesicle surface forming a complex actin mesh throughout the oocyte by Spir/FMN-2 mediated actin nucleation. Myosin Vb moves along these newly generated actin filaments to deliver Rab11-positive vesicles to the oocyte cortex. The Spir/FMN generated actin meshwork and the Rab11-positive vesicles are essential for proper spindle positioning during meiosis (256) and for the centred positioning of the oocyte nucleus (344). Here, a model has been proposed in which myosin Vb drives the so called *active diffusion* of the oocytic actin-coated vesicles to generate forces sufficient to move the nucleus.

In collaboration with Edward Ziff and Seonil Kim (NYU Medical Center, New York, USA) the localisation of fluorescently labelled Spir-1 proteins in primary mouse hippocampal neurons has been unravelled to be mainly at the spine base (Edward Ziff and Seonil Kim, personal communication). As already mentioned, Wang and co-workers have shown that the recycling endosome, containing the GluA1 subunits of AMPA receptors is also located at the spine base. By Ca^{2+} regulated mechanisms, MyoVb and Rab11 cooperate to pull these endosomal membranes into the spine head to facilitate AMPA receptor insertion into the postsynaptic densities (251), potentially by the motor moving along actin tracks. Combining the Spir-1 localisation pattern and the endosome pulling mechanism, it is intriguing to speculate that the MyoVb/Rab11 dependent AMPA receptor subunit transport, leading to LTP induction and synaptic plasticity, might be coupled to Spir (and putatively FMN family members) regulated actin assembly.

1.7.4 Overlapping functions of Rab11 GTPases and Spir actin nucleators in exocytosis and recycling

The functional correlation of Spir actin nucleators and Rab11 small GTPases has been described already a decade ago (325). Spir proteins colocalise with Rab11 on membrane surfaces of the trans-Golgi network, post-Golgi vesicles and the recycling endosome, the major locales of Rab11 in eukaryotic cells (212–214). Furthermore, by experiments employing dominant-negative Spir protein fragments, the role of Spir proteins in exocytic and recycling transport of the vesicular stomatitis virus (VSV) G membrane protein in conjunction with Rab11 has been revealed (325). Besides the insights on Spir and Rab11 colocalisation and functional cooperation, a direct physical interaction of both proteins *in vitro* and *in vivo* has never been identified (Eugen Kerkhoff, personal communication).

1.8 Aim of the thesis

This thesis was aimed to obtain a deeper insight into the principles of intracellular vesicle transport processes and the underlying molecular mechanisms controlling regulated vesicle trafficking. The combined recruitment of myosin actin motor proteins and actin assembly factors to sites of active membrane transport seems to be a general mechanism conserved from single cell to higher order organisms. Based on published data on myosin V, Rab11, FMN and Spir cooperation in vesicle transport, a functional as well as physical interaction of the Spir actin nucleators and myosin V actin motors was investigated that might add to these observations and further support the principle of actin assembly protein/actin motor protein complex formation and its involvement in intracellular traffic.

Spir and Rab11 proteins are functionally correlated in exocytic and recycling vesicle transport processes (325). However, a direct interaction of both proteins has not been identified and, thus, it is still unknown how Spir proteins specifically target Rab11-positive vesicles in order to contribute to distinct Rab11 driven transport processes. A recent study investigating the membrane targeting of the Spir/FMN actin nucleator complex revealed that the FYVE-type zinc-finger of the Spir-2 protein targets negatively charged intracellular membranes in a rather non-specific fashion without dependence on PIP_3 (327). These findings exclude a solely Spir driven specific membrane targeting based on its membrane interaction capacities. It is intriguing to speculate that additional factors, such as other membrane associated proteins, might contribute to Spir targeting to Rab11 vesicles. Therefore, the role of myosin V actin motors as a linker between Spir and Rab11 *in vitro* and in living cells at vesicle surfaces was analysed.

Accordingly, the thesis was intended to first unravel if Spir actin nucleators and myosin V actin motor proteins interact physically with each other *in vitro* and in eukaryotic cells at vesicle surfaces by

means of co-immunoprecipitation studies, GST-pulldowns and fluorescence microscopy studies in HeLa cells. The Spir/MyoV interaction at vesicle surfaces was analysed at the molecular level by FLIM-FRET (fluorescence lifetime, Förster resonance energy transfer) microscopy. This part of the thesis was performed in collaboration with Dr. Thomas Weidemann (Max Planck Institute of Biochemistry, Martinsried, Germany). Subsequently, the interaction sites of both proteins were further characterised by means of mapping essential amino acids and by determining the crystal structure of the Spir:MyoVa complex. The crystallisation studies were performed in collaboration with Prof. Dr. Anne Houdusse and Dr. Olena Pylypenko (Institut Curie, Paris, France).

The membrane targeting of Spir and myosin V was determined with respect to a potential mutual targeting of both proteins towards vesicle surfaces and putative regulatory mechanisms in membrane targeting, given the back-folded character of both Spir and myosin V full-length proteins at the inactive, cytoplasmic state. As it has been shown that the Rab27a effector protein melanophilin is able to open up and activate myosin Va *in vitro* by binding to its globular tail domain, a similar mechanism could apply for Spir proteins.

For the final part of this thesis, the eventual formation of a tripartite Spir:MyoV:Rab11 complex at vesicle surfaces was investigated, deciding on vesicle identity and the generation of a distinct vesicle subpopulation. This complex would first allow for the functional Spir/Rab11 interaction in distinct intracellular transport processes in which the myosin V protein might act as a linker between Rab11 and Spir. Second, the formation of a complex containing vesicle membrane receptors, actin assembly machineries and actin dependent motors could point towards a general mechanism used for trafficking of vesicles which require *de novo* generation of actin filaments.

2 Materials and methods

2.1 Multiple sequence alignments of Spir protein sequences

Multiple sequence alignments for GTBM and linker region of chosen Spir-1 and Spir-2 amino acid sequences were performed using the *Clustal Omega Multiple Sequence Alignment* tool (EMBL-EBI, Hinxton, UK) with manual confinements for the GTBM alignments. Calculations of protein sequence identities and similarities of Spir-linker and Spir-GTBM were done using the UniProt *Align* tool (UniProt Consortium). Respective cDNA sequences were obtained from the NCBI Gene database with the following accession numbers: Hs-Spir-1: NM_001128626.1, Hs-Spir-2: AJ422077, Mm-Spir-1: working sequence of the Kerkhoff Lab, Mm-Spir-2: AJ459115, Gg-Spir-1: XM_419119.4, Gg-Spir-2: XM_004944321.1, Xt-Spir-1: XM_012965027.1, Xt-Spir-2: XM_004913632.2, Br-Spir-1: NM_001044847.2, Br-Spir-2: NM_001007342.2. WebLogos (345) were generated from respective parts of the alignment of 223 Spir sequences and 44 MLPH sequences after reducing redundancy with CDhit (346), applying a 90% sequence similarity cut-off (in collaboration with Dr. Martin Kollmar, Max Planck Institute for Biophysical Chemistry, Göttingen, Germany).

2.2 Agarose gel electrophoresis

In order to separate PCR amplified DNA fragments and digested vectors and DNA inserts, PCR or restriction digest samples were mixed with 6x DNA loading dye and separated by agarose gel electrophoresis. Ultrapure agarose (ThermoFisher, Waltham, MA, USA) was solved in 0.5x TBE buffer by heating and shaking. Depending on the expected fragment size, agarose gels were used with suitable concentrations (in the range between 1% and 2.5%). Gel electrophoresis was usually performed at 120 V for 30 min in 0.5x TBE buffer.

2.3 Agarose gel clean-up

PCR amplified DNA fragments and digested vectors and DNA inserts were extracted from agarose gels for further processing. The DNA extraction was performed using the NucleoSpin Gel and PCR Clean-up kit (Macherey-Nagel, Düren, Germany). Respective bands in the gel were cut out and the gel slices were transferred into an Eppendorf tube. The slice was weighted and the double amount (mg to µl) of Binding Buffer (NTI) was added and subsequently incubated at 54°C to dissolve the gel completely. The solution was applied to a spin column containing a DNA binding membrane and centrifuged at 11,000 x *g*, 1 min, RT. The column was washed with 600 µl Wash Buffer (NT3) at 11,000 x *g*, 1 min, RT. The membrane was dried by centrifugation at 11,000 x *g*, 2 min, RT. Bound

DNA was eluted in 30 µl Elution Buffer (EB) by incubating for 1 min and subsequent centrifugation at 11,000 x *g*, 1 min, RT.

2.4 Measurement of DNA and RNA concentrations

The concentration of plasmid DNA, PCR amplified DNA fragments, isolated RNA as well as reverse transcribed cDNA was measured by spectrophotometric analysis using the GeneQuant photometer (GE Healthcare Life Sciences, Freiburg, Germany). The DNA was diluted 1:200 in autoclaved H_2O (1:40 for RNA preparations) and transferred into an opaque cuvette. The absorption of ultraviolet light (λ = 260 nm) by the DNA is measured and the concentration is calculated accordingly. The contamination of the DNA sample was estimated by concurrent measurement of sample absorption at 280 nm, since proteins absorb light at 280 nm. The ratio of absorbance at 260 nm and 280 nm ($A_{260/280}$) is calculated. An $A_{260/280}$ ratio around 1.8 is considered as indicating 100% DNA (2.0 for RNA).

2.5 PCR techniques

2.5.1 Amplification of cDNA fragments for cloning

DNA fragment amplification for cloning was performed using AccuPrime Pfx DNA Polymerase (ThermoFisher) employing 50 ng template DNA (plasmid DNA) (*Table 2*). The elongation time for DNA synthesis (t_E) was adjusted to the length of the amplified fragment (60 sec per 1000 bp). The primer annealing temperature (T_A) was usually set 5°C lower than the primers melting temperature. DMSO (5% to 10%) was added when using primers with high melting temperatures. Primers were designed manually, including restriction site overhangs, and ordered at Sigma-Aldrich (Taufkirchen, Germany) as lyophylised oligonucleotides. Very long primers or primers with high tendency to form secondary structures were purified by HPLC. An overview of all primers used in this thesis is provided in the supplements.

Reagents	Volume
Template DNA	50 ng
Primer 5' (10 µM)	3 µl
Primer 3' (10 µM)	3 µl
10x Pfx buffer	5 µl
Pfx DNA Polymerase	1 µl
DMSO (optional)	5% - 10%
H_20	fill up to 50 µl
Total volume	*50 µl*

Temperature	Time
95°C	5 min
95°C	1 min
T_A	30 sec
68°C	t_E
68°C	5 min
4°C	hold

Table 2 | Protocol and cycling parameters for DNA fragment amplification by Pfx DNA Polymerase.
T_A = 5°C less than primers melting temperature t_E = 60 sec for 1000 bp

2.5.2 Colony PCR from bacterial colonies

Colony PCR was performed to quickly check for positive bacterial colonies following transformation with newly generated plasmid DNA by using Taq DNA Polymerase with Standard Taq Buffer (New England Biolabs (NEB), Frankfurt am Main, Germany) (*Table 3*). Single colonies were picked and resuspended in 50 µl autoclaved H_2O. The mixture was heated to 95°C for 10 min and centrifuged at 16,000 x *g* for 5 min. 5 µl of the supernatant was used as template DNA. The respective cloning primers were used in order to obtain DNA bands with a specific length in agarose gel electrophoresis.

Reagent	**Volume**
Bacterial supernatant	5 µl
dNTP mix (25 mM each)	0.2 µl
Primer 5' (10 µM)	0.4 µl
Primer 3' (10 µM)	0.4 µl
10x Taq buffer	2 µl
Taq DNA Polymerase	0.2 µl
H_2O	11.8 µl
Total volume	*20 µl*

Temperature	**Time**
94°C	3 min
94°C	40 sec
T_A	40 sec
72°C	t_E
72°C	5 min
4°C	hold

Table 3 | Protocol and cycling parameters for Colony PCR using Taq DNA Polymerase.
T_A = 5°C less than primers melting temperature t_E = 60 sec for 1000 bp

2.5.3 QuikChange PCR for site-directed mutagenesis

To introduce mutations (changes in the nucleotide sequence) into existing plasmid DNAs, QuikChange PCR was performed using the QuikChange Site-Directed Mutagenesis Kit (Agilent Technologies (former Stratagene), Santa Clara, CA, USA) and Pfu DNA polymerase (Promega, Mannheim, Germany) (*Table 4*). Primers were designed manually, including the desired mutations in the middle of the primers, and ordered at Sigma-Aldrich (Taufkirchen, Germany) as lyophylised oligonucleotides. Usually, these primers were purified by HPLC. An overview of primers used in this thesis is provided in the supplements. For each reaction 50 ng of template plasmid DNA was applied.

Reagent	Volume
Plasmid DNA	50 ng
dNTP mix (25 mM each)	1 µl
Primer 5' (10 µM)	125 ng
Primer 3' (10 µM)	125 ng
10x Pfu buffer	5 µl
Pfu DNA Polymerase	1.5 µl
DMSO (optional)	5% - 10%
H_2O	fill up to 50 µl
Total volume	*50 µl*

	Cycles	Temperature	Time
1	1	95°C	30 sec
2	20	95°C	30 sec
		55°C	1 min
		68°C	t_E

Table 4 | Protocol and cycling parameters for QuikChange PCR with Pfu DNA Polymerase.
T_A = 55°C t_E = 120 sec for 1000 bp

To destroy the residual template plasmid DNA, 1 µl *Dpn*I endonuclease (NEB) was applied to each PCR reaction and incubated for 1 h at 37°C. *Dpn*I specifically cleaves methylated and hemi-methylated DNA (target sequence: 5'-Gm^{6}ATC-3'), therefore only targeting the parental, methylated, DNA and not the newly synthesised, non-methylated DNA. Finally, NEB10-beta Competent *E. coli* cells were transformed according to the standard transformation protocol (see below).

2.5.4 One-Step RT-PCR from RNA preparations

One-Step RT-PCR was performed using the QIAGEN One-Step RT-PCR Kit to amplify a corresponding cDNA fragment for cloning from template mRNA in a one-step reaction (*Table 5*). 200 ng RNA from mouse cerebellum preparations were used as template. Primers were designed manually, including restriction site overhangs, and ordered at Sigma-Aldrich as lyophylised oligonucleotides. An overview of primers used in this thesis is provided in the supplements.

Reagent	Volume
Template RNA	0.2 µg
5x RT-PCR buffer	10 µl
dNTP mix (10 mM each)	2 µl
Primer 5' (10 µM)	3 µl
Primer 3' (10 µM)	3 µl
RT-PCR Enzyme Mix	2 µl
RNase-free H_2O	fill up to 50 µl
Total volume	*50 µl*

Temperature	Time
50°C	30 min
95°C	15 min
94°C	30 sec
T_A	1 min
72°C	t_E
72°C	10 min
4°C	hold

Table 5 | Protocol and cycling parameters for One-Step RT-PCR from RNA.
T_A = 5°C less than primers melting temperature t_E = 60 sec for 1000 bp

2.6 Cloning

2.6.1 Restriction digest

For restriction digests, 2 µg plasmid DNA were incubated with restriction endonucleases (NEB) in the appropriate buffer for 2-5 h at 37°C (*Table 6, 7*). 1 µl CIP (Alkaline Phosphatase, Calf Intestinal; NEB) was added both, 1 h and 30 min before the desired ending. CIP removes phosphate groups at the 5' ends of the DNA and thus prevents re-ligation of the vector. Controls were used to check for proper digestion: undigested vector and the vector digested with only one of the two enzymes. For the digest of PCR amplified DNA fragments used as inserts, usually 7 µl of the gel extracted DNA was used. Following restriction digest, vector and inserts were separated by agarose gel electrophoresis and subsequently purified from gel for further processing.

Reagent	Volume			
	Undigested	Enzyme 1	Enzyme 2	Double digest
Plasmid DNA	0.5 µg	0.5 µg	0.5 µg	2 µg
Enzyme 1	-	Enzyme dependent	Enzyme dependent	Enzyme dependent
Enzyme 2	-	Enzyme dependent	Enzyme dependent	Enzyme dependent
10x NEBuffer	3 µl	3 µl	3 µl	3 µl
H_2O	up to 30 µl	up to 30 µl	up to 30 µl	up to 30 µl
Total volume	*30 µl*	*30 µl*	*30 µl*	*30 µl*

Table 6 | Protocol for vector digest. Enzyme: 2 µl for 5,000 U/ml, 1 µl for 10,000 U/ml, 0.5 µl for 20,000 U/ml.

Reagent	Volume
Linear DNA insert	7 µl
Enzyme 1	Enzyme dependent
Enzyme 2	Enzyme dependent
10x NEBuffer	3 µl
H_2O	fill up to 30 µl
Total volume	*30 µl*

Table 7 | Protocol for insert digest. Enzyme: 2 µl for 5,000 U/ml, 1 µl for 10,000 U/ml, 0.5 µl for 20,000 U/ml.

2.6.2 Ligation

In order to combine digested vectors and DNA fragment inserts, a ligation was performed using T4 DNA Ligase (NEB) at 16°C oN (alternatively for 1h, RT) (*Table 8*).

Reagent	Volume
Digested vector	1-2 µl
Digested insert	3-7 µl
10x T4-Ligase buffer	2 µl
T4 DNA Ligase	1 µl
H_2O	fill up to 20 µl
Total volume	*20 µl*

Table 8 | Protocol for ligation of digested vectors and inserts.

Following ligation, NEB10-beta Competent *E. coli* cells were transformed according to the standard transformation protocol (see below).

2.6.3 Transformation of *Escherichia coli* bacterial cells

The following chemo-competent *E.coli* strains were used for transformations: *E.coli* Rosetta(DE3)pLysS (F– *ompT hsdS*$_B$(r_B^- m_B^-) *gal dcm* (DE3) pLysSRARE^2 (Cam^R)) and *E.coli* Rosetta (F– *ompT hsdS*$_B$(r_B^- m_B^-) *gal dcm* pRARE^2 *(*Cam^R)) were used for bacterial expression vectors, and NEB10-beta Competent *E. coli* (Δ*(ara-leu) 7697 araD139 fhuA ΔlacX74 galK16 galE15 e14- φ80dlacZΔM15 recA1 relA1 endA1 nupG rpsL* (Str^R) *rph spoT1 Δ(mrr-hsdRMS-mcrBC)*; NEB) for cloning and plasmid DNA production and subsequent purification. Bacterial cells were thawed on ice. The complete ligation mixture (or 1 µl of existing plasmid DNA for re-transformations) was added to the cell suspension (100 µl) and incubated on ice for 1 h. A heat shock (42°C, 55 sec) followed to induce plasmid uptake. After a 2-min incubation on ice, 900 µl LB_0 medium was added to the bacteria and incubated for at least 1 h at 37°C while shaking. Bacteria were pelleted for 10 min at 4,600 x *g*, RT and 800 µl of the supernatant was removed. Bacterial cells were resuspended in the remaining supernatant and bacteria were plated and cultured on respective agar selection plates oN at 37°C.

2.6.4 Plasmid DNA extraction and purification from bacterial cells

Following successful vector generation and transformation of *E. coli* cells, single colonies were picked and incubated in LB medium, containing respective antibiotics, and incubated at 37°C, oN, while shaking in order to produce sufficient amounts of plasmid DNA. On the next day, plasmid DNA was extracted and purified from the bacterial cells for further processing, including control of vector correctness, sequencing and long-term storage. Plasmid DNA extraction from bacterial cells was performed either as Plasmid-Mini-Purification (MiniPrep) for control digests, Plasmid-Mini-Purification (MiniPrep) for sequencing, or Plasmid-Maxi-Purification (MaxiPrep). The QiaPrep Spin Miniprep Kit (Qiagen, Hilden, Germany) was used for MiniPrep and the Qiagen Plasmid Maxi Kit (Qiagen) was used for MaxiPrep.

2.6.5 Plasmid-Mini-Purification (MiniPrep) for control digests

Bacterial colonies were inoculated in 1.5 ml LB with respective antibiotics and incubated at 37°C, oN, while shaking. Cells were pelleted at 16,000 x *g*, 1 min and resuspended in 250 µl Resuspension Buffer P1 (QiaPrep Spin Miniprep Kit). 250 µl Lysis Buffer P2 was added and mixed gently. LyseBlue was added to the Resuspension Buffer so that now the cell solution turns blue which marks the right lysis conditions. Lysis was done for 5 min at RT. Afterwards, 250 µl Neutralisation Buffer P3 was added and mixed gently to turn the solution white. The solution was centrifuged at 16,000 x *g*, 5 min, RT to get rid of cell debris. 500 µl of the supernatant was added to 1 ml EtOH (100%) and incubated for 5 min at RT to precipitate the DNA. The solution was centrifuged at 16,000 x *g*, 10 min, RT. The DNA pellet was washed with 500 µl EtOH (70%) and centrifuged at 16,000 x *g*, 10 min, RT. Finally, the

supernatant was removed carefully, the DNA pellet was dried at 52°C and resuspended in 100 µl autoclaved H_2O for further processing, including control digest to check for successful DNA fragment insertion.

2.6.6 Plasmid-Mini-Purification (MiniPrep) for sequencing

Bacterial colonies were inoculated in 10 ml LB with respective antibiotics and incubated at 37°C, oN, while shaking. Cells were pelleted at 4,600 x *g*, 10 min, RT and resuspended in 250 µl Resuspension Buffer P1 (QiaPrep Spin Miniprep Kit). 250 µl Lysis Buffer P2 was added and mixed gently. LyseBlue was added to the Resuspension Buffer so that now the cell solution turns blue which marks the right lysis conditions. Lysis was done for 5 min at RT. Afterwards, 350 µl Neutralisation Buffer N3 was added and mixed gently to turn the solution white. The solution was centrifuged at 16,000 x *g*, 10 min, RT to get rid of cell debris. The supernatant was applied to a QIAprep spin column and centrifuged at 16,000 x *g*, 1 min, RT. The column was washed with 500 µl Binding Buffer PB and centrifuged at 16,000 x *g*, 1 min, RT. The column was again washed with 750 µl Wash Buffer PE and centrifuged at 16,000 x *g*, 1 min, RT. The membrane was dried by centrifugation at 16,000 x *g*, 2 min, RT. Bound DNA was eluted with 50 µl Elution Buffer EB by a 1-min incubation and centrifugation at 16,000 x *g*, 1 min, RT. The purified plasmid DNA is now ready for further processing, including sequencing and subsequent cloning steps.

2.6.7 Plasmid-Maxi-Purification

Bacterial colonies were inoculated in 100 ml LB with respective antibiotics and incubated at 37°C, oN, while shaking. Cells were pelleted at 4,600 x *g*, 15 min, 4°C and resuspended in 10 ml Resuspension Buffer P1 (Qiagen Plasmid Maxi Kit). 10 ml Lysis Buffer P2 was added and mixed gently. LyseBlue was added to the Resuspension Buffer so that now the cell solution turns blue which marks the right lysis conditions. Lysis was done for 5 min at RT. Afterwards, 10 ml Neutralisation Buffer P3 was added, mixed gently to turn the solution white and incubated on ice for 10 min. The solution was centrifuged at 4,600 x *g*, 10 min, 4°C. Meanwhile, a Qiagen column was equilibrated with 10 ml Buffer QBT by gravity flow. The centrifugal supernatant was poured into the column using a filter paper to pick up cell debris and allowed to enter the column by gravity flow. The column was washed two times, 30 ml each, with Wash Buffer QC. Bound DNA was eluted in 15 ml Elution Buffer QF into a clean 50 ml Falcon tube. DNA was precipitated using 10.5 ml isopropanol (100%) and centrifuged at 4,600 x *g*, 30 min, 4°C. The DNA pellet was washed with 5 ml ethanol (70%) and centrifuged at 4,600 x *g*, 10 min, 4°C. The supernatant was carefully removed and the DNA pellet was dried at 50°C. The pellet was finally resuspended in 300 µl Tris-EDTA, pH 8.0 for long-term storage and was now ready for further processing, including transfections of eukaryotic cells.

2.6.8 Control digests

Control digests were performed to check newly generated and isolated plasmid DNA for successful DNA fragment insertion. First, plasmid DNA was extracted and purified from bacterial colonies, and subsequently incubated with respective restriction endonucleases to obtain specific DNA bands on agarose gels. A master mix containing buffer, restriction endonucleases and H_2O was prepared (*Table 9*). 10 µl of plasmid DNA was incubated with 10 µl of the master mix for 2 h at 37°C. The presence of specific DNA bands was subsequently checked by agarose gel electrophoresis.

Reagent	Volume
Plasmid DNA	10 µl
10x NEBuffer	2 µl
Enzyme 1	Enzyme dependent
Enzyme 2	Enzyme dependent
H_2O	fill up to 20 µl
Total volume	*20 µl*

Table 9 | Protocol for control digests. Enzyme: 2 µl for 5,000 U/ml, 1 µl for 10,000 U/ml, 0.5 µl for 20,000 U/ml.

2.6.9 DNA Sequencing

In order to verify DNA sequence correctness of newly generated plasmid DNA, the sequence was checked by a commercially available sequencing service (LGC Genomics, Berlin, Germany). Plasmid DNA was diluted to a concentration of 100 ng/µl with autoclaved H_2O. Primers used for sequencing were either provided by the company, or own cloning primers or specifically synthesised sequencing primers were employed. Sequence correctness was verified by nucleotide sequence alignments (Nucleotide BLAST; NCBI) with the respective target cDNA sequence, and the correct reading frame throughout the desired sequence was analysed using Serial Cloner.

2.7 Cell culture techniques

HEK293 (human embryonic kidney) cells (ATCC, Manassas, Virginia, USA) and HeLa (human cervix carcinoma) cells (ATCC) were cultured in Dulbecco's Modified Eagle's Medium (DMEM; ThermoFisher) supplemented with 10% fetal calf serum (FCSIII; GE Healthcare Life Sciences, HyClone), 2 mM L-Glutamine (ThermoFisher), penicillin (100 units/ml; ThermoFisher) and streptomycin (100 µg/ml; ThermoFisher) (from now on referred to as *Full Medium*) at 37°C, 5% CO_2, 95% humidity and were passaged regularly at 80% confluency. For passaging, old medium was removed and cells were washed once with 1x PBS to get rid of residual serum. Cells were detached using Trypsin-EDTA solution (0.05%; ThermoFisher) for 2-5 min (until detachment) at RT. Trypsin-

EDTA was inactivated by adding Full Medium. A fraction of the cell suspension was then transferred into a new culture dish containing fresh medium, generally at a ratio of 1:5 for HeLa cells and 1:10 for HEK293 cells.

2.7.1 Thawing cells

Eukaryotic cells are kept in liquid nitrogen for long-term storage. A frozen stock was thawed rapidly at 37°C in a water bath and the cells were transferred into a 50 ml Falcon tube containing 15 ml Full Medium. The cell suspension was centrifuged at 800 x *g*, 6 min, RT. The supernatant was removed and cells were resuspended in 1 ml pre-warmed Full Medium. The cell suspension was finally transferred into a 10 cm dish (Greiner Bio-One, Frickenhausen, Germany) containing 9 ml pre-warmed Full Medium. Cells were cultured at 37°C, 5% CO_2.

2.7.2 Freezing cells

For long-term storage, cells were kept in liquid nitrogen. A specific *Freezing Medium* was prepared consisting of DMEM supplemented with 20% FCSIII, 2 mM L-Glutamine, penicillin (100 units/ml), streptomycin (100 µg/ml) and 10% DMSO. DMSO and FSCIII act as cyroprotective agents preventing the formation of ice crystals inside the cell. Eight 10 cm dishes with cells at approximately 80% confluency were normally used for one freezing procedure. The old medium was removed, cells were washed with 1x PBS and detached with Trypsin-EDTA as described above. Full medium was added to inactivate Trypsin-EDTA and the cell suspension was transferred into 5 ml Freezing Medium. After centrifugation at 800 x *g*, 6 min, RT the supernatant was removed and the cells were resuspended in 18 ml Freezing Medium. 1 ml aliquots were transferred into cryovials (ThermoFisher, Nunc). Vials were stored in a cryo-box filled with isopropanol at -80°C, oN, to allow slow freezing (-1°C per minute). The slow freezing induces cell shrinkage due to loss of water and prevents formation of ice crystals inside the cell which would cause damage. On the next day, cryovials containing the cells were transferred into liquid nitrogen for long-term storage.

2.7.3 Poly-L-Lysine coating of 6-well plates

Prior to seeding HEK293 cells for transfections in 6-well plastic plates, the wells need to be coated with Poly-L-Lysine to prevent cell loss during multiple washing steps because of the weak HEK293 cell adhesion capacity. Poly-L-Lysine (Sigma-Aldrich) was diluted 1:10 in sterile H_2O (Sigma-Aldrich). 1 ml of this dilution was added per well and shortly incubated. Wells were washed once with 1x PBS to get rid of residual solution and allowed to dry with a slightly open lid. Subsequently, cell seeding was perfomed as described.

2.7.4 Seeding cells

Cells were seeded on 6-well plates, WillCo dishes or microscope cover glasses in the respective densities prior to transfections. To seed cells, old medium was removed, cells were washed with 1x PBS and detached with Trypsin-EDTA as described above. Full Medium was added to inactivate Trypsin-EDTA, cells were transferred into a Falcon tube and centrifuged at 800 x *g*, 6 min, RT. The supernatant was removed and cells were resuspended in an appropriate volume of Full Medium, according to the expected cell number. 10 µl of the cell suspension was mixed with 10 µl Trypan Blue solution (0.4%; Sigma-Aldrich) to distinguish between viable and dead cells. Only the white, living cells were counted in a Neubauer counting chamber, considering all four major squares and calculating the mean ($\bar{X}$). One major square, consisting of 4×4 minor squares, is $1\ mm$ in length and $1\ mm$ in width. The distance between cover glass and counting chamber is $0.1\ mm$. Considering this, the counted cell number is in a volume of $1 \times 1 \times 0.1\ mm = 0.1\ mm^3 = 0.1\ \mu l$. To equal the dilution by Trypan Blue, the cell concentration is multiplied with 2. To normalise the concentration to ml volumes, the concentration is multiplied with 10^4 to get the number of cells per ml.

$$\bar{X} \times 2 \times 10^4 = cell\ concentration\ [\frac{cells}{ml}]$$

The volume of the cell suspension required to get the desired cell number was calculated as follows:

$$\frac{desired\ number\ of\ cells\ [cells]}{cell\ concentration\ [\frac{cells}{ml}]} = Y\ ml\ of\ cell\ suspension$$

The appropriate volume of the cell suspension was transferred into the respective culture plate or dish which was already filled with Full Medium. Seeded cells were allowed to attach over night at 37°C, 5% CO_2.

2.7.5 Transfection of eukaryotic cells using Lipofectamine Reagent

One day prior to transfection HEK293 and HeLa cells were seeded on 6-well plates, WillCo dishes or microscope cover glasses at densities as described individually for each experiment. Plasmid DNA was diluted in DMEM without supplements (DMEM w/s) to obtain a concentration of 0.1 µg/µl (e.g. 5 µg in 50 µl). 6 µL of Lipofectamine Reagent (ThermoFisher) was mixed with 100 µL DMEM w/s (per sample) and incubated for 5 min at RT. Per sample, 100 µl of the Lipofectamine dilution and 0.5 to 1.5 µg plasmid DNA (depending on the expected expression levels of the protein and on the number of transfected plamids per sample) were mixed and filled up with DMEM (w/s) to 200 µl. The mixture was incubated for 25-30 min at RT. Meanwhile, seeded cells were washed two times with DMEM w/s

to get rid of any residual serum that would disturb transfections. After the incubation time, 800 µl DMEM w/s was added to the transfection mixture and the whole solution (1 ml) was transferred to the cells. Transfections incubated for 4-5 hours at 37°C, 5% CO_2. Finally, the transfection solution was removed and fresh Full Medium was added. Cells were incubated at 37°C, 5% CO_2 for at least 24 hours to allow efficient protein production.

2.8 Protein work

2.8.1 SDS-PAGE

Protein preparations were mixed with SDS protein sample buffer (Laemmli buffer) and denatured at 95°C for 10 min. Proteins were separated on SDS gels with respective concentrations (depending on the molecular weight of the proteins to be separated, between 7.5% and 15%) at 50 mA per gel in 1x SDS-PAGE buffer. To obtain even separations for each lane, every lane was filled with the same amount of protein sample. The Precision Plus Protein Standard (Dual Color; Bio-Rad, Munich, Germany) was used as a molecular weight marker.

2.8.2 Western blotting – Protein transfer

Proteins were transferred from SDS gels to nitrocellulose membranes (Protran Nitrocellulose Transfer Membrane, 0.45 µm pore size; GE Healthcare Life Sciences) by use of the Mini Trans-Blot Cell system (Bio-Rad) in 1x Transfer Buffer (containing 20% methanol). Protein transfer was performed depending on the molecular weight of the respective proteins. Smaller proteins were typically transferred at 150 mA, RT for 2 h; larger proteins were typically transferred either at 150 mA, RT for 3h, or at 40V, 4°C, oN. Directly following the protein transfer, proteins were visualised by Ponceau S staining to check for equal loading of all lanes. Unspecific antibody binding sites were blocked with 5% milk powder solution in 1x PBST at 4°C, oN or for 1h, RT. Following blocking, blots were incubated with primary and secondary antibodies, and protein bands were detected as described below.

2.8.3 Western blotting - Ponceau S staining

Ponceau S staining was performed to show equal loading of all lanes. Membranes were incubated for 5 min in Ponceau S staining solution and subsequently washed with de-ionised H_2O to get clear bands without background. For complete decolouration the membrane was washed in 1x PBST.

2.8.4 Western blotting - Antibody treatment

After blocking, the membrane was incubated with the primary antibody according to antibody protocols (*Table 10*). To remove residual antibody solution, blots were washed in 1x PBST.

Subsequently, the blot was incubated with the secondary antibody, coupled to HRP (horse-radish-peroxidase), according to antibody protocols (*Table 11*). To remove residual antibody solution, blots were washed in 1x PBST. Protein bands were visualised by chemiluminescence signals (Luminata Forte Western HRP Substrate; Merck Millipore, Darmstadt, Germany). The signal was recorded with an ImageQuant LAS 4000 Lumineszent Image Analyser (GE Healthcare Life Sciences). Recorded images were processed in Adobe Photoshop and assembled in Adobe Illustrator. To prepare the blot for incubation with a second or third primary antibody, the blot was stripped and blocked again.

2.8.5 Antibody protocols

Primary antibody	Concentration and blocking solution	Incubation conditions
Living Colors® A.v. Peptide Antibody (Anti-GFP, rabbit polyclonal; TakaraBio/Clontech, Saint-Germain-en-Laye, France)	1:100; 5% milk ≙ 1 µg/ml	2 h, RT
Anti-Spir-1 (SA2133), rabbit polyclonal (322)	1:1000; 1x PBST ≙ 0.5 µg/mL	3 h, RT
Living Colors® DsRed, rabbit polyclonal antibody (TakaraBio/Clontech)	1:1000; 5% milk ≙ 0.5 µg/ml;	2 h, RT
Anti-c-Myc (9E10), mouse monoclonal antibody (Santa Cruz Biotechnology)	1:500; 5% milk ≙ 0.4 µg/ml	2 h, RT
Anti-myosin Va, rabbit polyclonal (Cell Signaling Technology, Leiden, Netherlands)	1:750; 5% milk	3 h, RT
Anti-Rab11a (D4F5 XP), rabbit monoclonal (Cell Signaling Technology)	1:1000; 5% milk	3 h, RT

Table 10 | Overview on primary antibody protocols for Western blotting.

Secondary antibody	Concentration and blocking solution	Incubation conditions
Donkey anti-rabbit, HRP-linked (GE Healthcare Life Sciences)	1:5000; 1.6 % milk	1 h, RT
Sheep anti-mouse, HRP-linked (GE Healthcare Life Sciences)	1:5000; 1.6 % milk	1 h, RT

Table 11 | Overview on secondary antibody protocols for Western blotting.

2.8.6 Western blotting – Blot stripping

In order to remove primary and secondary antibodies from the membrane and to prepare it for following antibody treatments, blots were stripped in Stripping Buffer. 50 ml Stripping Buffer per membrane were supplemented with 345 µl β-Mercaptoethanol solution (12.8 M stock) and warmed to 50°C. Blots were incubated in warm Stripping Buffer for $3 \times 20\ min$ at 50°C. To remove residual Stripping Buffer, blots were washed extensivly for $4 \times 15\ min$ in 1x PBST. Finally, blots were blocked in 5% milk powder solution in 1x PBST as described and incubated with new antibody solutions.

2.9 Production and purification of recombinant proteins in *E.coli* bacteria

Escherichia coli strains were transformed with expression vectors generated for recombinant protein expression. GST-MyoVa/b-GTD proteins were expressed in *E.coli* Rosetta(DE3)pLysS (F– *ompT* *hsdS*$_B$(r_B^- m_B^-) *gal dcm* (DE3) pLysSRARE^2 (Cam^R); Merck Millipore, Novagen). His$_6$-mCherry-Spir-2-linker(LALA), GST-Rab11a-Q70L and GST-Spir-2-GTBM-SB-FYVE proteins were expressed in *E.coli* Rosetta (F– *ompT* *hsdS*$_B$(r_B^- m_B^-) *gal dcm* pRARE^2 *(*Cam^R); Merck Millipore, Novagen).

The whole protein purification procedure was performed in two sequential purification steps. At first, a batch purification using specific beads for affinity based purification was done with Glutathione Sepharose 4B beads (GE Healthcare Life Sciences) for GST-tags, and Ni-NTA Agarose beads (Qiagen) for His$_6$-tags, respectively. Second, a size exclusion chromatography (SEC) was performed using an ÄKTApurifier system (GE Healthcare Life Sciences) and High Load 16/60 Superdex 200 SEC column (GE Healthcare Life Sciences). For SEC, the column was first calibrated with Gelfiltration buffer (1.5 CV, flow rate: 1 ml/min). The protein solution was then loaded on the column and separated in Gelfiltration buffer using a pre-designed method (Sdex1660completerun; 1.2 CV, flow rate: 1 ml/min). 2-ml fractions were collected automatically. Single fractions were analysed by SDS gel electrophoresis and Coomassie staining for presence of respective protein bands with the desired size, and the right fractions were pooled using Amicon Ultra centrifugal filters (Merck Millipore) with respective molecular weight cut offs in order to increase the protein concentration. All purification steps were performed at 4°C. Protein concentrations were measured by Bradford assay as described below. Small aliquots were prepared (30-100 µl, depending on the protein concentration), quickly frozen in liquid nitrogen, and stored at -80°C.

2.9.1 Purification of GST-MyoVa/b-GTD

The bacterial expression vectors pGEX-4T1-NTEV-mm-MyoVa-GTD or pGEX-4T1-NTEV-hs-MyoVb-GTD were expressed in *E.coli* Rosetta(DE3)pLysS. A 37°C oN culture was used to inoculate 1 l LB medium (1:50), supplemented with 100 mg/l ampicillin, 30 mg/l chloramphenicol. Bacteria were grown at 37°C until an OD_{600} ~0.8. Protein expression was induced by adding 0.1 mM Isopropyl-β-D-thiogalactopyranoside (IPTG; Sigma-Aldrich), and continued at 20°C, 18 h. Bacteria were harvested by pelleting at 5,500 x *g*, 30 min, 4°C and the bacterial pellet was washed in 1x PBST. Bacteria were pelleted again at 4,600 x *g*, 30 min, 4°C, resuspended in 5 times the pellet mass (v/w) Lysis buffer and subsequently lysed by ultra-sonication (6 x 30 sec, 6 cycles, 60% amplitude) on ice. The lysates were centrifuged at 75,000 x *g*, 2 x 30 min, 4°C, and the cleared supernatant was incubated with 1 ml Glutathion Sepharose 4B beads (1:1 suspension) for 2 h at 4°C on a rotating wheel. The beads were pelleted (500 x *g*, 5 min, 4°C) and washed 5 times in 5 ml Wash buffer. Bound proteins were eluted from the beads by Elution buffer for 5 x 30 min in 1 ml buffer for each elution step. The eluted fractions were concentrated via Amicon 50K centrifugal filters at 4,000 x *g*, 4°C in 10-min steps until ~1 ml protein solution is left. The concentrated protein solution was loaded on the ÄKTApurifier (2 ml loop) by a syringe and the proteins were separated by size exclusion chromatography. All buffers for the respective purification steps are listed in *Table 12*.

Wash buffer for GST-MyoVa/b-GTD **Lysis buffer**	- 1x PBS, pH 8.0 - 2 mM β-Mercaptoethanol - 5% (v/v) Glycerol - 2 mM $MgCl_2$ - 0.05% Tween20 - add freshly: 1 mM PMSF, complete Mini Protease Inhibitor Cocktail
Elution buffer for GST-MyoVa/b-GTD	- 20 mM Tris-HCl, pH 8.0 - 150 mM NaCl - 2 mM β-Mercaptoethanol - 2 mM $MgCl_2$ - 5% Glycerol - 20 mM Glutathion
Gelfiltration buffer for GST-MyoVa/b-GTD	- 20 mM Tris-HCl, pH 8.0 - 150 mM NaCl - 2 mM DTE - 2 mM $MgCl_2$ - 5% Glycerol - filter sterile, de-gas, store at 4°C

Table 12 | Buffers for purification of GST-MyoVa/b-GTD proteins.

2.9.2 Purification of His_6-mCherry-Spir-2-linker(LALA)

The bacterial expression vector pProEx-HTb-mCherry-hs-Spir-2-linker(LALA) was expressed in *E. coli* Rosetta. A 37°C oN culture was used to inoculate 1 l LB medium (1:50), supplemented with 100 mg/l ampicillin, 30 mg/l chloramphenicol. Bacteria were grown at 37°C until an OD_{600} ~0.8. Protein expression was induced by 0.1 mM IPTG, and continued at 20°C, 18 h. Bacteria were harvested by pelleting at 5,500 x *g*, 30 min, 4°C and the bacterial pellet was washed in cold 1x PBST. Bacteria were pelleted again at 4,600 x *g*, 30 min, 4°C, resuspended in 5 times the pellet mass (v/w) Lysis buffer, and subsequently lysed by ultra-sonication (6 x 30 sec, 6 cycles, 60% amplitude) on ice. The lysates were centrifuged at 75,000 x *g*, 2 x 30 min, 4°C, and the cleared supernatant was incubated with 1 ml Ni-NTA Agarose beads (1:1 suspension) for 2 h at 4°C on a rotating wheel. The beads were pelleted (500 x *g*, 5 min, 4°C) and washed 5 times in 5 ml Wash buffer. Bound proteins were eluted from the beads by Elution buffer for 5 x 30 min in 1 ml buffer for each elution step. The eluted fractions were concentrated via Amicon 30K centrifugal filters at 4,000 x *g*, 4°C in 10-min steps until ~1 ml protein solution is left. The concentrated protein solution was loaded on the ÄKTApurifier (2 ml loop) by a syringe and the proteins were separated by size exclusion chromatography. All buffers for the respective purification steps are listed in *Table 13*.

Wash buffer for His_6-mCherry-Spir-2-linker (LALA)	-	20 mM Tris-HCl, pH 8.0
	-	300 mM NaCl
	-	20 mM Imidazol
	-	5 mM β-Mercaptoethanol
Lysis buffer	-	add freshly: 1 mM PMSF, complete Mini Protease Inhibitor Cocktail
Elution buffer for His_6-mCherry-Spir-2-linker (LALA)	-	20 mM Tris-HCl, pH 8.0
	-	300 mM NaCl
	-	300 mM Imidazol
	-	5 mM β-Mercaptoethanol
Gelfiltration buffer for His_6-mCherry-Spir-2-linker (LALA)	-	2x PBS, pH 7.2
	-	10% Glycerol
	-	filter sterile, de-gas, store at 4°C

Table 13 | Buffers for purification of His_6-mCherry-Spir-2-linker(LALA) proteins.

2.9.3 Purification of GST-Rab11a-Q70L

The bacterial expression vector pGEX-4T1-NTEV-cl-Rab11a-Q70L was expressed in *E. coli* Rosetta. A 37°C oN culture was used to inoculate 1 l LB medium (1:50), supplemented with 100 mg/l ampicillin, 30 mg/l chloramphenicol. Bacteria were grown at 37°C until an OD_{600} ~0.8. Protein expression was induced with 0.1 mM IPTG, and continued at 20°C, 18 h. Bacteria were harvested by pelleting at 5,500 x *g*, 30 min, 4°C and the bacterial pellet was washed in 1x PBST. Bacteria were pelleted again at 4,600 x *g*, 30 min, 4°C, resuspended in 5 times the pellet mass (v/w) Lysis buffer, and subsequently lysed by ultra-sonication (6 x 1 min, 6 cycles, 60% amplitude) on ice. The lysates were centrifuged at 75,000 x *g*, 2 x 30 min, 4°C and the cleared supernatant was incubated with 1 ml Glutathion Sepharose 4B beads (1:1 suspension) for 3 h at 4°C on a rotating wheel. The beads were pelleted (500 x *g*, 5 min, 4°C) and washed 5 times in 5 ml Wash buffer. Bound proteins were eluted from the beads by Elution buffer for 5 x 30 min in 1 ml buffer for each elution step. The eluted fractions were concentrated via Amicon 50K centrifugal filters at 4,000 x *g*, 4°C in 10-min steps until ~1 ml protein solution is left. The concentrated protein solution was loaded on the ÄKTApurifier (2 ml loop) by a syringe and the proteins were separated by size exclusion chromatography. All buffers for the respective purification steps are listed in *Table 14*.

Wash buffer for GST-Rab11a-Q70L **Lysis buffer**	- 1x PBS, pH 7.8 - 2 mM β-Mercaptoethanol - 5% Glycerol (v/v) - 2 mM $MgCl_2$ - 0.05% Tween20 - add freshly: 1 mM PMSF, complete Mini Protease Inhibitor Cocktail
Elution buffer for GST-Rab11a-Q70L	- 20 mM Tris-HCl, pH 7.8 - 150 mM NaCl - 2 mM β-Mercaptoethanol - 2 mM $MgCl_2$ - 5% Glycerol (v/v) - 20 mM Glutathion
Gelfiltration buffer for GST-Rab11a-Q70L	- 20 mM Tris-HCl, pH 7.8 - 150 mM NaCl - 2 mM DTE - 2 mM $MgCl_2$ - 5% Glycerol - filter sterile, de-gas, store at 4°C

Table 14 | Buffers for purification of GST-Rab11a-Q70L proteins.

2.9.4 Purification of GST-Spir-2-GTBM-SB-FYVE

The bacterial expression vector pGEX-4T3-hs-Spir-2-GTBM-SB-FYVE was expressed in *E. coli* Rosetta. A 37°C oN culture was used to inoculate 1 l LB medium (1:50), supplemented with 100 mg/l ampicillin, 30 mg/l chloramphenicol. Bacteria were grown at 37°C until an OD_{600} ~0.8. Protein expression was induced with 0.15 mM IPTG, and continued at 18°C, 20 h. Bacteria were harvested by pelleting at 5,500 x *g*, 30 min, 4°C, and the bacterial pellet was washed in 1x PBST. Bacteria were pelleted again at 4,600 x *g*, 30 min, 4°C, resuspended in 40 ml Lysis buffer (supplemented with 0.1% Triton-X100, 2 protease inhibitor cocktail tablets (complete Mini, EDTA-free; Roche, Penzberg, Germany), 1 mM Phenylmethylsulfonylfluoride (PMSF; Sigma-Aldrich)) and subsequently lysed by ultra-sonication (6 x 1 min, 6 cycles, 60% amplitude) on ice. The lysates were centrifuged at 27,000 x *g*, 2 x 30 min, 4°C, and the cleared supernatant was incubated with 1 ml Glutathion Sepharose 4B beads (1:1 suspension) for 2.5 h at 4°C on a rotating wheel. The beads were pelleted (500 x *g*, 5 min, 4°C) and washed 5 times in 5 ml Wash buffer. Bound proteins were eluted from the beads by Elution buffer for 4 x 30 min in 1 ml buffer for each elution step. 2 ml of the collected elution fractions were directly loaded on the ÄKTApurifier (2 ml loop) by a syringe and the proteins were separated by size exclusion chromatography. The residual 2 ml elution was loaded afterwards and the SEC was repeated with the same conditions to both, increase protein yield and avoide excess protein concentrations that could lead to protein precipitation. All buffers for the respective purification steps are listed in *Table 15*.

Wash buffer	-	2x PBS, pH 7.2
for GST-Spir-2-GTBM-SB-FYVE	-	10% Glycerol (v/v)
Lysis buffer	-	add freshly: 1 mM PMSF, complete Mini Protease Inhibitor Cocktail, 0.1% Triton-X100
Elution buffer	-	2x PBS, pH 7.2
for GST-Spir-2-GTBM-SB-FYVE	-	10% Glycerol (v/v)
	-	20 mM Glutathion
Gelfiltration buffer	-	2x PBS, pH 7.2
for GST-Spir-2-GTBM-SB-FYVE	-	10% Glycerol (v/v)
	-	filter sterile, de-gas, store at 4°C

Table 15 | Buffers for purification of GST-Spir-2-GTBM-SB-FYVE proteins.

2.9.5 Bradford assay to determine protein concentrations

Bradford assay was used to determine concentrations of recombinant, bacterially expressed, purified proteins. The lab uses a self-prepared Bradford solution which needs an initial calibration to use for subsequent measurements. The Bradford stock solution (Coomassie Plus Protein Assay Reagent; ThermoFisher) was mixed 2:1 with de-ionised H_2O. A calibration line was determined with H_2O only, Bradford solution only and Bradford solution supplemented with BSA protein standard rising from 1 µg to 15 µg in 1 µg steps. The absorption at 595 nm of the solution was measured and a calibration line was calculated with:

$$y = a \times x + b$$

For subsequent measurements of protein concentrations, 1 ml calibrated Bradford solution was adjusted to RT in a transparent cuvette. 1 µl protein solution was added and incubated for 10 min at RT. The absorption of the solution at 595 nm was determined and the concentration of the protein solution as calculated with:

$$x = (A_{595} - b) / a$$

2.10 Co-immunoprecipitation

HEK293 cells were seeded on Poly-L-Lysine coated 6-well plates (6×10^5 cells per well) as described above, one day prior to transfection. HEK293 cells were transfected with expression vectors encoding Myc-epitope-tagged Spir proteins and AcGFP-tagged myosin V fragments as described above in triplicates (the cells of three wells are pooled and handled as one sample). 48 hours post transfection, cells were washed two times with 1x PBS to remove residual medium and serum. Cells were scraped off the wells in 333 µl Lysis buffer (25 mM Tris-HCl pH 7.4, 150 mM NaCl, 5 mM $MgCl_2$, 10% (v/v) glycerol, 0.1% (v/v) Nonidet P-40, 1 mM PMSF, protease inhibitor cocktail) per well. The cells of three wells were pooled per sample and the cells were lysed for 40 min, 4°C on a rotating wheel. Cell lysates were centrifuged at 20,000 x *g*, 20 min, 4°C, to remove insoluble debris. Meanwhile, respective amounts of Protein G-Agarose beads (Roche) were washed three times in Pulldown Buffer (25 mM Tris-HCl pH 7.4, 150 mM NaCl, 5 mM $MgCl_2$, 10% (v/v) glycerol, 0.1% (v/v) Nonidet P-40) and a 1:1 suspension of beads and Pulldown Buffer was prepared for subsequent use. The cleared supernatant was pre-incubated with 20 µl Protein G-Agarose beads (1:1 suspension) for 1 h, 4°C on a rotating wheel to get rid of proteins unspecifically binding to the beads. 40 µl of the cleared supernatant were mixed with 5x Laemmli buffer and used as cleared lysates in Western blots to check for protein expression levels. Beads from the pre-incubation step were pelleted at 500 x *g*, 3 min, 4°C and the supernatant was transferred into a new tube. The supernatant was subsequently incubated with 4 µg anti-c-Myc antibody (9E10, mouse monoclonal; Santa Cruz Biotechnology, Dallas,

TX, USA) for 1 h on ice. Subsequently, 40 µl Protein G-Agarose beads (1:1 suspension) were added and incubated for 2 h, 4°C on a rotating wheel. Beads were washed in Pulldown Buffer four times, 500 µl each, and every time beads were pelleted at 500 x *g*, 2 min, 4°C. Beads were pelleted finally and any residual fluid was removed carefully but completely. Bound proteins were eluted by 40 µl 1x Laemmli buffer and denatured for 10 min at 95°C. Potential protein interactions in co-IPs and the protein expression levels in the cleared lysates were analysed by immunoblotting using respective antibodies.

2.11 GST-pulldown from HEK293 lysates

HEK293 cells were seeded on Poly-L-Lysine coated 6-well plates (6×10^5 cells per well) as described above, one day prior to transfection. HEK293 cells were co-transfected with expression vectors encoding Myc-Spir-2-FL, mStrawberry-FMN-2-FH2-FSI, eGFP-MyoVa-D-FL and eGFP-MyoVa-D-Q1753R, respectively, as described above, in triplicates (the cells of three wells are pooled and handled as one sample). 24 hours post transfection, cells were washed two times with 1x PBS to remove residual medium and serum. Cells were scraped off the wells in 333 µl Lysis buffer (25 mM Tris-HCl pH 7.4, 150 mM NaCl, 5 mM $MgCl_2$, 10% (v/v) glycerol, 0.1% (v/v) Nonidet P-40, 1 mM PMSF, protease inhibitor cocktail) per well. The cells of three wells were pooled per sample and cells were lysed for 40 min at 4°C on a rotating wheel. Cell lysates were centrifuged at 20,000 x *g*, 20 min, 4°C, to remove insoluble debris. Meanwhile, respective amounts of GSH-Sepharose 4B beads were washed three times in Pulldown Buffer (25 mM Tris-HCl pH 7.4, 150 mM NaCl, 5 mM $MgCl_2$, 10% (v/v) glycerol, 0.1% (v/v) Nonidet P-40) and a 1:1 suspension of beads and Pulldown Buffer was prepared for subsequent use. The cleared supernatant was pre-incubated with 20 µl GSH-Sepharose 4B beads (1:1 suspension) for 1 h, 4°C on a rotating wheel to get rid of proteins unspecifically binding to the beads. 40 µl of the cleared supernatant were mixed with 5x Laemmli buffer and used as cleared lysates in Western blots to check for protein expression levels. For GST-pulldown assays, 65 µg GST-Rab11a-Q70L protein and 25 µg GST protein as a control, respectively, was coupled to 40 µl GSH-Sepharose 4B beads (1:1 suspension) in 500 µl Pulldown Buffer for 1:20 h, 4°C on a rotating wheel. Beads were pelleted at 500 x g, 2 min, 4°C and washed two times with Pulldown Buffer, 500 µl each, by pelleting beads each time at 500 x *g*, 2 min, 4°C. Beads were pelleted again and any residual fluid was removed completely. Beads from the pre-incubation step were pelleted at 500 x *g*, 3 min, 4°C, and the supernatant (cell lysates) were transferred to the GST-protein coupled GSH-Sepharose 4B beads and incubated for 2:15 h, 4°C on a rotating wheel. Beads were pelleted at 500 x *g*, 2 min, 4°C and washed four times with Pulldown buffer, 500 µl each. Beads were pelleted finally and any residual fluid was removed carefully but completely. Bound proteins were eluted by 40 µl 1x Laemmli

buffer and denatured for 10 min at 95°C. Potential protein interactions in Pulldowns and the protein expression in cleared lysates were analysed by immunoblotting using respective antibodies.

2.12 GST-pulldown from mouse brain

Wild-type C57BL/6N mice were killed by cervical dislocation. One brain was used for one experiment. The brain was isolated immediately, washed three times in ice-cold 1x PBS and lysed in 1 ml Lysis Buffer (25 mM Tris-HCl pH 7.4, 150 mM NaCl, 5 mM $MgCl_2$, 10% (v/v) glycerol, 0.1% (v/v) Nonidet P-40, 0.1 M NaF, 1 mM Na_3VO_4, 1 mM PMSF, protease inhibitor cocktail) using a TissueRuptor (Qiagen). Cell lysis was completed for 45 min on ice by inverting regularly. Lysates were centrifuged at 20,000 x *g*, 4°C until the supernatant was clear (usually 3-4 times, 30 min each). 40 µl of the cleared supernatant were mixed with 5x Laemmli buffer and used as cleared brain lysates in Western blots to check for protein expression levels. 50 µg GST-fusion proteins were coupled to 40 µl washed (see above) GSH-Sepharose 4B beads (1:1 suspension) in 500 µl Pulldown Buffer for 1 h, 4°C on a rotating wheel. Beads were pelleted at 500 x g, 2 min, 4°C and washed two times with Pulldown Buffer, 500 µl each, by pelleting beads each time at 500 x *g*, 2 min, 4°C. Beads were pelleted again and any residual fluid was removed completely. Cleared brain lysates were incubated with GST-protein coupled beads for 2.5 h at 4°C on a rotating wheel. Beads were pelleted at 500 x *g*, 2 min, 4°C and washed five times with Pulldown Buffer, 500 µl each. Beads were pelleted finally and any residual fluid was removed carefully but completely. Bound proteins were eluted by 20 µl 1x Laemmli buffer and denatured for 10 min at 95°C. Potential protein interactions in Pulldowns and the protein expression levels in cleared brain lysates were analysed by immunoblotting using respective antibodies.

2.13 GST-pulldown experiments with purified proteins

Respective amounts of GSH-Sepharose 4B beads were washed three times in Pulldown Buffer (25 mM Tris-HCl pH 7.4, 150 mM NaCl, 5 mM $MgCl_2$, 10% (v/v) glycerol, 0.1% (v/v) Nonidet P-40) and a 1:1 suspension of beads and Pulldown Buffer was prepared for subsequent use. 50 µg GST-fusion proteins were coupled to 40 µl GSH-Sepharose 4B beads (1:1 suspension) in 500 µl Pulldown Buffer for 1 h, 4°C on a rotating wheel. Beads were pelleted at 500 x g, 2 min, 4°C and washed two times with Pulldown Buffer, 500 µl each, by pelleting beads each time at 500 x *g*, 2 min, 4°C. Beads were pelleted again and any residual fluid was removed completely. GST-protein coupled beads were incubated with 20 µg His_6-mCherry-fusion peptides in 1 ml Pulldown Buffer for 2 h at 4°C on a rotating wheel. In order to identify the tripartite Rab11a/MyoVa/Spir-2 complex, 65 µg GST-Spir-2-GTBM-SB-FYVE was coupled to beads. Subsequently, beads were incubated with 40 µg MyoVa and 35 µg Rab11a proteins simultaneously for 2 h. Beads were pelleted at 500 x *g*, 2 min, 4°C and washed four times with Pulldown Buffer, 500 µl each. Beads were pelleted finally and any residual fluid was

removed carefully but completely. Bound proteins were eluted by 20 µl 1x Laemmli buffer and denatured for 10 min at 95°C. Potential protein interactions in Pulldowns were analysed by immunoblotting using respective antibodies.

2.14 Quantitative GST-pulldown assays

Respective amounts of GSH-Sepharose 4B beads were washed three times in Pulldown Buffer (25 mM Tris-HCl pH 7.4, 150 mM NaCl, 5 mM $MgCl_2$, 10% (v/v) glycerol, 0.1% (v/v) Nonidet P-40) and a 1:1 suspension of beads and Pulldown Buffer was prepared for subsequent use. Increasing amounts of GST-MyoVa/b-GTD fusion proteins were coupled to 20 µl GSH-Sepharose 4B beads (1:1 suspension) in 500 µl Pulldown Buffer for 1 h, 4°C on a rotating wheel. Beads were pelleted at 500 x *g*, 2 min, 4°C and washed two times with Pulldown Buffer, 500 µl each, by pelleting beads each time at 500 x *g*, 2 min, 4°C. Beads were pelleted again and any residual fluid was removed completely. GST-protein coupled beads were incubated with 100 nM His_6-mCherry-Spir-2-linker peptide in SPECS buffer (1x PBS pH 7.2, 50 mM NaCl) for 2 h at 4°C on a rotating wheel. Beads were pelleted at 500 x *g*, 2 min, 4°C and the supernatant was transferred into new tube. The supernatant was centrifuged for 10 min at 20,000 x *g* at 4°C to remove potential debris that could disturb fluorescence measurements.

Each protein sample was allowed to adapt to 20°C for 15 min in a water bath. The concentration dependent binding of GST-MyoVa/b-GTD to the His_6-mCherry-Spir-2-linker was determined by fluorospectrometric analysis using the FluoroMax-4 Spectrofluorometer (Horiba Jobin Yvon, Bensheim, Germany). The mCherry red fluorescent protein was excited at 548 nm and the emission at 610 nm was recorded (emission maximum of mCherry). The data were calculated as “fraction bound” compared to the fluorescence signals of His_6-mCherry-Spir-2-linker alone, without any GST-MyoV-GTD protein:

$$y = 1 - \frac{y_0 - y_c}{y_0}$$

With y_0 is the fluorescence signal of His_6-mCherry-Spir-2-linker alone, without GST-MyoV-GTD and y_c is the signal at the respective GST-MyoV-GTD concentration.

The data were further processed in SigmaPlot 12.3 software (Systat Software, Erkrath, Germany) and the equilibrium binding data were fitted according to the equation:

$$\mathrm{y} = \frac{B_{max} \cdot x}{K_d + x}$$

assuming a single binding site, and with B_{max} representing the maximal amplitude, K_d representing the equilibrium constant, and x representing the concentration of GST-MyoV-GTD. The binding curves saturated at 40% since the His_6-mCherry-Spir-2-linker protein preparation contained C-terminal incomplete protein products, which are still fluorescent but cannot interact with MyoV-GTD. The Spir-2-linker region is predicted to be highly unstructured, which may be the reason for the relative instability of the recombinant His_6-mCherry-Spir-2-linker fusion protein.

2.15 Immunostaining

HeLa cells were seeded on microscope cover glasses in a 6-well plate (3×10^5 cells per well) and transfected with in each experiment indicated expression vectors encoding Myc-epitope-tagged and fluorescently tagged proteins, as described above, on the next day. One day post transfection, cells were washed three times with 1x PBS to remove any residual medium and serum. Cells were fixed with paraformaldehyde (3.7% in 1x PBS) for 20 min at 4°C. Cells were again washed three times with 1x PBS and subsequently permeabilised using 0.2% Triton X-100 (in 1x PBS) for 3.5 min, RT. After washing three times with 1x PBS, cells were incubated with 50 µl of an anti-c-Myc antibody solution (9E10, mouse monoclonal, 2 µg/ml; Santa Cruz Biotechnology) for 1:30 h, RT, in the dark. Cells were washed three times in 1x PBS and subsequently incubated with 50 µl of a conjugated anti-mouse secondary antibody solution (Cy5, from donkey, 3.25 µg/ml, Dianova; and TRITC, from donkey, 3.125 µg/ml, Dianova, Hamburg, Germany) for 1:30 h, RT, in the dark. Primary and secondary antibody solutions were always prepared in 1x PBS, supplemented with 1% FCSIII. Cells were washed again three times in 1x PBS and once in de-ionised H_2O to get rid of residual salts. Finally, cells were mounted on microscope slides with Mowiol solution, dried at RT in the dark and stored at 4°C.

Immunostainings were subsequently analysed with a Leica AF6000LX fluorescence microscope, equipped with a Leica HCX PL APO 63x/1.3 GLYC objective and a Leica DFC350 FX digital camera (1392 x 1040 pixels, 6.45 µm x 6.45 µm pixel size) (all from Leica, Wetzlar, Germany). 3D stacks were recorded and processed with the Leica 3D-deconvolution software module.

In case of the MyoVa autoregulation/activation experiments, the eGFP-MyoVa-FL expression levels were quantified. High expression levels of GFP-MyoVa-FL induced a vesicular localisation, whereas an even cytoplasmic distribution was only observed at low expression levels. In order to distinguish clearly between vesicular and cytoplasmic MyoVa localisation, cells were imaged at either state, and the sum of pixel grey values per cell was determined as a measure for the eGFP-MyoVa-FL expression levels. Based on that, only those cells were used for autoregulation analysis that have a sum of pixel grey values less than 20×10^6 for the expression of GFP-MyoVa-FL.

Images were recorded using the Leica LASX software, further processed with Adobe Photoshop and subsequently assembled in Adobe Illustrator.

2.16 Colocalisation analysis

The extent of colocalisation of Rab11a, Spir-2 and MyoVa was analysed using the ImageJ (V2.0.0) plug-in Coloc2. Here, the colocalisation rate for signals of individual fluorescence channels within one image is indicated by the Pearson's Correlation Coefficient (PCC) as a standard statistical measure to unravel a linear correlation between the intensity of different fluorescent signals. A PCC value of 1 indicates a perfect colocalisation, 0 indicates a random colocalisation and a PCC value of -1 indicates a mutually exclusive localisation of the analysed signals. To take the noise of each image into account and to gain an objective evaluation of PCC significance, a Costes significance test was performed. To do so, the pixels in one image were scrambled randomly and the correlation with the other (unscrambled) image was measured. PCC significance was observed when at least 95% of the randomised images show a PCC less than that of the original image, meaning that the probability for the measured correlation of two colours is significantly greater than the correlation of random overlap (347, 348). Statistical data analysis was done using the Student's t-test to compare two mean values for co-expression conditions with a confidence interval of 95%, and was performed using SPSS 22 (IBM, Armonk, NY).

3 Results

In order to characterise the functional correlation of Spir and MyoV proteins, a set of eukaryotic expression vectors encoding fluorescent protein and Myc-epitope tagged MyoVa, MyoVb, Spir-2, FMN-2 and Rab11a full-length proteins, deletion mutants and point mutants were employed, as well as prokaryotic expression vectors encoding Glutathione-S-transferase (GST) or His_6-mCherry tagged and untagged MyoVa, MyoVb, Spir-2, FMN-2 and Rab11a full-length proteins, deletion mutants and point mutants. For better orientation throughout the results section, all proteins, protein fragments and mutants are depicted in *Figure 16* (Spir-1/-2, FMN-2) and *Figure 17* (MyoVa, MyoVb, Rab11a). A detailed list on all expression vectors, including information about vector backbone, amino acid boundaries, respective species, restriction sites used for cloning, method of protein purification and the purpose of each plasmid is presented in the supplements (*Tables 16, 17*). All expression vectors which were kindly provided by other research groups and laboratories are indicated and described.

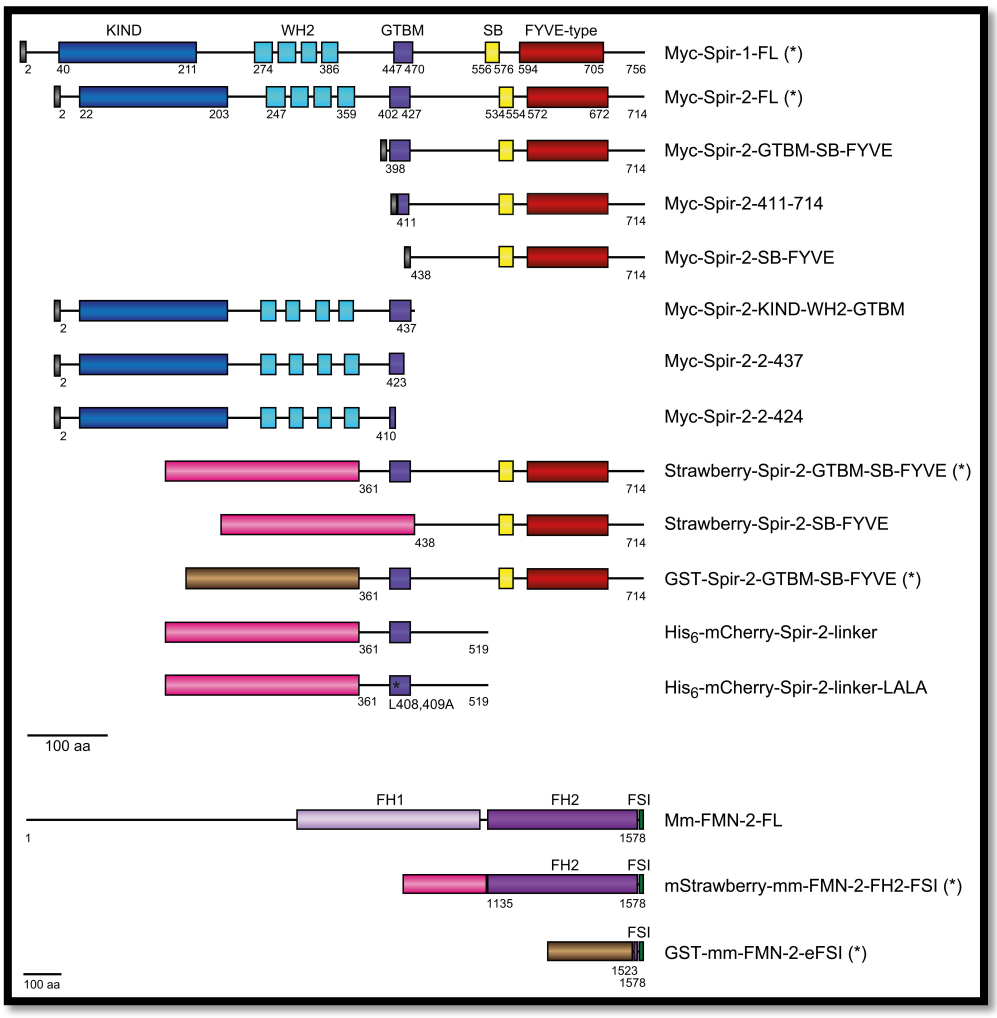

Figure 16 | Overview on Spir-1/-2 and FMN-2 protein fragments used in this thesis. (*) These vectors already existed in the lab of Eugen Kerkhoff. Spir-1/-2 proteins are all the human (Hs) isoforms. Numbers indicate amino acids. *GTBM*, globular tail domain binding motif; *SB*, Spir-box; *FH*, formin homology; *FL*, full-length; *Mm*, Mus musculus; *aa*, amino acid.

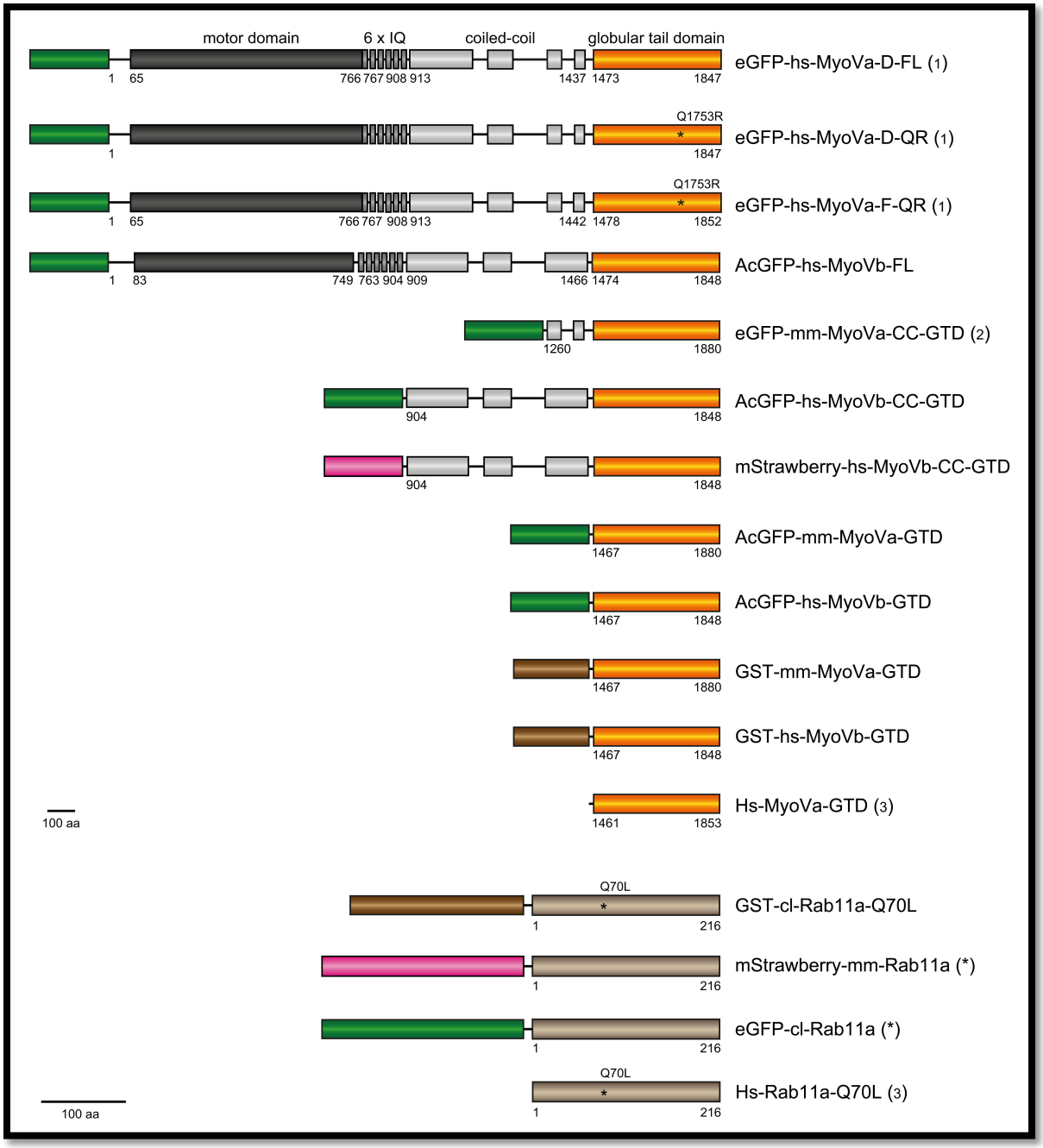

Figure 17 | Overview on myosin Va, myosin Vb and Rab11a protein fragments used in this thesis. (1), these expression vectors were generated and kindly provided by the lab of Bruno Goud, Institut Curie, Paris, France; (2), this expression vector was generated and kindly provided by the lab of Alistair Hume, University of Nottingham, Nottingham, UK. (3), these expression vectors were generated and kindly provided by the lab of Anne Houdusse, Institut Curie, Paris, France. (*) This expression vector already existed in the lab of Eugen Kerkhoff. Numbers indicate amino acids. *D*, isoform D; *F*, isoform F; *CC*, coiled-coil; *GTD*, globular tail domain; *FL*, full-length; *Hs*, Homo sapiens; *Mm*, Mus musculus; *Cl*, Canis lupus familiaris; *aa*, amino acid.

3.1 Spir and MyoV proteins co-exist in a protein complex

Spir actin nucleators and MyoV actin motor proteins colocalise with the Rab11 small GTPase at vesicular structures and cooperate in exocytic vesicle transport processes (7, 222, 256, 325, 334). Despite extensive efforts, a direct interaction of Spir and Rab11 proteins could not be demonstrated, and it remained unclear how Spir proteins are targeted towards Rab11 vesicles. Furthermore, recent work of our lab could show that Spir proteins rather non-specifically bind to negatively charged lipid membranes by their FYVE-type zinc-finger (327), which precludes the possibility of lipid-specific vesicle targeting of Spir proteins. Altogether, this led to the assumption that other factors, such as membrane associated proteins, might function to induce the formation of a distinct vesicle subpopulation, i.e. vesicles harbouring both, Spir and Rab11 proteins. Due to the cooperative mechanisms of MyoV and Rab11 proteins in a diversity of cellular processes (222, 251, 253, 256, 334, 349), the intriguing idea came up that the myosin V actin motor proteins possibly acts as a linker between Spir and Rab11 at vesicle membranes, therefore deciding on the vesicle identity. To follow this suggestion, an initial GST-pulldown from mouse brain lysates could show that a GST-tagged MyoVb globular tail domain protein (GST-MyoVb-GTD) is able to pull the Spir-1 protein from brain lysates (*Figure 18*). This finding manifests the co-existence of MyoV and Spir proteins in a protein complex. A GST-tagged C-terminal Formin-2 fragment (GST-FMN2-eFSI) also pulls the Spir-1 protein from brain lysates as expected, considering the well-established KIND-FSI interaction of Spir and FMN proteins (324, 338, 350). In the same experiment, MyoVa was pulled as well, further supporting the co-existence of Spir-1 and myosin V proteins in a protein complex. No interactions were observed for both, GST and buffer controls.

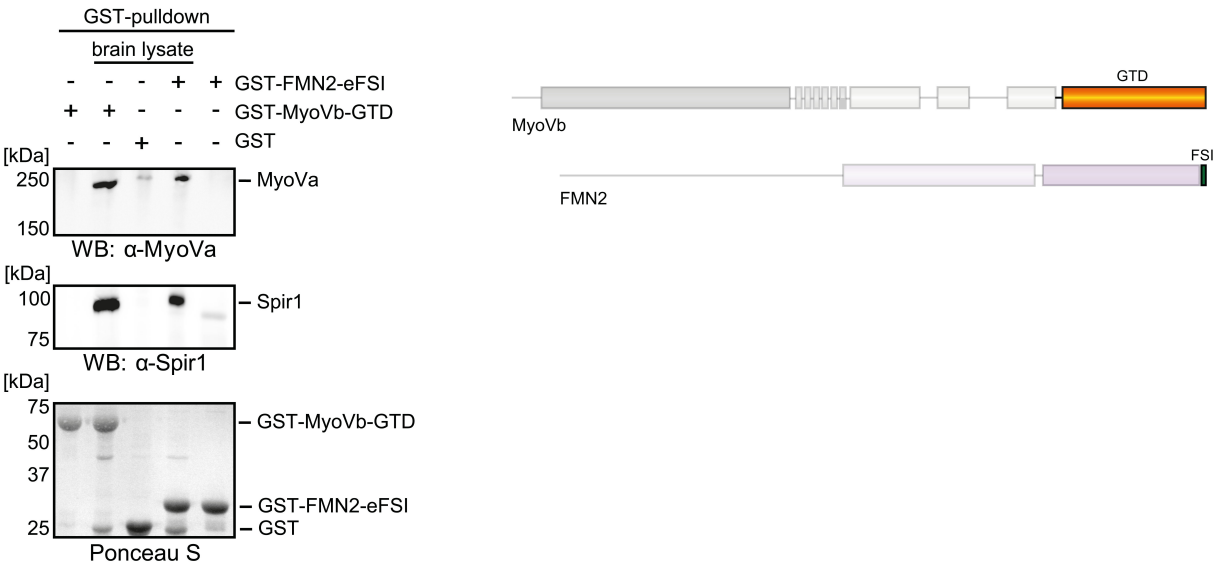

Figure 18 | Myosin V and Spir-1 proteins co-exist in a protein complex. GST-pulldown assays from mouse brain lysates with the GST-tagged MyoVb globular tail domain (GST-MyoVb-GTD) shows that GST-MyoVb-GTD strongly pulls Spir-1 as detected by immunoblotting (anti-Spir-1). A GST-tagged C-terminal FMN-2 fragment (GST-FMN2-eFSI) also strongly pulls Spir-1 from brain lysates. Interestingly, in the same experiment, MyoVa is also pulled, showing that Spir-1 and MyoVa co-exist in a protein complex. No interactions are observed for the GST control and for buffer controls. Ponceau S staining shows equal loading of GST and GST-fusion proteins. An overview of the employed protein fragments is presented and the domains and sequence parts used for pulldowns are highlighted. N = 3 experimental repeats. *eFSI*, extended formin/Spir interaction sequence; *GTD*, globular tail domain; *WB*, Western blot.

3.2 Identification of a highly conserved sequence motif within the central Spir linker region

After revealing that Spir and MyoV proteins co-exist in a protein complex, initial co-immunoprecipitation (co-IP) studies revealed that a potential Spir/MyoV interaction is neither mediated by the very N-terminal part of the Spir protein (KIND and WH2), nor by the very C-terminal part (Spir-box and FYVE) (not shown). Therefore, the putative MyoV interaction site is likely to be located within the central Spir linker region, between the WH2 domains and the Spir-box, a region that was formerly not known to contain distinct conserved domains or sequence motifs, and that was not shown before to serve distinct functions. A multiple sequence alignment of chosen vertebrate Spir-1 and Spir-2 amino acid sequences was performed for the central Spir region, starting from the last of the four WH2 domains (WH2-D), spanning the linker region until the FYVE-type zinc-finger (*Figure 19*). The multiple sequence alignment reveals the high sequence conservation within WH2-D, the Spir-box and the FYVE-type zinc-finger, as was expected. Considering the central linker region, the sequence similarity between Spir-1 and Spir-2 protein sequences is rather low (3.74% identity, 8.41% similarity). Taking only the Spir-1 or the Spir-2 proteins into account, some sequence homology can be found within the linker, but not between Spir-1 and Spir-2 proteins, for most of the linker region.

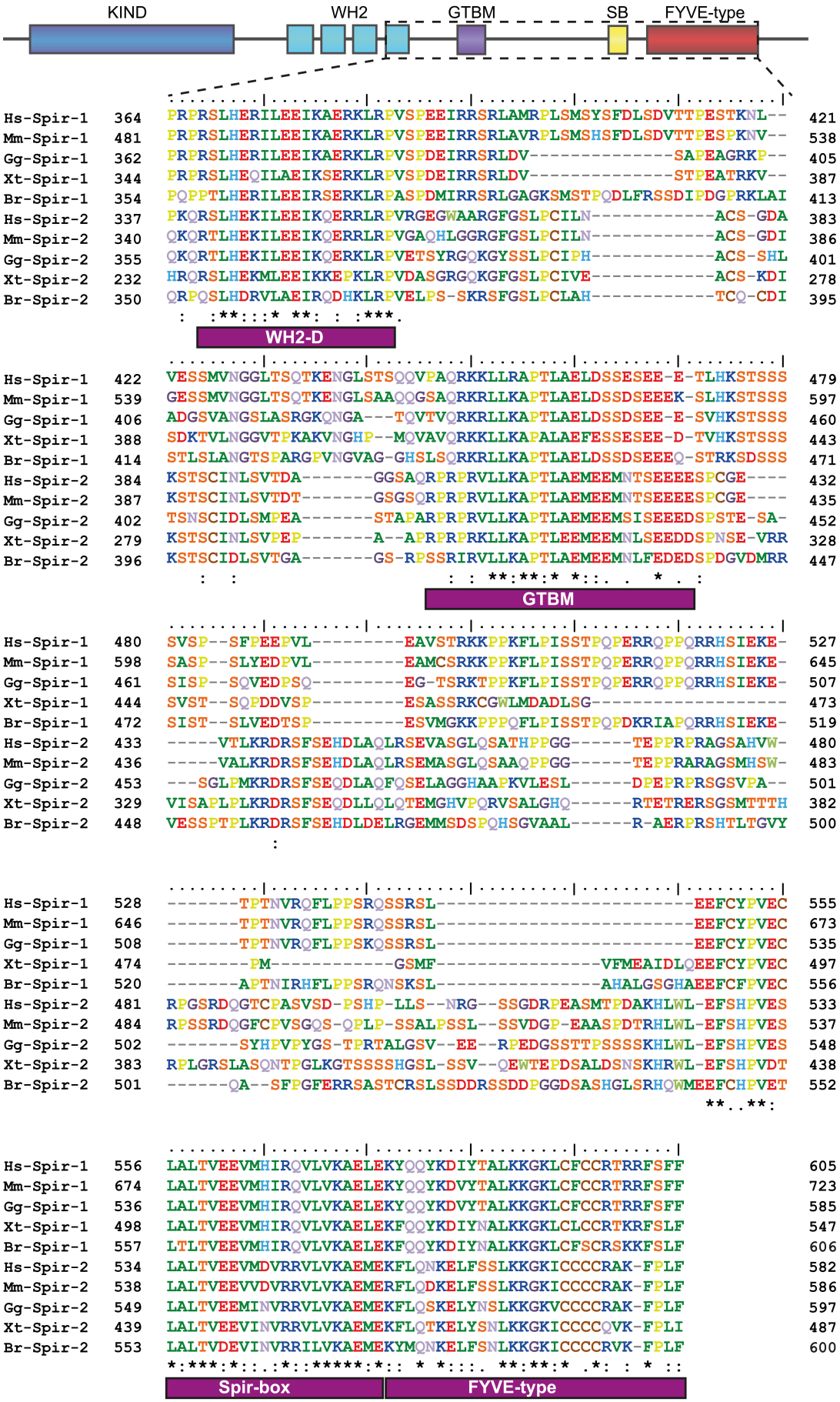
KIND
WH2
GTBM
SB
FYVE-type
WH2-D
GTBM
Spir-box
FYVE-type

Figure 19 | The central Spir linker region contains a highly conserved sequence motif. A multiple sequence alignment of linker regions from chosen vertebrate Spir-1 and Spir-2 amino acid sequences is presented starting from the last WH2 domain (WH2-D) and ending with the FYVE-type zinc-finger. High sequence homology between all sequences was only observed for WH2-D, Spir-box, FYVE-type zinc-finger and GTBM, but not for other parts of the linker region. Species abbreviations are: *Homo sapiens* (Hs), *Mus musculus* (Mm), *Gallus gallus* (Gg), *Xenopus tropicalis* (Xt), *Brachydanio rerio* (Br). 100% sequence identity is indicated with an asterisk (*). Numbers indicate amino acids.

Besides this, in the approximate middle of the linker region, a previously unrecognised short sequence motif of 27 amino acids is located which shows high sequence conservation also between Spir-1 and Spir-2 proteins (*Figure 20*). A subsequent multiple sequence alignment of this short sequence motif of vertebrate Spir-1 and Spir-2 amino acid sequences further strengthens the high rate of homology across those sequences (25.93% identity, 33.33% similarity). Throughout this thesis, the newly identified sequence motif is from now on referred to as *globular tail domain binding motif* (GTBM). By definition, this conserved sequence must be rather considered as a sequence motif than as a protein domain, because it does not show a defined higher order structural organisation by itself. The GTBM is composed of a positively charged basic amino acid cluster at the beginning and two negatively charged acidic clusters in the middle and at the end of the motif. A WebLogo of the respective sequence parts from 223 Spir sequences shows the abundance of individual amino acids for each sequence position (in collaboration with Dr. Martin Kollmar, Max-Planck-Institute for Biophysical Chemistry, Göttingen, Germany). Of significance, there are two highly conserved leucine residues (L408, L409 for human Spir-2), which are identical in almost all Spir sequences analysed. Considering the assumed role for the Spir linker region in MyoV interaction and the newly discovered highly conserved sequence motif within the linker region, it is intriguing to speculate that this short sequence motif is critical for mediating a Spir/MyoV interaction.

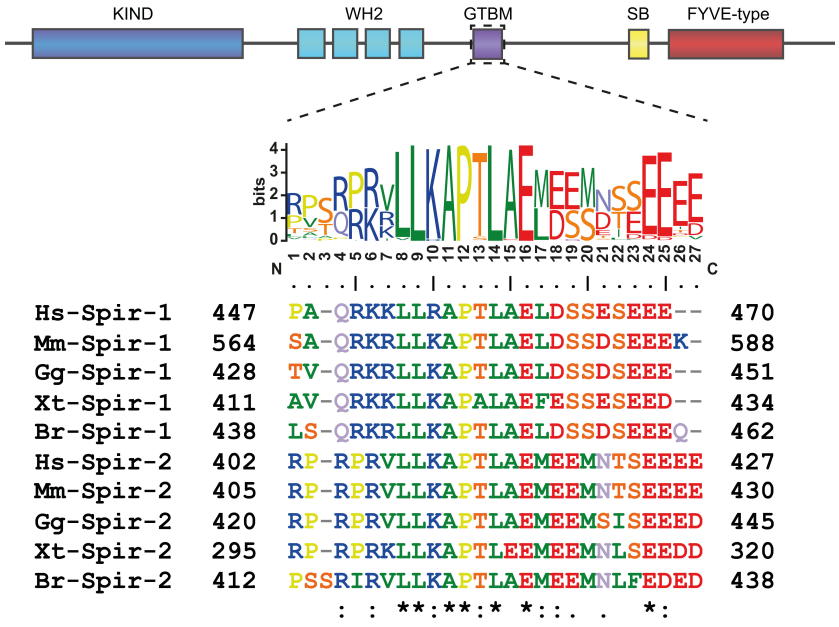

Figure 20 | The Spir GTBM contains highly conserved amino acid clusters with distinct chemical properties. A multiple sequence alignment of the 27 amino acid spanning conserved sequence motif within the central Spir linker region from chosen vertebrate Spir-1 and Spir-2 amino acid sequences is presented. The motif is composed of a positively charged basic amino acid cluster at the beginning and two negatively charged acidic clusters in the middle and at the end. Note the two highly conserved leucine residues within the basic cluster (L408, L409 for human Spir-2). The WebLogo of the respective sequence parts from 223 Spir sequences shows the abundance of individual amino acids at each sequence position. Species abbreviations: *Homo sapiens* (Hs), *Mus musculus* (Mm), *Gallus gallus* (Gg), *Xenopus tropicalis* (Xt), *Brachydanio rerio* (Br). 100% sequence identity is indicated with an asterisk (*). Numbers indicate amino acids.

3.3 Spir/MyoV complex formation depends on the highly conserved sequence motif

In order to analyse if the newly identified Spir GTBM is indeed required for the Spir/MyoV interaction, co-IP studies were performed employing several GFP-tagged MyoVb and Myc-epitope-tagged Spir-1 and Spir-2 full-length proteins and deletion mutants (*Figure 21*). A C-terminal MyoVb protein (AcGFP-MyoVb-CC-GTD) co-precipitates with both full-length Spir proteins (Myc-Spir-1-FL and Myc-Spir-2-FL), which again proves the co-existence of Spir and MyoV in a protein complex. Importantly, also the globular tail domain of MyoVb (AcGFP-MyoVb-GTD) alone co-precipitates with Spir-2 showing that the MyoVb GTD is required and sufficient for Spir interaction. In order to reveal if the newly identified short sequence motif within the Spir linker region (GTBM) is indeed essential for MyoV interaction, Myc-tagged Spir-2 deletion mutants were generated which either express (Myc-Spir2-GTBM-SB-FYVE) or not express (Myc-Spir2-SB-FYVE) the conserved motif and were analysed if they co-precipitate with AcGFP-MyoVb-GTD. Interestingly, Myc-Spir2-GTBM-SB-FYVE indeed co-precipitates with the MyoVb GTD, whereas Myc-Spir2-SB-FYVE does not. This strongly points towards the necessity of the Spir GTBM for MyoV interaction.

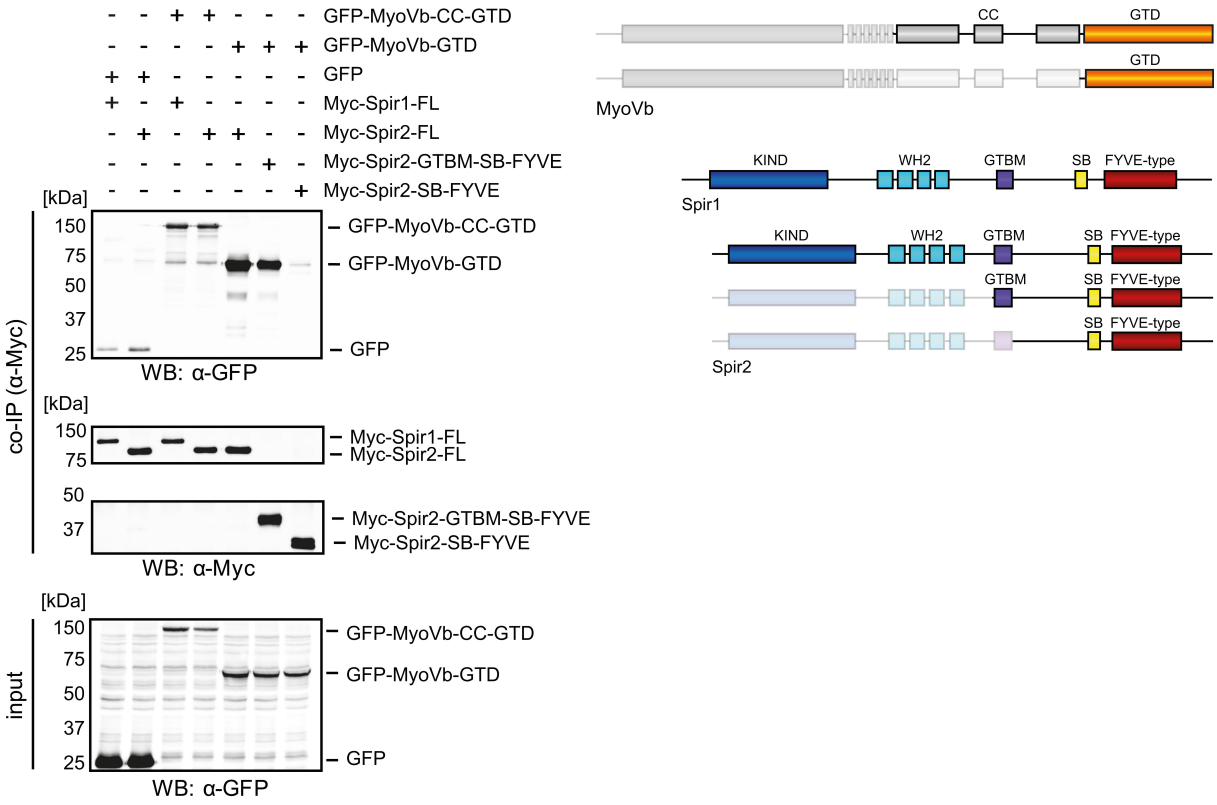

Figure 21 | Complex formation of Spir and MyoVb depends on the MyoVb GTD and the Spir GTBM. Co-immunoprecipitation (co-IP) assays of HEK293 cells expressing AcGFP-tagged MyoVb deletion mutants and Myc-epitope tagged Spir-1 and Spir-2 proteins. Cell lysates were immunoprecipitated with anti-c-Myc antibodies. Cell lysates (input) and immunoprecipitates were analysed by immunoblotting (anti-GFP, anti-c-Myc). The Spir-2 GTBM and the MyoVb GTD were identified to be essential for the Spir/MyoV interaction. Only faint background bands are observed when using AcGFP as a negative control. An overview of the employed protein fragments is presented and the domains used for interaction studies are highlighted. N = 4 experimental repeats. *CC*, coiled-coil; *GTD*, globular tail domain; *FL*, full-length; *WB*, Western blot.

Important to note, also the MyoVa GTD binds to Spir-2 as was shown by co-IP experiments (*Figure 22*). Again, the Spir-2 GTBM was crucial for the Spir/MyoVa interaction in the same way as it was shown for MyoVb. These results are in accordance with overlapping cellular functions of MyoVa and MyoVb proteins, common interaction partners and mechanisms for Rab11 vesicle transport.

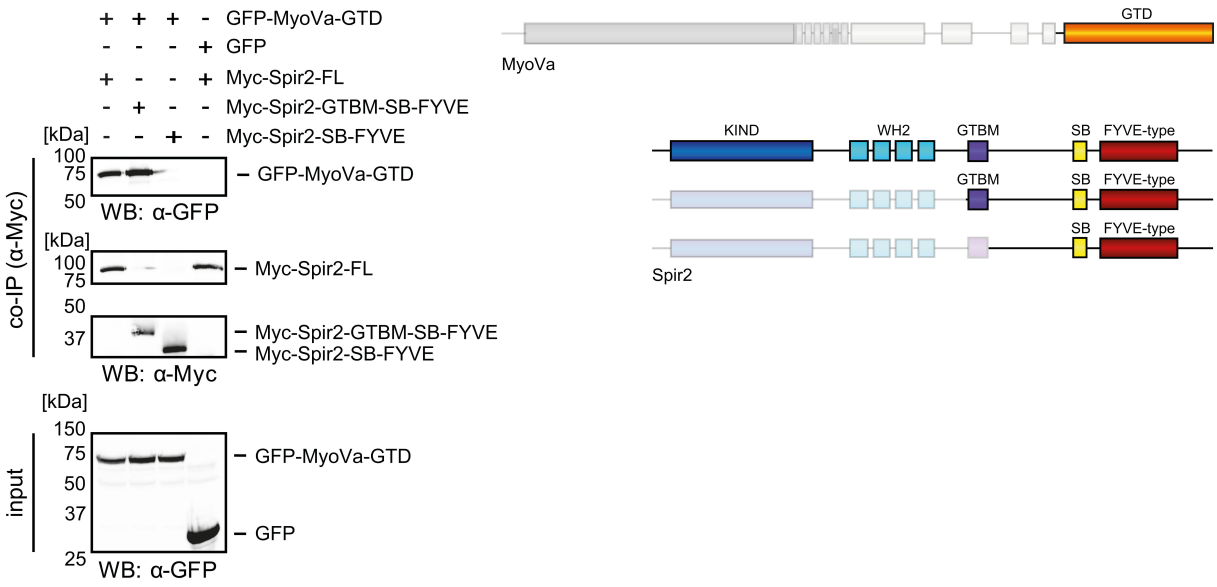

Figure 22 | Complex formation of Spir-2 and MyoVa-GTD depends on the Spir-2 GTBM. Co-immunoprecipitation (co-IP) assays of HEK293 cells expressing AcGFP-tagged MyoVa-GTD and Myc-epitope tagged Spir-2 deletion mutants. Cell lysates were immunoprecipitated with anti-Myc antibodies. The cell lysates (input) and immunoprecipitates were analysed by immunoblotting (anti-GFP, anti-Myc). The Spir-2 GTBM is crucial for MyoVa-GTD interaction. An overview of the employed protein fragments is presented and the domains used for interaction studies are highlighted. N = 2 experimental repeats. *GTD*, globular tail domain; *SB*, Spir-box; *FL*, full-length; *WB*, Western blot.

The Spir GTBM consists of distinct amino acid clusters with distinct chemical properties (compare *Figure 20*), i.e. positive and negative charge distributions and hydrophobic residues. In order to identify essential residues involved in the Spir/MyoV interaction, the minimal interaction sequence of the Spir-2 GTBM was mapped (*Figure 23*). Co-IP studies employing a set of Myc-epitope-tagged N-terminal and C-terminal Spir-2 deletion mutants starting or ending with distinct amino acid clusters (*Figure 23B*) and AcGFP-tagged MyoVb-GTD proteins shows that the C-terminal Myc-Spir2-398-714 (complete GTBM) and the N-terminal Myc-Spir2-2-423 (ending after the first acidic cluster) co-precipitate with AcGFP-MyoVb-GTD, whereas the C-terminal Myc-Spir2-411-714 (starting after the basic cluster) and the N-terminal Myc-Spir2-2-410 (ending after the basic cluster) do not (*Figure 23A*). Taken together, only the basic cluster at the beginning and the first acidic cluster in the middle of the conserved Spir GTBM are indispensable for Spir/MyoV interaction (*Figure 23C*). This means that the

second acidic cluster at the end is not necessarily required for MyoV interaction, although an indirect involvement in terms of strength, stability and specificity of the interaction might not be excluded.

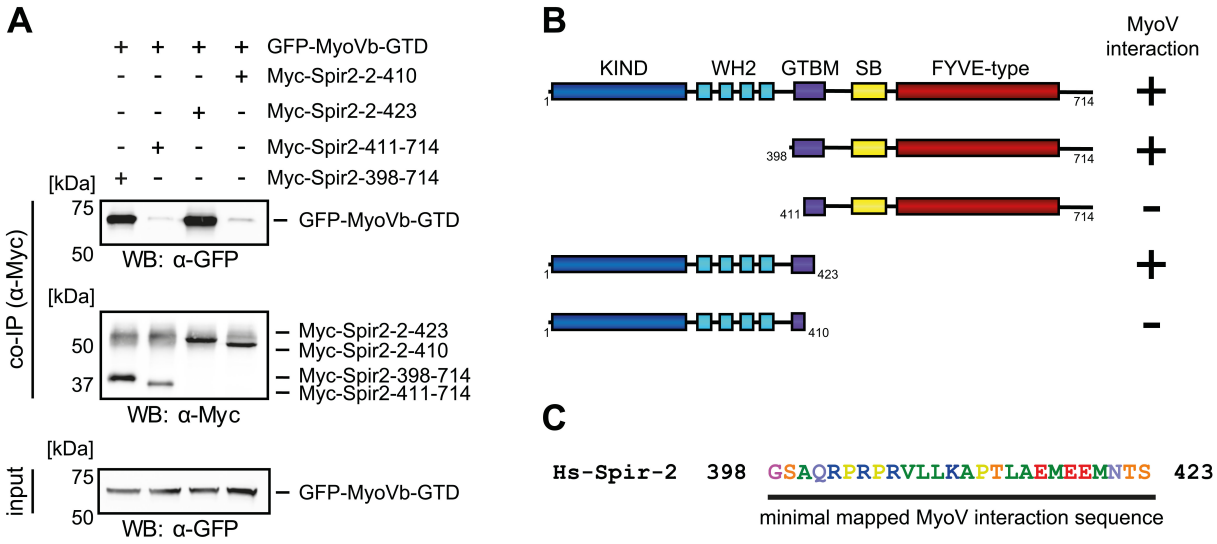

Figure 23 | Mapping of the Spir-2 myosin V interaction sequence. (*A*) Co-immunoprecipitation (co-IP) experiments employing AcGFP-tagged MyoVb-GTD (GFP-MyoVb-GTD) as well as N-terminal and C-terminal Spir-2 deletion mutants show MyoVb-GTD co-precipitation with the C-terminal Myc-Spir2-398-714 and the N-terminal Myc-Spir2-2-423 fragments. MyoVb-GTD does not co-precipitate with C-terminal Myc-Spir2-411-714 and N-terminal Myc-Spir2-2-410 fragments. Numbers indicate amino acids. N = 2-4 experimental repeats. **(*B*)** Overview of the Spir-2 deletion mutants used in (*A*) compared to full-length Spir-2 (amino acids 1-714) and their capacity to interact (+) or not interact (-) with MyoVb-GTD. **(*C*)** The minimal mapped Spir/MyoV interaction sequence of human Spir-2 contains amino acids 398 to 423 and involves the basic cluster at the beginning and the first acidic cluster in the middle of the Spir-2 GTBM. *GTD*, globular tail domain; *SB*, Spir-box; *WB*, Western blot.

3.4 Spir-2 and MyoV proteins interact directly *in vitro*

The data obtained so far showed that Spir proteins co-exist in a protein complex with MyoVa and MyoVb, respectively, which is mediated by the MyoV GTD and the Spir GTBM. Nevertheless, the formation of a protein complex including Spir and MyoV proteins could also be mediated or supported by additional proteins and complex members and does *per se* not argue for a direct interaction of both proteins. Thus, to examine a direct physical interaction of Spir and MyoV proteins, GST-pulldown studies were performed using bacterially expressed and purified recombinant Spir-2-linker peptides and MyoVa/MyoVb-GTD proteins (*Figure 24A*). Here, both, GST-MyoVa-GTD and GST-MyoVb-GTD, are able to pull a His_6-mCherry-tagged Spir-2-linker protein (mCherry-Spir2-linker), strongly suggesting a direct protein interaction of Spir and MyoV. As mentioned above, the Spir GTBM contains two highly conserved leucine residues (L408, 409 for human Spir-2), which might contribute to the protein interactions. The binding of a mutant Spir-2-linker peptide in which these two leucines are substituted by alanines (L408A, L409A; His_6-mCherry-Spir-2-linker-LALA, mCherry-

Spir2-linker-LALA) is strongly reduced compared to the wild-type GTBM, emphasising the relevance of the two leucine residues for the Spir/MyoV interaction. GST and His_6-mCherry proteins were used as controls and did not show any binding.

In order to gain deeper insights about binding strength and significance of the His_6-mCherry-Spir-2-linker:MyoV-GTD complexes, the equilibrium constants (or dissociation constants, K_d) for the His_6-mCherry-Spir-2-linker:MyoVa-GTD and His_6-mCherry-Spir-2-linker:MyoVb-GTD complexes were determined by fluorescence-spectroscopic measurements of the His_6-mCherry-tagged Spir-2-linker peptide with increasing concentrations of GST-MyoVa-GTD and GST-MyoVb-GTD, respectively (*Figure 24B*). For both complexes, the K_d is in the higher nanomolar range (728 ± 113 nM for His_6-mCherry-Spir-2-linker:MyoVa-GTD, and 377 ± 84 nM for His_6-mCherry-Spir-2-linker:MyoVb-GTD). The binding curves saturated at 40% since the His_6-mCherry-Spir-2-linker protein preparation contained C-terminal incomplete protein products, which are still fluorescent but cannot interact with MyoV-GTD. The Spir-2-linker region is predicted to be highly unstructured, which may be the reason for the relative instability of the recombinant His_6-mCherry-Spir-2-linker fusion protein.

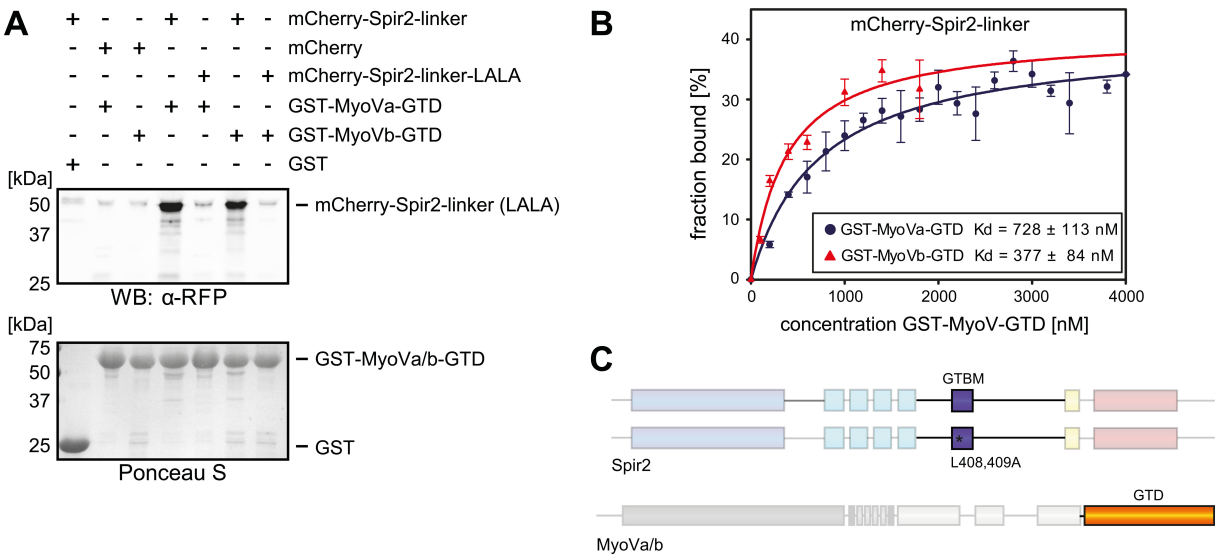

Figure 24 | Spir-2 directly interacts with MyoVa and MyoVb GTDs. (*A*) GST-pulldown studies employing purified bacterially expressed recombinant proteins to analyse a direct interaction of Spir-2 with MyoVa and MyoVb are shown. Both, GST-MyoVa-GTD and GST-MyoVb-GTD, pull the His_6-mCherry-Spir-2-linker (mCherry-Spir2-linker) protein as detected by immunoblotting (anti-RFP), arguing for a direct protein interaction. The substitution of two highly conserved leucine residues within the Spir-2 GTBM to alanines (human Spir-2-L408A,L409A; mCherry-Spir2-linker-LALA; compare *Figure 20*) largely impairs binding of this mutant to GST-MyoVa/Vb-GTD. Only faint background bands are detected using the GST protein or the His_6-mCherry protein as controls. Ponceau S staining shows equal loading of GST-fusion proteins. N = 4 experimental repeats. **(*B*)** Fluorescence spectroscopy was used to determine the dissociation constants (K_d) for MyoVa (blue) and MyoVb GTD (red) binding to mCherry-Spir2-linker (aa 361-519 of human Spir-2). *Error bars* represent SEM (n = 4 experimental repeats). **(*C*)** An overview of the employed protein fragments is presented and the domains used for interaction studies are highlighted. *GTD*, globular-tail-domain; *LALA*, L408,409A; *WB*, Western blot.

3.5 The Spir GTBM is necessary for colocalisation of Spir-2 and MyoV at vesicle membranes

Spir and MyoV proteins were shown to directly interact with each other *in vitro*. It was assumed that the functional cooperation of Spir actin nucleators and Rab11 small GTPases in vesicle transport processes is mediated by MyoV actin motor proteins linking Spir and Rab11 at the same vesicle membranes thereby determining the vesicle identity. In line with that, further analysis was aimed to decipher if Spir and MyoV proteins also colocalise and interact in eukaryotic cells at vesicle membranes. Co-expression of GFP-tagged full-length MyoVa and MyoVb proteins (eGFP-MyoVa-FL, AcGFP-MyoVb-FL), respectively, and Myc-epitope-tagged full-length Spir-2 (Myc-Spir2-FL) in HeLa cells revealed that both, MyoVa and MyoVb, perfectly colocalise with Spir-2 at vesicle membranes (*Figure 25*).

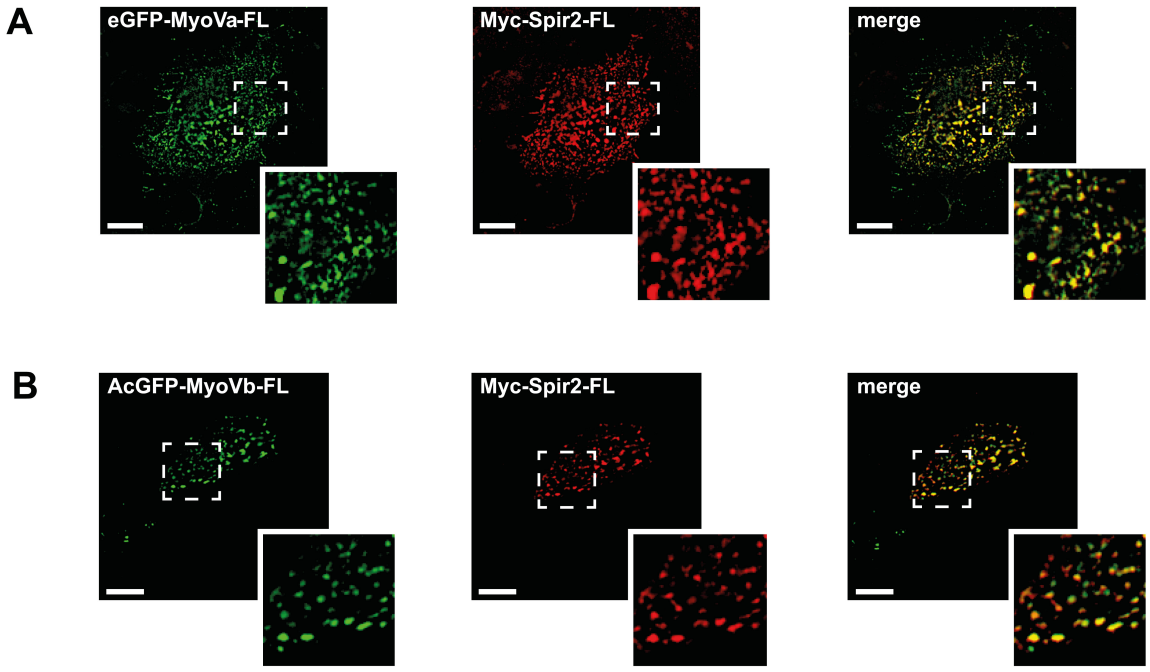

Figure 25 | Myosin V and Spir-2 colocalise at vesicle membranes. Both, GFP-tagged full-length MyoVa (eGFP-MyoVa-FL; green; ***A***) and GFP-tagged full-length MyoVb (AcGFP-MyoVb-FL; green; ***B***), colocalise with Myc-epitope-tagged full-length Spir-2 (Myc-Spir2-FL; red) at vesicle membranes when transiently co-expressed in HeLa cells, as indicated by overlapping punctae (merge; yellow; see also higher magnification in insets). 5 cells were recorded for each condition and one representative cell is presented here. *Scale bars* represent 10 µm.

As a proof of principle, the requirement of the Spir GTBM for Spir-2 colocalisation with MyoV at vesicle membranes was investigated by co-expression of GFP-tagged MyoVa and MyoVb GTD (AcGFP-MyoVa-GTD, AcGFP-MyoVb-GTD), respectively, and Myc-tagged Spir-2 deletion mutants carrying (Myc-Spir2-GTBM-SB-FYVE) or not carrying (Myc-Spir2-SB-FYVE) the conserved sequence motif necessary for MyoV binding *in vitro* (*Figure 26*). All proteins show a vesicular localisation by itself when expressed alone, as expected (*Figure 26A*). AcGFP-MyoVa-GTD perfectly colocalises with

Myc-Spir2-GTBM-SB-FYVE (*Figure 26B, upper panel*) just as the full-length proteins do (compare *Figure 25*). In contrast, Myc-Spir2-SB-FYVE does only in part colocalise with MyoVa-GTD and is also localised to vesicles on which MyoVa-GTD is not present (*Figure 26B, lower panel*). Here, MyoVa-GTD is also largely localised to the nucleus which was not observed when co-expressed with Myc-Spir2-GTBM-SB-FYVE. Identical results were obtained employing the MyoVb GTD. AcGFP-MyoVb-GTD perfectly colocalises with Myc-Spir2-GTBM-SB-FYVE at vesicle membranes (*Figure 26C, upper panel*), whereas the localisation of MyoVb-GTD and Myc-Spir2-SB-FYVE does not largely overlap (*Figure 26C, lower panel*). In summary, these data indeed show that the highly conserved Spir GTBM is not only essential for the direct interaction of Spir and MyoV proteins *in vitro*, but for the colocalisation of both proteins in eukaryotic cells at vesicle membranes as well.

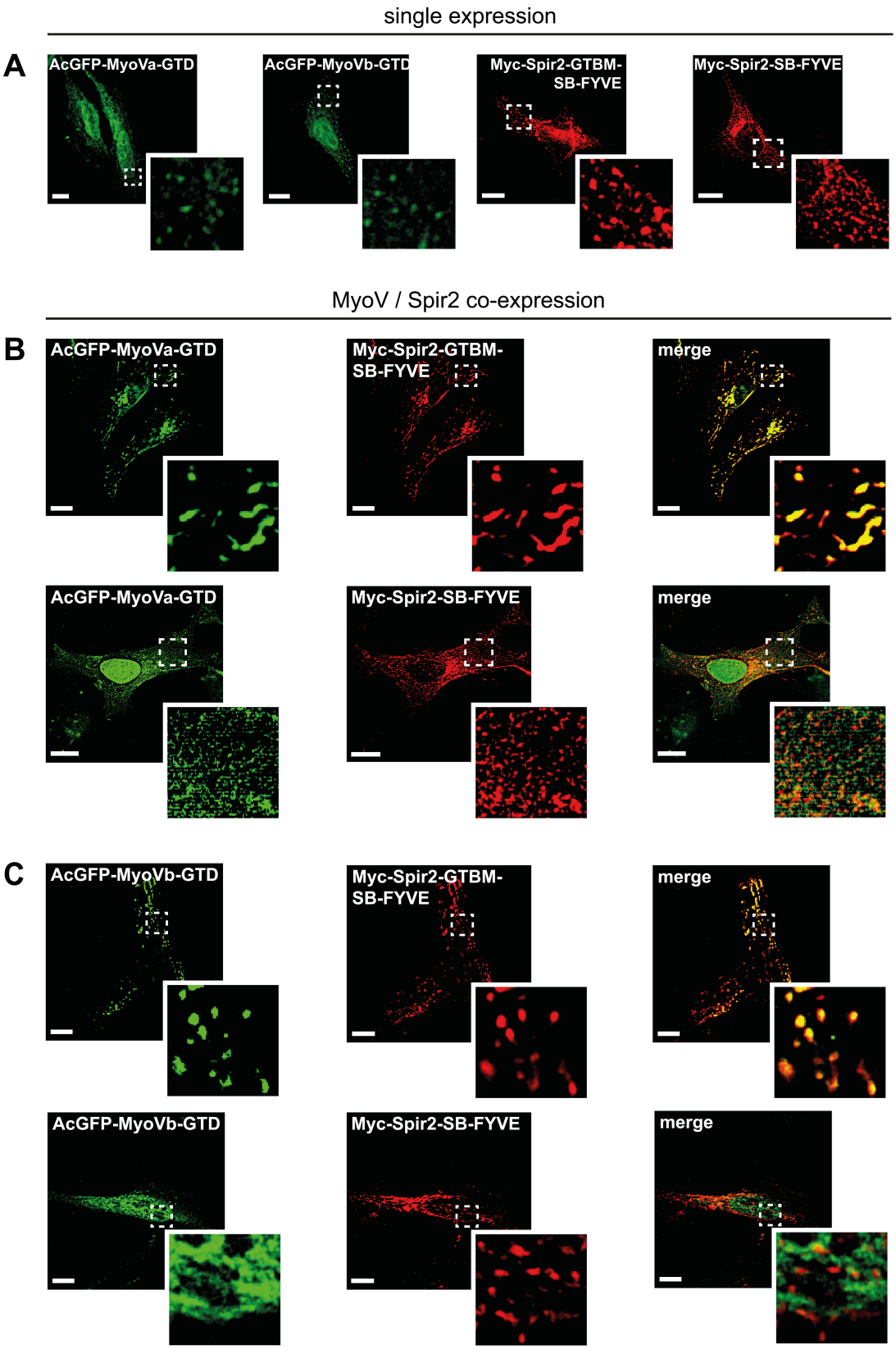

Figure 26 | MyoVa and MyoVb GTDs colocalise with Spir-2 at vesicle membranes depending on the Spir-2 GTBM. (*A*) AcGFP-MyoVa-GTD, AcGFP-MyoVb-GTD, Myc-Spir2-GTBM-SB-FYVE and Myc-Spir2-SB-FYVE show a typical vesicular localisation pattern when expressed alone. **(*B and C*)** AcGFP-tagged GTDs of MyoVa (*B*) and MyoVb (*C*), respectively, (green) were transiently co-expressed with Myc-tagged Spir-2 deletion mutants (red) in HeLa cells. **(*B*)** MyoVa-GTD perfectly colocalises with Spir-2 in a vesicular pattern only in presence of the Spir-2 GTBM (Myc-Spir2-GTBM-SB-FYVE; upper panel) as indicated by overlapping punctae (merge; yellow; see also higher magnification in insets) but not in its absence (Myc-Spir2-SB-FYVE; lower panel). **(*C*)** MyoVb-GTD also perfectly colocalises with Spir-2 only in presence of the Spir-2 GTBM

(Myc-Spir2-GTBM-SB-FYVE; upper panel) as indicated by overlapping punctae (merge; yellow; see also higher magnification in insets) but not in its absence (Myc-Spir2-SB-FYVE; lower panel). Fixed cells are shown in each case, using the auto-fluorescence of the GFP-tag and immunostainings against the Myc-epitope tag (TRITC-conjugated secondary antibodies) for fluorescence microscopic image recording. 5 cells were recorded for each condition and one representative cell is presented here. *Scale bars* represent 10 µm.

3.6 Spir-2 and MyoV proteins directly interact at vesicle membranes

In order to exclude a random colocalisation of Spir-2 and MyoV proteins at vesicle membranes and, thus, to prove a direct MyoVa and Spir-2 interaction at vesicle surfaces, FLIM-FRET (fluorescence lifetime imaging, Förster resonance energy transfer) microscopy studies were performed to unravel the molecular interactions of Spir-2 and MyoVa in living cells at vesicle membranes, depending on the Spir-2 GTBM (*Figure 27*). These experiments were done in collaboration with Dr. Thomas Weidemann (Max Planck Institute of Biochemistry, Martinsried, Germany). The fluorescence lifetime of a donor fluorophore is measured in presence of an acceptor fluorophore. If donor and acceptor fluorophores are in close proximity (max. distance of 10 nm; (351)), the fluorescence energy is transferred from the excited donor to the acceptor, reducing the fluorescence lifetime of the donor. If donor and acceptor fluorophores are spatially separated, the energy transfer is not possible and the fluorescence lifetime is comparable to that of the donor alone. AcGFP-MyoVa-GTD was used here as the fluorescence donor. Several C-terminal Spir-2 fragments were used as the fluorescence acceptors: the MyoV binding incompetent mStrawberry-Spir2-SB-FYVE and mStrawberry-Spir2-GTBM-SB-FYVE-LALA mutants, and the MyoV interacting mStrawberry-Spir2-GTBM-SB-FYVE fragment. The fluorescence lifetime of the AcGFP-MyoVa-GTD donor was measured at vesicle membranes when expressed alone or when co-expressed with either of the fluorescence acceptors. The fluorescence lifetime of AcGFP alone was measured to test for AcGFP-MyoVa-GTD homo-FRET signals. As a positive FLIM-FRET control, an AcGFP-linker-mStrawberry construct was used. The isolated GTDs of MyoV proteins have been observed to be monomeric in solution, showing that they do not interact with each other by themselves (revealed by gel filtration experiments) (211). Therefore, AcGFP-MyoVa-GTD was co-expressed with an mStrawberry-tagged version (mStrawberry-MyoVa-GTD) to exclude FRET signals due to dense vesicle packaging (high protein concentrations at the vesicle surface). Based on the measured donor fluorescence lifetime, the FRET efficiency *E* was calculated for each condition with:

$$E = 1 - \frac{\tau_{DA}}{\tau_D}$$

with τ_D is the fluorescence lifetime of the donor alone and τ_{DA} in presence of an acceptor (352).

The positive FLIM-FRET control (AcGFP-linker-mStrawberry) reveals a FRET efficiency of 20.9% (median value; *Figure 27C*). Compared to that, the FRET efficiency of AcGFP-MyoVa-GTD alone is

completely abolished (0.0% FRET efficiency) and is even lower than that of the AcGFP fluorescent protein alone (1.4% FRET efficiency). Only a slight increase in FRET efficiency is observed when AcGFP-MyoVa-GTD is co-expressed with free floating mStrawberry proteins (2.2% FRET efficiency). A strong increase in FRET efficiency of the AcGFP-MyoVa-GTD donor is observed when co-expressed with a C-terminal Spir-2 fragment containing the GTBM for MyoV interaction, and the Spir-box and FYVE-type zinc-finger for vesicle membrane targeting (mStrawberry-Spir2-GTBM-SB-FYVE; 14.7% FRET efficiency). As the donor fluorescence lifetime reduction is only possible if MyoVa and Spir-2 proteins are in close proximity (within 10 nm of distance between the fluorophores), these results strongly support a direct interaction of MyoVa and Spir-2 at vesicle membranes. In contrast, co-expression of a C-terminal Spir-2 fragment only encoding Spir-box and the FYVE-type zinc-finger (mStrawberry-Spir2-SB-FYVE; 1.6% FRET efficiency) and the Spir-2 GTBM-LALA mutant protein (mStrawberry-Spir2-GTBM-SB-FYVE-LALA; 2.4% FRET efficiency), respectively, both of which do not interact with MyoVa-GTD, do not alter the fluorescence lifetime of the AcGFP-MyoVa-GTD donor. Co-expression of mStrawberry-MyoVa-GTD (2.0% FRET efficiency) does also not increase the FRET efficiency compared to AcGFP-MyoVa-GTD alone. This shows that there is no false positive FRET signal due to dense protein packing on vesicle surfaces and further indicates that a direct interaction of MyoVa-GTD and the Spir-2-GTBM is required for the observed FLIM-FRET signal.

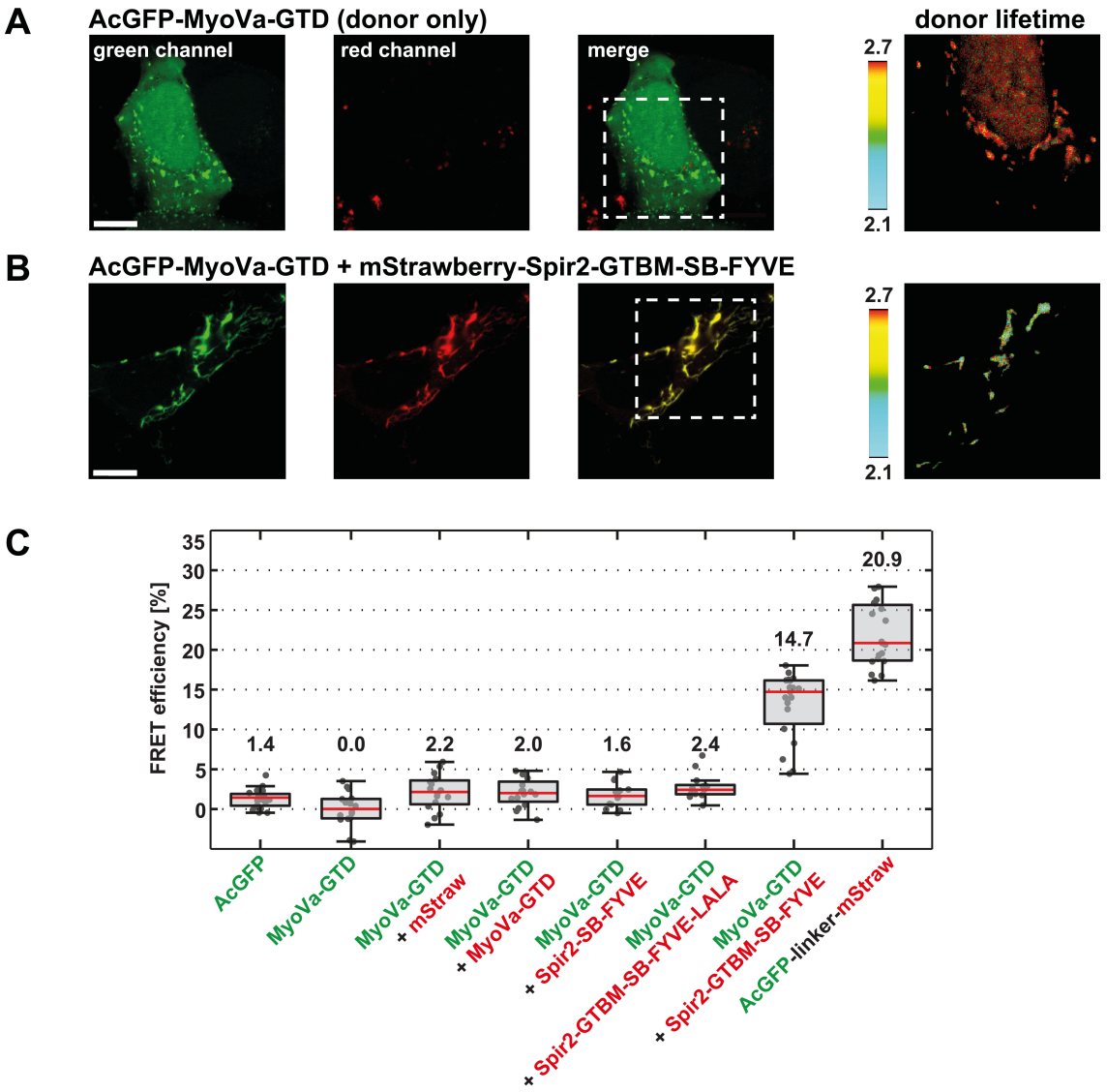

Figure 27 | FLIM-FRET analysis of transiently expressed AcGFP-tagged MyoVa-GTD (donor) and mStrawberry-tagged C-terminal Spir proteins (acceptors) at vesicle membranes in HeLa cells. (*A and B*) Representative cells showing the lifetime shift due to FRET. Confocal fluorescence images (green channel, AcGFP; red channel, mStrawberry; and fluorescence lifetime images of the AcGFP-tagged donor) of AcGFP-MyoVa-GTD expressed alone (*A*), and in presence of the interacting acceptor mStrawberry-Spir-2-GTBM-SB-FYVE (*B*) are shown. *Scale bar* represents 10 µm. **(*C*)** The average FRET efficiencies per cell measured at vesicle membranes are presented for the indicated transiently expressed donor-acceptor combinations. A box-and-whisker plot is shown with every dot representing a single cell. The region of interest (ROI) was manually confined to the cytoplasm (average FRET efficiencies for AcGFP alone and the AcGFP-linker-mStrawberry positive control). For all other experiments, the ROI was further reduced by a threshold algorithm that identifies vesicles in the AcGFP channel. Box-and-whisker plots indicate 2nd and 3rd quartile (box), median (red horizontal line), and 1.5x interquartile range (whiskers). The median value is also indicated above each box. 10-15 cells have been analysed for each condition.

3.7 Crystal structure of the MyoVa-GTD:Spir-2-GTBM complex

In collaboration with Prof. Dr. Anne Houdusse and Dr. Olena Pylypenko (Institut Curie, Paris, France), the direct interaction of Spir and MyoVa proteins was further characterized by solving the crystal structure of the MyoVa-GTD:Spir-2-GTBM complex (PDB ID 5JCY; *Figure 28*) to get a deeper insight into the contributing amino acids and the underlying molecular interactions within the complex at atomic detail. The MyoV globular tail domain is composed of two subdomains, the N-terminal subdomain 1 (SD-1) and the C-terminal SD-2 (210). The Spir-2-GTBM peptide binds to SD-1 of the MyoVa GTD in an extended conformation in the cleft between helices H3 and H5 of the GTD. At the end, the peptide forms a two-turn alpha helix. Importantly, the Spir-2-GTBM residues involved in MyoV-GTD interaction (see *Figure 30* for more detail) are conserved among Spir proteins (compare *Figure 20),* which is also consistent with the data obtained from Spir-1 binding assays (compare *Figure 21*). The MyoVa GTD undergoes only minor conformational changes when bound to the Spir-2 GTBM (211). The Spir-GTBM binding pocket is structurally conserved in MyoVa and MyoVb (211), which is also in line with the Spir capacity to physically interact with both, MyoVa and MyoVb GTDs (compare *Figure 24*). The Spir binding pockets of MyoVa and MyoVc differ in some way, although the overall structures of MyoVa and MyoVc proteins are similar (211). Direct protein interaction studies revealed binding of Spir-2-GTBM to MyoVc-GTD in a micromolar range (211). Nevertheless, MyoVc is considerably different from MyoVa and MyoVb regarding functionality, expression patterns and in terms of its inability to bind to Rab11 (207), and was therefore not further investigated here.

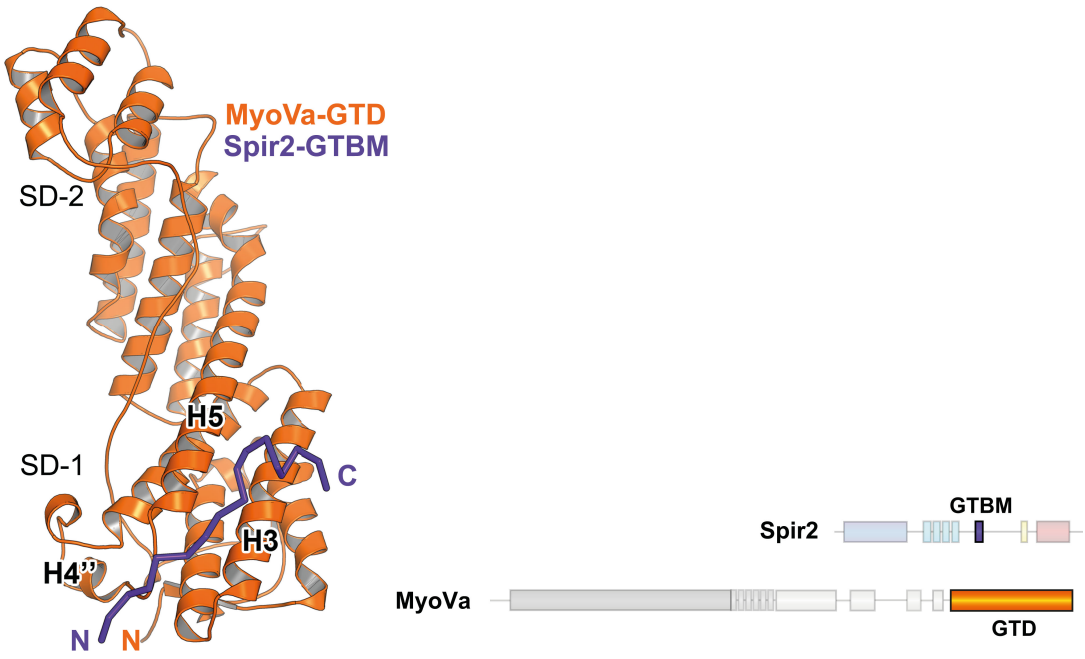

Figure 28 | Crystal structure of the MyoVa-GTD:Spir-2-GTBM complex. The Spir-2 GTBM peptide (purple) binds in an extended conformation to subdomain 1 (SD-1) of MyoVa-GTD (orange), between helix 3 (H3) and helix 5 (H5). An overview of employed proteins is presented and the domains used for structural analysis are highlighted. *GTD*, globular tail domain; *SD*, subdomain; *H*, helix.

3.8 Similarities and differences between Spir and MLPH binding to MyoVa-GTD

Of importance, the Spir GTBM was found to bind to the same site of MyoVa-GTD as was shown before to be involved in the direct interaction with the melanophilin (MLPH) protein (210, 353). MLPH is a critical component for the transport of melanosomes to the periphery of melanocytes, which ultimately drives skin and hair pigmentation (80, 83, 175). Here, MLPH forms a tripartite complex with the myosin Va actin motor protein and the melanosome associated Rab27a GTPase (83). Interestingly, MLPH and Spir proteins share a similar domain organisation with similar functions (*Figure 29*). In principle, both proteins consist of a vesicle membrane targeting unit, a MyoV/MyoVa interaction unit, and an actin nucleation (Spir: KIND and WH2) and F-actin binding (MLPH: ABD) unit, respectively.

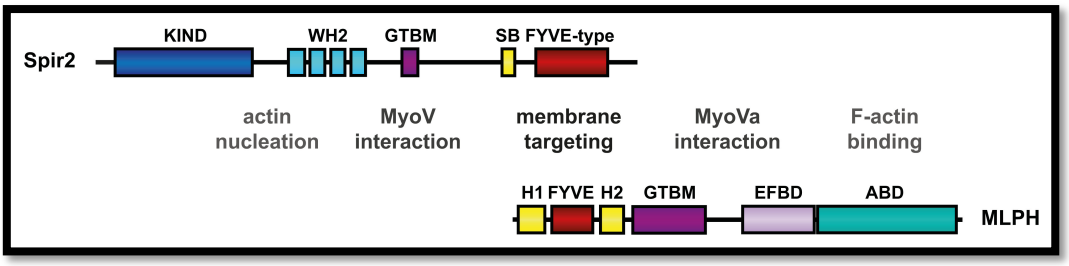

Figure 29 | Spir and MLPH proteins share a similar domain organisation. Comparison of the Spir-2 and MLPH protein domain organisation shows the presence of similar functional units. Both proteins share a MyoV protein interaction unit in their central regions (GTBM for Spir-2; GTBM and exon-F binding domain (EFBD) for MLPH). Both proteins encode a membrane targeting unit at their C-terminus (Spir-2) and N-terminus (MLPH), respectively, consisting of a FYVE-type zinc-finger and a related potential small GTPase binding Spir-box (SB, in Spir-2) and synaptotagmin-like protein homology domains (H1 and H2, in MLPH). The MLPH-H1-FYVE-H2 cluster is essential for MLPH interaction with Rab27a (354). Both proteins share an actin interaction cluster as well, where Spir-2 encodes an actin nucleating KIND/WH2 cluster at its N-terminus, and MLPH encodes an F-actin binding domain (ABD) at its C-terminus. Adapted and modified from Pylypenko, Welz et al., 2016 (211). Information on the MLPH domain organisation from Hume et al., 2006 (355).

By its synaptotagmin homology domains (SHD1, SHD2), MLPH binds to activated Rab27a on melanosome membranes and recruits MyoVa (81, 83, 84, 354–357), probably supported by the FYVE-type zinc-finger located between SHD1 and SHD2. Spir proteins non-specifically bind to negatively charged intracellular membranes by its FYVE-type zinc-finger (327). In contrast to Spir proteins, MLPH owns two MyoVa binding regions. First, the GTBD which interacts with the globular tail domain (originally, this binding site was termed GTBD (355); due to its characteristics of being rather a short sequence motif instead of a structured domain and for better comparison with the Spir GTBM it will here also be termed *MLPH GTBM*). Second, the exon-F binding domain (EFBD) interacts with exon F encoded myosin Va sequences (see also *Introduction, Figure 9*) (108, 355).

Both, Spir-2-GTBM and MLPH-GTBM, bind to MyoVa-GTD within a similar range of micromolar affinities (210, 211). Spir-2-GTBM and MLPH-GTBM are similar regarding the N-terminal regions of the conserved sequence motifs (*Figure 30B,C*) and comparing the two complex structures

demonstrates that both GTBMs interact with MyoVa-GTD in an analogical way. A network of hydrogen bonds is formed with the H4''-H5-loop of the GTD and two conserved leucine residues of the motifs (L408 and L409 in human Spir-2; L188 and L189 in mouse MLPH) are located in equivalent positions within cavities of the MyoVa-GTD surface (*Figure 30B,C; lower panels*). As mentioned before, the substitution of the two highly conserved Spir-2 leucine residues by alanines significantly impairs Spir-2 binding to MyoVa/b-GTD (*Figure 24A*). The C-terminal parts of the Spir-2 GTBM and the MLPH GTBM differ from each other and, thus, show distinct binding modes (*Figure 30B,C; upper panels*). The MLPH GTBM specifically binds to the GTD of MyoVa, in contrast to the Spir GTBM interacting with all three MyoV isoforms. The MLPH-GTBM:MyoVa-GTD complex formation requires a conformational flexibility of the MyoVa GTD to accommodate F191, a conserved hydrophobic residue (Phe, Ile or Val) in melanophilin (210, 353) (*Figure 30C, upper panel*). At the position corresponding to MLPH-F191, Spir-2-GTBM has the highly conserved A411 residue. This alanine residue allows binding without conformational changes of MyoV-GTD (*Figure 30B, upper panel*).

Spir GTBM and MLPH GTBM present a similar charge distribution along the sequence motifs. Whereas each N-terminal sequence part is positively charged, their C-terminal parts carry negatively charged residues (*Figure 30B,C*). The charge complementarity described for binding of MLPH-GTBM to MyoVa-GTD (210) is therefore potentially also used by Spir-2-GTBM.

In summary, three characteristics of the conserved sequence motif within Spir (and MLPH) proteins can be described which are demanded for the Spir-GTBM:MyoV-GTD interaction. First, clusters of positive and negative charges in the N-terminal and C-terminal regions, respectively, may facilitate the proper orientation of the peptide towards the GTD surface. Second, an extended N-terminal region of the motif may form hydrogen bonds with backbone atoms of the GTD. Third, hydrophobic residues (for instance L408, L409 in human Spir-2) may anchors in small surface pockets of the GTD.

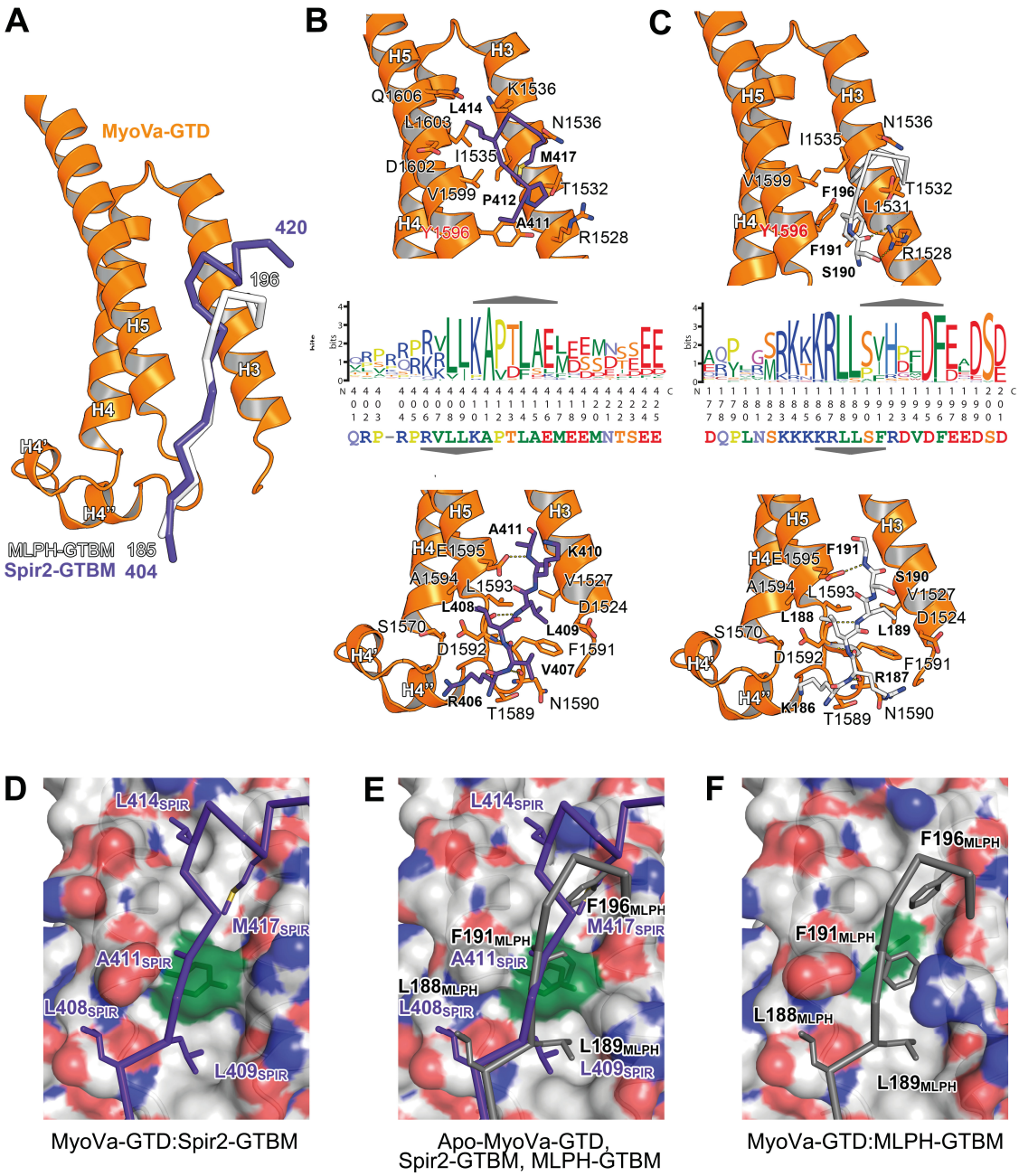

Figure 30 | Direct binding of Spir and MLPH to MyoVa-GTD exhibits similarities and differences. (*A*) Spir-2-GTBM (purple) and MLPH-GTBM (white) bind to the same site of MyoVa-GTD (orange) with binding similarities at the N-termini of Spir and MLPH GTBMs but with differences at their C-termini. **(*B and C*)** *Middle panels*: The Spir GTBM sequence logo indicates sequence conservation in Spir-1 and Spir-2 proteins (compare *Figure 20*); The MLPH GTBM sequence logo indicates sequence conservation in MLPH proteins. The sequence motifs of Spir and MLPH involved in MyoV-GTD binding show a similar charge distribution with positively charged N-terminal regions and negatively charged C-terminal regions and display two highly conserved leucine residues within the N-terminal part of the motif (L408, L409 for human Spir-2; L188, L189 for mouse MLPH). *Lower panels*: N-terminal regions of the Spir-2 GTBM and the MLPH GTBM show some sequence similarities and form similar contacts with MyoVa-GTD. An identical network of hydrogen bonds (dashed lines) involves the side chain of MyoVa-E1595 and main chain atoms of D1592 and N1590 which interact with backbone atoms of the Spir/MLPH peptide. The R406 side chain and the two conserved leucine residues L408 and L409 of human Spir-2 are packed on the MyoVa-GTD surface in a similar way as the K186 side chain, and the conserved leucine residues L188 and L189 of MLPH. *Upper panels*: C-terminal regions of Spir-2-GTBM and MLPH-GTBM are less similar regarding their MyoVa-GTD binding mode. Thus, MLPH-GTBM forms specific contacts with MyoVa-GTD. The Spir-2 hydrophobic residues A411, P412, L414 and M417 are packed in the hydrophobic cleft between the helices H3 and H5 of the MyoVa GTD. Within Spir-2, the conserved L414 side chain anchors the C-terminal Spir-2 fragment. Therefore, the interacting hydrophobic surface is extended in comparison to the binding of MLPH-GTBM. The F191 and F196 side chains of the MLPH GTBM form hydrophobic contacts with residues in the cleft between H3 and H5 of the MyoVa GTD. The side chain of MyoVa-R1528 stabilises the MLPH GTBM by forming

hydrogen bonds with MLPH-S190. The side chain conformation of MyoVa-Y1596 (marked in *red*) is different within the two complexes. That would allow a modulation of the binding surface in order to optimise the binding to the respective target peptide. **(*D*)** Hydrophobic residues anchoring Spir-2-GTBM (purple) on the MyoVa-GTD surface. Spir-2-A411 is packed on top of MyoVa-Y1596 (*green*) side chain. **(*E*)** Spir-2 (purple) and MLPH (grey) GTBMs projected on the surface of apo-MyoVa (PDB ID 4LX1). The apo-MyoVa hydrophobic cleft between the H5 and H3 is compatible with Spir-2 binding, but not with MLPH binding, in which the side chain of F191 clashes with MyoVa-Y1596 (*green*). In the Spir-2 GTBM, the conserved L414 side chain anchors the C-terminal Spir-2 fragment extending the interacting hydrophobic surface compared to MLPH-GTBM binding. (***F***) Hydrophobic residues anchoring MLPH-GTBM (grey) in the MyoVa-GTD pocket (PDB ID 4LX2). MyoVa-Y1596 (*green*) side chain is rotated to bury the side chain within the protein core (see also panel *D*) to accommodate MLPH-F191 in the binding pocket. *GTD*, globular tail domain; *H*, helix; MLPH:MyoVa-GTD complex (PDB ID 4LX2).

3.9 Spir proteins induce MyoVa targeting to vesicle membranes

Up to here, the direct interaction of Spir and MyoV proteins *in vitro* and at vesicle membranes in living cells was shown. The coordination and regulation of a mutual Spir and MyoV membrane targeting is so far unknown. At the inactive state, the myosin V dimer is structurally back-folded by an intramolecular interaction of its two GTDs with its motor domains (98–100) (*Figure 5*). At this state, the ATPase activity of the motor is inhibited (101, 102), and binding of cargo to the GTD or increased Ca^{2+} levels are able to release this inhibition, thereby activating the MyoV dimer (98, 104, 252). The MLPH GTBM was described before to have the capacity to open up the back-folded MyoV conformation and to convert it into an extended conformation (109). In accordance, the ATPase activity of the MyoV dimer was observed to be activated by MLPH *in vitro* (108, 109, 124). Based on the structural similarity between Spir GTBM and MLPH GTBM, as described before, it is intriguing to speculate that the Spir GTBM could play an identical role in opening and activating the MyoV dimer, and finally in the mutual targeting of both proteins to vesicle membranes. Transiently over-expressed GFP-tagged full-length MyoVa proteins (eGFP-MyoVa-FL) show an even cytoplasmic distribution, and known activators, such as Ca^{2+} influx into cells, reorient MyoVa towards vesicular structures, as presented by a punctate pattern across the cell (103). Considering a function of Spir proteins in MyoV activation, the presence of Spir proteins should also reorient MyoVa from a cytoplasmic state towards a vesicular pattern, similar to what was observed before for known activators, in a way that Spir is able to bind to back-folded MyoV in the cytoplasm, probably release the back-folding, and subsequently targets it to vesicle membranes.

In order to test this hypothesis, GFP-tagged full-length MyoVa (eGFP-MyoVa-FL) was transiently expressed in HeLa cells. Unfortunately, the previously described cytoplasmic localisation of MyoVa (103) was not as clear-cut as expected. It was rather the case that the localisation of MyoVa was strongly dependent on the protein expression levels, with high expression leading to vesicular localisation of the protein by itself, and only at low expression levels MyoVa showed the desired even cytoplasmic distribution (*Figure 31B*). Therefore, individual cells were recorded and the sum of pixel grey values, representing the expression levels of eGFP-MyoVa-FL, was measured for each cell. Subsequently, the protein localisation (cytoplasmic vs. vesicular) was correlated to the measured

protein expression levels for individual cells (*Figure 31A*). A box-and-whisker plot was generated that nicely demonstrates the dependence of cellular eGFP-MyoVa-FL localisation on its expression levels. Based on these analyses, the sum of pixel grey values were measured for all cells in the following experimental setups, and only those cells were recorded and further investigated which showed a sum of pixel grey value below 20×10^6, to exclude vesicular MyoVa localisation by itself induced by over-expression artefacts.

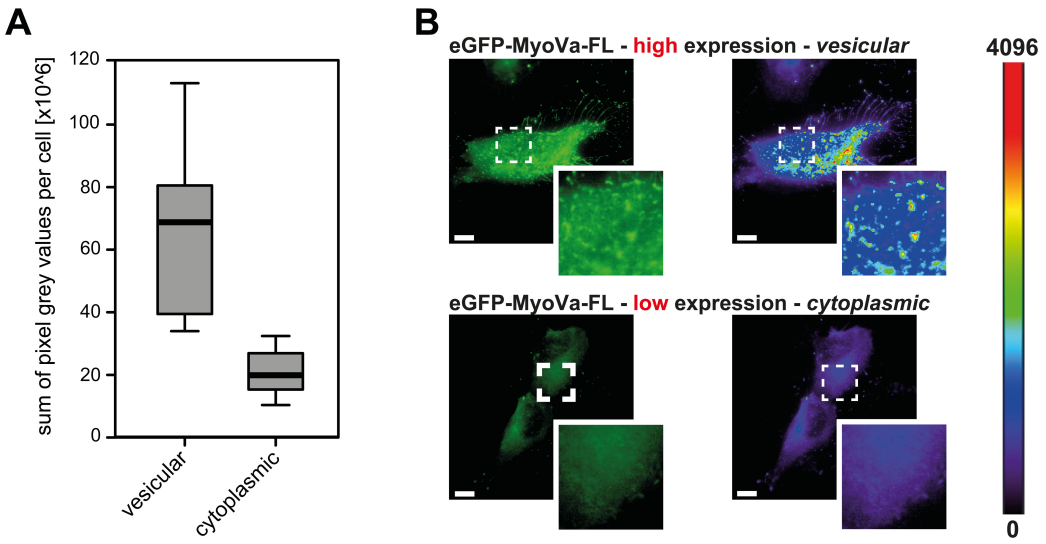

Figure 31 | Myosin Va protein localisation depends on protein expression levels. (*A*) The sum of pixel grey values was determined for individual cells expressing eGFP-MyoVa-FL, and each cell was classified into either *vesicular* or *cytoplasmic* localisation of the MyoVa protein. For both groups, a box-and-whisker plot was generated showing the sum of pixel grey value distribution for each localisation state. A clear correlation was found between protein expression levels and protein localisation with low expression levels leading to cytoplasmic localisation and vice versa. **(*B*)** Representative cells are shown for both, high protein expression leading to vesicular localisation of eGFP-MyoVa-FL (*green* and as *heat map*), and low protein expression leading to cytoplasmic MyoVa localisation. Heat maps represent grey values for MyoVa fluorescence intensities, rising from "0" (black) to "4096" (red), for better demonstration of expression levels and protein accumulation at vesicle membranes under high protein expression conditions.

In subsequent fluorescence microscopy studies, eGFP-MyoVa-FL was co-expressed with N-terminal Spir-2 deletion mutants either carrying (Myc-Spir-2-KIND-WH2-GTBM, Myc-Spir2-KWM) or not carrying (Myc-Spir-2-KIND-WH2, Myc-Spir2-KW) the Spir GTBM required for MyoV interaction (*Figure 32*). As those Spir-2 mutants miss the Spir-box and the FYVE-type zinc-finger, they are not targeted to vesicle membranes by themselves and show a cytoplasmic (and nuclear) localisation when expressed alone (*Figure 32A*). Single expression of eGFP-MyoVa-FL (*Figure 32A*) and co-expression with Myc-Spir2-KW (*Figure 32B, upper panel*) shows and even cytoplasmic distribution of the MyoVa protein. In contrast, co-expression with Myc-Spir2-KWM, which interacts with MyoV proteins *in vitro*, significantly changes the localisation of the MyoVa protein and targets it to vesicular structures (*Figure 32B, middle panel*). Importantly, also the N-terminal Spir-2 mutant is now localised to vesicles

which is not observed when expressed alone (*Figure 32A*), and colocalises with MyoVa at vesicle surfaces.

Furthermore, the melanocyte specific F isoform of MyoVa (carries exon F, but not exon D, preventing interaction with Rab8a and Rab10), which additionally carries the Q1753R point mutation, preventing Rab11 interaction (103) (eGFP-MyoVa-FL-QR), was used as a negative control for membrane targeting. Co-expression of the mutant eGFP-MyoVa-FL-QR and Myc-Spir2-KWM does not change the localisation of mutant MyoVa (*Figure 32B, lower panel*), in contrast to the wild-type MyoVa protein. These results strongly suggest a coordinated and mutual membrane targeting of Spir and MyoV proteins to Rab11 vesicles, most likely to subsequently form a multimeric membrane associated protein complex.

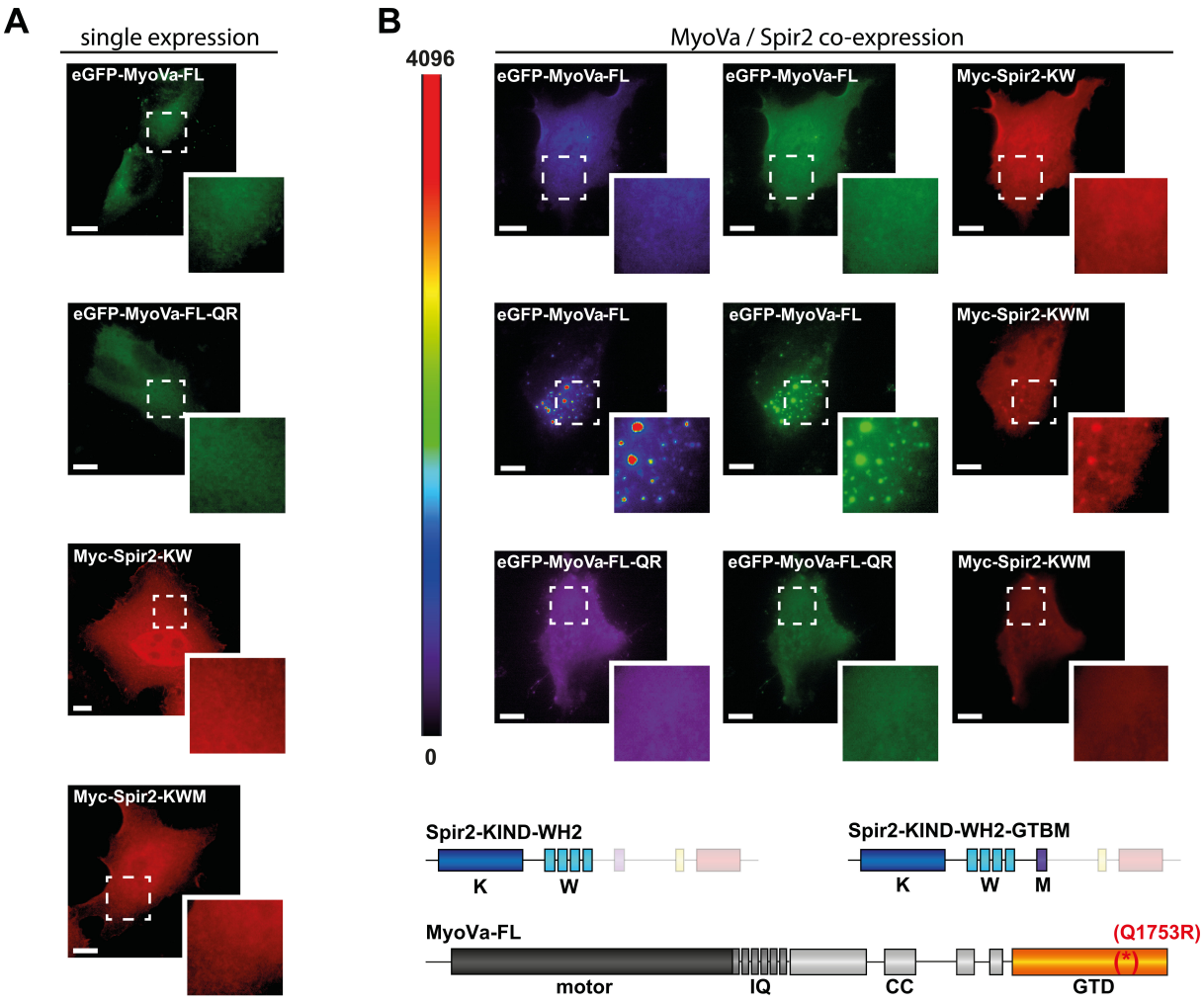

Figure 32 | Spir-2 facilitates myosin Va recruitment to vesicle membranes. (*A*) N-terminal Myc-epitope-tagged Spir fragments (Myc-Spir2-KIND-WH2, Myc-Spir2-KW; Myc-Spir2-KIND-WH2-GTBM, Myc-Spir2-KWM; *red*) and GFP-tagged full-length MyoVa proteins (eGFP-MyoVa-FL, eGFP-MyoVa-FL-QR; *green*) show an even cytoplasmic and nuclear localisation when transiently expressed in HeLa cells (single expression). **(*B*)** eGFP-MyoVa-FL (*green* and as *heat map*) shows an even cytoplasmic distribution that is not changed by co-expression of an N-terminal Spir-2 fragment (Myc-Spir2-KW; *red*), which is not able to bind to MyoV and lipid membranes (*upper panel*). In contrast, co-expression of a MyoV binding N-terminal Spir-2 fragment (Myc-Spir2-KWM; *red*) induces targeting of MyoVa to vesicle membranes and to overlapping Spir-2 and MyoVa localisation at vesicle surfaces (*middle panel*, see also higher magnification in insets). Heat maps represent grey

values for eGFP-MyoVa fluorescence intensities, rising from “0” (black) to “4096” (red), to document equal expression levels of MyoVa proteins in each depicted cell, and accumulation of fluorescent proteins at vesicle membranes induced by Myc-Spir2-KWM. To address the dependence of motor protein vesicle targeting on membrane associated small GTPases, the GFP-tagged melanocyte specific F isoform of MyoVa (carries exon F, but not exon D), which additionally carries the Q1753R mutation (eGFP-MyoVa-FL-QR) was expressed. The point mutation prevents MyoVa binding to Rab11. Expression of the eGFP-MyoVa-FL-QR mutant shows an even cytoplasmic distribution that was not changed upon co-expression of the MyoV binding N-terminal Spir-2 fragment (Myc-Spir2-KWM; *red*, *lower panel*), in contrast to what is observed for the wild-type MyoVa protein. At least 5 cells were recorded for each condition and one representative cell is depicted here. For all cells recorded, the fluorescence intensities of the eGFP-tagged MyoVa protein were measured and only those cells were further processed which have below-threshold levels of MyoVa protein expression (compare *Figure 31*). *Scale bars* represent 10 µm. An overview of employed proteins is presented and the domains used for localisation studies are highlighted. *K*, KIND; *W*, WH2; *M*, GTBM; *IQ*, isoleucine/glutamine motifs for calmodulin light chain binding; *CC*, coiled-coil; *GTD*, globular tail domain; *FL*, full-length.

3.10 A tripartite Spir:MyoV:Rab11 complex determines vesicle specificity

Spir actin nucleators and Rab11 small GTPases have been demonstrated to colocalise on vesicular structures and cooperate in exocytic and recycling transport processes (325), although a direct interaction of both proteins has never been observed. Furthermore, Rab11 and myosin V actin motor proteins directly interact with each other on vesicle membranes and function together in a wide range of cellular processes (222, 251, 256–260). Finally, Spir proteins have been shown to directly interact with MyoV proteins *in vitro* and at vesicle membranes. Therefore, the intriguing idea came up that myosin V actin motor proteins might act as a linker between Rab11 and Spir to form a tripartite Spir:MyoV:Rab11 complex at vesicle membranes, which in turn specifies a distinct vesicle subpopulation of Rab11- and Spir-positive vesicles, which possibly require *de novo* generation of actin filaments for transport through the cell.

The crystal structures of the MyoVa-GTD:Spir-2-GTBM complex (PDB ID 5JCY; see also *Figure 28*) and the MyoVa-GTD:Rab11a complex (PDB ID 5JCZ) (211) reveal that the MyoVa-GTD binding sites for Rab11a and Spir-2-GTBM are distinct and on opposite ends of the domain. So, in theory, Spir and Rab11 proteins might be able to bind to the MyoV GTD simultaneously, which would support a linker function of the MyoV GTD for Spir and Rab11 at vesicle surfaces. To test this hypothesis, a series of experiments was performed in order to analyse the putative formation of a tripartite Spir-2:MyoVa:Rab11a complex which is suggested to contribute in determining vesicle identity.

An initial pulldown assay showed that a bacterially expressed and purified recombinant constitutively active Rab11a protein (GST-Rab11a-Q70L) is able to pull transiently co-expressed eGFP-tagged full-length MyoVa (GFP-MyoVa-FL), Myc-epitope-tagged full-length Spir-2 (Myc-Spir2) and mStrawberry-tagged C-terminal FMN-2 (Straw-FMN2-FH2-FSI) from HEK293 cell lysates (*Figure 33A*). GST-Rab11a-Q70L is not able to pull a mutated MyoVa protein (GFP-MyoVa-Q1753R), as expected due to its mutation induced Rab11 binding deficit (103), which subsequently reduces the amount of pulled Myc-Spir2 and Straw-FMN2-FH2-FSI proteins. These data allow arguing on the formation of a large protein complex containing Rab11a, MyoVa, Spir-2 and FMN-2. Considering the markedly reduced

co-precipitation of Spir-2 and FMN-2 proteins in the case of Rab11a not binding to MyoVa (MyoVa-Q1753R mutant), the idea of a linker function of MyoVa for Spir and Rab11 proteins within this complex is further supported.

Next, the colocalisation of Spir-2 and Rab11a depending on MyoVa was determined by fluorescence microscopic analysis (*Figure 33B*). Immunostainings of Myc-epitope-tagged C-terminal Spir-2 deletion mutants, co-expressed with fluorescent-protein labelled C-terminal MyoVa (eGFP-MyoVa-CC-GTD) and Rab11a (mStrawberry-Rab11a) were examined. The MyoV-binding Myc-Spir2-GTBM-SB-FYVE protein perfectly colocalised with eGFP-MyoVa-CC-GTD and mStrawberry-Rab11a in a vesicular pattern (*upper panel*). In opposite, Myc-Spir2-SB-FYVE, missing the MyoV binding site, is still localised to vesicle membranes driven by its FYVE-type zinc-finger (327), but is largely targeted to vesicles other than those carrying MyoVa and Rab11a, both of which still perfectly colocalise (*lower panel*). To further decipher these findings, the Pearson's correlation coefficient (PCC) was determined to quantify the colocalisation of Spir-2 and Rab11a at vesicle surfaces in a MyoVa dependent manner (*Figure 33C*). The PCC for the colocalisation of Spir2-SB-FYVE was significantly reduced compared to the PCC for the colocalisation of Spir2-GTBM-SB-FYVE, demonstrating the dependence of the Rab11a/Spir-2 colocalisation on the Spir/MyoV binding site (Spir GTBM). Furthermore, the complete absence of MyoVa also significantly reduced the PCC for colocalisation of Spir2-GTBM-SB-FYVE with Rab11a compared to when MyoVa is present. The PCC for colocalisation of MyoVa and Rab11a is not altered in each of the experimental setups. Taken together, these data show that both, the capacity of Spir proteins to bind to MyoV (presence of the Spir GTBM), and the presence of MyoV itself, is critical to induce overlapping Spir-2/Rab11a localisation at vesicle membranes, and is in line with the concept of MyoV connecting Spir and Rab11 proteins into a tripartite Spir:MyoV:Rab11 complex at vesicle membranes. The same results were obtained for MyoVb (*Figure 34*). Fluorescence microscopy analysis revealed colocalisation of eGFP-tagged Rab11a, mStrawberry-tagged MyoVb-CC-GTD and Myc-epitope-tagged C-terminal Spir-2-GTBM-SB-FYVE at vesicle surfaces (*Figure 34A*). The PCC was determined to quantify the colocalisation of Spir-2 and Rab11a at vesicle surfaces in a MyoVb dependent manner (*Figure 34B*). The PCC for the colocalisation of Spir-2-GTBM-SB-FYVE and Rab11a was significantly reduced when MyoVb-CC-GTD is not present. MyoVb and Rab11a completely colocalise in each condition which does not depend on the presence of Spir-2. Thus, the PCC for colocalisation of MyoVb and Rab11a is not altered in each of the experimental setups.

Finally, a GST-pulldown assay was performed to prove the formation of a tripartite Spir-2:MyoVa:Rab11a complex *in vitro* without the support by additional factors (*Figure 33D*). Here, bacterially expressed and purified recombinant GST-Spir-2-GTBM-SB-FYVE, Rab11a-Q70L and MyoVa-GTD proteins were employed. As expected, GST-Spir-2-GTBM-SB-FYVE was not able to pull Rab11a-Q70L by itself, but strongly pulls MyoVa-GTD. Importantly, in presence of MyoVa-GTD, GST-Spir-2-

GTBM-SB-FYVE is now also able to pull the Rab11a-Q70L protein. In summary, these data strongly support the role of the MyoVa GTD as a linker between Spir-2 and Rab11a as a prerequisite to form a tripartite complex at vesicle membranes allowing the specification of vesicle identity for a distinct Rab11- and Spir-positive vesicle subpopulation.

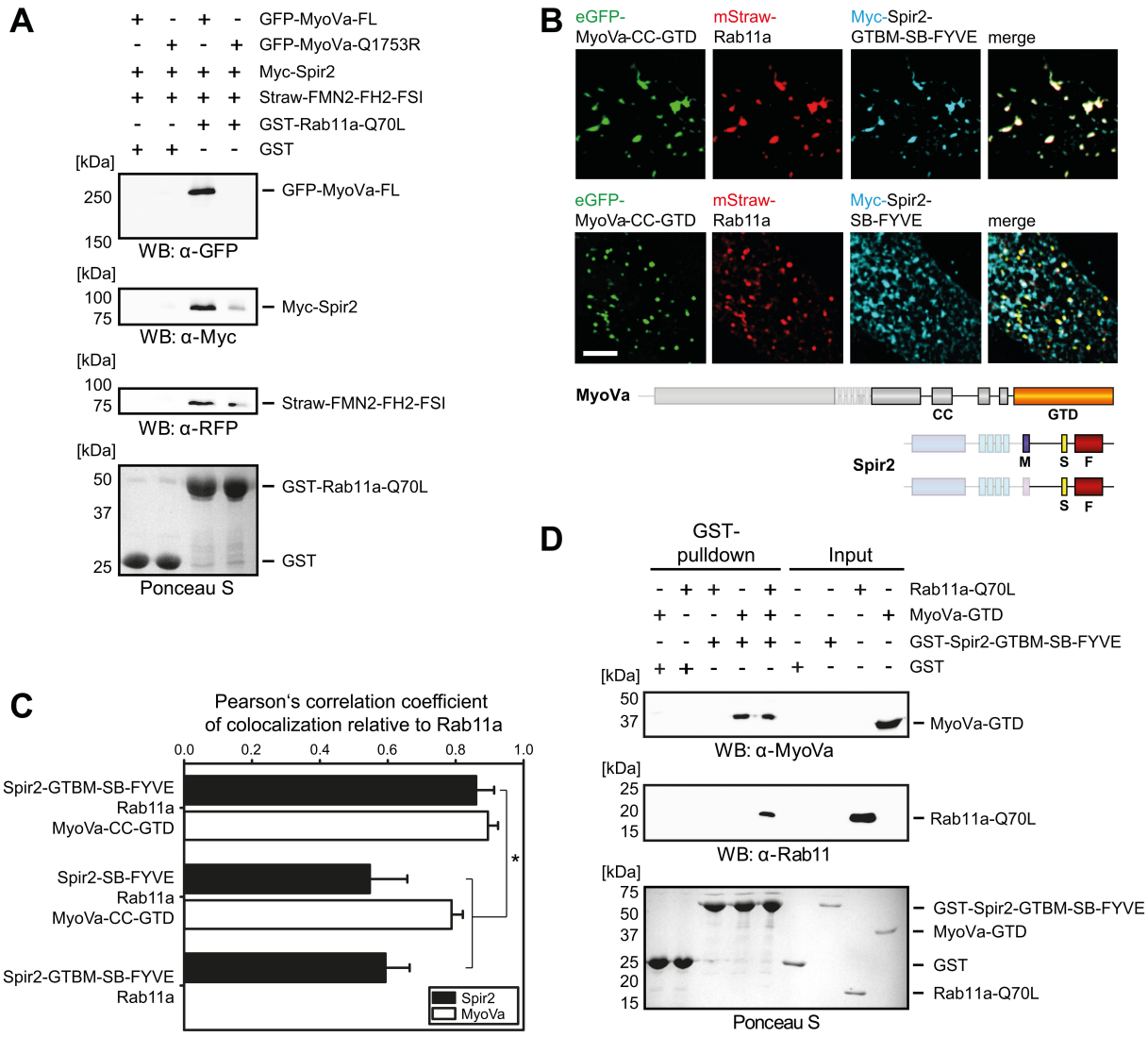

Figure 33 | Myosin Va links Spir-2 and Rab11a into a tripartite complex. (*A*) GST-pulldown assay with bacterially expressed, purified GTP-locked GST-Rab11a-Q70L mutant from HEK293 cell lysates transiently expressing full-length Myc-epitope-tagged Spir-2 (Myc-Spir2), mStrawberry-tagged C-terminal Formin-2 (Straw-FMN2-FH2-FSI), eGFP-tagged full-length MyoVa (D isoform; GFP-MyoVa-FL) or eGFP-tagged full-length MyoVa, carrying the Q1753R point mutation (D isoform; GFP-MyoVa-Q1753R). GST-Rab11a-Q70L pulls GFP-MyoVa-FL from cell lysates, but not the GFP-MyoVa-Q1753R mutant. In presence of GFP-MyoVa-FL, GST-Rab11a-Q70L is also able to pull Myc-Spir2, as well as Straw-FMN2-FH2-FSI. Only faint Myc-Spir2 and Straw-FMN2-FH2-FSI bands were detected using the GFP-MyoVa-Q1753R mutant. Pulled proteins were detected by immunoblotting (anti-GFP, anti-Myc, anti-RFP). No bands were detected employing a GST control. Ponceau S staining reveals equal loading of GST-fusion proteins. N = 2 experimental repeats. **(*B*)** The localisation of transiently co-expressed tagged Rab11a (mStrawberry, mStraw-Rab11a; *red*), MyoVa-CC-GTD (eGFP, eGFP-MyoVa-CC-GTD; *green*) and the Myc-epitope-tagged (Myc; *cyan*) C-terminal Spir-2 proteins encoding (Myc-Spir2-GTBM-SB-FYVE) or lacking (Myc-Spir2-SB-FYVE) the MyoV binding motif was analysed by fluorescence microscopy. 3D-deconvoluted images indicate the localisation of the proteins on vesicular structures. 5 cells were recorded for each condition and one representative cell is presented here. *Scale bars* represent 5 µm. An overview of employed proteins is presented and the domains used for colocalisation studies are highlighted. **(*C*)** The colocalisation of tagged proteins as described in (*C*) was quantified for the indicated co-expressions by determining the Pearson's correlation coefficient (PCC) as shown in a bar diagram. Each bar

represents the mean PCC value for at least 4 cells analysed. *Error bars* represent SEM. Statistical analysis was performed using Student's t-test to compare the mean PCC values of two co-expression conditions with a confidence interval of 95%. *, $p < 0.05$. **(*D*)** GST-pulldown assay employing bacterially expressed, purified GST-tagged Spir-2-GTBM-SB-FYVE protein (GST-Spir2-GTBM-SB-FYVE), MyoVa-GTD and the GTP-locked Rab11a-Q70L mutant. GST-Spir2-GTBM-SB-FYVE by itself does not pull Rab11a-Q70L. In contrast, the presence of the MyoVa GTD allows GST-Spir2-GTBM-SB-FYVE to pull Rab11a-Q70L, as indicated by immunoblotting (anti-MyoVa and anti-Rab11a). No bands were detected employing a GST control. Ponceau S staining reveals equal loading of GST-fusion proteins. N = 3 experimental repeats.

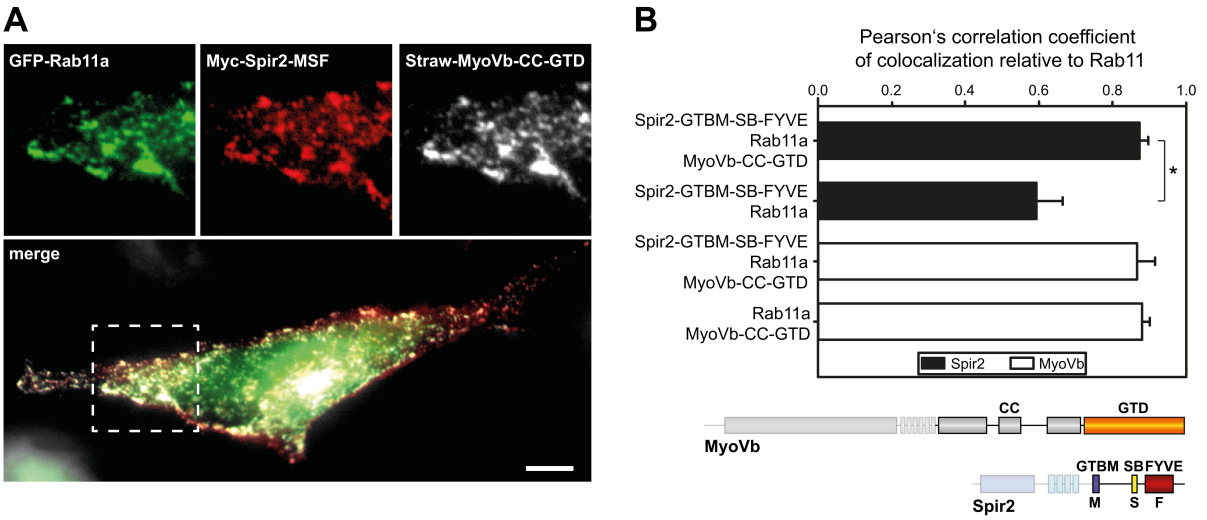

Figure 34 | Myosin Vb links Spir-2 and Rab11a into a tripartite complex. (*A*) The localisation of transiently co-expressed tagged Rab11a (eGFP, GFP-Rab11a; *green*), MyoVb-CC-GTD (mStrawberry, Straw-MyoVb-CC-GTD; *grey*) and the Myc-epitope-tagged C-terminal Spir-2 fragment encoding the MyoV binding motif (Spir-2-GTBM-SB-FYVE, Myc-Spir2-MSF; *red*) was analysed by fluorescence microscopy. 3D-deconvoluted images indicate the co-localisation of the proteins on vesicular structures. 5 cells were recorded and one representative cell is presented here. *Scale bar* represents 10 µm. **(*B*)** The colocalisation of tagged proteins as described in (*A*) was quantified for the indicated co-expressions by determining the Pearson's correlation coefficient (PCC) as shown in a bar diagram. Each bar represents the mean PCC value for at least 4 cells analysed. *Error bars* represent SEM. Statistical analysis was performed using Student's t-test to compare the mean PCC values of two co-expression conditions with a confidence interval of 95%. *, $p < 0.05$. An overview of employed proteins is presented and the domains used for colocalisation studies are highlighted.

Accordingly, in collaboration with Prof. Dr. Anne Houdusse and Dr. Olena Pylypenko (Institut Curie, Paris, France), a model for the tripartite Spir-2-GTBM:MyoVa-GTD:Rab11a complex was generated by superimposition of the MyoVa-GTD from the MyoVa-GTD:Spir-2-GTBM complex and the MyoVa-GTD:Rab11a complex crystal structures which nicely shows the distinct Rab11 and Spir-GTBM binding sites on the MyoVa GTD and the connecting character of MyoVa-GTD between Spir-2 and Rab11a (*Figure 35*).

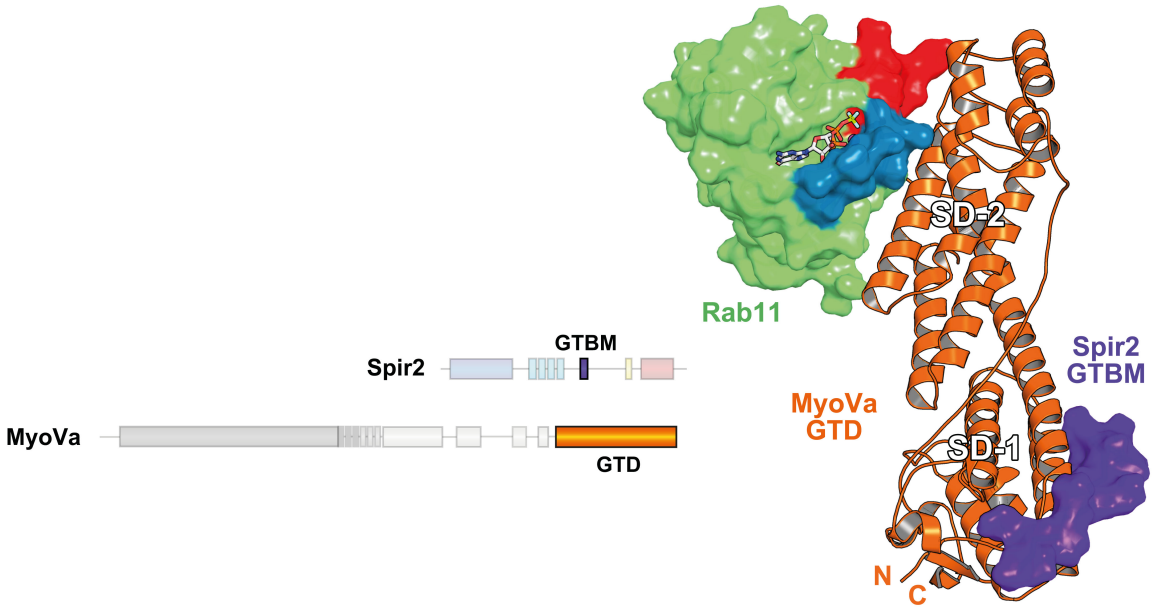

Figure 35 | Model for the Spir-2-GTBM:MyoVa-GTD:Rab11a complex. This complex was generated by superimposition of the MyoVa GTD from the MyoVa-GTD:Rab11a complex (PDB ID 5JCZ; (211)) and the MyoVa-GTD:Spir-2-GTBM complex (PDB ID 5JCY; see also *Figure 28*) crystal structures. The Spir-2-GTBM peptide (purple) binds to subdomain 1 (SD-1) of the MyoVa GTD (orange) and Rab11a (green; Switch-1 in blue, Switch-2 in red) binds to its SD-2. An overview of the employed proteins is presented and the domains used for structural analysis are highlighted.

4 Discussion

Accumulating evidence was generated for the cooperation of myosin actin motor proteins and actin assembly factors in intracellular membrane transport processes. In yeast, as well as in mammalian cells, the co-recruitment of the Arp2/3 complex and class I myosin motors has been described to facilitate endocytic events (340–343). Myosin Vb cooperates with Spir and FMN actin nucleators to peripherally transport Rab11-positive vesicles in metaphase mouse oocytes (222, 334), but the underlying mechanisms how the Spir/FMN actin nucleation activity and Rab11/MyoV motor activity are coordinated at the same vesicle surfaces remained unknown.

The present thesis was aimed to gain deeper insights into the processes of actin dependent vesicle transport, and unravelled a direct physical interaction of Spir actin nucleators and myosin V actin motor proteins driving a mutual targeting towards intracellular vesicle membranes. The Spir/myosin V interaction is mediated by a newly identified highly conserved sequence motif within the central Spir linker region (globular tail domain binding motif, GTBM) and the myosin V globular tail domain (GTD). The Spir GTBM is highly conserved across species, from choanoflagellata to mammals, and decides on the targeting of the MyoV GTD to Spir-positive vesicles.

Rab family small GTPases are well known to act as master regulators at different steps of intracellular transport. Rab11 is localised to intracellular membranes of the trans-Golgi-network (TGN), post-Golgi vesicles and the recycling endosome, and is thus involved in exocytic and recycling pathways (7). The Spir proteins have been identified to localise to Rab11-positive vesicles and cooperate in these intracellular trafficking pathways (325). So far, a direct interaction of Rab11 and Spir proteins has not been demonstrated. In line with that, this thesis revealed the formation of a tripartite Spir:MyoV:Rab11 complex both, *in vitro* and in living cells at vesicle membranes. The Spir-GTBM mediated interaction with MyoVa-GTD is critical for the tripartite complex formation and is required to target the complex to the same vesicle population. Superimposition of the Rab11a:MyoVa-GTD complex (PDB ID 5JCZ; (211)) and the Spir-2-GTBM:MyoVa-GTD complex (PDB ID 5JCY; see also *Figure 28*) showed that the binding sites for Spir and Rab11 are distinct and on opposite ends of the MyoVa GTD. Together, these data unravel a role for the myosin V actin motors as a linker between Rab11 and Spir proteins at vesicle membranes, which therefore determines the vesicle identity by mediating the formation of a specific Rab11- and Spir-positive vesicle subpopulation. This finally allows the coordination of Spir/FMN dependent actin nucleation and Rab11/MyoV mediated motor activity at the same vesicle population.

The melanophilin (MLPH) protein shows a similar domain organisation as the Spir proteins (see *Figure 29*), containing a membrane targeting unit, a myosin V binding unit, and an F-actin binding domain (compared to the actin nucleating KIND/WH2 unit in Spir proteins). MLPH mediates the interaction between the melanosome associated small GTPase Rab27a and myosin Va, in order to drive melanosome transport to the periphery of melanocytes, a process required for skin and hair pigmentation (80, 124, 169, 172–174). The polypeptide sequence of the Spir GTBM is similar to the MLPH GTBM binding to MyoVa-GTD, and also the Spir-2-GTBM:MyoVa-GTD (*Figure 28*) and MLPH-GTBM:MyoVa-GTD (PDB ID 4LX2; (210)) complex structures share some similarities. Both GTBMs target the same site of the globular tail domain of MyoVa. These findings open the possibility that there might be a general mechanism for the association of Rab family GTPases, myosin actin motor proteins and actin monomer/F-actin binding proteins which contribute to specific vesicle transport processes.

4.1 Mechanisms for Spir/MLPH induced unfolding of MyoV motors

The inactive full-length myosin V dimer is back-folded by an intramolecular interaction of the motor domains and globular tail domains (GTDs) (98–100), and has been shown to be evenly distributed in the cytoplasm (103). MLPH has been observed to open up the back-folded myosin V dimer, to activate its ATPase activity and to facilitate its movement on actin filaments *in vitro* (107–109).

However, the exact mechanism here has not yet been deciphered completely. Several studies have shown that the GTD binding sites for MLPH and for the MyoV motor domain are distinct and not overlapping (109, 358). Whereas the MLPH GTBM binds, as does the Spir-2 GTBM, to subdomain 1 (SD-1) of the MyoVa GTD, the motor domain is suggested to bind to SD-2, and specific residues within the GTD are essentially involved in binding to MLPH and to the motor domain, respectively (98, 109, 210, 353, 358, 359). Consequently, an allosteric mechanism has been proposed in which MLPH-GTBM binding to MyoVa-GTD induces the release of the GTD-motor interaction, and in which the GTD-motor interaction competes with the GTD-MLPH interaction (109). It is suggested that binding of the MLPH GTBM does not induce a major conformational change within the GTD, but the GTD-motor interaction does so. MLPH is thought to prevent these conformational changes by binding to the GTD, thus inhibiting the GTD-motor interaction. The back-folded structure of the full-length MyoVa protein might therefore inhibit the binding of MLPH-GTBM to the GTD by allosteric effects as well, and thus strongly reduces its binding affinity. This is supported by studies demonstrating differences in the binding affinities of MLPH-GTBM binding to the isolated GTD (~0.5 µM) (210, 353, 360) and to the GTD of full-length MyoVa (~20 µM) (109).

In a very recent study, the decreased binding capacity of the MLPH GTBM to the GTD of the back-folded myosin Va dimer was attributed to a dimerising interaction between both GTDs of the heavy chain dimer, formed by the N-terminal linkers of the GTDs (*Figure 36*) (361). Both GTDs of the dimer are supposed to dimerise in a head-to-head orientation by which both SD-1 bind to each other, preventing MLPH binding to the GTD. Two conserved residues, R1490 and K1491, correspond to the respective R187 and K186 of the MLPH GTBM, and bind to the MLPH binding site of the opposing GTD-SD-1. Mutations of these two residues (R1490A and K1491A) increased the binding of MLPH to the GTDs of a full-length MyoVa dimer. Furthermore, it has been revealed that the GTD dimerisation by mutual binding to the opposing MLPH binding site is essential for the efficient binding of both GTDs to the motor domains of the dimer and to support the stabilisation of the typical triangular back-folded MyoVa structure (361).

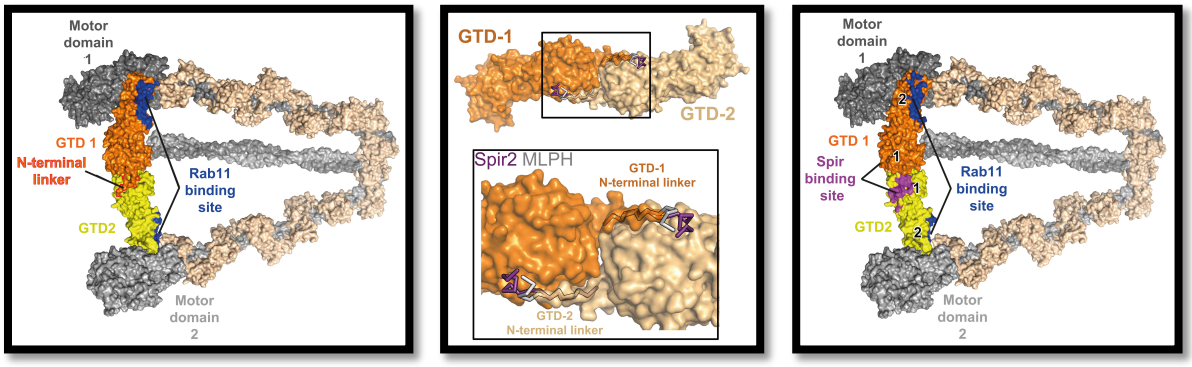

Figure 36 | Back-folding of the MyoV dimer is stabilised by the GTD N-terminal linkers. A model for the back-folded MyoV dimer is shown and the N-terminal linker of the GTD 1, as well as the Rab11 binding sites are indicated on left. The binding of the N-terminal linkers (orange and beige) to the opposing GTD, as well as the binding of the Spir (purple) and MLPH (white) GTBMs to the GTDs are presented in greater structural detail in the middle. The Spir GTBM, as does the MLPH GTBM, binds to the same site of the MyoVa GTD as the N-terminal linker from the opposing GTD does in the back-folded state, which also shows the distinct GTD binding sites for Spir/MLPH and the motor domains. Images provided by Olena Pylypenko (*left and right*) and adapted from Pylypenko, Welz et al., 2016 (211) (*middle*).

Taking all these considerations into account, MLPH might be able to open and activate MyoVa in a dual-step manner with the auto-inhibited MyoVa dimer traversing two distinct states (361). First, a state in which MyoVa is strongly back-folded, supported by the GTD-GTD interaction mediated by their N-terminal linkers occupying the sites for MLPH and preventing MLPH-GTBM binding. Second, a pre-activated state in which the MLPH binding sites are exposed by the previous release of the N-terminal linkers, allowing MLPH-GTBM to bind to the GTD which allosterically blocks the binding of the GTDs to the motor domains and consequently induces the unfolding of MyoVa.

Besides the GTBM, melanophilin carries a second MyoVa binding site that interacts with the exon F encoded regions of MyoVa, the exon F binding domain (EFBD) (355). It has been shown that the presence of both MyoVa binding sites increases the affinity of MLPH to MyoVa compared to

presence of the GTBM alone, and accordingly, the binding of EFBD to MyoVa-exon F might be able to weaken the GTD-GTD interaction, thereby inducing the pre-activated state and paving the way for GTBM binding to the GTD (108).

As Spir-2 was able to target the back-folded, cytoplasmic, GFP-tagged full-length myosin Va protein to vesicle membranes in a GTBM dependent fashion (see *Figure 32*), it is intriguing to speculate about a similar role for Spir proteins in the opening and activation of full-length myosin V motors. The overall protein organisation of Spir and MLPH proteins is very similar, as well as the amino acid sequence of both GTBMs (*Figure 37*), explaining a similar binding mode of the Spir GTBM and the MLPH GTBM to the MyoVa GTD, although there are differences, as well (see *Figure 30*).

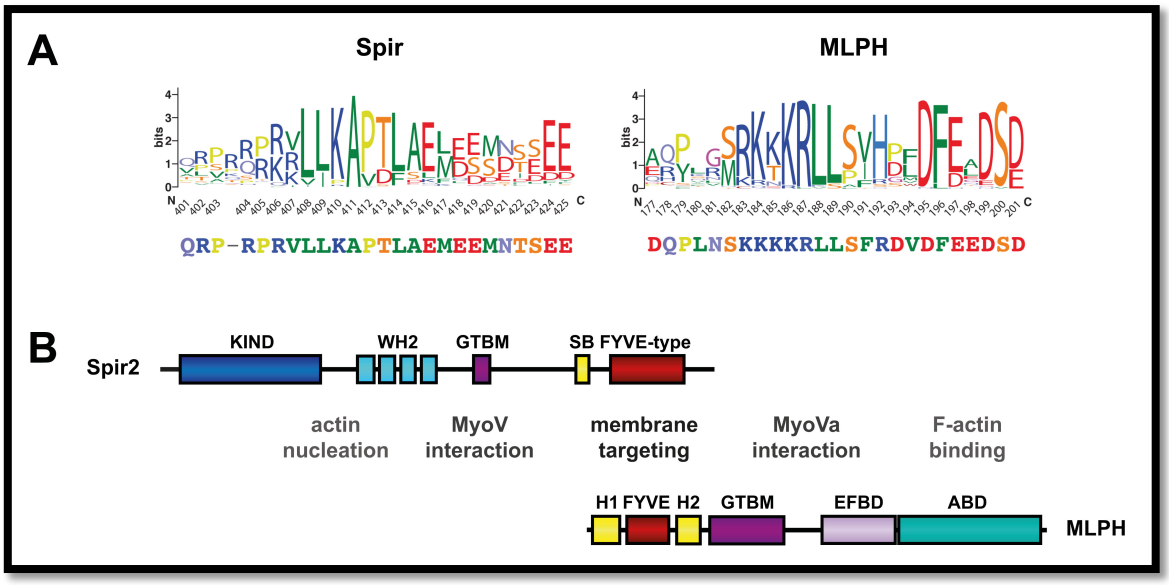

Figure 37 | Comparison of Spir and melanophilin proteins. (*A*) The Spir-GTBM sequence is highly conserved in Spir-1 and Spir-2 proteins as indicated by the sequence logo (*left*). The respective human Spir-2-GTBM sequence is shown below the WebLogo. The melanophilin (MLPH)-GTBM sequence is also highly conserved in MLPH proteins (*right*). The respective murine MLPH-GTBM sequence is shown below the WebLogo. The WebLogos (345) for both GTBMs were generated from the alignment of 223 Spir protein sequences and 44 MLPH sequences. Both, Spir and MLPH GTBMs, show a similar charge distribution with positive charges at the N-terminus and negative charges at the C-terminus, and have two highly conserved leucine residues within the positively charged cluster. **(*B*)** Comparison of the Spir-2 and MLPH protein domain organisation shows the presence of similar functional units. Both proteins share a MyoV protein interaction unit in their central regions (GTBM for Spir-2; GTBM and exon-F binding domain (EFBD) for MLPH). Both proteins encode a membrane targeting unit at their C-terminus (Spir-2) and N-terminus (MLPH), respectively, consisting of a FYVE-type zinc-finger and a related potential small GTPase binding Spir-box (SB in Spir-2) and synaptotagmin-like protein homology domains (H1 and H2 in MLPH). The MLPH-H1-FYVE-H2 cluster is essential for MLPH interaction with Rab27a (354). Both proteins share an actin interaction cluster as well, in which Spir-2 encodes an actin nucleating KIND/WH2 cluster at its N-terminus, and MLPH encodes an F-actin binding domain (ABD) at its C-terminus. Adapted and modified from Pylypenko, Welz et al., 2016 (211). Information on the MLPH domain organisation from Hume et al., 2006 (355).

The similarity of GTD binding by MLPH and Spir GTBMs strongly suggests a mechanism for MyoV activation in accordance to the MLPH induced opening of MyoVa, in a way that the Spir GTBM is able to weaken the GTD-motor interaction in an allosteric manner in order to release the back-folded conformation and induce motor activity (*Figure 38*).

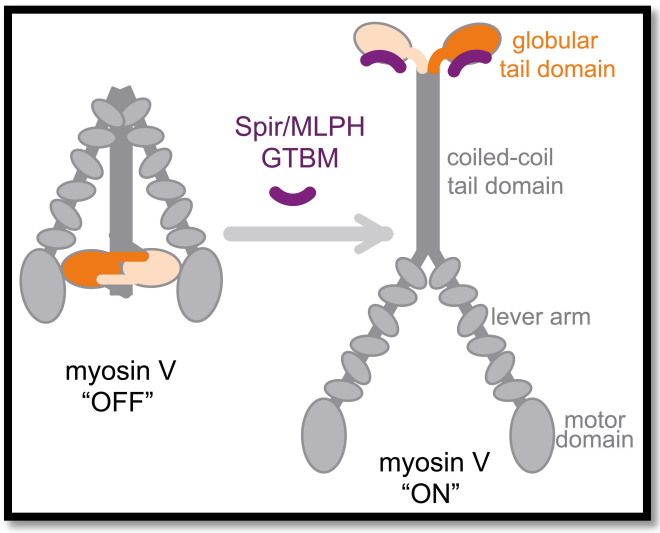

Figure 38 | Schematic representation of MyoV activation. In the myosin V OFF state, MyoV is back-folded supported by the mutual binding of the GTDs N-terminal linkers (orange and beige). Spir/MLPH GTBM (purple) binding to MyoV globular tail domains induces unfolding into an extended structure, and activation of MyoV motors. Adapted from Pylypenko, Welz et al., 2016 (211).

However, a second MyoV binding site was not detected within the Spir-2 protein, a finding which would disagree with a two-step opening mechanism as proposed for MLPH. The binding patterns of the C-terminal regions of Spir-2 and MLPH GTBMs differ as Spir-2-GTBM forms a larger hydrophobic interaction surface compared to MLPH-GTBM. It could be the case that such minor differences in terms of molecular interactions are sufficient to induce the Spir dependent opening of MyoV proteins. However, no significant conformational changes in the MyoV GTD following Spir-2-GTBM binding have been observed (211). Therefore, it would be of great importance to further analyse the effects of Spir-GTBM binding to MyoV-GTD as well as the exact molecular mechanisms leading to MyoV activation in more detail. Mutational analysis of both the Spir GTBM and the MyoV GTD in combination with protein interaction studies, fluorescence microscopy, electron microscopy, fractional ultracentrifugation and ATPase activity assays would help to gain deeper insights on Spir induced myosin V opening, membrane targeting and activation. In accordance to studies on the MLPH GTBM, it would be very helpful to show if the isolated Spir GTBM is able to induce unfolding of the full-length MyoV protein and to induce the ATPase activity of the motor domain by itself, using purified proteins and peptides. Additionally, it would be meaningful to unravell if there are similar differences in the binding affinities of Spir-GTBM to the isolated GTDs and to full-length myosin V proteins, as was observed for the MLPH GTBM.

4.2 Rab11 by itself is not able to activate MyoV *in vivo*

It has been recently revealed that the *Drosophila* Rab11 protein (dRab11) is able to activate the motor function of *Drosophila* myosin V (Dm-MyoV) *in vitro* (362). It was proposed that dRab11 either directly blocks the binding of Dm-MyoV GTDs to its motor domains by occupying identical binding sites, or by allosteric inhibition of Dm-MyoV-GTD-motor interactions. Recent data shows that the binding sites for the motor domain and for Rab11 on the MyoV GTD are both located at subdomain 2 (SD-2), but on opposite surfaces (211, 362). The E1791 residue within the loop connecting helix 11 and helix 12 of the MyoVa GTD-SD-2 (H11-H12 loop) is involved in binding to the motor domain and to Rab11 (109, 211). Therefore, it might be a competing interaction between GTD-motor and GTD-Rab11 binding which leads to motor activation following vesicle targeting. However, when expressed in living cells, the back-folded full-length myosin Va protein is not targeted to vesicle surfaces by the active, membrane associated Rab11 GTPase alone (see *Figure 32*) (103), demonstrating the importance of additional mechanisms besides the presence of Rab11 at vesicle surfaces, which are demanded for myosin V opening and targeting to Rab11 vesicle membranes. A sterical hindrance might exist which inhibits the association of the membrane bound Rab11 and the large cytoplasmic MyoV dimer, preventing an active Rab11 driven MyoV opening mechanism. Co-expression of N-terminal Spir-2 fragments induced a re-orientation of full-length myosin Va proteins to Rab11-positive vesicle membranes (see *Figure 32*). One may speculate about a mechanism by which Spir proteins activate back-folded MyoV proteins in the cytoplasm, induce the release of the auto-inhibitory GTD-motor interaction, and target the motor towards vesicle surfaces. Once they reach the vesicle membrane, active Rab11 binds to the MyoV GTD and stabilises the opened, active MyoV conformation in order to fulfil its role in vesicle transport.

4.3 Coordinated recruitment of Spir and MyoV proteins to vesicle surfaces

Based on the data obtained in this thesis the following model is proposed for the coordinated recruitment of Spir actin nucleators and myosin V actin motor proteins to Rab11 vesicle membranes (*Figure 39*). In this model, both, Spir and MyoV proteins exist in two distinct states. There is an inactive cytoplasmic state in which the myosin V dimer is back-folded and auto-inhibited, a condition that is also suggested for Spir proteins (327). At this state, the ATPase activity of MyoV is inhibited and the motor only weakly interacts with actin filaments (101, 102). The potentially auto-inhibited, cytoplasmic Spir proteins do not interact with FMN proteins, preventing efficient actin nucleation in the cytoplasm. However, Spir proteins have been shown to transiently interact non-specifically with negatively charged intracellular membranes during which the back-folding is released and Spir is opened up (327). By so far unknown activating mechanisms, Spir and MyoV proteins are co-recruited

to Rab11-positive vesicles forming a vesicle associated tripartite Rab11:MyoV:Spir protein complex. The newly identified Spir-GTBM is essentially involved in the opening mechanism of MyoV proteins and the interaction of the MyoV GTD and Rab11 is thought to further stabilise the whole protein complex and supports its functionality at the vesicle membrane. Here, the MyoV actin motor acts as a linker between Rab11 and Spir at vesicle surfaces. Furthermore, Spir proteins are thought to dimerise once they are targeted to vesicle membranes (321, 333), and interact with FMN proteins to form a functional actin nucleator complex which generates actin filaments directly at the vesicle surface. These *de novo* generated actin filaments are supposed to associate with MyoV motors to finally exert forces on membrane vesicles. Therefore, the Spir/myosin V interaction provides the base to coordinate Spir/FMN actin nucleation activity and Rab11/MyoV motor activity at the same vesicle population. The existence of two distinct activity states, including auto-inhibited back-folded MyoV and Spir proteins, allows for induced, specific targeting of actin nucleation and motor activity to vesicle membranes.

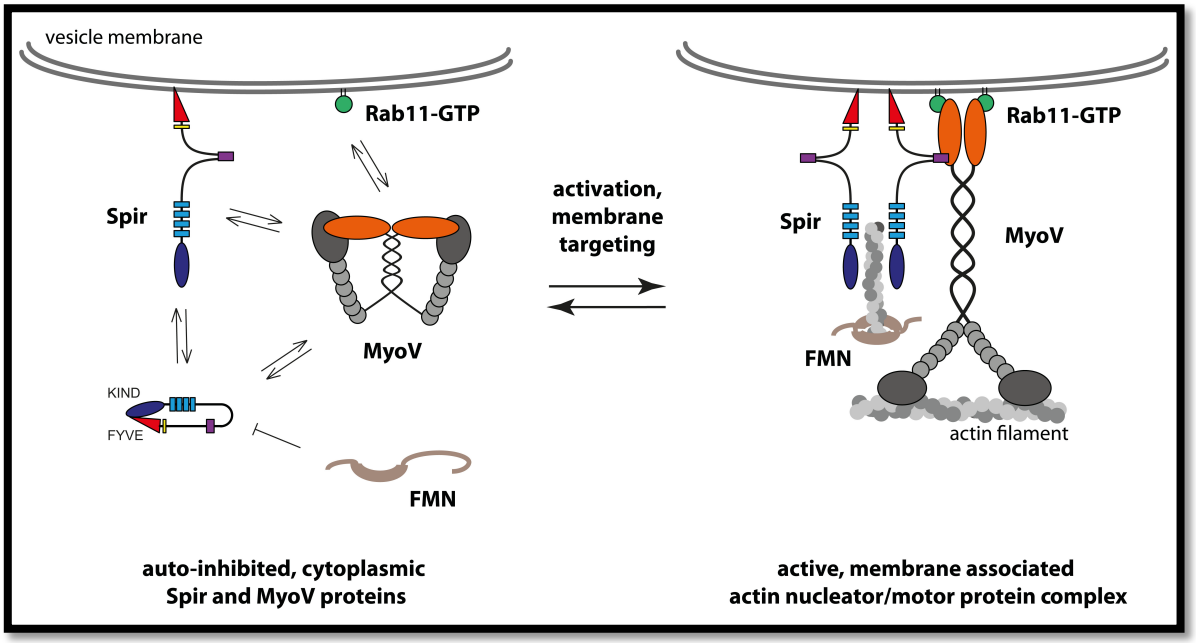

Figure 39 | Model for the formation of a Spir/FMN actin nucleator/MyoV actin motor complex at Rab11 vesicle membranes. Spir and MyoV proteins adopt an auto-inhibited, (potentially in case of Spir) back-folded and cytoplasmic conformation on the one hand, and an active, open conformation on the other hand in which the proteins are targeted to vesicle membranes as part of a multimeric protein complex. The recently discovered Spir-KIND/FYVE interaction is thought to induce a back-folded, cytoplasmic Spir protein conformation which does not interact with Formin family formin (FMN) proteins (327). Spir proteins have also been shown to transiently interact with vesicle membranes, mediated by the FYVE-type zinc-finger, during which the protein opens up. MyoV at its inactive state is back-folded by the interaction of the globular tail domains (GTDs) with the motor domains of the dimer. By yet poorly understood activation mechanisms, Spir and MyoV proteins are targeted to Rab11-positve (Rab11-GTP) vesicle membranes. The newly identified Spir-GTBM is essentially involved in the opening mechanism of MyoV proteins. The interaction of MyoV-GTD and Rab11 is thought to further stabilise the whole protein complex and supports its functionality at the vesicle membrane. The membrane targeted, unfolded Spir protein is consequently free to interact with FMN proteins to form a functional actin nucleator complex to generate new actin filaments directly at vesicle surfaces. These *de novo* generated actin tracks might then be used by MyoV actin motors to either move the whole vesicle, or to pull out tubular membrane structures in order to reach microtubule tracks.

This model is supported by two studies showing the influence of the actin nucleotide state on myosin V run length (363, 364). It has been revealed that younger, ADP+P_i rich actin filaments increase the run length of myosin Va by 1.3- to 1.5-fold. Furthermore, younger actin filaments also induce a rise in landing rates (the rate at which myosin V attaches to F-actin and starts a processive run) of myosin Va on actin filaments (363). These findings perfectly fit to a cooperation of an actin nucleation machinery (Spir/FMN) and myosin V motor activity, generating new actin filaments at vesicle membranes which might be subsequently available for actin motor proteins.

4.4 Nanotube formation as a potential mechanism for switching vesicle transport tracks

The final role of a functional interaction of actin nucleation factors, F-actin binding proteins and actin motor proteins at vesicle surfaces needs to be further investigated. The Spir/FMN and Rab11/MyoVb dependent actin driven long-range vesicle transport has been revealed in metaphase oocytes in which the microtubules are trapped in the mitotic spindle and are thus not available for vesicle transport. In contrast, somatic cells harbour a very complex microtubule network which enables rapid transport towards the cell periphery and backwards. Therefore, a completely actin based long-range transport, similar to metaphase oocytes, seems to be rather unlikely in somatic cells.

Live cell imaging studies of Spir-2-positive vesicles in HeLa cells have revealed the existence of different vesicle states, including resting phases and fast movement on microtubule tracks (321). During the resting phases, a dynamic and continuous outgrowth of membrane nanotubes from the vesicle surface has been observed (321). Accordingly, a model is proposed in which the interaction of Spir, FMN and MyoV proteins at Rab11 vesicles induces the formation of such nanotubules by Spir/FMN dependent actin nucleation and polymerisation, and subsequent myosin V motility along *de novo* generated F-actin tracks (*Figure 40*). The indirect membrane association of myosin V (by interactions with Rab11, Ra11-FIP2 and Spir proteins) might therefore enable the motor to exert a pulling force on the vesicle membrane and to generate tubular structures. Those might then be used to reach the microtubule network in more centred regions of the cell, and allow vesicle switching to microtubule tracks for fast long-range transport.

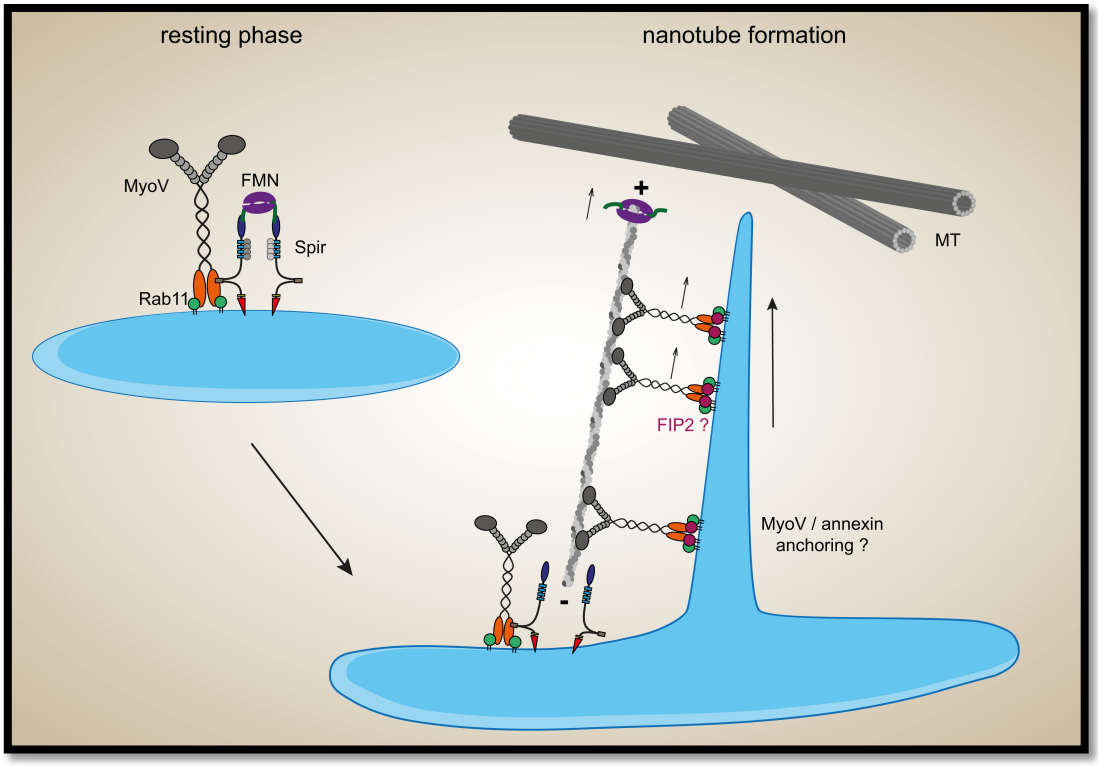

Figure 40 | Model for the formation of nanotubes from somatic cell vesicles. Somatic cell vesicles have been shown to exist in different states, including resting phases and fast movement on microtubule (MT) tracks (321). During the resting phases, a dynamic and continuous outgrowth of nanotubes from the vesicle surface has been observed (321). Spir, Formin (FMN), Rab11 and MyoV proteins are supposed to form a functional complex at the vesicle surface. The Spir/FMN actin nucleator complex mediates *de novo* generation of actin filaments at the vesicle surface with the barbed end (+) potentially pointing away from the vesicle. These newly generated actin tracks are then supposed to be used by Rab11/MyoV motor complexes to move along and exert a pulling force on the vesicle membrane inducing nanotube formation. Anchoring of actin filaments might be provided by annexin actin binding proteins (365), or directly by MyoV motors by forming complexes with other membrane associated proteins (e.g. Rab11-FIP2). FMN, processively moving with the elongating actin barbed end, might account for the initial contact with the MT tracks (366), in order to induce vesicle switching to MT based fast transport. Additional proteins, such as MT dependent motors, might contribute to these processes.

This theory gets support as the myosin motors myosin Vb, myosin VI and myosin Ib have been reported to be involved in membrane tabulation *in vivo* (196, 367–369). Myosin Ib (MyoIb) is a membrane associated single-headed motor, which directly binds to lipid membranes by its highly basic C-terminal tail homology 1 (TH1) domain (370, 371), and is essential for the formation of membrane tubules from the TGN and from sorting endosomes (368, 369). The process and mechanism of nanotube formation was described in detail for MyoIb recently (372). By means of a reconstituted system engaging purified proteins and giant unilamellar vesicles (GUVs), it has been shown that myosin Ib is able to form membrane tubules along F-actin bundles at physiologically relevant densities (372). A similar mechanism of membrane tabulation induced by motor proteins has been described before for microtubule associated motors (373, 374). *In vitro* studies have revealed the formation of tubular networks along microtubules emanating from the Golgi and endoplasmatic reticulum (375–377), and processive microtubule associated motors generated forces

on the membranes to which they are attached to, in order to form nanotubues along microtubules (378–380).

Formin family formins have been shown to directly interact with microtubules via their FH2 domains and the C-terminal Formin/Spir interaction (FSI) sequence (366). When bound to microtubules, formins are not able to nucleate and elongate actin filaments anymore as the FH2 domain is occupied. Formin proteins processively move with the elongating barbed end of actin filaments and could therefore mediate the initial contact of the vesicle associated protein complex with the microtubule network. As soon as the formin reaches the microtubule, actin polymerisation would be stopped right in time. Additional vesicle membrane associated proteins that may join the protein complex, such as kinesin or dynein microtubule dependent motors, would be able to attach to the microtubules and mediate long-rang vesicle transport.

Open questions remain regarding the orientation and attachment of actin filaments when newly generated at vesicle surfaces. Spir proteins are attached to the membrane via their C-terminal FYVE-type zinc-finger. The KIND and WH2 domains are thus oriented away from the vesicle surface. Spir induced actin nucleation starts with actin monomer binding to WH2C and WH2D domains and is followed by G-actin binding to WH2B and WH2A (with A to D in N-to-C-terminal direction) (318). The actin nucleus formed at the WH2 domains has consequently an orientation with the barbed end pointing towards the KIND domain and the pointed end towards the vesicle. Formin binds to Spir-KIND and consequently polymerises Spir-generated actin nuclei by moving processively with the growing actin filament barbed end. Taken together, it seems obvious that the actin filament pointed end is oriented towards the vesicle surface, and the barbed end towards the cytoplasm, away from the vesicle. Myosin V motors move towards the barbed end of actin filaments which would thus allow myosin V movement away from the vesicle surface and a potential nanotube formation. Nothing is currently known about the attachment of actin filaments at vesicle surfaces. Annexins as actin binding proteins might be potential candidates in capturing newly generated F-actin tracks at the vesicle membrane. Another possibility might be provided by the myosin V motors themselves which have also been reported to act as tethering factors (4, 35, 381–388). The high abundance of myosin V and Rab11 proteins in the cell would allow for the association of multiple Rab11/MyoV complexes at the surface of one vesicle, and a situation in which some complexes are used to capture the actin tracks and attach them to the surface, and some are used to mediate the actin based movement. Myosin V motors also directly bind to the Rab11-interacting protein Rab11-FIP2 (264). Rab11-FIP2 carries a C2 membrane binding domain (244, 247) which provides the possibility that myosin V forms at least two distinct protein complexes at Rab11-positive membranes; one complex with Rab11 and one complex with Rab11-FIP2, both of which could have distinct functions in tethering of actin filaments and movement along those, respectively.

Undoubtedly, further investigations are required to analyse in detail the molecular processes occuring on vesicle membranes. *In vitro* reconstitution of intracellular membranes and associated proteins by means of giant unilamellar vesicles (GUVs) and purified Spir, MyoV, Rab11 and FMN-2 proteins as well as actin will help to shed light into the interplay of these interaction partners in terms of actin nucleation and elongation, myosin V motor movement and subsequent changes in membrane morphology.

So far, one might not exclude the presence of additional proteins that might also be included in a much larger protein complex assembling at vesicle surfaces. The role of actin anchoring proteins, such as annexins, as well as other Spir interacting proteins, including Arf family GTPases should be in focus of future studies. The presence of MyoV/Rab11-FIP2 complexes could broaden the spectrum of protein interactions at vesicle surfaces, as well as the presence of microtubule associated motor proteins (kinesins and dynein). Consistently, a proteomics approach of Spir- and Rab11-positive vesicles would tremendously help to identify additional proteins that might join Spir, MyoV and Rab11 at vesicle membranes.

Live cell imaging experiments of HeLa cells expressing fluorescently tagged Spir-2 and Rab11-FIP2 proteins revealed a very dynamic exchange of both proteins at vesicle membranes (unpublished observations). Some vesicles only carry Spir-2, some carry only FIP2, and some vesicles carry both proteins. Time-lapse imaging also revealed the conversion of Spir-2-positive vesicles into FIP2-positive ones and vice versa. Having this in mind, the formation of such multimeric protein complexes might be considered as a dynamic process of proteins joining and leaving the complex and not as a static clump of proteins sitting at one spot of the vesicle surface.

The association of a large set of proteins into a protein complex requires the exact and well-regulated timing and order of events for protein joining, including here the opening and activation of MyoV and Spir proteins. In order to form a multimeric protein complex, both, the total and relative protein concentrations decide on proper complex functioning. There is a roughly 20-fold excess of myosin V motor proteins over the Spir-1 and Spir-2 proteins in a single HeLa cell (~50,000 MyoV proteins, ~1830 Spir-1 and ~815 Spir-2 proteins) (389), arguing that only a small subset of MyoV proteins can actually associate with Spir proteins at vesicle surfaces. The low abundance of Spir proteins in total and especially in relation to the myosin V motors, leads the so far employed cell biological approaches by means of transient protein over-expression to the edge of obtaining meaningful results. Thus, it will be indispensable in the future, to study the protein dynamics at endogenous expression levels in order to precisely define the temporal and spatial steps involved in MyoV and Spir activation and recruitment towards Rab11-positve vesicles. The combination of state-of-the-art gene editing tools, such as CRISPR/Cas9 and the MIN-tag technology (390), and the latest

advances in the development of novel fluorescent proteins, for instance mNeonGreen and mRuby3 (391, 392), will be very useful to generate stable cell lines allowing the visualisation of low abundant proteins such as Spir. The use of modern fluorescence microscopy methods, including TIRF (total internal reflection) microscopy and FCS / FCCS (fluorescence correlation spectroscopy / fluorescence cross-correlation spectroscopy) (393–395), would enable protein quantification as well as determining the dynamics of Spir, FMN, MyoV, Rab11 and additional associated proteins at vesicle surfaces, and their correlation with vesicular motility and morphological changes.

4.5. Diverse Rab/MyoV interactions suggest similar mechanisms for other transport processes

Myosin V actin motor proteins interact, next to Rab11a, with a large set of Rab family GTPases and are thus involved in diverse cellular functions (*Figure 42*). Several studies have revealed the direct or indirect interactions of myosin Va with Rab3A (194), Rab3b, Rab3c, Rab3d, Rab6a, Rab6a', Rab6b (103), Rab8a, Rab10 (55), Rab11b, Rab14, Rab11c (or Rab25) (103), Rab27a (81, 83, 84) and Rab39b (103). Rab39b has been shown to be a neuronal specific Rab GTPase which is localised to the Golgi complex, a broad range of cytoplasmic vesicles and within neurites at which overlapping localisation with myosin Va has been revealed (103). Rab3A as well as Rab27b form complexes with myosin Va in order to enable exocytosis of synaptic vesicles for synaptic transmission (194, 195).

Myosin Vb has been shown to interact with Rab8a (196, 197) and Rab10 (196) and myosin Vc has been revealed to interact with Rab10 (55), Rab38 and the closely related Rab32 (which do not interact with MyoVa or MyoVb) playing a role in melanosome biogenesis (207). Additionally, myosin Vc interacts with Rab7a and Rab8a within melanocytes which localise to immature (Rab7a) and mature (Rab8a) melanosomes (396, 397) and could provide a Rab32/38 independent pathway during melanosome biogenesis (207).

Due to the large diversity of Rab/MyoV protein interactions and the herein newly identified Spir/MyoV interaction, it might be intriguing that a functional Spir:MyoV:Rab-GTPase complex might exist in different flavours depending on the participating MyoV motor and Rab GTPase. A differential complex composition would allow targeting actin nucleation and motor protein function to different vesicle subpopulations in order to drive distinct vesicle transport processes that require *de novo* generation of actin filaments directly at vesicle surfaces. In line with that, initial experiments employing Rab8a revealed a colocalisation with Spir-2 and MyoVa at vesicle surfaces, comparable to the Rab11a:MyoVa:Spir-2 tripartite complex (*Figure 41*). Accordingly, a similar tripartite complex formation is suggested which might also be involved in exocytic as well as endocytic transport processes described for Rab8 (126, 164). However, further investigations, including detailed colocalisation analyses, indirect and direct protein interaction studies and functional cell based

assays are required to describe the exact interplay between Rab8, Spir and myosin V proteins and its functional consequences.

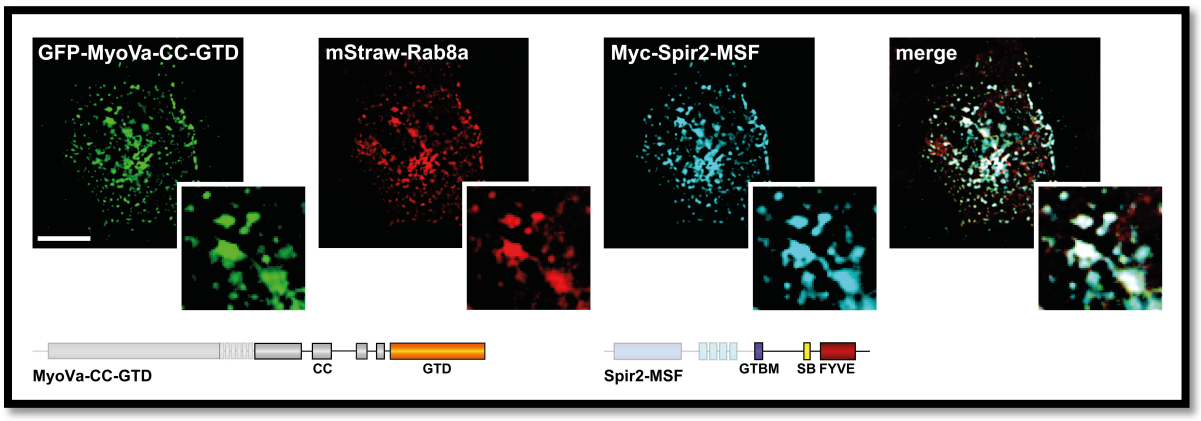

Figure 41 | Spir-2 forms a tripartite complex with Rab8a and MyoVa at vesicle surfaces. Preliminary data on HeLa cells transiently over-expressing Myc-epitope-tagged Spir-2-GTBM-SB-FYVE (Myc-Spir2-MSF; *cyan*), eGFP-tagged MyoVa-CC-GTD (GFP-MyoVa-CC-GTD; *green*) and mStrawberry-tagged Rab8a (mStraw-Rab8a; *red*) as analysed by fluorescence microscopy. All proteins show a vesicular localisation pattern when expressed alone (not shown) and colocalise at vesicle surfaces under co-expression conditions, indicated by overlapping punctae (*merge;* see also higher magnification insets). *Scale bar* represents 10 µm. An overview of employed MyoVa and Spir-2 proteins is presented and the domains used for colocalisation studies are highlighted.

On top of the multitude of interactions between Rab GTPases and MyoV motor proteins, the concept of a *Rab cascade*, also named *Rab conversion* or *Rab maturation*, has been described, which would make the principle of Rab GTPase/MyoV motor interaction as the base of vesicle transport much more complex and complicated (398–400). In this network of Rab GTPases and motor proteins, different Rabs are sequentially targeted to the vesicle surface, which in turn recruit Rab-GEFs and Rab-GAPs to activate the “new” Rab GTPase and to inactivate the “old” one (162, 220, 223, 401). This sequence of events might be a decisive element in the determination of the compartment identity, and therefore for the compartment/vesicle maturation (162). The exchange of Rab proteins at the vesicle membrane could also influence the recruitment of specific MyoV motors in a temporal and spatial fashion. Rab cascades have been described for both, endocytic (223, 399, 402–404) and exocytic, secretory pathways (401, 405–408). A well-established Rab-MyoV network is the Rab11-Rab8-MyoVb network as described during ciliogenesis and apical lumen formation, and in yeast secretory pathways (220, 223, 405, 409, 410). Here, Rab11 is located at an upstream membrane compartment and recruits a GEF for Rab8, for instance Rabin8, in order to activate Rab8 for subsequent membrane targeting (220). The active Rab8 protein now recruits Rab8 specific effector proteins to the membrane to drive further vesicle maturation. One of those effectors is a Rab11-GAP to inactivate Rab11 and to release it from the membrane surface (162, 223, 401). A similar

mechanism is proposed for an interplay between Rab11, Rab8 and MyoVb in the secretion of discoidal/fusiform-shaped vesicles (DFVs) in bladder umbrella cells (398).

The complex formation of Rab11 (and potentially Rab8), MyoV and Spir proteins at vesicle membranes might open the possibility that Spir proteins could be somehow differentially regulated in the processes of Rab cascades or might even influence those by itself.

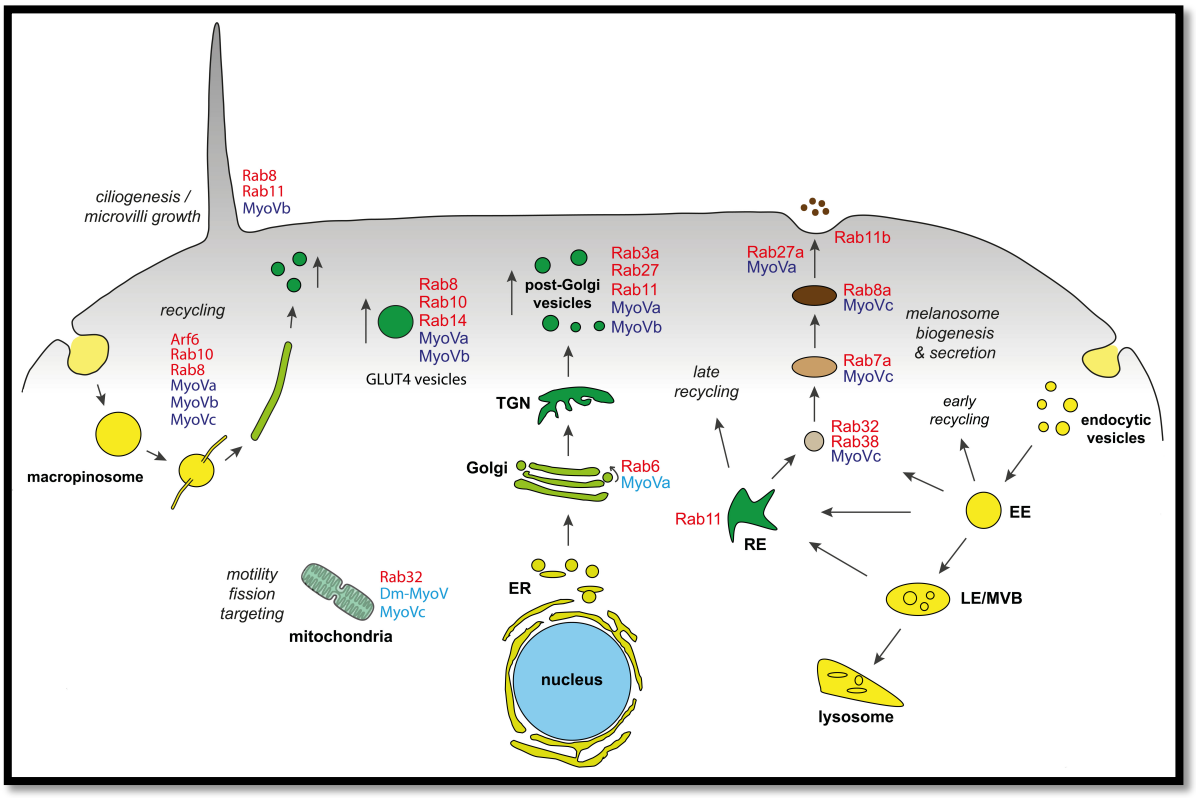

Figure 42 | Overview on Rab GTPase contributions to intracellular transport processes and their potential interactions with MyoV motor proteins in these processes. This overview shortly summarises the function of Rab GTPases in distinct subcellular processes and the therein established interactions with the indicated MyoV motor proteins (*dark blue*). Known Rab/MyoV protein interactions, which might contribute to these processes but what has not been proven to date, are indicated in *light blue*. Endocytic events are drawn in *yellow* and exocytic events in *green*. In general, Rab GTPases are crucial for exocytosis from post-Golgi vesicles (e.g. Rab3A) and by recycling pathways (e.g. Rab11), but also for endocytic uptake (not shown here). Rab8 is involved in recycling processes via macropinocytosis, a tubular membrane network and exocytic vesicles, e.g. for recycling of the transferrin receptor. Rab10 is localised to the same tubular network and might thus function in a similar way. A number of Rab GTPases are critically involved in different steps of melanosome biogenesis, maturation and transport (Rab32/Rab38, Rab7a, Rab8a, Rab27a), arising from the early endosome (EE) and the recycling endosome (RE), and in the release of melanin for subsequent endocytic uptake by keratinocytes (Rab11b) (411). Rab GTPases are also involved in intra-organelle trafficking (e.g. Rab6). Not much is known about the role of Rab GTPases in mitochondria function, but a body of evidence exists for MyoV proteins mediating mitochondria dynamics, including fission and motility (412–414). Rab GTPases furthermore contribute to specific transport processes in specific cell types (e.g. Rab3A, Rab27b and Rab39b in neuronal cells; Rab8 and Rab11 in epithelial cells) which are not shown here. *EE*, early endosome; *LE/MVB*, late endosome/multi-vesicular body; *RE*, recycling endosome; *ER*, endoplasmatic reticulum; *TGN*, trans-Golgi network; *GLUT4*, glucose transporter type 4.

4.6 The Spir/MyoV interaction in context of cellular processes

Myosin V motor proteins have been implicated in the trafficking and dynamics of mitochondria (412–414). Mitochondria are generally transported bidirectional over longer distances along microtubule tracks by kinesin and dynein driven mechanisms (413). Two distinct roles for myosin V motors are proposed, especially within neuronal cells. First, myosin V is expected to act as a tethering factor, which removes mitochondria from transporting microtubule tracks and transfers them to actin networks to create a stationary pool of mitochondria (412). This has been shown as the depletion of myosin V induced an increase of mitochondrial transport, affecting both, velocity and duty cycle along microtubule tracks. Additionally, MyoV depletion induced an increase in mitochondrial length, supposing a role for MyoV in mitochondrial fission (412). Together, it might be the case that the myosin V driven pausing of mitochondria during their transport along microtubules is necessary for mitochondrial fission when attached to actin networks in a stationary phase. Both, mitochondria fission but also the storage at stationary pools itself might be essential processes to evenly distribute mitochondria along the length of the axons and within the axon terminals in order to provide sufficient energy for synaptic activity. Actin networks and the associated myosin V motors might also be involved in rather short range transport of mitochondria within the actin rich presynaptic terminals (414).

The newly discovered and described splice isoform of Spir-1, containing the alternatively spliced exon C and accordingly named Spire1C, has been shown to localise to mitochondrial membranes and drives mitochondrial fission in collaboration with the endoplasmatic reticulum associated inverted formin 2 (INF2) (339). Exon C mediates the Spire1C mitochondrial targeting and is located downstream of the GTBM which would allow MyoV binding of Spire1C in the cytoplasm and, thus, a potential Spire1C induced targeting of MyoV proteins to mitochondrial membranes. The exact targeting mechanism of myosin V motors to mitochondria is still unknown which might open the possibility that a Spir-GTBM mediated Spire1C/MyoV interation induces MyoV localisation to mitochondria membranes.

A study by Wang and co-workers showed a cooperation of Rab11 and MyoVb in the activity dependent transport of AMPA receptor subunits into the postsynaptic densities (PSD) of dendritic spines (251). Synaptic activity induced influx of Ca^{2+} ions into the spine drives the opening of the back-folded MyoVb protein leading to the subsequent association with Rab11 located at the AMPA receptor containing recycling endosome. The Rab11/MyoVb motor protein complex now provides the force to pull the endosomal membrane into the spine head to reach the PSD and to finally facilitate the AMPA receptor subunit insertion. So far, the origin of the actin filaments used for the MyoVb driven motility is not clear. In collaboration with Prof. Dr. Edward Ziff and Dr. Seonil Kim (NYU

Medical Centre, New York, USA) a localisation of the Spir-1 protein at the spine base of mouse primary hippocampal neurons was already revealed (unpublished observations). Therefore, and based on the data presented here, a functional cooperation of Spir proteins, Rab11 and MyoVb in actin filament nucleation and MyoV driven motor activity seems intriguing as an underlying process for this type of AMPA receptor transport and insertion into the PSD.

Recent studies report that mutations and deletions of the FMN-2 protein lead to non-syndromic intellectual disability in humans (415–417). Together with the already described phenotypes for *spir-1*$^{gt/gt}$ mutant mice (defects in emotional learning and memory) (418), as well as for *Fmn-2*$^{-/-}$ knockout mice (defects in age-related associative learning and memory) (419), a cooperative mechanism of Spir, FMN, Rab11 and MyoV proteins in processes underlying learning and memory might be intriguing.

Spir-1 proteins have been shown to be recruited to invadosomes of Src-transformed cells in which they participate in a protein complex containing Src kinase, the formin mDia1 and actin (420). Spir-1 is thereby involved in the proteolytic activity of these cells by the release of membrane-type matrix metalloproteinases (MT-MMPs). MMPs are required to drive ECM degradation and disruption of tissue and cellular barriers, and need to be specifically targeted to invadosomal sites before their release. Consistently, Spir-1 over-expression in such cells induced cell invasions that were faster and increased in number (420). In the same study, an interaction of the C-terminal part of Spir-1 (including Spir-box and FYVE-type domain) and the Rab3A GTPase has been identified, and thus, a role for Spir-1 in the directed trafficking of MMPs to invadosomal sites and in conjunction with Rab3A has been proposed. Considering the reported direct interaction of Rab3A and myosin Va (194) and the functional cooperation of Rab3A and Spir-1 in invadosome activity, it might point towards the formation of a similar tripartite complex including a Rab family GTPase, an actin motor protein and an actin nucleating or elongating protein, which finally decides on cell invasion and cancer metastasis. Nevertheless, the exact role of the myosin V actin motor proteins in these processes need to be further investigated. This assumption is supported by a study on Rab27a, highly related to Rab3A, which has been described to be involved in cell invasion and the metastatic potential of breast cancer cells by regulating the transport of ECM degrading enzymes (421).

Besides the transport of cell originating vesicles, desired vesicles which are readily transported, there are processes of hijacking the cellular transport machineries by extracellular cargo, such as by pathogens, including virus and bacteria. Rab GTPases, such as Rab7, Rab8b and Rab11, are generally involved in the endocytic and exocytic transport of different types of virus (422–427). Rab11 is important for the successful budding and processing of influenza A virus particles (422). Rab11

dependent transport also underlies the release of mumps virus from polarised epithelial cells (423). Rab7a is essentially involved in the late stages of the HIV-1 replication cycle (424). Both, Rab8 and Rab11 have been shown to significantly contribute to the secretion of the New World hantavirus (Andes virus) particles via the recycling endosome (425), and Rab8b has also been observed to be involved in the release of West Nile virus particles (426). Not much is known about the exact Rab GTPase mediated transport and release mechanisms of virus particles, especially about the involvement of myosin V motor proteins. However, there is a study demonstrating the necessity of MyoVc in complex with Rab8 for the release of dengue virus particles (427) which could point towards a general role of Rab GTPase/MyoV motor protein complexes in virus particle transport. Also here, Spir proteins could play a major role in collaboration with Rab GTPases and MyoV motor proteins.

Furthermore, Spir-1 and Spir-2 proteins have been reported to contribute to the invasion process of *Salmonella typhimurium*, although both proteins influence different invasion steps (428), and Spir-2 has been also implicated in the invasion process of *Listeria monocytogenes* (429).

4.7 Conclusion

In summary, this thesis revealed that the coordination of an actin nucleation machinery (Spir/FMN) and Rab11/MyoV based motor activity at the surface of intracellular vesicle membranes is mediated by a direct interaction of Spir and myosin V proteins. This interaction involves a herein newly identified short sequence motif within the Spir proteins that is highly conserved across species, and the globular tail domain of the myosin V actin motors. The Spir/MyoV interaction drives the formation of a tripartite Rab11:MyoV:Spir protein complex at vesicle membranes that is suggested to facilitate vesicle transport by combining *de novo* actin filament nucleation and myosin dependent force generation. Nevertheless, a lot of open questions still remain regarding the molecular dynamics of protein complex formation, the whole spectrum of proteins finally involved in the functional multimeric complex, and the factors inducing activation and membrane targeting of Spir and MyoV proteins. The diversity of interactions of Rab GTPases and MyoV motors, as well as initial findings on other Rab GTPase cooperations with Spir proteins, allows speculating on far reaching contributions of such protein complexes including Rab GTPases, MyoV motors, and actin nucleating, elongating and binding proteins in intracellular transport processes underlying a multitude of cellular processes.

Deciphering these molecular and cellular aspects will be of fundamental importance for future studies and might be indispensable to understand intracellular transport processes as the base of proper cell function, development and survival, but also in terms of disease manifestation and potential treatment targets.

5 References

1. Chavarría, A., and Cárdenas, G. (2013) Neuronal influence behind the central nervous system regulation of the immune cells. *Front. Integr. Neurosci.* **7**, 64
2. Clainche, C. Le, and Carlier, M.-F. F. (2008) Regulation of actin assembly associated with protrusion and adhesion in cell migration. *Physiol. Rev.* **88**, 489–513
3. Langford, G. M. (1995) Actin- and microtubule-dependent organelle motors: interrelationships between the two motility systems. *Curr. Opin. Cell Biol.* **7**, 82–88
4. Woolner, S., and Bement, W. M. (2009) Unconventional myosins acting unconventionally. *Trends Cell Biol.* **19**, 245–52
5. Evans, R. D., Robinson, C., Briggs, D. a, Tooth, D. J., Ramalho, J. S., Cantero, M., Montoliu, L., Patel, S., Sviderskaya, E. V, and Hume, A. N. (2014) Myosin-Va and dynamic actin oppose microtubules to drive long-range organelle transport. *Curr. Biol.* **24**, 1743–50
6. Schroeder, H. W., Mitchell, C., Shuman, H., Holzbaur, E. L. F., and Goldman, Y. E. (2010) Motor Number Controls Cargo Switching at Actin-Microtubule Intersections In Vitro. *Curr. Biol.* **20**, 687–696
7. Welz, T., Wellbourne-Wood, J., and Kerkhoff, E. (2014) Orchestration of cell surface proteins by Rab11. *Trends Cell Biol.* **24**, 407–414
8. Kneussel, M., and Wagner, W. (2013) Myosin motors at neuronal synapses: drivers of membrane transport and actin dynamics. *Nat. Rev. Neurosci.* **14**, 233–47
9. Lawrence, C. J., Dawe, R. K., Christie, K. R., Cleveland, D. W., Dawson, S. C., Endow, S. A., Goldstein, L. S. B., Goodson, H. V., Hirokawa, N., Howard, J., Malmberg, R. L., McIntosh, J. R., Miki, H., Mitchison, T. J., Okada, Y., Reddy, A. S. N., Saxton, W. M., Schliwa, M., Scholey, J. M., Vale, R. D., Walczak, C. E., and Wordeman, L. (2004) A standardized kinesin nomenclature. *J. Cell Biol.* **167**, 19–22
10. Miki, H., Okada, Y., and Hirokawa, N. (2005) Analysis of the kinesin superfamily: Insights into structure and function. *Trends Cell Biol.* **15**, 467–476
11. Hirokawa, N., Noda, Y., Tanaka, Y., and Niwa, S. (2009) Kinesin superfamily motor proteins and intracellular transport. *Nat. Rev. Mol. Cell Biol.* **10**, 682–96
12. Dagenbach, E. M., and Endow, S. A. (2004) A new kinesin tree. *J. Cell Sci.* **117**, 3–7
13. Matsuzaki, F., Shirane, M., Matsumoto, M., and Nakayama, K. I. (2011) Protrudin serves as an adaptor molecule that connects KIF5 and its cargoes in vesicular transport during process formation. *Mol. Biol. Cell*. **22**, 4602–20
14. Vale, R. D., and Fletterick, R. J. (1997) The design plan of kinesin motors. *Annu Rev Cell Dev Biol.* **13**, 745–77
15. Svoboda, K., Schmidt, C., Schnapp, B., and Block, S. (1993) Direct observation of kinesin stepping by optical trapping interferometry. *Nature*
16. Vale, R. D. (2003) The molecular motor toolbox for intracellular transport. *Cell.* **112**, 467–480
17. Bhabha, G., Johnson, G. T., Schroeder, C. M., and Vale, R. D. (2016) How Dynein Moves Along Microtubules. *Trends Biochem. Sci.* **41**, 94–105
18. Allan, V. J. (2011) Cytoplasmic dynein. *Biochem. Soc. Trans.* **39**, 1169–78
19. Kikkawa, M. (2013) Big steps toward understanding dynein. *J. Cell Biol.* **202**, 15–23
20. Roberts, A. J., Kon, T., Knight, P. J., Sutoh, K., and Burgess, S. a (2013) Functions and mechanics of dynein motor proteins. *Nat. Rev. Mol. Cell Biol.* **14**, 713–26
21. Raaijmakers, J. A., and Medema, R. H. (2014) Function and regulation of dynein in mitotic chromosome segregation. *Chromosoma*. **123**, 407–422
22. Tanenbaum, M. E., Vale, R. D., and McKenney, R. J. (2013) Cytoplasmic dynein crosslinks and slides anti-parallel microtubules using its two motor domains. *Elife*. **2013**, 1–20
23. Heald, R., Tournebize, R., Blank, T., Sandaltzopoulos, R., Becker, P., Hyman, A., and Karsenti, E. (1996) Self-organization of microtubules into bipolar spindles around artificial chromosomes in Xenopus egg extracts. *Nature*. **382**, 420–5
24. Rusan, N. M., Serdar Tulu, U., Fagerstrom, C., and Wadsworth, P. (2002) Reorganization of the microtubule array in prophase/prometaphase requires cytoplasmic dynein-dependent microtubule transport. *J. Cell Biol.* **158**, 997–1003
25. Howell, B. J., McEwen, B. F., Canman, J. C., Hoffman, D. B., Farrar, E. M., Rieder, C. L., and Salmon, E. D. (2001) Cytoplasmic dynein/dynactin drives kinetochore protein transport to the spindle poles and has a role in mitotic spindle checkpoint inactivation. *J. Cell Biol.* **155**, 1159–1172
26. Varma, D., Monzo, P., Stehman, S. A., and Vallee, R. B. (2008) Direct role of dynein motor in stable kinetochore-

microtubule attachment, orientation, and alignment. *J. Cell Biol.* **182**, 1045–1054

27. Carminati, J. L., and Stearns, T. (1997) Microtubules orient the mitotic spindle in yeast through dynein- dependent interactions with the cell cortex. *J. Cell Biol.* **138**, 629–641
28. Niedner, A., Edelmann, F. T., and Niessing, D. (2014) Of social molecules: The interactive assembly of ASH1 mRNA-transport complexes in yeast. *RNA Biol.* **11**, 998–1009
29. Tsai, J. W., Bremner, K. H., and Vallee, R. B. (2007) Dual subcellular roles for LIS1 and dynein in radial neuronal migration in live brain tissue. *Nat Neurosci*. **10**, 970–979
30. Burke, B., and Roux, K. J. (2009) Nuclei Take a Position: Managing Nuclear Location. *Dev. Cell*. **17**, 587–597
31. Wynshaw-Boris, A., Pramparo, T., Youn, Y. H., and Hirotsune, S. (2010) Lissencephaly: mechanistic insights from animal models and potential therapeutic strategies. *Semin. Cell Dev. Biol.* **21**, 823–30
32. Qiu, W., Derr, N. D., Goodman, B. S., Villa, E., Wu, D., Shih, W., and Reck-Peterson, S. L. (2012) Dynein achieves processive motion using both stochastic and coordinated stepping. *Nat. Struct. Mol. Biol.* **19**, 193–200
33. Ma, S., and Chisholm, R. L. (2002) Cytoplasmic dynein-associated structures move bidirectionally in vivo. *J. Cell Sci.* **115**, 1453–1460
34. Odronitz, F., and Kollmar, M. (2007) Drawing the tree of eukaryotic life based on the analysis of 2,269 manually annotated myosins from 328 species. *Genome Biol.* **8**, R196
35. Hammer, J. a, and Sellers, J. R. (2012) Walking to work: roles for class V myosins as cargo transporters. *Nat. Rev. Mol. Cell Biol.* **13**, 13–26
36. Sakamoto, T., Wang, F., Schmitz, S., Xu, Y., Xu, Q., Molloy, J. E., Veigel, C., and Sellers, J. R. (2003) Neck length and processivity of myosin V. *J. Biol. Chem.* **278**, 29201–7
37. Howard, J., and Spudich, J. A. (1996) Is the lever arm of myosin a molecular elastic element? *Proc. Natl. Acad. Sci. U. S. A.* **93**, 4462–4
38. Warshaw, D. M., Guilford, W. H., Freyzon, Y., Krementsova, E., Palmiter, K. A., Tyska, M. J., Baker, J. E., and Trybus, K. M. (2000) The light chain binding domain of expressed smooth muscle heavy meromyosin acts as a mechanical lever. *J. Biol. Chem.* **275**, 37167–72
39. Ruff, C., Furch, M., Brenner, B., Manstein, D. J., and Meyhöfer, E. (2001) Single-molecule tracking of myosins with genetically engineered amplifier domains. *Nat. Struct. Biol.* **8**, 226–9
40. Sellers, J. R. (2004) Fifty years of contractility research post sliding filament hypothesis. *J. Muscle Res. Cell Motil.* **25**, 475–482
41. Vicente-Manzanares, M., Ma, X., Adelstein, R. S., and Horwitz, A. R. (2009) Non-muscle myosin II takes centre stage in cell adhesion and migration. *Nat. Rev. Mol. Cell Biol.* **10**, 778–90
42. Medeiros, N. A., Burnette, D. T., and Forscher, P. (2006) Myosin II functions in actin-bundle turnover in neuronal growth cones. **8**, 215–226
43. Pasapera, A. M., Schneider, I. C., Rericha, E., Schlaepfer, D. D., and Waterman, C. M. (2010) Myosin II activity regulates vinculin recruitment to focal adhesions through FAK-mediated paxillin phosphorylation. *J. Cell Biol.* **188**, 877–890
44. Ma, X., Kovacs, M., Conti, M. A., Wang, A., Zhang, Y., Sellers, J. R., and Adelstein, R. S. (2012) Nonmuscle myosin II exerts tension but does not translocate actin in vertebrate cytokinesis. *Proc. Natl. Acad. Sci.* **109**, 4509–4514
45. Straight, A. F., Cheung, A., Limouze, J., Chen, I., Westwood, N. J., Sellers, J. R., and Mitchison, T. J. (2003) Dissecting temporal and spatial control of cytokinesis with a myosin II Inhibitor. *Science*. **299**, 1743–7
46. Taylor Eves, P., Jin, Y., Brunner, M., and Weisman, L. S. (2012) Overlap of cargo binding sites on myosin V coordinates the inheritance of diverse cargoes. *J. Cell Biol.* **198**, 69–85
47. Cheney, R. E., Shea, M. K. O., Heuser, J. E., Coelho, M. V, Wolenski, J. S., Espraafico, E. M., Forecher, P., Larson, R. E., and Mooseker, M. S. (1993) Brain Myosin-V Is a Two-Headed Unconventional I ll. **75**, 13–23
48. Watanabe, S., Mabuchi, K., Ikebe, R., and Ikebe, M. (2006) Mechanoenzymatic characterization of human myosin Vb. *Biochemistry*. **45**, 2729–2738
49. Tóth, J., Kovács, M., Wang, F., Nyitray, L., and Sellers, J. R. (2005) Myosin V from Drosophila reveals diversity of motor mechanisms within the myosin V family. *J. Biol. Chem.* **280**, 30594–603
50. Nelson, S. R., Trybus, K. M., and Warshaw, D. M. (2014) Motor coupling through lipid membranes enhances transport velocities for ensembles of myosin Va. *Proc. Natl. Acad. Sci. U. S. A.* **111**, E3986-95
51. Berg, J. S., Powell, B. C., and Cheney, R. E. (2001) A millennial myosin census. *Mol. Biol. Cell*. **12**, 780–94
52. Zhao, L. P., Koslovsky, J. S., Reinhard, J., Bähler, M., Witt, a E., Provance, D. W., and Mercer, J. a (1996) Cloning and characterization of myr 6, an unconventional myosin of the dilute/myosin-V family. *Proc. Natl. Acad. Sci. U. S. A.* **93**, 10826–31
53. Mercer, J. A., Seperack, P. K., Strobel, M. C., Copeland, N. G., and Jenkins, N. A. (1991) Novel myosin heavy chain encoded by murine dilute coat colour locus. *Nature*. **349**, 709–713
54. Rodriguez, O. C., and Cheney, R. E. (2002) Human myosin-Vc is a novel class V myosin expressed in epithelial cells.

J. Cell Sci. **115**, 991–1004

55. Roland, J. T., Lapierre, L. a, and Goldenring, J. R. (2009) Alternative splicing in class V myosins determines association with Rab10. *J. Biol. Chem.* **284**, 1213–23
56. Espreafico, E. M., Cheney, R. E., Matteoli, M., Nascimento, A. A. C., De Camilli, P. V., Larson, R. E., and Mooseker, M. S. (1992) Primary structure and cellular localization of chicken brain myosin-V (p190), an unconventional myosin with calmodulin light chains. *J. Cell Biol.* **119**, 1541–1557
57. Lisé, M. F., Tak, P. W., Trinh, A., Hines, R. M., Liu, L., Kang, R., Hines, D. J., Lu, J., Goldenring, J. R., Yu, T. W., and El-Husseini, A. (2006) Involvement of myosin Vb in glutamate receptor trafficking. *J. Biol. Chem.* **281**, 3669–3678
58. Tilelli, C. Q., Martins, A. R., Larson, R. E., and Garcia-Cairasco, N. (2003) Immunohistochemical localization of myosin Va in the adult rat brain. *Neuroscience*. **121**, 573–586
59. Cheney, R. E., O'Shea, M. K., Heuser, J. E., Coelho, M. V, Wolenski, J. S., Espreafico, E. M., Forscher, P., Larson, R. E., and Mooseker, M. S. (1993) Brain myosin-V is a two-headed unconventional myosin with motor activity. *Cell*. **75**, 13–23
60. Ishmael, J. E., Safic, M., Amparan, D., Vogel, W. K., Pham, T., Marley, K., Filtz, T. M., and Maier, C. S. (2007) Nonmuscle myosins II-B and Va are components of detergent-resistant membrane skeletons derived from mouse forebrain. *Brain Res.* **1143**, 46–59
61. Petralia, R. S., Wang, Y. X., Sans, N., Worley, P. F., Hammer, J. A., and Wenthold, R. J. (2001) Glutamate receptor targeting in the postsynaptic spine involves mechanisms that are independent of myosin Va. *Eur. J. Neurosci.* **13**, 1722–1732
62. Naisbitt, S., Valtschanoff, J., Allison, D. W., Sala, C., Kim, E., Craig, A. M., Weinberg, R. J., and Sheng, M. (2000) Interaction of the postsynaptic density-95/guanylate kinase domain-associated protein complex with a light chain of myosin-V and dynein. *J. Neurosci.* **20**, 4524–34
63. Seperack, P. K., Mercer, J. A., Strobel, M. C., Copeland, N. G., and Jenkins, N. A. (1995) Retroviral sequences located within an intron of the dilute gene alter dilute expression in a tissue-specific manner. *EMBO J.* **14**, 2326–2332
64. Huang, J. D., Mermall, V., Strobel, M. C., Russell, L. B., Mooseker, M. S., Copeland, N. G., and Jenkins, N. A. (1998) Molecular genetic dissection of mouse unconventional myosin-VA: Tail region mutations. *Genetics*. **148**, 1963–1972
65. Lambert, J., Naeyaert, J. M., Callens, T., De Paepe, A., and Messiaen, L. (1998) Human myosin V gene produces different transcripts in a cell type-specific manner. *Biochem. Biophys. Res. Commun.* **252**, 329–33
66. Wagner, W., Fodor, E., Ginsburg, A., and Hammer, J. A. (2006) The binding of DYNLL2 to myosin Va requires alternatively spliced exon B and stabilizes a portion of the myosin's coiled-coil domain. *Biochemistry*. **45**, 11564–11577
67. Hódi, Z., Németh, A. L., Radnai, L., Hetényi, C., Schlett, K., Bodor, A., Perczel, A., and Nyitray, L. (2006) Alternatively spliced exon B of myosin Va is essential for binding the tail-associated light chain shared by dynein. *Biochemistry*. **45**, 12582–95
68. Sakamoto, T., Webb, M. R., Forgacs, E., White, H. D., and Sellers, J. R. (2008) Direct observation of the mechanochemical coupling in myosin Va during processive movement. *Nature*. **455**, 128–132
69. Mehta, A. D., Rock, R. S., Rief, M., Spudich, J. A., Mooseker, M. S., and Cheney, R. E. (1999) Myosin-V is a processive actin-based motor. *Nature*. **400**, 590–3
70. Sakamoto, T., Amitani, I., Yokota, E., and Ando, T. (2000) Direct observation of processive movement by individual myosin V molecules. *Biochem. Biophys. Res. Commun.* **272**, 586–590
71. Kodera, N., Yamamoto, D., Ishikawa, R., and Ando, T. (2010) Video imaging of walking myosin V by high-speed atomic force microscopy. *Nature*. **468**, 72–6
72. Murphy, C. T., Rock, R. S., and Spudich, J. a (2001) A myosin II mutation uncouples ATPase activity from motility and shortens step size. *Nat. Cell Biol.* **3**, 311–315
73. Warshaw, D. M., Kennedy, G. G., Work, S. S., Krementsova, E. B., Beck, S., and Trybus, K. M. (2005) Differential labeling of myosin V heads with quantum dots allows direct visualization of hand-over-hand processivity. *Biophys. J.* **88**, L30-2
74. Churchman, L. S., Okten, Z., Rock, R. S., Dawson, J. F., and Spudich, J. A. (2005) Single molecule high-resolution colocalization of Cy3 and Cy5 attached to macromolecules measures intramolecular distances through time. *Proc. Natl. Acad. Sci. U. S. A.* **102**, 1419–23
75. Walker, M. L., Burgess, S. A., Sellers, J. R., Wang, F., Hammer, J. A., Trinick, J., and Knight, P. J. (2000) Two-headed binding of a processive myosin to F-actin. *Nature*. **405**, 804–7
76. Purcell, T. J., Morris, C., Spudich, J. A., and Sweeney, H. L. (2002) Role of the lever arm in the processive stepping of myosin V. *Pnas*. **99**, 14159–14164
77. Sakamoto, T., Yildez, A., Selvin, P. R., and Sellers, J. R. (2005) Step-size is determined by neck length in myosin V. *Biochemistry*. **44**, 16203–16210
78. Nagy, A., Piszczek, G., and Sellers, J. R. (2009) Extensibility of the extended tail domain of processive and

nonprocessive myosin V molecules. *Biophys. J.* **97**, 3123–31

79. Schilstra, M. J., and Martin, S. R. (2006) An elastically tethered viscous load imposes a regular gait on the motion of myosin-V. Simulation of the effect of transient force relaxation on a stochastic process. *J. R. Soc. Interface*. **3**, 153–65
80. Wu, X. S., Rao, K., Zhang, H., Wang, F., Sellers, J. R., Matesic, L. E., Copeland, N. G., Jenkins, N. A., and Hammer, J. A. (2002) Identification of an organelle receptor for myosin-Va. *Nat. Cell Biol.* **4**, 271–278
81. Wu, X., Wang, F., Rao, K., Sellers, J. R., and Hammer, J. A. (2002) Rab27a is an essential component of melanosome receptor for myosin Va. *Mol. Biol. Cell*. **13**, 1735–49
82. Fukuda, M., Kuroda, T. S., and Mikoshiba, K. (2002) Slac2-a/melanophilin, the missing link between Rab27 and myosin Va: Implications of a tripartite protein complex for melanosome transport. *J. Biol. Chem.* **277**, 12432–12436
83. Strom, M., Hume, A. N., Tarafder, A. K., Barkagianni, E., and Seabra, M. C. (2002) A family of Rab27-binding proteins: Melanophilin links Rab27a and myosin Va function in melanosome transport. *J. Biol. Chem.* **277**, 25423–25430
84. Nagashima, K., Torii, S., Yi, Z., Igarashi, M., Okamoto, K., Takeuchi, T., and Izumi, T. (2002) Melanophilin directly links Rab27a and myosin Va through its distinct coiled-coil regions. *FEBS Lett.* **517**, 233–8
85. Ali, M. Y., Krementsova, E. B., Kennedy, G. G., Mahaffy, R., Pollard, T. D., Trybus, K. M., and Warshaw, D. M. (2007) Myosin Va maneuvers through actin intersections and diffuses along microtubules. *Proc. Natl. Acad. Sci. U. S. A.* **104**, 4332–6
86. De La Cruz, E. M., Wells, A. L., Rosenfeld, S. S., Ostap, E. M., and Sweeney, H. L. (1999) The kinetic mechanism of myosin V. *Proc Natl Acad Sci U S A*. **96**, 13726–13731
87. De La Cruz, E. M., and Ostap, E. M. (2004) Relating biochemistry and function in the myosin superfamily. *Curr. Opin. Cell Biol.* **16**, 61–67
88. Veigel, C., Schmitz, S., Wang, F., and Sellers, J. R. (2005) Load-dependent kinetics of myosin-V can explain its high processivity. *Nat. Cell Biol.* **7**, 861–869
89. Rosenfeld, S. S., and Sweeney, H. L. (2004) A model of myosin V processivity. *J. Biol. Chem.* **279**, 40100–40111
90. Purcell, T. J., Sweeney, H. L., and Spudich, J. A. (2005) A force-dependent state controls the coordination of processive myosin V. *Proc. Natl. Acad. Sci. U. S. A.* **102**, 13873–13878
91. Forgacs, E., Cartwright, S., Sakamoto, T., Sellers, J. R., Corrie, J. E. T., Webb, M. R., and White, H. D. (2008) Kinetics of ADP dissociation from the trail and lead heads of actomyosin V following the power stroke. *J. Biol. Chem.* **283**, 766–773
92. Takagi, Y., Yang, Y., Fujiwara, I., Jacobs, D., Cheney, R. E., Sellers, J. R., and Kovacs, M. (2008) Human Myosin Vc Is a Low Duty Ratio, Nonprocessive Molecular Motor. *J. Biol. Chem.* **283**, 8527–8537
93. Watanabe, S., Watanabe, T. M., Sato, O., Awata, J., Homma, K., Umeki, N., Higuchi, H., Ikebe, R., and Ikebe, M. (2008) Human myosin Vc is a low duty ratio nonprocessive motor. *J. Biol. Chem.* **283**, 10581–10592
94. Taft, M. H., Hartmann, F. K., Rump, A., Keller, H., Chizhov, I., Manstein, D. J., and Tsiavaliaris, G. (2008) Dictyostelium myosin-5b is a conditional processive motor. *J. Biol. Chem.* **283**, 26902–26910
95. Dunn, B. D., Sakamoto, T., Hong, M. S. S., Sellers, J. R., and Takizawa, P. A. (2007) Myo4p is a monomeric myosin with motility uniquely adapted to transport mRNA. *J. Cell Biol.* **178**, 1193–1206
96. Hodges, A. R., Bookwalter, C. S., Krementsova, E. B., and Trybus, K. M. (2009) A Nonprocessive Class V Myosin Drives Cargo Processively When a Kinesin- Related Protein Is a Passenger. *Curr. Biol.* **19**, 2121–2125
97. Hodges, A. R., Krementsova, E. B., and Trybus, K. M. (2008) She3p binds to the rod of yeast myosin V and prevents it from dimerizing, forming a single-headed motor complex. *J. Biol. Chem.* **283**, 6906–6914
98. Li, X.-D., Jung, H. S., Wang, Q., Ikebe, R., Craig, R., and Ikebe, M. (2008) The globular tail domain puts on the brake to stop the ATPase cycle of myosin Va. *Proc. Natl. Acad. Sci. U. S. A.* **105**, 1140–5
99. Liu, J., Taylor, D. W., Krementsova, E. B., Trybus, K. M., and Taylor, K. A. (2006) Three-dimensional structure of the myosin V inhibited state by cryoelectron tomography. *Nature*. **442**, 208–11
100. Thirumurugan, K., Sakamoto, T., Hammer, J. A., Sellers, J. R., and Knight, P. J. (2006) The cargo-binding domain regulates structure and activity of myosin 5. *Nature*. **442**, 212–5
101. Sato, O., Li, X. D., and Ikebe, M. (2007) Myosin Va becomes a low duty ratio motor in the inhibited form. *J. Biol. Chem.* **282**, 13228–13239
102. Lu, H., Krementsova, E. B., and Trybus, K. M. (2006) Regulation of myosin V processivity by calcium at the single molecule level. *J. Biol. Chem.* **281**, 31987–31994
103. Lindsay, A. J., Jollivet, F., Horgan, C. P., Khan, A. R., Raposo, G., McCaffrey, M. W., and Goud, B. (2013) Identification and characterization of multiple novel Rab-myosin Va interactions. *Mol. Biol. Cell*. **24**, 3420–34
104. Wang, F., Thirumurugan, K., Stafford, W. F., Hammer, J. A., Knight, P. J., and Sellers, J. R. (2004) Regulated Conformation of Myosin V. *J. Biol. Chem.* **279**, 2333–2336
105. Trybus, K. M., Gushchin, M. I., Lui, H., Hazelwood, L., Krementsova, E. B., Volkmann, N., and Hanein, D. (2007)

Effect of calcium on calmodulin bound to the IQ motifs of myosin V. *J. Biol. Chem.* **282**, 23316–23325

106. Nguyen, H., and Higuchi, H. (2005) Motility of myosin V regulated by the dissociation of single calmodulin. *Nat. Struct. Mol. Biol.* **12**, 127–132
107. Wu, X., Sakamoto, T., Zhang, F., Sellers, J. R., and Hammer, J. A. (2006) In vitro reconstitution of a transport complex containing Rab27a, melanophilin and myosin Va. *FEBS Lett.* **580**, 5863–5868
108. Li, X. D., Ikebe, R., and Ikebei, M. (2005) Activation of myosin Va function by melanophilin, a specific docking partner of myosin Va. *J. Biol. Chem.* **280**, 17815–17822
109. Yao, L. L., Cao, Q. J., Zhang, H. M., Zhang, J., Cao, Y., and Li, X. D. (2015) Melanophilin Stimulates Myosin-5a Motor Function by Allosterically Inhibiting the Interaction between the Head and Tail of Myosin-5a. *Sci Rep*. **5**, 10874
110. Nascimento, A. A. C., Amaral, R. G., Bizario, J. C. S., Larson, R. E., and Espreafico, E. M. (1997) Subcellular localization of myosin-V in the B16 melanoma cells, a wild-type cell line for the dilute gene. *Mol. Biol. Cell*. **8**, 1971–88
111. Tabb, J. S., Molyneaux, B. J., Cohen, D. L., Kuznetsov, S. a, and Langford, G. M. (1998) Transport of ER vesicles on actin filaments in neurons by myosin V. *J. Cell Sci.* **111**, 3221–3234
112. Gross, S. P., Carolina Tuma, M., Deacon, S. W., Serpinskaya, A. S., Reilein, A. R., and Gelfand, V. I. (2002) Interactions and regulation of molecular motors in Xenopus melanophores. *J. Cell Biol.* **156**, 855–865
113. Klumpp, S., and Lipowsky, R. (2005) Cooperative cargo transport by several molecular motors. *Proc. Natl. Acad. Sci. USA*. **102**, 17284–9
114. Vershinin, M., Carter, B. C., Razafsky, D. S., King, S. J., and Gross, S. P. (2007) Multiple-motor based transport and its regulation by Tau. *Proc. Natl. Acad. Sci. U. S. A.* **104**, 87–92
115. Conway, L., Wood, D., Tüzel, E., and Ross, J. L. (2012) Motor transport of self-assembled cargos in crowded environments. *Proc. Natl. Acad. Sci.* **109**, 20814–9
116. Hariadi, R. F., Cale, M., and Sivaramakrishnan, S. (2014) Myosin lever arm directs collective motion on cellular actin network. *Proc. Natl. Acad. Sci.* **111**, 4091–4096
117. Böhm, K. J., Stracke, R., and Unger, E. (2000) Speeding up kinesin-driven microtubule gliding in vitro by variation of cofactor composition and physicochemical parameters. *Cell Biol. Int.* **24**, 335–41
118. Beeg, J., Klumpp, S., Dimova, R., Gracià, R. S., Unger, E., and Lipowsky, R. (2008) Transport of Beads by Several Kinesin Motors. *Biophys. J.* **94**, 532–541
119. Rogers, A. R., Driver, J. W., Constantinou, P. E., Kenneth Jamison, D., and Diehl, M. R. (2009) Negative interference dominates collective transport of kinesin motors in the absence of load. *Phys. Chem. Chem. Phys.* **11**, 4882–9
120. Sivaramakrishnan, S., and Spudich, J. A. (2009) Coupled myosin VI motors facilitate unidirectional movement on an F-actin network. *J. Cell Biol.* **187**, 53–60
121. Kad, N. M., Trybus, K. M., and Warshaw, D. M. (2008) Load and Pi control flux through the branched kinetic cycle of myosin V. *J. Biol. Chem.* **283**, 17477–17484
122. Clemen, A. E.-M., Vilfan, M., Jaud, J., Zhang, J., Bärmann, M., and Rief, M. (2005) Force-dependent stepping kinetics of myosin-V. *Biophys. J.* **88**, 4402–4410
123. Efremov, A. K., Radhakrishnan, A., Tsao, D. S., Bookwalter, C. S., Trybus, K. M., and Diehl, M. R. (2014) Delineating cooperative responses of processive motors in living cells. *Proc. Natl. Acad. Sci. U. S. A.* **111**, E334-43
124. Sckolnick, M., Krementsova, E. B., Warshaw, D. M., and Trybus, K. M. (2013) More than just a cargo adapter, melanophilin prolongs and slows processive runs of myosin Va. *J. Biol. Chem.* **288**, 29313–22
125. Ali, M. Y., Lu, H., Bookwalter, C. S., Warshaw, D. M., and Trybus, K. M. (2008) Myosin V and Kinesin act as tethers to enhance each others' processivity. *Proc. Natl. Acad. Sci. U. S. A.* **105**, 4691–4696
126. Stenmark, H. (2009) Rab GTPases as coordinators of vesicle traffic. *Nat. Rev. Mol. Cell Biol.* **10**, 513–25
127. Rojas, A. M., Fuentes, G., Rausell, A., and Valencia, A. (2012) The Ras protein superfamily: Evolutionary tree and role of conserved amino acids. *J. Cell Biol.* **196**, 189–201
128. Heasman, S. J., and Ridley, A. J. (2008) Mammalian Rho GTPases: new insights into their functions from in vivo studies. *Nat. Rev. Mol. Cell Biol.* **9**, 690–701
129. Hall, A. (2012) Rho family GTPases. *Biochem. Soc. Trans.* **40**, 1378–82
130. Park, H.-O., and Bi, E. (2007) Central roles of small GTPases in the development of cell polarity in yeast and beyond. *Microbiol. Mol. Biol. Rev.* **71**, 48–96
131. Wennerberg, K., Rossman, K. L., and Der, C. J. (2005) The Ras superfamily at a glance. *J. Cell Sci.* **118**, 843–846
132. Reiner, D. J., and Lundquist, E. A. (2016) Small GTPases. *WormBook*. 10.1002/ejoc.201200111
133. Holbrook, S. R., and Kim, S. H. (1989) Molecular model of the G protein alpha subunit based on the crystal structure of the HRAS protein. *Proc. Natl. Acad. Sci. U. S. A.* **86**, 1751–5
134. Bos, J., Rehmann, H., and Wittinghofer, A. (2007) GEFs and GAPs : Critical Elements in the Control of Small G Proteins. *Cell*. **129**, 865–877

135. Pechlivanis, M., and Kuhlmann, J. (2006) Hydrophobic modifications of Ras proteins by isoprenoid groups and fatty acids-More than just membrane anchoring. *Biochim. Biophys. Acta - Proteins Proteomics*. **1764**, 1914–1931

136. Zhang, F. L., and Casey, P. J. (1996) Protein prenylation: molecular mechanisms and functional consequences. *Annu. Rev. Biochem.* **65**, 241–269

137. Alexandrov, K., Horiuchi, H., Steele-Mortimer, O., Seabra, M. C., and Zerial, M. (1994) Rab escort protein-1 is a multifunctional protein that accompanies newly prenylated rab proteins to their target membranes. *EMBO J.* **13**, 5262–5273

138. Pereira-Leal, J. B., Hume, A. N., and Seabra, M. C. (2001) Prenylation of Rab GTPases: Molecular mechanisms and involvement in genetic disease. *FEBS Lett.* **498**, 197–200

139. Seabra, M. C. (1996) Nucleotide dependence of rab geranylgeranylation rab escort protein interacts preferentially with GDP-bound Rab. *J. Biol. Chem.* **271**, 14398–14404

140. Shen, F., and Seabra, M. C. (1996) Mechanism of digeranylgeranylation of rab proteins: Formation of a complex between Monogeranylgeranyl-Rab and Rab escort protein. *J. Biol. Chem.* **271**, 3692–3698

141. Fried, H., and Kutay, U. (2003) Nucleocytoplasmic transport: Taking an inventory. *Cell. Mol. Life Sci.* **60**, 1659–1688

142. Schmick, M., Kraemer, A., and Bastiaens, P. I. H. (2015) Ras moves to stay in place. *Trends Cell Biol.* **25**, 190–197

143. Matsui, Y., Kikuchi, a, Araki, S., Hata, Y., Kondo, J., Teranishi, Y., and Takai, Y. (1990) Molecular cloning and characterization of a novel type of regulatory protein (GDI) for smg p25A, a ras p21-like GTP-binding protein. *Mol. Cell. Biol.* **10**, 4116–22

144. Garcia-Mata, R., Boulter, E., and Burridge, K. (2011) The "invisible hand": regulation of RHO GTPases by RHOGDIs. *Nat. Rev. Mol. Cell Biol.* **12**, 493–504

145. Chandra, A., Grecco, H. E., Pisupati, V., Perera, D., Cassidy, L., Skoulidis, F., Ismail, S. a., Hedberg, C., Hanzal-Bayer, M., Venkitaraman, A. R., Wittinghofer, A., and Bastiaens, P. I. H. (2012) The GDI-like solubilizing factor PDEδ sustains the spatial organization and signalling of Ras family proteins. *Nat. Cell Biol.* **14**, 329–329

146. Wandinger-Ness, A., and Zerial, M. (2014) Rab Proteins and the Compartmentalization of the Endosomal system. *Cold Spring Harb. Perspect. Biol.* **6**, 1–25

147. Ullrich, O., Horiuchi, H., Bucci, C., and Zerial, M. (1994) Membrane association of Rab5 mediated by GDP-dissociation inhibitor and accompanied by GDP/GTP exchange. *Nature*. **368**, 157–160

148. Ullrich, O., Stenmark, H., Alexandrov, K., Huber, L. A., Kaibuchi, K., Sasaki, T., Takai, Y., and Zerial, M. (1993) Rab GDP dissociation inhibitor as a general regulator for the membrane association of rab proteins. *J. Biol. Chem.* **268**, 18143–18150

149. Soldati, T., Shapiro, a D., Svejstrup, a B., and Pfeffer, S. R. (1994) Membrane targeting of the small GTPase Rab9 is accompanied by nucleotide exchange. *Nature*. **369**, 76–78

150. Schwartz, S. L., Cao, C., Pylypenko, O., Rak, A., and Wandinger-Ness, A. (2007) Rab GTPases at a glance. *J. Cell Sci.* **120**, 3905–3910

151. Pereira-Leal, J. B., and Seabra, M. C. (2001) Evolution of the Rab family of small GTP-binding proteins. *J. Mol. Biol.* **313**, 889–901

152. Zerial, M., and McBride, H. (2001) Rab proteins as membrane organizers. *Nat. Rev. Mol. Cell Biol.* **2**, 107–117

153. Chavrier, P., Parton, R. G., Hauri, H. P., Simons, K., and Zerial, M. (1990) Localization of Low-Molecular-Weight Gtp Binding-Proteins to Exocytic and Endocytic Compartments. *Cell*. **62**, 317–329

154. Pfeffer, S. R. (2005) Structural clues to rab GTPase functional diversity. *J. Biol. Chem.* **280**, 15485–15488

155. Eathiraj, S., Pan, X., Ritacco, C., and Lambright, D. G. (2005) Structural basis of family-wide Rab GTPase recognition by rabenosyn-5. *Nature*. **436**, 415–9

156. Albert, Š., and Gallwitz, D. (1999) Two new members of a family of Ypt/Rab GTPase activating proteins. Promiscuity of substrate recognition. *J. Biol. Chem.* **274**, 33186–33189

157. Albert, Š., Will, E., and Gallwitz, D. (1999) Identification of the catalytic domains and their functionally critical arginine residues of two yeast GTPase-activating proteins specific for Ypt/Rab transport GTPases. *EMBO J.* **18**, 5216–5225

158. Strom, M., Vollmer, P., Tan, T. J., and Gallwitz, D. (1993) A yeast GTPase-activating protein that interacts specifically with a member of the Ypt/Rab family. *Nature*. **361**, 736–9

159. Pan, X., Eathiraj, S., Munson, M., and Lambright, D. G. (2006) TBC-domain GAPs for Rab GTPases accelerate GTP hydrolysis by a dual-finger mechanism. *Nature*. **442**, 303–306

160. Rak, A., Fedorov, R., Alexandrov, K., Albert, S., Goody, R. S., Gallwitz, D., and Scheidig, a J. (2000) Crystal structure of the GAP domain of Gyp1p: first insights into interaction with Ypt/Rab proteins. *EMBO J.* **19**, 5105–5113

161. Nottingham, R. M., Pusapati, G. V., Ganley, I. G., Barr, F. A., Lambright, D. G., and Pfeffer, S. R. (2012) RUTBC2 protein, a Rab9A effector and GTPase-activating protein for Rab36. *J. Biol. Chem.* **287**, 22740–22748

162. Barr, F., and Lambright, D. G. (2010) Rab GEFs and GAPs. *Curr. Opin. Cell Biol.* **22**, 461–470

163. Sivars, U., Aivazian, D., and Pfeffer, S. R. (2003) Yip3 catalyses the dissociation of endosomal Rab–GDI complexes.

Nature. **425**, 856–859

164. Peränen, J. (2011) Rab8 GTPase as a regulator of cell shape. *Cytoskeleton (Hoboken).* **68**, 527–39
165. Vitelli, R., Santillo, M., Lattero, D., Chiariello, M., Bifulco, M., Bruni, C. B., and Bucci, C. (1997) Role of the small GTPase RAB7 in the late endocytic pathway. *J. Biol. Chem.* **272**, 4391–4397
166. Yang, M., Chen, T., Han, C., Li, N., Wan, T., and Cao, X. (2004) Rab7b, a novel lysosome-associated small GTPase, is involved in monocytic differentiation of human acute promyelocytic leukemia cells. *Biochem. Biophys. Res. Commun.* **318**, 792–799
167. Progida, C., Cogli, L., Piro, F., De Luca, A., Bakke, O., and Bucci, C. (2010) Rab7b controls trafficking from endosomes to the TGN. *J. Cell Sci.* **123**, 1480–1491
168. Arai, S., Noda, Y., Kainuma, S., Wada, I., and Yoda, K. (2008) *Ypt11 Functions in Bud-Directed Transport of the Golgi by Linking Myo2 to the Coatomer Subunit Ret2*, 10.1016/j.cub.2008.06.028
169. Seabra, M. C., and Coudrier, E. (2004) Rab GTPases and Myosin Motors in Organelle Motility. *Traffic*. **5**, 393–399
170. Itoh, T., Watabe, A., Toh-e, A., and Matsui, Y. (2002) Complex Formation with Ypt11p, a rab-Type Small GTPase, Is Essential To Facilitate the Function of Myo2p, a Class V Myosin, in Mitochondrial Distribution in Saccharomyces cerevisiae. *Mol. Cell. Biol.* **22**, 7744–7757
171. Schott, D., Ho, J., Pruyne, D., and Bretscher, A. (1999) The COOH-terminal domain of Myo2p, a yeast myosin V, has a direct role in secretory vesicle targeting. *J. Cell Biol.* **147**, 791–808
172. Hume, A. N., Collinson, L. M., Rapak, A., Gomes, A. Q., Hopkins, C. R., and Seabra, M. C. (2001) Rab27a regulates the peripheral distribution of melanosomes in melanocytes. *J. Cell Biol.* **152**, 795–808
173. Matesic, L. E., Yip, R., Reuss, A. E., Swing, D. A., O'Sullivan, T. N., Fletcher, C. F., Copeland, N. G., and Jenkins, N. A. (2001) Mutations in Mlph, encoding a member of the Rab effector family, cause the melanosome transport defects observed in leaden mice. *Proc. Natl. Acad. Sci. U. S. A.* **98**, 10238–43
174. Ménasché, G., Pastural, E., Feldmann, J., Certain, S., Ersoy, F., Dupuis, S., Wulffraat, N., Bianchi, D., Fischer, A., Le Deist, F., and de Saint Basile, G. (2000) Mutations in RAB27A cause Griscelli syndrome associated with haemophagocytic syndrome. *Nat. Genet.* **25**, 173–176
175. Wu, X., Rao, K., Bowers, M. B., Copeland, N. G., Jenkins, N. a, and Hammer, J. a (2001) Rab27a enables myosin Va-dependent melanosome capture by recruiting the myosin to the organelle. *J. Cell Sci.* **114**, 1091–1100
176. Cağdaş, D., Ozgür, T. T., Asal, G. T., Tezcan, I., Metin, A., Lambert, N., de Saint Basile, G., and Sanal, O. (2012) Griscelli syndrome types 1 and 3: analysis of four new cases and long-term evaluation of previously diagnosed patients. *Eur. J. Pediatr.* **171**, 1527–31
177. Arico, M., Zecca, M., Santoro, N., Caselli, D., Maccario, R., Danesino, C., de Saint Basile, G., and Locatelli, F. (2002) Successful treatment of Griscelli syndrome with unrelated donor allogeneic hematopoietic stem cell transplantation. *Bone Marrow Transplant.* **29**, 995–998
178. Dessinioti, C., Stratigos, A. J., Rigopoulos, D., and Katsambas, A. D. (2009) A review of genetic disorders of hypopigmentation: Lessons learned from the biology of melanocytes. *Exp. Dermatol.* **18**, 741–749
179. Ménasché, G., Ho, C. H., Sanal, O., Feldmann, J., Tezcan, I., Ersoy, F., Houdusse, A., Fischer, A., and De Saint Basile, G. (2003) Griscelli syndrome restricted to hypopigmentation results from a melanophilin defect (GS3) or a MYO5A F-exon deletion (GS1). *J. Clin. Invest.* **112**, 450–456
180. Thomas, E. R., Walker, L. J., Pullaperuma, S., Cooper, B., Brueton, L. A., Basile, G. de Saint, Suri, M., and Brady, A. F. (2009) Griscelli syndrome type 1: a report of two cases and review of the literature. *Clin. Dysmorphol.* **18**, 145–8
181. Sakai, T., Jung, H. S., Sato, O., Yamada, M. D., You, D. J., Ikebe, R., and Ikebe, M. (2015) Structure and regulation of the movement of human myosin VIIA. *J. Biol. Chem.* **290**, 17587–17598
182. Watanabe, S., Ikebe, R., and Ikebe, M. (2006) Drosophila myosin VIIA is a high duty ratio motor with a unique kinetic mechanism. *J. Biol. Chem.* **281**, 7151–7160
183. Yang, Y., Kovács, M., Sakamoto, T., Zhang, F., Kiehart, D. P., and Sellers, J. R. (2006) Dimerized Drosophila myosin VIIa: a processive motor. *Proc. Natl. Acad. Sci. U. S. A.* **103**, 5746–5751
184. Weil, D., Blanchard, S., Kaplan, J., Guilford, P., Gibson, F., Walsh, J., Mburu, P., Varela, A., Levilliers, J., Weston, M. D., Kelley, P. M., Kimberling, W. J., Wagenaar, M., Levi-Acobas, F., Larget-Piet, D., Munnich, A., Steel, K. P., Brown, S. D. M., and Petit, C. (1995) Defective myosin VIIA gene responsible for Usher syndrome type 1B. *Nature*. **374**, 60–61
185. Hasson, T., Gillespie, P. G., Garcia, J. A., MacDonald, R. B., Zhao, Y. D., Yee, A. G., Mooseker, M. S., and Corey, D. P. (1997) Unconventional myosins in inner-ear sensory epithelia. *J. Cell Biol.* **137**, 1287–1307
186. Hasson, T., Heintzelman, H. B., Santos-sacchi, J. T., Coreyii, D. P., and Mooseker, M. S. (1995) Expression in cochlea and retina of myosin VIIa, the gene product defective in Usher syndrome type 1B. *Cell Biol.* **92**, 9815–9819
187. Liu, X., Udovichenko, I. P., Brown, S. D., Steel, K. P., and Williams, D. S. (1999) Myosin VIIa participates in opsin transport through the photoreceptor cilium. *J. Neurosci.* **19**, 6267–74
188. Futter, C. E., Ramalho, J. S., Jaissle, G. B., Seeliger, M. W., and Seabra, M. C. (2004) The Role of Rab27a in the Regulation of Melanosome Distribution within Retinal Pigment Epithelial Cells. *Mol. Biol. Cell*. **15**, 2264–2275

189. Lopes, V. S., Ramalho, J. S., Owen, D. M., Karl, M. O., Strauss, O., Futter, C. E., and Seabra, M. C. (2007) The ternary Rab27a-Myrip-Myosin VIIa complex regulates melanosome motility in the retinal pigment epithelium. *Traffic*. **8**, 486–499

190. El-Amraoui, A., and Petit, C. (2005) Usher I syndrome: unravelling the mechanisms that underlie the cohesion of the growing hair bundle in inner ear sensory cells. *J. Cell Sci.* **118**, 4593–603

191. Kimberling, W. J., Möller, C. G., Davenport, S., Priluck, I. A., Beighton, P. H., Greenberg, J., Reardon, W., Weston, M. D., Kenyon, J. B., and Grunkemeyer, J. A. (1992) Linkage of Usher syndrome type I gene (USH1B) to the long arm of chromosome 11. *Genomics*. **14**, 988–94

192. Brozzi, F., Diraison, F., Lajus, S., Rajatileka, S., Philips, T., Regazzi, R., Fukuda, M., Verkade, P., Molnár, E., and Váradi, A. (2012) Molecular mechanism of Myosin Va recruitment to dense core secretory granules. *Traffic*. **13**, 54–69

193. Schlüter, O. M., Khvotchev, M., Jahn, R., and Südhof, T. C. (2002) Localization versus function of Rab3 proteins: Evidence for a common regulatory role in controlling fusion. *J. Biol. Chem.* **277**, 40919–40929

194. Wöllert, T., Patel, A., Lee, Y. L., Provance, D. W., Vought, V. E., Cosgrove, M. S., Mercer, J. A., and Langford, G. M. (2011) Myosin5a tail associates directly with Rab3A-containing compartments in neurons. *J. Biol. Chem.* **286**, 14352–14361

195. Pavlos, N. J., Grønborg, M., Riedel, D., Chua, J. J. E., Boyken, J., Kloepper, T. H., Urlaub, H., Rizzoli, S. O., and Jahn, R. (2010) Quantitative analysis of synaptic vesicle Rabs uncovers distinct yet overlapping roles for Rab3a and Rab27b in Ca2+-triggered exocytosis. *J. Neurosci.* **30**, 13441–53

196. Roland, J. T., Kenworthy, A. K., Peranen, J., Caplan, S., and Goldenring, J. R. (2007) Myosin Vb interacts with Rab8a on a tubular network containing EHD1 and EHD3. *Mol. Biol. Cell*. **18**, 2828–37

197. Knowles, B. C., Roland, J. T., Krishnan, M., Tyska, M. J., Lapierre, L. A., Dickman, P. S., Goldenring, J. R., and Shub, M. D. (2014) Myosin Vb uncoupling from RAB8A and RAB11A elicits microvillus inclusion disease. *J. Clin. Invest.* **124**, 2947–2962

198. Randhawa, V. K., Ishikura, S., Talior-Volodarsky, I., Cheng, A. W. P., Patel, N., Hartwig, J. H., and Klip, A. (2008) GLUT4 vesicle recruitment and fusion are differentially regulated by Rac, AS160, and Rab8A in muscle cells. *J. Biol. Chem.* **283**, 27208–27219

199. Sun, Y., Chiu, T. T., Foley, K. P., Bilan, P. J., and Klip, A. (2014) Myosin Va mediates Rab8A-regulated GLUT4 vesicle exocytosis in insulin-stimulated muscle cells. *Mol. Biol. Cell*. **25**, 1159–70

200. Klip, A., Sun, Y., Chiu, T. T., and Foley, K. P. (2014) Signal transduction meets vesicle traffic: the software and hardware of GLUT4 translocation. *Am. J. Physiol. Cell Physiol.* **306**, C879-86

201. Chen, Y., Wang, Y., Zhang, J., Deng, Y., Jiang, L., Song, E., Wu, X. S., Hammer, J. A., Xu, T., and Lippincott-Schwartz, J. (2012) Rab10 and myosin-va mediate insulin-stimulated GLUT4 storage vesicle translocation in adipocytes. *J. Cell Biol.* **198**, 545–560

202. Chen, Y. T., Holcomb, C., and Moore, H. P. (1993) Expression and localization of two low molecular weight GTP-binding proteins, Rab8 and Rab10, by epitope tag. *Proc. Natl. Acad. Sci. U. S. A.* **90**, 6508–6512

203. Babbey, C. M., Ahktar, N., Wang, E., Chih-Hsiung Chen, C., Grant, B. D., and Dunn, K. W. (2006) Rab10 Regulates Membrane Transport through Early Endosomes of Polarized Madin-Darby Canine Kidney Cells. *Mol. Biol. Cell*. **17**, 3156–3175

204. Ishikura, S., Bilan, P. J., and Klip, A. (2007) Rabs 8A and 14 are targets of the insulin-regulated Rab-GAP AS160 regulating GLUT4 traffic in muscle cells. *Biochem. Biophys. Res. Commun.* **353**, 1074–1079

205. Sano, H., Eguez, L., Teruel, M. N., Fukuda, M., Chuang, T. D., Chavez, J. A., Lienhard, G. E., and McGraw, T. E. (2007) Rab10, a Target of the AS160 Rab GAP, Is Required for Insulin-Stimulated Translocation of GLUT4 to the Adipocyte Plasma Membrane. *Cell Metab.* **5**, 293–303

206. Schuck, S., Gerl, M. J., Ang, A., Manninen, A., Keller, P., Mellman, I., and Simons, K. (2007) Rab10 is involved in basolateral transport in polarized Madin-Darby canine kidney cells. *Traffic*. **8**, 47–60

207. Bultema, J. J., Boyle, J. A., Malenke, P. B., Martin, F. E., Dell'Angelica, E. C., Cheney, R. E., and Di Pietro, S. M. (2014) Myosin Vc interacts with Rab32 and Rab38 proteins and works in the biogenesis and secretion of melanosomes. *J. Biol. Chem.* **289**, 33513–33528

208. Provance, D. W., James, T. L., and Mercer, J. a (2002) Melanophilin, the product of the leaden locus, is required for targeting of myosin-Va to melanosomes. *Traffic*. **3**, 124–132

209. Au, J. S. Y., and Huang, J. D. (2002) A tissue-specific exon of Myosin Va is responsible for selective cargo binding in melanocytes. *Cell Motil. Cytoskeleton*. **53**, 89–102

210. Pylypenko, O., Attanda, W., Gauquelin, C., Lahmani, M., Coulibaly, D., Baron, B., Hoos, S., Titus, M. a, England, P., and Houdusse, A. M. (2013) Structural basis of myosin V Rab GTPase-dependent cargo recognition. *Proc. Natl. Acad. Sci. U. S. A.* **110**, 20443–8

211. Pylypenko, O., Welz, T., Tittel, J., Kollmar, M., Chardon, F., Malherbe, G., Weiss, S., Michel, C. I. L., Samol-Wolf, A., Grasskamp, A. T., Hume, A., Goud, B., Baron, B., England, P., Titus, M. A., Schwille, P., Weidemann, T., Houdusse, A., and Kerkhoff, E. (2016) Coordinated recruitment of Spir actin nucleators and myosin V motors to Rab11 vesicle

membranes. *Elife*. **5**, 1–25

212. Urbé, S., Huber, L. A., Zerial, M., Tooze, S. A., and Parton, R. G. (1993) Rab11, a small GTPase associated with both constitutive and regulated secretory pathways in PC12 cells. *FEBS Lett.* **334**, 175–182

213. Ullrich, O., Reinsch, S., Urbé, S., Zerial, M., and Parton, R. G. (1996) Rab11 regulates recycling through the pericentriolar recycling endosome. *J. Cell Biol.* **135**, 913–924

214. Sönnichsen, B., De Renzis, S., Nielsen, E., Rietdorf, J., and Zerial, M. (2000) Distinct membrane domains on endosomes in the recycling pathway visualized by multicolor imaging of Rab4, Rab5, and Rab11. *J. Cell Biol.* **149**, 901–14

215. Goldenring, J. R., Smith, J., Vaughan, H. D., Cameron, P., Hawkins, W., and Navarre, J. (1996) Rab11 is an apically located small GTP-binding protein in epithelial tissues. *Am. J. Physiol.* **270**, G515–G525

216. Casanova, J. E., Wang, X., Kumar, R., Bhartur, S. G., Navarre, J., Woodrum, J. E., Altschuler, Y., Ray, G. S., and Goldenring, J. R. (1999) Association of Rab25 and Rab11a with the apical recycling system of polarized Madin-Darby canine kidney cells. *Mol. Biol. Cell*. **10**, 47–61

217. Apodaca, G., Gallo, L. I., and Bryant, D. M. (2012) Role of membrane traffic in the generation of epithelial cell asymmetry. *Nat. Cell Biol.* **14**, 1235–1243

218. Desclozeaux, M., Venturato, J., Wylie, F. G., Kay, J. G., Joseph, S. R., Le, H. T., and Stow, J. L. (2008) Active Rab11 and functional recycling endosome are required for E-cadherin trafficking and lumen formation during epithelial morphogenesis. *Am. J. Physiol. Cell Physiol.* **295**, C545–C556

219. Kelly, E. E., Horgan, C. P., and McCaffrey, M. W. (2012) Rab11 proteins in health and disease. *Biochem. Soc. Trans.* **40**, 1360–7

220. Knödler, A., Feng, S., Zhang, J., Zhang, X., Das, A., Peränen, J., and Guo, W. (2010) Coordination of Rab8 and Rab11 in primary ciliogenesis. *Proc. Natl. Acad. Sci. U. S. A.* **107**, 6346–51

221. Shirane, M., and Nakayama, K. I. (2006) Protrudin induces neurite formation by directional membrane trafficking. *Science*. **314**, 818–21

222. Schuh, M. (2011) An actin-dependent mechanism for long-range vesicle transport. *Nat. Cell Biol.* **13**, 1431–1436

223. Bryant, D. M., Datta, A., Rodríguez-Fraticelli, A. E., Peränen, J., Martín-Belmonte, F., and Mostov, K. E. (2010) A molecular network for de novo generation of the apical surface and lumen. *Nat. Cell Biol.* **12**, 1035–45

224. Gálvez-Santisteban, M., Rodriguez-Fraticelli, A. E., Bryant, D. M., Vergarajauregui, S., Yasuda, T., Bañón-Rodríguez, I., Bernascone, I., Datta, A., Spivak, N., Young, K., Slim, C. L., Brakeman, P. R., Fukuda, M., Mostov, K. E., and Martín-Belmonte, F. (2012) Synaptotagmin-like proteins control the formation of a single apical membrane domain in epithelial cells. *Nat. Cell Biol.* **14**, 838–49

225. Golachowska, M. R., Hoekstra, D., and van IJzendoorn, S. C. D. (2010) Recycling endosomes in apical plasma membrane domain formation and epithelial cell polarity. *Trends Cell Biol.* **20**, 618–626

226. Winter, J. F., Höpfner, S., Korn, K., Farnung, B. O., Bradshaw, C. R., Marsico, G., Volkmer, M., Habermann, B., and Zerial, M. (2012) Caenorhabditis elegans screen reveals role of PAR-5 in RAB-11-recycling endosome positioning and apicobasal cell polarity. *Nat. Cell Biol.* **14**, 666–676

227. Wilcke, M., Johannes, L., Galli, T., Mayau, V., Goud, B., and Salamero, J. (2000) Rab11 regulates the compartmentalization of early endosomes required for efficient transport from early endosomes to the trans-Golgi network. *J. Cell Biol.* **151**, 1207–1220

228. Cox, D., Lee, D. J., Dale, B. M., Calafat, J., and Greenberg, S. (2000) A Rab11-containing rapidly recycling compartment in macrophages that promotes phagocytosis. *Proc. Natl. Acad. Sci. U. S. A.* **97**, 680–5

229. Yu, X., Prekeris, R., and Gould, G. W. (2007) Role of endosomal Rab GTPases in cytokinesis. *Eur. J. Cell Biol.* **86**, 25–35

230. Goldenring, J. R., Soroka, C. J., Shen, K. R., Tang, L. H., Rodriguez, W., Vaughan, H. D., Stoch, S. A., and Modlin, I. M. (1994) Enrichment of rab11 , a small GTP-binding protein, in gastric parietal cells. *Am. J. Physiol.* **267**, 187–194

231. Lai, F., Stubbs, L., and Artzt, K. (1994) Molecular analysis of mouse Rab11b: a new type of mammalian YPT/Rab protein. *Genomics*. **22**, 610–616

232. Goldenring, J. R., Shen, K. R., Vaughan, H. D., and Modlin, I. M. (1993) Identification of a small GTP-binding protein, Rab25, expressed in the gastrointestinal mucosa, kidney, and lung. *J. Biol. Chem.* **268**, 18419–18422

233. Zhang, X. M., Walsh, B., Mitchell, C. A., and Rowe, T. (2005) TBC domain family, member 15 is a novel mammalian Rab GTPase-activating protein with substrate preference for Rab7. *Biochem. Biophys. Res. Commun.* **335**, 154–161

234. Dabbeekeh, J. T. S., Faitar, S. L., Dufresne, C. P., and Cowell, J. K. (2006) The EVI5 TBC domain provides the GTPase-activating protein motif for RAB11. *Oncogene*. **26**, 2804–2808

235. Fuchs, E., Haas, A. K., Spooner, R. A., Yoshimura, S. I., Lord, J. M., and Barr, F. A. (2007) Specific Rab GTPase-activating proteins define the Shiga toxin and epidermal growth factor uptake pathways. *J. Cell Biol.* **177**, 1133–1143

236. Laflamme, C., Assaker, G., Ramel, D., Dorn, J. F., She, D., Maddox, P. S., and Emery, G. (2012) Evi5 promotes collective cell migration through its Rab-GAP activity. *J. Cell Biol.* **198**, 57–67

237. Assaker, G., Ramel, D., Wculek, S. K., González-Gaitán, M., and Emery, G. (2010) Spatial restriction of receptor tyrosine kinase activity through a polarized endocytic cycle controls border cell migration. *Proc. Natl. Acad. Sci. U. S. A.* **107**, 22558–63

238. Hehnly, H., Chen, C. T., Powers, C. M., Liu, H. L., and Doxsey, S. (2012) The centrosome regulates the Rab11-dependent recycling endosome pathway at appendages of the mother centriole. *Curr. Biol.* **22**, 1944–1950

239. Xiong, B., Bayat, V., Jaiswal, M., Zhang, K., Sandoval, H., Charng, W. L., Li, T., David, G., Duraine, L., Lin, Y. Q., Neely, G. G., Yamamoto, S., and Bellen, H. J. (2012) Crag Is a GEF for Rab11 Required for Rhodopsin Trafficking and Maintenance of Adult Photoreceptor Cells. *PLoS Biol.* **10**, e1001438

240. Yoshimura, S. I., Gerondopoulos, A., Linford, A., Rigden, D. J., and Barr, F. A. (2010) Family-wide characterization of the DENN domain Rab GDP-GTP exchange factors. *J. Cell Biol.* **191**, 367–381

241. Sakaguchi, A., Sato, M., and Sato, K. (2016) REI-1, a Novel Rab11 GEF with a SH3BP5 domain. *Commun. Integr. Biol.* **9**, e1208325

242. Li, X., Sapp, E., Valencia, A., Kegel, K. B., Qin, Z., Alexander, J., Masso, N., Reeves, P., Ritch, J. J., Zeitlin, S., Aronin, N., and Difiglia, M. (2008) A function of huntingtin in guanine nucleotide exchange on Rab11. *Neuroreport*. **19**, 1643–7

243. Li, X., Standley, C., Sapp, E., Valencia, A., Qin, Z.-H., Kegel, K. B., Yoder, J., Comer-Tierney, L. A., Esteves, M., Chase, K., Alexander, J., Masso, N., Sobin, L., Bellve, K., Tuft, R., Lifshitz, L., Fogarty, K., Aronin, N., and DiFiglia, M. (2009) Mutant Huntingtin Impairs Vesicle Formation from Recycling Endosomes by Interfering with Rab11 Activity. *Mol. Cell. Biol.* **29**, 6106–6116

244. Prekeris, R., Klumperman, J., and Scheller, R. H. (2000) A Rab11/Rip11 protein complex regulates apical membrane trafficking via recycling endosomes. *Mol. Cell*. **6**, 1437–1448

245. Hales, C. M., Griner, R., Hobdy-Henderson, K. C., Dorn, M. C., Hardy, D., Kumar, R., Navarre, J., Chan, E. K. L., Lapierre, L. A., and Goldenring, J. R. (2001) Identification and Characterization of a Family of Rab11-interacting Proteins. *J. Biol. Chem.* **276**, 39067–39075

246. Lindsay, A. J., Hendrick, A. G., Cantalupo, G., Senic-Matuglia, F., Goud, B., Bucci, C., and McCaffrey, M. W. (2002) Rab coupling protein (RCP), a novel Rab4 and Rab11 effector protein. *J. Biol. Chem.* **277**, 12190–12199

247. Horgan, C. P., and McCaffrey, M. W. (2009) The dynamic Rab11-FIPs. *Biochem. Soc. Trans.* **37**, 1032–1036

248. Lapierre, L. A., Kumar, R., Hales, C. M., Navarre, J., Bhartur, S. G., Burnette, J. O., Provance, D. W., Mercer, J. A., Bähler, M., and Goldenring, J. R. (2001) Myosin vb is associated with plasma membrane recycling systems. *Mol. Biol. Cell*. **12**, 1843–57

249. Henley, J. M., Barker, E. A., and Glebov, O. O. (2011) Routes, destinations and delays: Recent advances in AMPA receptor trafficking. *Trends Neurosci.* **34**, 258–268

250. Malenka, R. C., and Bear, M. F. (2004) LTP and LTD: An embarrassment of riches. *Neuron*. **44**, 5–21

251. Wang, Z., Edwards, J. G., Riley, N., Provance, D. W., Karcher, R., Li, X. dong, Davison, I. G., Ikebe, M., Mercer, J. A., Kauer, J. A., and Ehlers, M. D. (2008) Myosin Vb Mobilizes Recycling Endosomes and AMPA Receptors for Postsynaptic Plasticity. *Cell*. **135**, 535–548

252. Sellers, J. R., Thirumurugan, K., Sakamoto, T., Hammer, J. A., and Knight, P. J. (2008) Calcium and cargoes as regulators of myosin 5a activity. *Biochem. Biophys. Res. Commun.* **369**, 176–181

253. Correia, S. S., Bassani, S., Brown, T. C., Lisé, M.-F., Backos, D. S., El-Husseini, A., Passafaro, M., and Esteban, J. A. (2008) Motor protein–dependent transport of AMPA receptors into spines during long-term potentiation. *Nat. Neurosci.* **11**, 457–466

254. Schnell, E., and Nicoll, R. A. (2001) Hippocampal synaptic transmission and plasticity are preserved in myosin Va mutant mice. *J. Neurophysiol.* **85**, 1498–501

255. van Diepen, M. T., Parsons, M., Downes, C. P., Leslie, N. R., Hindges, R., and Eickholt, B. J. (2009) MyosinV controls PTEN function and neuronal cell size. *Nat. Cell Biol.* **11**, 1191–1196

256. Holubcová, Z., Howard, G., and Schuh, M. (2013) Vesicles modulate an actin network for asymmetric spindle positioning. *Nat. Cell Biol.* **15**, 937–47

257. Li, B. X., Satoh, A. K., and Ready, D. F. (2007) Myosin V, Rab11, and dRip11 direct apical secretion and cellular morphogenesis in developing Drosophila photoreceptors. *J. Cell Biol.* **177**, 659–669

258. Ossipova, O., Chuykin, I., Chu, C.-W., and Sokol, S. Y. (2015) Vangl2 cooperates with Rab11 and Myosin V to regulate apical constriction during vertebrate gastrulation. *Development*. **142**, 99–107

259. Gidon, A., Bardin, S., Cinquin, B., Boulanger, J., Waharte, F., Heliot, L., de la Salle, H., Hanau, D., Kervrann, C., Goud, B., and Salamero, J. (2012) A Rab11A/myosin Vb/Rab11-FIP2 complex frames two late recycling steps of langerin from the ERC to the plasma membrane. *Traffic*. **13**, 815–33

260. Dhekne, H. S., Hsiao, N.-H., Roelofs, P., Kumari, M., Slim, C. L., Rings, E. H. H. M., and van Ijzendoorn, S. C. D. (2014) Myosin Vb and Rab11a regulate phosphorylation of ezrin in enterocytes. *J. Cell Sci.* **127**, 1007–17

261. Fehon, R. G., McClatchey, A. I., and Bretscher, A. (2010) Organizing the cell cortex: the role of ERM proteins. *Nat. Rev. Mol. Cell Biol.* **11**, 276–87

262. LaLonde, D. P., Garbett, D., and Bretscher, A. (2010) A regulated complex of the scaffolding proteins PDZK1 and EBP50 with ezrin contribute to microvillar organization. *Mol. Biol. Cell*. **21**, 1519–29

263. Wang, W., Soroka, C. J., Mennone, A., Rahner, C., Harry, K., Pypaert, M., and Boyer, J. L. (2006) Radixin Is Required to Maintain Apical Canalicular Membrane Structure and Function in Rat Hepatocytes. *Gastroenterology*. **131**, 878–884

264. Hales, C. M., Vaerman, J. P., and Goldenring, J. R. (2002) Rab11 family interacting protein 2 associates with myosin Vb and regulates plasma membrane recycling. *J. Biol. Chem.* **277**, 50415–50421

265. Horgan, C. P., Hanscom, S. R., Jolly, R. S., Futter, C. E., and McCaffrey, M. W. (2010) Rab11-FIP3 links the Rab11 GTPase and cytoplasmic dynein to mediate transport to the endosomal-recycling compartment. *J. Cell Sci.* **123**, 181–191

266. Horgan, C. P., Hanscom, S. R., Jolly, R. S., Futter, C. E., and McCaffrey, M. W. (2010) Rab11-FIP3 binds dynein light intermediate chain 2 and its overexpression fragments the Golgi complex. *Biochem. Biophys. Res. Commun.* **394**, 387–392

267. Horgan, C. P., Walsh, M., Zurawski, T. H., and McCaffrey, M. W. (2004) Rab11-FIP3 localises to a Rab11-positive pericentrosomal compartment during interphase and to the cleavage furrow during cytokinesis. *Biochem. Biophys. Res. Commun.* **319**, 83–94

268. Wilson, G. M., Fielding, A. B., Simon, G. C., Yu, X., Andrews, P. D., Hames, R. S., Frey, A. M., Peden, A. A., Gould, G. W., and Prekeris, R. (2005) The FIP3-Rab11 protein complex regulates recycling endosome targeting to the cleavage furrow during late cytokinesis. *Mol. Biol. Cell*. **16**, 849–60

269. Schonteich, E., Wilson, G. M., Burden, J., Hopkins, C. R., Anderson, K., Goldenring, J. R., and Prekeris, R. (2008) The Rip11/Rab11-FIP5 and kinesin II complex regulates endocytic protein recycling. *J. Cell Sci.* **121**, 3824–33

270. Gil, J. E., Kim, E., Kim, I. S., Ku, B., Park, W. S., Oh, B. H., Ryu, S. H., Cho, W., and Heo, W. Do (2012) Phosphoinositides differentially regulate protrudin localization through the FYVE domain. *J. Biol. Chem.* **287**, 41268–41276

271. Nishimura, N., Nakamura, H., Takai, Y., and Sano, K. (1994) Molecular cloning and characterization of two rab GDI species from rat brain: Brain-specific and ubiquitous types. *J. Biol. Chem.* **269**, 14191–14198

272. Pollard, T. D., and Borisy, G. G. (2003) Cellular motility driven by assembly and disassembly of actin filaments. *Cell*. **112**, 453–465

273. Chhabra, E. S., and Higgs, H. N. (2007) The many faces of actin: matching assembly factors with cellular structures. *Nat. Cell Biol.* **9**, 1110–21

274. Le Clainche, C., and Carlier, M.-F. (2008) Regulation of Actin Assembly Associated With Protrusion and Adhesion in Cell Migration. *Physiol. Rev.* **88**, 489–513

275. Galletta, B. J., and Cooper, J. A. (2009) Actin and endocytosis: mechanisms and phylogeny. *Curr. Opin. Cell Biol.* **21**, 20–27

276. Dominguez, R. (2009) Actin filament nucleation and elongation factors--structure-function relationships. *Crit. Rev. Biochem. Mol. Biol.* **44**, 351–66

277. Winterhoff, M., and Faix, J. (2015) Actin-filament disassembly: it takes two to shrink them fast. *Curr. Biol.* **25**, R450-2

278. Hild, G., Kalmár, L., Kardos, R., Nyitrai, M., and Bugyi, B. (2014) The other side of the coin: Functional and structural versatility of ADF/cofilins. *Eur. J. Cell Biol.* **93**, 238–251

279. Blanchoin, L., and Pollard, T. D. (1999) Mechanism of Interaction of Acanthamoeba Mechanism of Interaction of Acanthamoeba Actophorin (ADF / Cofilin) with Actin Filaments. *J. Biol. Chem.* **274**, 15538–15546

280. Carlier, M., Laurent, V., Santolini, J., Melki, R., Xia, G., Hong, Y., Chua, N., Pantaloni, D., Laurent, V., Santolini, J., and Didry, D. (1997) Factor (ADF / Cofilin) Enhances the Rate of Actin Depolymerizing Filament Turnover : Motility Implication in Actin-based. *J. Cell Biol.* **136**, 1307–1322

281. Suarez, C., Roland, J., Boujemaa-Paterski, R., Kang, H., McCullough, B. R., Reymann, A. C., Guérin, C., Martiel, J. L., De La Cruz, E. M., and Blanchoin, L. (2011) Cofilin tunes the nucleotide state of actin filaments and severs at bare and decorated segment boundaries. *Curr. Biol.* **21**, 862–868

282. Sept, D., and McCammon, J. A. (2001) Thermodynamics and kinetics of actin filament nucleation. *Biophys. J.* **81**, 667–74

283. Kerkhoff, E. (2006) Cellular functions of the Spir actin-nucleation factors. *Trends Cell Biol.* **16**, 477–83

284. Robinson, R. C., Turbedsky, K., Kaiser, D. A., Marchand, J. B., Higgs, H. N., Choe, S., and Pollard, T. D. (2001) Crystal structure of Arp2/3 complex. *Science*. **294**, 1679–84

285. Pollard, T. D., and Cooper, J. A. (2009) Actin, a central player in cell shape and movement. *Science*. **326**, 1208–12

286. Pollard, T. D., and Beltzner, C. C. (2002) Structure and function of the Arp2/3 complex. *Curr. Opin. Struct. Biol.* **12**, 768–774

287. Mullins, R. D., Heuser, J. A., and Pollard, T. D. (1998) The interaction of Arp2/3 complex with actin: nucleation, high affinity pointed end capping, and formation of branching networks of filaments. *Proc. Natl. Acad. Sci. U. S. A.* **95**,

6181–6186

288. Machesky, L. M., and Insall, R. H. (1998) Scar1 and the related Wiskott–Aldrich syndrome protein, WASP, regulate the actin cytoskeleton through the Arp2/3 complex. *Curr. Biol.* **8**, 1347–1356

289. Goley, E. D., and Welch, M. D. (2006) The ARP2/3 complex: an actin nucleator comes of age. *Nat. Rev. Mol. Cell Biol.* **7**, 713–26

290. Pollard, T. D. (2007) Regulation of actin filament assembly by Arp2/3 complex and formins. *Annu. Rev. Biophys. Biomol. Struct.* **36**, 451–477

291. Chesarone, M. A., and Goode, B. L. (2009) Actin nucleation and elongation factors: mechanisms and interplay. *Curr. Opin. Cell Biol.* **21**, 28–37

292. Ridley, A. J., Paterson, H. F., Johnston, C. L., Diekmann, D., and Hall, A. (1992) The small GTP-binding protein rac regulates growth factor-induced membrane ruffling. *Cell*. **70**, 401–410

293. Ridley, A. J., and Hall, A. (1992) The small GTP-binding protein rho regulates the assembly of focal adhesions and actin stress fibers in response to growth factors. *Cell*. **70**, 389–399

294. Jaffe, A. B., and Hall, A. (2005) RHO GTPASES: Biochemistry and Biology. *Annu. Rev. Cell Dev. Biol.* **21**, 247–269

295. Higgs, H. N., and Pollard, T. D. (2000) Activation by Cdc42 and PIP2 of Wiskott-Aldrich Syndrome protein (WASp) stimulates actin nucleation by Arp2/3 complex. *J. Cell Biol.* **150**, 1311–1320

296. Rohatgi, R., Ho, H. Y. H., and Kirschner, M. W. (2000) Mechanism of N-WASP activation by CDC42 and phosphatidylinositol 4,5-bisphosphate. *J. Cell Biol.* **150**, 1299–1309

297. Wallar, B. J., and Alberts, A. S. (2003) The formins: Active scaffolds that remodel the cytoskeleton. *Trends Cell Biol.* **13**, 435–446

298. Otomo, T., Tomchick, D. R., Otomo, C., Panchal, S. C., Machius, M., and Rosen, M. K. (2005) Structural basis of actin filament nucleation and processive capping by a formin homology 2 domain. *Nature*. **433**, 488–494

299. Romero, S., Le Clainche, C., Didry, D., Egile, C., Pantaloni, D., and Carlier, M. F. (2004) Formin is a processive motor that requires profilin to accelerate actin assembly and associated ATP hydrolysis. *Cell*. **119**, 419–429

300. Vavylonis, D., Kovar, D. R., O'Shaughnessy, B., and Pollard, T. D. (2006) Model of formin-associated actin filament elongation. *Mol. Cell*. **21**, 455–466

301. Witke, W. (2004) The role of profilin complexes in cell motility and other cellular processes. *Trends Cell Biol.* **14**, 461–469

302. Harris, E. S., Li, F., and Higgs, H. N. (2004) The Mouse Formin, FRLa, Slows Actin Filament Barbed End Elongation, Competes with Capping Protein, Accelerates Polymerization from Monomers, and Severs Filaments. *J. Biol. Chem.* **279**, 20076–20087

303. Kovar, D. R., Kuhn, J. R., Tichy, A. L., and Pollard, T. D. (2003) The fission yeast cytokinesis formin Cdc12p is a barbed end actin filament capping protein gated by profilin. *J. Cell Biol.* **161**, 875–887

304. Paul, A., and Pollard, T. (2008) The Role of the FH1 Domain and Profilin in Formin-Mediated Actin-Filament Elongation and Nucleation. *Curr. Biol.* **18**, 9–19

305. Kovar, D. R., Harris, E. S., Mahaffy, R., Higgs, H. N., and Pollard, T. D. (2006) Control of the assembly of ATP- and ADP-actin by formins and profilin. *Cell*. **124**, 423–435

306. Higashida, C., Miyoshi, T., Fujita, A., Oceguera-Yanez, F., Monypenny, J., Andou, Y., Narumiya, S., and Watanabe, N. (2004) Actin polymerization-driven molecular movement of mDia1 in living cells. *Science*. **303**, 2007–2010

307. Qualmann, B., and Kessels, M. M. (2009) New players in actin polymerization--WH2-domain-containing actin nucleators. *Trends Cell Biol.* **19**, 276–85

308. Gasca, S., Hill, D. P., Klingensmith, J., and Rossant, J. (1995) Characterization of a gene trap insertion into a novel gene, cordon-bleu, expressed in axial structures of the gastrulating mouse embryo. *Dev. Genet.* **17**, 141–154

309. Carroll, E. A., Gerrelli, D., Gasca, S., Berg, E., Beier, D. R., Copp, A. J., and Klingensmith, J. (2003) Cordon-bleu is a conserved gene involved in neural tube formation. *Dev. Biol.* **262**, 16–31

310. Ahuja, R., Pinyol, R., Reichenbach, N., Custer, L., Klingensmith, J., Kessels, M. M., and Qualmann, B. (2007) Cordon-bleu is an actin nucleation factor and controls neuronal morphology. *Cell*. **131**, 337–50

311. Chereau, D., Boczkowska, M., Skwarek-Maruszewska, A., Fujiwara, I., Hayes, D. B., Rebowski, G., Lappalainen, P., Pollard, T. D., and Dominguez, R. (2008) Leiomodin is an actin filament nucleator in muscle cells. *Science*. **320**, 239–43

312. Zuchero, J. B., Coutts, A. S., Quinlan, M. E., Thangue, N. B. La, and Mullins, R. D. (2009) p53-cofactor JMY is a multifunctional actin nucleation factor. *Nat. Cell Biol.* **11**, 451–459

313. Manseau, L. J., and Schupbach, T. (1989) cappucino and spire: two unique maternal effect loci required fro both the anteroposterior and dorsoventral patterns of the Drosophila embryo. *Genes Dev.* **3**, 1437–1452

314. Wellington, A., Emmons, S., James, B., Calley, J., Grover, M., Tolias, P., and Manseau, L. (1999) Spire contains actin binding domains and is related to ascidian posterior end mark-5. *Development*. **126**, 5267–74

315. Otto, I. M., Raabe, T., Rennefahrt, U. E. E., Bork, P., Rapp, U. R., and Kerkhoff, E. (2000) The p150-Spir protein

provides a link between c-Jun N-terminal kinase function and actin reorganization. *Curr. Biol.* **10**, 345–348

316. Ciccarelli, F. D., Bork, P., and Kerkhoff, E. (2003) The KIND module: A putative signalling domain evolved from the C lobe of the protein kinase fold. *Trends Biochem. Sci.* **28**, 349–352
317. Kerkhoff, E. (2011) Actin dynamics at intracellular membranes: the Spir/formin nucleator complex. *Eur. J. Cell Biol.* **90**, 922–5
318. Quinlan, M. E., Heuser, J. E., Kerkhoff, E., and Mullins, R. D. (2005) Drosophila Spire is an actin nucleation factor. *Nature*. **433**, 382–388
319. Bosch, M., Le, K. H. D., Bugyi, B., Correia, J. J., Renault, L., and Carlier, M. F. (2007) Analysis of the Function of Spire in Actin Assembly and Its Synergy with Formin and Profilin. *Mol. Cell*. **28**, 555–568
320. Sitar, T., Gallinger, J., Ducka, A. M., Ikonen, T. P., Wohlhoefler, M., Schmoller, K. M., Bausch, A. R., Joel, P., Trybus, K. M., Noegel, A. A., Schleicher, M., Huber, R., and Holak, T. A. (2011) Molecular architecture of the Spire-actin nucleus and its implication for actin filament assembly. *Proc. Natl. Acad. Sci. U. S. A.* **108**, 19575–19580
321. Dietrich, S., Weiß, S., Pleiser, S., and Kerkhoff, E. (2013) Structural and functional insights into the Spir/formin actin nucleator complex. *Biol. Chem.* **394**, 1649–60
322. Schumacher, N., Borawski, J. M., Leberfinger, C. B., Gessler, M., and Kerkhoff, E. (2004) Overlapping expression pattern of the actin organizers Spir-1 and formin-2 in the developing mouse nervous system and the adult brain. *Gene Expr. Patterns*. **4**, 249–55
323. Pleiser, S., Rock, R., Wellmann, J., Gessler, M., and Kerkhoff, E. (2010) Expression patterns of the mouse Spir-2 actin nucleator. *Gene Expr. Patterns*. **10**, 345–50
324. Pechlivanis, M., Samol, A., and Kerkhoff, E. (2009) Identification of a short Spir interaction sequence at the C-terminal end of formin subgroup proteins. *J. Biol. Chem.* **284**, 25324–33
325. Kerkhoff, E., Simpson, J. C., Leberfinger, C. B., Otto, I. M., Doerks, T., Bork, P., Rapp, U. R., Raabe, T., and Pepperkok, R. (2001) The Spir actin organizers are involved in vesicle transport processes. *Curr. Biol.* **11**, 1963–1968
326. Ostermeier, C., and Brunger, A. T. (1999) Structural Basis of Rab Effector Specificity: Crystal Structure of the Small G Protein Rab3A Complexed with the Effector Domain of Rabphilin-3A. *Cell*. **96**, 363–374
327. Tittel, J., Welz, T., Czogalla, A., Dietrich, S., Samol-Wolf, A., Schulte, M., Schwille, P., Weidemann, T., and Kerkhoff, E. (2015) Membrane Targeting of the Spir/FMN Actin Nucleator Complex Requires a Sequential Handshake of Polar Interactions. *J. Biol. Chem.* **290**, 6428–6444
328. Stenmark, H., Aasland, R., Toh, B. H., and D'Arrigo, A. (1996) Endosomal localization of the autoantigen EEA1 is mediated by a zinc- binding FYVE finger. *J. Biol. Chem.* **271**, 24048–24054
329. Kutateladze, T. G. (2006) Phosphatidylinositol 3-phosphate recognition and membrane docking by the FYVE domain. *Biochim. Biophys. Acta - Mol. Cell Biol. Lipids*. **1761**, 868–877
330. Misra, S., and Hurley, J. H. (1999) Crystal structure of a phosphatidylinositol 3-phosphate-specific membrane-targeting motif, the FYVE domain of Vps27p. *Cell*. **97**, 657–666
331. Dumas, J. J., Merithew, E., Sudharshan, E., Rajamani, D., Hayes, S., Lawe, D., Corvera, S., and Lambright, D. G. (2001) Multivalent endosome targeting by homodimeric EEA1. *Mol. Cell*. **8**, 947–958
332. Montaville, P., Jégou, A., Pernier, J., Compper, C., Guichard, B., Mogessie, B., Schuh, M., Romet-Lemonne, G., and Carlier, M.-F. (2014) Spire and Formin 2 synergize and antagonize in regulating actin assembly in meiosis by a ping-pong mechanism. *PLoS Biol.* **12**, e1001795
333. Quinlan, M. E., Hilgert, S., Bedrossian, A., Mullins, R. D., and Kerkhoff, E. (2007) Regulatory interactions between two actin nucleators, Spire and Cappuccino. *J. Cell Biol.* **179**, 117–128
334. Pfender, S., Kuznetsov, V., Pleiser, S., Kerkhoff, E., and Schuh, M. (2011) Spire-type actin nucleators cooperate with Formin-2 to drive asymmetric oocyte division. *Curr. Biol.* **21**, 955–60
335. Dahlgaard, K., Raposo, A. a S. F., Niccoli, T., and St Johnston, D. (2007) Capu and Spire assemble a cytoplasmic actin mesh that maintains microtubule organization in the Drosophila oocyte. *Dev. Cell*. **13**, 539–53
336. Quinlan, M. E. (2013) Direct interaction between two actin nucleators is required in Drosophila oogenesis. *Development*. **140**, 4417–25
337. Zeth, K., Pechlivanis, M., Samol, A., Pleiser, S., Vonrhein, C., and Kerkhoff, E. (2011) Molecular basis of actin nucleation factor cooperativity: Crystal structure of the Spir-1 KIND / formin-2 FSI complex. *J. Biol. Chem.* **286**, 30732–30749
338. Vizcarra, C. L., Kreutz, B., Rodal, A. A., Toms, A. V, Lu, J., Zheng, W., Quinlan, M. E., and Eck, M. J. (2011) Structure and function of the interacting domains of Spire and Fmn-family formins. *Proc. Natl. Acad. Sci. U. S. A.* **108**, 11884–9
339. Manor, U., Bartholomew, S., Golani, G., Christenson, E., Kozlov, M., Higgs, H., Spudich, J., and Lippincott-Schwartz, J. (2015) A mitochondria-anchored isoform of the actin-nucleating spire protein regulates mitochondrial division. *Elife*. **4**, 1–27
340. Cheng, J., Grassart, A., and Drubin, D. G. (2012) Myosin 1E coordinates actin assembly and cargo trafficking during clathrin-mediated endocytosis. *Mol. Biol. Cell*. **23**, 2891–904

341. Sirotkin, V., Beltzner, C. C., Marchand, J. B., and Pollard, T. D. (2005) Interactions of WASp, myosin-I, and verprolin with Arp2/3 complex during actin patch assembly in fission yeast. *J. Cell Biol.* **170**, 637–648

342. Sun, Y., Martin, A. C., and Drubin, D. G. (2006) Endocytic Internalization in Budding Yeast Requires Coordinated Actin Nucleation and Myosin Motor Activity. *Dev. Cell*. **11**, 33–46

343. Jung, G., Remmert, K., Wu, X., Volosky, J. M., and Hammer, J. A. (2001) The Dictyostelium CARMIL protein links capping protein and the Arp2/3 complex to type I myosins through their SH3 domains. *J. Cell Biol.* **153**, 1479–1497

344. Almonacid, M., Ahmed, W. W., Bussonnier, M., Mailly, P., Betz, T., Voituriez, R., Gov, N. S., and Verlhac, M.-H. (2015) Active diffusion positions the nucleus in mouse oocytes. *Nat. Cell Biol.* **17**, 470–9

345. Crooks, G. E., Hon, G., Chandonia, J.-M., and Brenner, S. E. (2004) WebLogo: a sequence logo generator. *Genome Res.* **14**, 1188–1190

346. Li, W., and Godzik, A. (2006) Cd-hit: A fast program for clustering and comparing large sets of protein or nucleotide sequences. *Bioinformatics*. **22**, 1658–1659

347. Costes, S. V, Daelemans, D., Cho, E. H., Dobbin, Z., Pavlakis, G., and Lockett, S. (2004) Automatic and quantitative measurement of protein-protein colocalization in live cells. *Biophys. J.* **86**, 3993–4003

348. Pompey, S. N., Michaely, P., and Luby-phelps, K. (2013) Protein-Ligand Interactions. **1008**, 439–453

349. Hammer, J. A., and Wagner, W. (2013) Functions of class v myosins in neurons. *J. Biol. Chem.* **288**, 28428–28434

350. Zeth, K., Pechlivanis, M., Samol, A., Pleiser, S., Vonrhein, C., and Kerkhoff, E. (2011) Molecular basis of actin nucleation factor cooperativity: crystal structure of the Spir-1 kinase non-catalytic C-lobe domain (KIND)•formin-2 formin SPIR interaction motif (FSI) complex. *J. Biol. Chem.* **286**, 30732–9

351. Sun, Y., Rombola, C., Jyothikumar, V., and Periasamy, A. (2013) Förster Resonance Energy Transfer Microscopy and Spectroscopy for Localizing Protein – Protein Interactions in Living Cells. *Cytom. Part A*. **Early View**, 1–14

352. Austen, K., Ringer, P., Mehlich, A., Chrostek-Grashoff, A., Kluger, C., Klingner, C., Sabass, B., Zent, R., Rief, M., and Grashoff, C. (2015) Extracellular rigidity sensing by talin isoform-specific mechanical linkages. *Nat. Cell Biol.* **17**, 1597–1606

353. Wei, Z., Liu, X., Yu, C., and Zhang, M. (2013) Structural basis of cargo recognitions for class V myosins. *Proc. Natl. Acad. Sci. U. S. A.* **110**, 11314–9

354. Kukimoto-Niino, M., Sakamoto, A., Kanno, E., Hanawa-Suetsugu, K., Terada, T., Shirouzu, M., Fukuda, M., and Yokoyama, S. (2008) Structural basis for the exclusive specificity of Slac2-a/melanophilin for the Rab27 GTPases. *Structure*. **16**, 1478–90

355. Hume, A. N., Tarafder, A. K., Ramalho, J. S., Sviderskaya, E. V, and Seabra, M. C. (2006) A Coiled-Coil Domain of Melanophilin Is Essential for Myosin Va Recruitment and Melanosome Transport in Melanocytes. *Mol. Biol. Cell*. **17**, 4720–4735

356. Kuroda, T. S., Fukuda, M., Ariga, H., and Mikoshiba, K. (2002) The Slp homology domain of synaptotagmin-like proteins 1-4 and Slac2 functions as a novel Rab27A binding domain. *J. Biol. Chem.* **277**, 9212–9218

357. Hume, A. N., and Seabra, M. C. (2011) Melanosomes on the move: a model to understand organelle dynamics. *Biochem. Soc. Trans.* **39**, 1191–1196

358. Pashkova, N., Jin, Y., Ramaswamy, S., and Weisman, L. S. (2006) Structural basis for myosin V discrimination between distinct cargoes. *EMBO J.* **25**, 693–700

359. Xie, J., Hao, X., Azeloglu, E. U., Ren, H., Wang, Z., Ma, J., Liu, J., Ma, X., Wang, W., Pan, X., Zhang, W., Zhong, F., Li, Y., Meng, G., Kiryluk, K., He, J. C., Gharavi, A. G., and Chen, N. (2015) Novel mutations in the inverted formin 2 gene of Chinese families contribute to focal segmental glomerulosclerosis. *Kidney Int.* **88**, 593–604

360. Geething, N. C., and Spudich, J. A. (2007) Identification of a minimal myosin Va binding site within an intrinsically unstructured domain of melanophilin. *J. Biol. Chem.* **282**, 21518–21528

361. Zhang, W.-B., Yao, L.-L., and Li, X. (2016) The Globular Tail Domain of Myosin-5a Functions As a Dimer in Regulating the Motor Activity. *J. Biol. Chem.* **291**, jbc.M116.724328

362. Ji, H.-H., Zhang, H.-M., Shen, M., Yao, L.-L., and Li, X. (2015) The motor function of Drosophila melanogaster myosin-5 is activated by calcium and cargo-binding protein dRab11. *Biochem. J.* **469**, 135–44

363. Zimmermann, D., Santos, A., Kovar, D. R., and Rock, R. S. (2015) Actin age orchestrates myosin-5 and myosin-6 run lengths. *Curr. Biol.* **25**, 2057–62

364. Semenova, I., Burakov, A., Berardone, N., Zaliapin, I., Slepchenko, B., Svitkina, T., Kashina, A., and Rodionov, V. (2008) Actin Dynamics Is Essential for Myosin-Based Transport of Membrane Organelles. *Curr. Biol.* **18**, 1581–1586

365. Morel, E., Parton, R. G., and Gruenberg, J. (2009) Annexin A2-dependent polymerization of actin mediates endosome biogenesis. *Dev. Cell*. **16**, 445–57

366. Roth-Johnson, E. A., Vizcarra, C. L., Bois, J. S., and Quinlan, M. E. (2014) Interaction between microtubules and the drosophila formin cappuccino and its effect on actin assembly. *J. Biol. Chem.* **289**, 4395–4404

367. Chibalina, M. V, Seaman, M. N. J., Miller, C. C., Kendrick-Jones, J., and Buss, F. (2007) Myosin VI and its interacting protein LMTK2 regulate tubule formation and transport to the endocytic recycling compartment. *J. Cell Sci.* **120**,

4278–4288

368. Salas-Cortes, L., Ye, F., Tenza, D., Wilhelm, C., Theos, A., Louvard, D., Raposo, G., and Coudrier, E. (2005) Myosin Ib modulates the morphology and the protein transport within multi-vesicular sorting endosomes. *J. Cell Sci.* **118**, 4823–4832

369. Almeida, C. G., Yamada, A., Tenza, D., Louvard, D., Raposo, G., and Coudrier, E. (2011) Myosin 1b promotes the formation of post-Golgi carriers by regulating actin assembly and membrane remodelling at the trans-Golgi network. *Nat. Cell Biol.* **13**, 779–789

370. Hokanson, D. E., Laakso, J. M., Lin, T., Sept, D., and Ostap, E. M. (2006) Myo1c Binds Phosphoinositides through a Putative Pleckstrin Homology Domain. *Mol. Biol. Cell*. **17**, 4856–4865

371. Komaba, S., and Coluccio, L. M. (2010) Localization of myosin 1b to actin protrusions requires phosphoinositide binding. *J. Biol. Chem.* **285**, 27686–27693

372. Yamada, A., Mamane, A., Lee-Tin-Wah, J., Di Cicco, A., Prévost, C., Lévy, D., Joanny, J.-F., Coudrier, E., and Bassereau, P. (2014) Catch-bond behaviour facilitates membrane tubulation by non-processive myosin 1b. *Nat. Commun.* **5**, 3624

373. Soldati, T., and Schliwa, M. (2006) Powering membrane traffic in endocytosis and recycling. *Nat. Rev. Mol. Cell Biol.* **7**, 897–908

374. Anitei, M., and Hoflack, B. (2011) Bridging membrane and cytoskeleton dynamics in the secretory and endocytic pathways. *Nat. Cell Biol.* **14**, 11–19

375. Dabora, S. L., and Sheetz, M. F. (1988) The microtubule-dependent formation of a tubulovesicular network with characteristics of the ER from cultured cell extracts. *Cell*. **54**, 27–35

376. Allan, V. J., and Vale, R. D. (1991) Cell cycle control of microtuble-based membrane transport and tubule formation in vitro. *J. Cell Biol.* **113**, 347–359

377. Fullerton, A. T., Bau, M. Y., Conrad, P. A., and Bloom, G. S. (1998) In vitro reconstitution of microtubule plus end-directed, GTP gamma S-sensitive motility of Golgi membranes. *Mol. Biol. Cell*. **9**, 2699–2714

378. Roux, A., Cappello, G., Cartaud, J., Prost, J., Goud, B., and Bassereau, P. (2002) A minimal system allowing tubulation with molecular motors pulling on giant liposomes. *Proc. Natl. Acad. Sci. U. S. A.* **99**, 5394–5399

379. Koster, G., VanDuijn, M., Hofs, B., and Dogterom, M. (2003) Membrane tube formation from giant vesicles by dynamic association of motor proteins. *Proc. Natl. Acad. Sci. U. S. A.* **100**, 15583–15588

380. Leduc, C., Campàs, O., Zeldovich, K. B., Roux, A., Jolimaitre, P., Bourel-Bonnet, L., Goud, B., Joanny, J.-F., Bassereau, P., and Prost, J. (2004) Cooperative extraction of membrane nanotubes by molecular motors. *Proc. Natl. Acad. Sci. U. S. A.* **101**, 17096–17101

381. Desnos, C., Huet, S., and Darchen, F. (2007) "Should I stay or should I go?": myosin V function in organelle trafficking. *Biol. cell*. **99**, 411–23

382. Wu, X., Bowers, B., Rao, K., Wei, Q., and Hammer, J. A. (1998) Visualization of melanosome dynamics within wild-type and dilute melanocytes suggests a paradigm for myosin v function in vivo. *J. Cell Biol.* **143**, 1899–1918

383. Provance, D. W., Addison, E. J., Wood, P. R., Chen, D. Z., Silan, C. M., and Mercer, J. a (2008) Myosin-Vb functions as a dynamic tether for peripheral endocytic compartments during transferrin trafficking. *BMC Cell Biol.* **9**, 44

384. Desnos, C., Huet, S., Fanget, I., Chapuis, C., Böttiger, C., Racine, V., Sibarita, J.-B., Henry, J.-P., and Darchen, F. (2007) Myosin va mediates docking of secretory granules at the plasma membrane. *J. Neurosci.* **27**, 10636–45

385. Kögel, T., Bittins, C. M., Rudolf, R., and Gerdes, H.-H. (2010) Versatile roles for myosin Va in dense core vesicle biogenesis and function. *Biochem. Soc. Trans.* **38**, 199–204

386. Coudrier, E. (2007) Myosins in melanocytes: To move or not to move? *Pigment Cell Res.* **20**, 153–160

387. Loubéry, S., and Coudrier, E. (2008) Membrane traffic in the secretory pathway: Myosins in the secretory pathway: Tethers or transporters? *Cell. Mol. Life Sci.* **65**, 2790–2800

388. Watanabe, M. (2005) Myosin-Va Regulates Exocytosis through the Submicromolar Ca2+-dependent Binding of Syntaxin-1A. *Mol. Biol. Cell*. **16**, 4519–4530

389. Kulak, N. a, Pichler, G., Paron, I., Nagaraj, N., and Mann, M. (2014) Minimal, encapsulated proteomic-sample processing applied to copy-number estimation in eukaryotic cells. *Nat. Methods*. **11**, 319–24

390. Mulholland, C. B., Smets, M., Schmidtmann, E., Leidescher, S., Markaki, Y., Hofweber, M., Qin, W., Manzo, M., Kremmer, E., Thanisch, K., Bauer, C., Rombaut, P., Herzog, F., Leonhardt, H., and Bultmann, S. (2015) A modular open platform for systematic functional studies under physiological conditions. *Nucleic Acids Res.* 10.1093/nar/gkv550

391. Shaner, N. C., Lambert, G. G., Chammas, A., Ni, Y., Cranfill, P. J., Baird, M. A., Sell, B. R., Allen, J. R., Day, R. N., Israelsson, M., Davidson, M. W., and Wang, J. (2013) A bright monomeric green fluorescent protein derived from Branchiostoma lanceolatum. *Nat. Methods*. **10**, 407–409

392. Bajar, B. T., Wang, E. S., Lam, A. J., Kim, B. B., Jacobs, C. L., Howe, E. S., Davidson, M. W., Lin, M. Z., and Chu, J. (2016) Improving brightness and photostability of green and red fluorescent proteins for live cell imaging and FRET reporting. *Sci. Rep.* **6**, 20889

393. Bacia, K., Kim, S. a, and Schwille, P. (2006) Fluorescence cross-correlation spectroscopy in living cells. *Nat. Methods*. **3**, 83–9

394. Haustein, E., and Schwille, P. (2004) Single-molecule spectroscopic methods. *Curr. Opin. Struct. Biol.* **14**, 531–40

395. Weidemann, T., Mücksch, J., and Schwille, P. (2014) Fluorescence fluctuation microscopy: a diversified arsenal of methods to investigate molecular dynamics inside cells. *Curr. Opin. Struct. Biol.* **28C**, 69–76

396. Jordens, I., Fernandez-Borja, M., Marsman, M., Dusseljee, S., Janssen, L., Calafat, J., Janssen, H., Wubbolts, R., and Neefjes, J. (2001) The Rab7 effector protein RILP controls lysosomal transport by inducing the recruitment of dynein-dynactin motors. *Curr. Biol.* **11**, 1680–1685

397. Chabrillat, M. L., Wilhelm, C., Wasmeier, C., Sviderskaya, E. V., Louvard, D., and Coudrier, E. (2005) Rab8 Regulates the Actin-based Movement of Melanosomes. *Mol. Biol. Cell*. **16**, 1640–1650

398. Khandelwal, P., Prakasam, H. S., Clayton, D. R., Ruiz, W. G., Gallo, L. I., van Roekel, D., Lukianov, S., Peränen, J., Goldenring, J. R., and Apodaca, G. (2013) A Rab11a-Rab8a-Myo5B network promotes stretch-regulated exocytosis in bladder umbrella cells. *Mol. Biol. Cell*. **24**, 1007–19

399. Rink, J., Ghigo, E., Kalaidzidis, Y., and Zerial, M. (2005) Rab conversion as a mechanism of progression from early to late endosomes. *Cell*. **122**, 735–749

400. Hutagalung, A. H., and Novick, P. J. (2011) Role of Rab GTPases in membrane traffic and cell physiology. *Physiol. Rev.* **91**, 119–49

401. Rivera-Molina, F. E., and Novick, P. J. (2009) A Rab GAP cascade defines the boundary between two Rab GTPases on the secretory pathway. *Proc. Natl. Acad. Sci. U. S. A.* **106**, 14408–13

402. Eitzen, G., Will, E., Gallwitz, D., Haas, A., and Wickner, W. (2000) Sequential action of two GTPases to promote vacuole docking and fusion. *EMBO J.* **19**, 6713–6720

403. Zhu, H., Liang, Z., and Li, G. (2009) Rabex-5 Is a Rab22 Effector and Mediates a Rab22-Rab5 Signaling Cascade in Endocytosis. *Mol. Biol. Cell*. **20**, 4720–4729

404. Poteryaev, D., Datta, S., Ackema, K., Zerial, M., and Spang, A. (2010) Identification of the switch in early-to-late endosome transition. *Cell*. **141**, 497–508

405. Ortiz, D., Medkova, M., Walch-solimena, C., and Novick, P. (2002) Cascade in Yeast. *Cell*. **157**, 1005–1015

406. Morozova, N., Liang, Y., Tokarev, A. a, Chen, S. H., Cox, R., Andrejic, J., Lipatova, Z., Sciorra, V. a, Emr, S. D., and Segev, N. (2006) TRAPPII subunits are required for the specificity switch of a Ypt-Rab GEF. *Nat Cell Biol.* **8**, 1263–1269

407. Starr, T., Sun, Y., Wilkins, N., and Storrie, B. (2010) Rab33b and Rab6 are functionally overlapping regulators of Golgi homeostasis and trafficking. *Traffic*. **11**, 626–636

408. Grigoriev, I., Yu, K. Lou, Martinez-Sanchez, E., Serra-Marques, A., Smal, I., Meijering, E., Demmers, J., Peränen, J., Pasterkamp, R. J., Van Der Sluijs, P., Hoogenraad, C. C., and Akhmanova, A. (2011) Rab6, Rab8, and MICAL3 cooperate in controlling docking and fusion of exocytotic carriers. *Curr. Biol.* **21**, 967–974

409. Medkova, M., France, Y. E., Coleman, J., and Novick, P. (2006) The rab Exchange Factor Sec2p Reversibly Associates with the Exocyst. *Mol. Biol. Cell*. **17**, 2757–2769

410. Jin, Y., Sultana, A., Gandhi, P., Franklin, E., Hamamoto, S., Khan, A. R., Munson, M., Schekman, R., and Weisman, L. S. (2011) Myosin V transports secretory vesicles via a Rab GTPase cascade and interaction with the exocyst complex. *Dev. Cell*. **21**, 1156–1170

411. Tarafder, A. K., Bolasco, G., Correia, M. S., Pereira, F. J. C., Iannone, L., Hume, A. N., Kirkpatrick, N., Picardo, M., Torrisi, M. R., Rodrigues, I. P., Ramalho, J. S., Futter, C. E., Barral, D. C., and Seabra, M. C. (2013) Rab11b Mediates Melanin Transfer between Donor Melanocytes and Acceptor Keratinocytes via Coupled Exo/Endocytosis. *J. Invest. Dermatol.* **134**, 1–11

412. Pathak, D., Sepp, K. J., and Hollenbeck, P. J. (2010) Evidence That Myosin Activity Opposes Microtubule-Based Axonal Transport of Mitochondria. *J. Neurosci.* **30**, 8984–8992

413. Schwarz, T. L. (2013) Mitochondrial trafficking in neurons. *Cold Spring Harb. Perspect. Med.* **3**, 1–16

414. Sheng, Z. H. (2014) Mitochondrial trafficking and anchoring in neurons: New insight and implications. *J. Cell Biol.* **204**, 1087–1098

415. Law, R., Dixon-Salazar, T., Jerber, J., Cai, N., Abbasi, A. a, Zaki, M. S., Mittal, K., Gabriel, S. B., Rafiq, M. A., Khan, V., Nguyen, M., Ali, G., Copeland, B., Scott, E., Vasli, N., Mikhailov, A., Khan, M. N., Andrade, D. M., Ayaz, M., Ansar, M., Ayub, M., Vincent, J. B., and Gleeson, J. G. (2014) Biallelic truncating mutations in FMN2, encoding the actin-regulatory protein Formin 2, cause nonsyndromic autosomal-recessive intellectual disability. *Am. J. Hum. Genet.* **95**, 721–8

416. Almuqbil, M., Hamdan, F. F., Mathonnet, G., Rosenblatt, B., and Srour, M. (2013) De novo deletion of FMN2 in a girl with mild non-syndromic intellectual disability. *Eur. J. Med. Genet.* **56**, 686–8

417. Perrone, M. D., Rocca, M. S., Bruno, I., Faletra, F., Pecile, V., and Gasparini, P. (2012) De novo 911 Kb interstitial deletion on chromosome 1q43 in a boy with mental retardation and short stature. *Eur. J. Med. Genet.* **55**, 117–119

418. Pleiser, S., Banchaabouchi, M. Al, Samol-Wolf, A., Farley, D., Welz, T., Wellbourne-Wood, J., Gehring, I., Linkner, J.,

Faix, J., Riemenschneider, M. J., Dietrich, S., and Kerkhoff, E. (2014) Enhanced fear expression in Spir-1 actin organizer mutant mice. *Eur. J. Cell Biol.* **93**, 225–37

419. Peleg, S., Sananbenesi, F., Zovoilis, A., Burkhardt, S., Bahari-Javan, S., Agis-Balboa, R. C., Cota, P., Wittnam, J. L., Gogol-Doering, A., Opitz, L., Salinas-Riester, G., Dettenhofer, M., Kang, H., Farinelli, L., Chen, W., and Fischer, A. (2010) Altered histone acetylation is associated with age-dependent memory impairment in mice. *Science (80-.).* **328**, 753–756

420. Lagal, V., Abrivard, M., Gonzalez, V., Perazzi, a., Popli, S., Verzeroli, E., and Tardieux, I. (2013) Spire-1 contributes to the invadosome and its associated invasive properties. *J. Cell Sci.* **127**, 328–340

421. Tedone, T., Correale, M., and Barbarossa, G. (1997) Release of the aspartyl protease cathepsin D is associated with and facilitates human breast cancer cell invasion. *FASEB J.* **11**, 785–792

422. Bruce, E. A., Digard, P., and Stuart, A. D. (2010) The Rab11 pathway is required for influenza A virus budding and filament formation. *J. Virol.* **84**, 5848–5859

423. Katoh, H., Nakatsu, Y., Kubota, T., Sakata, M., Takeda, M., and Kidokoro, M. (2015) Mumps Virus Is Released from the Apical Surface of Polarized Epithelial Cells, and the Release Is Facilitated by a Rab11-Mediated Transport System. *J. Virol.* **89**, 12026–12034

424. Caillet, M., Janvier, K., Pelchen-Matthews, A., Delcroix-Genête, D., Camus, G., Marsh, M., and Berlioz-Torrent, C. (2011) Rab7A is required for efficient production of infectious HIV-1. *PLoS Pathog.* 10.1371/journal.ppat.1002347

425. Rowe, R. K., Suszko, J. W., and Pekosz, A. (2008) Roles for the recycling endosome, Rab8, and Rab11 in hantavirus release from epithelial cells. *Virology*. **382**, 239–249

426. Kobayashi, S., Suzuki, T., Kawaguchi, A., Phongphaew, W., Yoshii, K., Iwanofi, T., Harada, A., Kariwa, H., Orba, Y., and Sawa, H. (2016) Rab8b regulates transport of West Nile virus particles from recycling endosomes. *J. Biol. Chem.* **291**, 6559–6568

427. Xu, X. F., Chen, Z. T., Gao, N., Zhang, J. L., and An, J. (2009) Myosin Vc, a member of the actin motor family associated with Rab8, is involved in the release of DV2 from HepG2 cells. *Intervirology*. **52**, 258–265

428. Andritschke, D., Dilling, S., Emmenlauer, M., Welz, T., Schmich, F., Misselwitz, B., Rämö, P., Rottner, K., Kerkhoff, E., Wada, T., Penninger, J. M., Beerenwinkel, N., Horvath, P., Dehio, C., and Hardt, W.-D. (2016) A Genome-Wide siRNA Screen Implicates Spire1/2 in SipA-Driven Salmonella Typhimurium Host Cell Invasion. *PLoS One*. **11**, e0161965

429. Kühbacher, A., Emmenlauer, M., Rämo, P., Kafai, N., Dehio, C., Cossart, P., and Pizarro-Cerdá, J. (2015) Genome-Wide siRNA Screen Identifies Complementary Signaling Pathways Involved in Listeria Infection and Reveals Different Actin Nucleation Mechanisms during Listeria Cell Invasion and Actin Comet Tail Formation. *MBio*. **6**, e00598-15

6 Supplement

6.1 Sequence related data

Spir-1, *homo sapiens* (756 amino acids)

NM_001128626.1 NP_001122098.1

MAQAAGPAGGGEPRTEAVGGEGPREPGAAGGAAGGSRDALSLEEILRLYNQPINEEQAWAVCYQCCGS
LRAAARRRQPRHRVRSAAQIRVWRDGAVTLAPAADDAGEPPPVAGKLGYSQCMETEVIESLGIIIYKA
LDYGLKENEERELSPPLEQLIDHMANTVEADGSNDEGYEAAEEGLGDEDEKRKISAIRSYRDVMKLCA
AHLPTESDAPNHYQAVCRALFAETMELHTFLTKIKSAKENLKKIQEMEKSDESSTDLEELKNADWARF
WVQVMRDLRNGVKLKKVQERQYNPLPIEYQLTPYEMLMDDIRCKRYTLRKVMVNGDIPPRLKKSAHEI
ILDFIRSRPPLNPVSARKLKPTPPRPRSLHERILEEIKAERKLRPVSPEEIRRSRLAMRPLSMSYSFD
LSDVTTPESTKNLVESSMVNGGLTSQTKENGLSTSQQVPAQRKKLLRAPTLAELDSSESEEETLHKST
SSSSVSPSFPEEPVLEAVSTRKKPPKFLPISSTPQPERRQPPQRRHSIEKETPTNVRQFLPPSRQSSR
SLEEFCYPVECLALTVEEVMHIRQVLVKAELEKYQQYKDIYTALKKGKLCFCCRTRRFSFFTWSYTCQ
FCKRPVCSQCCKKMRLPSKPYSTLPIFSLGPSALQRGESSMRSEKPSTAHHRPLRSIARFSSKSKSMD
KSDEELQFPKELMEDWSTMEVCVDCKKFISEIISSSRRSLVLANKRARLKRKTQSFYMSSPGPSEYCP
SERTISEI

KIND WH2 GTBM Spir-box FYVE-type

Spir-2, *homo sapiens* (714 amino acids)

AJ422077 CAD19439.1

MARAGSCGGAAAGAGRPEPWELSLEEVLKAYEQPLNEEQALAVCFQGCRGLRGSPGRRLRDTGDLLLR
GDGSVGAREPEAAEPATMVVPLASSEAQTVQSLGFAIYRALDWGLDESEERELSPQLERLIDLMANND
SEDSGCGAADEGYGGPEEEEEAEGVPRSVRTFAQAMRLCAARLTDPRGAQAHYQAVCRALFVETLELR
AFLARVREAKEMLQKLREDEPHLETPRAELDSLGHTDWARLWVQLMRELRRGVKLKKVQEQEFNPLPT
EFQLTPFEMLMQDIRARNYKLRKVMVDGDIPPRVKKDAHELILDFIRSRPPLKQVSERRLRPLPPKQR
SLHEKILEEIKQERRLRPVRGEGWAARGFGSLPCILNACSGDAKSTSCINLSVTDAGGSAQRPRPRVL
LKAPTLAEMEEMNTSEEEESPCGEVTLKRDRSFSEHDLAQLRSEVASGLQSATHPPGGTEPPRPRAGS
AHVWRPGSRDQGTCPASVSDPSHPLLSNRGSSGDRPEASMTPDAKHLWLEFSHPVESLALTVEEVMDV
RRVLVKAEMEKFLQNKELFSSLKKGKICCCCRAKFPLFSWPPSCLFCKRAVCTSCSIKMKMPSKKFGH
IPVYTLGFESPQRVSAAKTAPIQRRDIFQSLQGPQWQSVEEAFPHIYSHGCVLKDVCSECTSFVADVV
RSSRKSVDVLNTTPRRSRQTQSLYIPNTRTLDFK

KIND WH2 GTBM Spir-box FYVE-type

Myosin Va, *Mus musculus,* Transcript variant X1 (1880 amino acids)

XM_006510827.2 XP_006510890.1

MAASELYTKFARVWIPDPEEVWKSAELLKDYKPGDKVLLLHLEEGKDLEYRLDPKTGELPHLRNPDIL
VGENDLTALSYLHEPAVLHNLRVRFIDSKLIYTYCGIVLVAINPYEQLPIYGEDIINAYSGQNMGDMD
PHIFAVAEEAYKQMARDERNQSIIVSGESGAGKTVSAKYAMRYFATVSGSASEANVEEKVLASNPIME
SIGNAKTTRNDNSSRFGKYIEIGFDKRYRIIGANMRTYLLEKSRVVFQAEEERNYHIFYQLCASAKLP
EFKMLRLGNADSFHYTKQGGSPMIEGVDDAKEMAHTRQACTLLGISESYQMGIFRILAGILHLGNVGF
ASRDSDSCTIPPKHEPLTIFCDLMGVDYEEMCHWLCHRKLATATETYIKPISKLQATNARDALAKHIY
AKLFNWIVDHVNQALHSAVKQHSFIGVLDIYGFETFEINSFEQFCINYANEKLQQQFNMHVFKLEQEE
YMKEQIPWTLIDFYDNQPCINLIESKLGILDLLDEECKMPKGTDDTWAQKLYNTHLNKCALFEKPRMS
NKAFIIKHFADKVEYQCEGFLEKNKDTVFEEQIKVLKSSKFKMLPELFQDDEKAISPTSATSSGRTPL
TRVPVKPTKGRPGQTAKEHKKTVGHQFRNSLHLLMETLNATTPHYVRCIKPNDFKFPFTFDEKRAVQQ
LRACGVLETIRISAAGFPSRWTYQEFFSRYRVLMKQKDVLGDRKQTCKNVLEKLILDKDKYQFGKTKI
FFRAGQVAYLEKLRADKLRAACIRIQKTIRGWLLRKRYLCMQRAAITVQRYVRGYQARCYAKFLRRTK
AATTIQKYWRMYVVRRRYKIRRAATIVIQSYLRGYLTRNRYRKILREYKAVIIQKRVRGWLARTHYKR
TMKAIVYLQCCFRRMMAKRELKKLKIEARSVERYKKLHIGMENKIMQLQRKVDEQNKDYKCLMEKLTN
LEGVYNSETEKLRNDVERLQLSEEEAKVATGRVLSLQEEIAKLRKDLEQTRSEKKSIEERADKYKQET
DQLVSNLKEENTLLKQEKETLNHRIVEQAKEMTETMERKLVEETKQLELDLNDERLRYQNLLNEFSRL
EERYDDLKEEMTLMLNVPKPGHKRTDSTHSSNESEYTFSSEFAETEDIAPRTEEPIEKKVPLDMSLFL
KLQKRVTELEQEKQLMQDELDRKEEQVFRSKAKEEERPQIRGAELEYESLKRQELESENKKLKNELNE
LRKALSEKSAPEVTAPGAPAYRVLMEQLTSVSEELDVRKEEVLILRSQLVSQKEAIQPKDDKNTMTDS
TILLEDVQKMKDKGEIAQAYIGLKETNRSSTMDYQELNEDGELWMVYEGLKQANRLLESQLQSQKRSH
ENEAEALRGEIQSLKEENNRQQQLLAQNLQLPPEARIEASLQHEITRLTNENLYFEELYADDPKKYQS
YRISLYKRMIDLMEQLEKQDKTVRKLKKQLKVFAKKIGELEVGQMENISPGQIIDEPIRPVNIPRKEK
DFQGMLEYKREDEQKLVKNLILELKPRGVAVNLIPGLPAYILFMCVRHADYLNDDQKVRSLLTSTINS
IKKVLKKRGDDFETVSFWLSNTCRFLHCLKQYSGEEGFMKHNTSRQNEHCLTNFDLAEYRQVLSDLAI
QIYQQLVRVLENILQPMIVSGMLEHETIQGVSGVKPTGLRKRTSSIADEGTYTLDSILRQLNSFHSVM
CQHGMDPELIKQVVKQMFYIVGAITLNNLLLRKDMCSWSKGMQIRYNVSQLEEWLRDKNLMNSGAKET
LEPLIQAAQLLQVKKKTDDDAEAICSMCNALTTAQIVKVLNLYTPVNEFEERVSVSFIRTIQMRLRDR
KDSPQLLMDAKHIFPVTFPFNPSSLALETIQIPASLGLGFIARV

motor IQ/IQ coiled-coil GTD

Exon A Exon B Exon C Exon D Exon E ExonF

Myosin Va, *homo sapiens*, Transcript variant_X2 (1879 amino acids)

XM_011521607.1 XP_011519909.1

MLTCLDETALKFARVWIPDPEEVWKSAELLKDYKPGDKVLLLHLEEGKDLEYHLDPKTKELPHLRNPD
ILVGENDLTALSYLHEPAVLHNLRVRFIDSKLIYTYCGIVLVAINPYEQLPIYGEDIINAYSGQNMGD
MDPHIFAVAEEAYKQMARDERNQSIIVSGESGAGKTVSAKYAMRYFATVSGSASEANVEEKVLASNPI
MESIGNAKTTRNDNSSRFGKYIEIGFDKRYRIIGANMRTYLLEKSRVVFQAEEERNYHIFYQLCASAK
LPEFKMLRLGNADNFNYTKQGGSPVIEGVDDAKEMAHTRQACTLLGISESHQMGIFRILAGILHLGNV
GFTSRDADSCTIPPKHEPLCIFCELMGVDYEEMCHWLCHRKLATATETYIKPISKLQATNARDALAKH
IYAKLFNWIVDNVNQALHSAVKQHSFIGVLDIYGFETFEINSFEQFCINYANEKLQQQFNMHVFKLEQ
EEYMKEQIPWTLIDFYDNQPCINLIESKLGILDLLDEECKMPKGTDDTWAQKLYNTHLNKCALFEKPR
LSNKAFIIQHFADKVEYQCEGFLEKNKDTVFEEQIKVLKSSKFKMLPELFQDDEKAISPTSATSSGRT
PLTRTPAKPTKGRPGQMAKEHKKTVGHQFRNSLHLLMETLNATTPHYVRCIKPNDFKFPFTFDEKRAV
QQLRACGVLETIRISAAGFPSRWTYQEFFSRYRVLMKQKDVLSDRKQTCKNVLEKLILDKDKYQFGKT
KIFFRAGQVAYLEKLRADKLRAACIRIQKTIRGWLLRKKYLRMRKAAITMQRYVRGYQARCYAKFLRR
TKAATIIQKYWRMYVVRRRYKIRRAATIVLQSYLRGFLARNRYRKILREHKAVIIQKRVRGWLARTHY
KRSMHAIIYLQCCFRRMMAKRELKKLKIEARSVERYKKLHIGMENKIMQLQRKVDEQNKDYKCLVEKL
TNLEGIYNSETEKLRSDLERLQLSEEEAKVATGRVLSLQEEIAKLRKDLEQTRSEKKCIEEHADRYKQ
ETEQLVSNLKEENTLLKQEKEALNHRIVQQAKEMTETMEKKLVEETKQLELDLNDERLRYQNLLNEFS
RLEERYDDLKEEMTLMVHVPKPGHKRTDSTHSSNESEYIFSSEIAEMEDIPSRTEEPSEKKVPLDMSL
FLKLQKRVTELEQEKQVMQDELDRKEEQVLRSKAKEEERPQIRGAELEYESLKRQELESENKKLKNEL
NELRKALSEKSAPEVTAPGAPAYRVLMEQLTSVSEELDVRKEEVLILRSQLVSQKEAIQPKNTMTDST
ILLEDVQKMKDKGEIAQAYIGLKETNRSSALDYHELNEDGELWLVYEGLKQANRLLESQLQSQKRSHE
NEAEALRGEIQSLKEENNRQQQLLAQNLQLPPEARIEASLQHEITRLTNENLYFEELYADDPKKYQSY
RISLYKRMIDLMEQLEKQDKTVRKLKKQLKVFAKKIGELEVGQMENISPGQIIDEPIRPVNIPRKEKD
FQGMLEYKKEDEQKLVKNLILELKPRGVAVNLIPGLPAYILFMCVRHADYLNDDQKVRSLLTSTINSI
KKVLKKRGDDFETVSFWLSNTCRFLHCLKQYSGEEGFMKHNTSRQNEHCLTNFDLAEYRQVLSDLAIQ
IYQQLVRVLENILQPMIVSGMLEHETIQGVSGVKPTGLRKRTSSIADEGTYTLDSILRQLNSFHSVMC
QHGMDPELIKQVVKQMFYIIGAITLNNLLLRKDMCSWSKGMQIRYNVSQLEEWLRDKNLMNSGAKETL
EPLIQAAQLLQVKKKTDDDAEAICSMCNALTTAQIVKVLNLYTPVNEFEERVSVSFIRTIQMRLRDRK
DSPQLLMDAKHIFPVTFPFNPSSLALETIQIPASLGLGFISRV

motor IQ/IQ coiled-coil GTD

Exon A Exon C Exon D Exon E ExonF

Myosin Vb, *homo sapiens* (1848 amino acids)

NM_001080467.2 NP_001073936.1

MSVGELYSQCTRVWIPDPDEVWRSAELTKDYKEGDKSLQLRLEDETILEYPIDVQRNQLPFLRNPDIL
VGENDLTALSYLHEPAVLHNLKVRFLESNHIYTYCGIVLVAINPYEQLPIYGQDVIYTYSGQNMGDMD
PHIFAVAEEAYKQMARDEKNQSIIVSGESGAGKTVSAKYAMRYFATVGGSASETNIEEKVLASSPIME
AIGNAKTTRNDNSSRFGKYIQIGFDKRYHIIGANMRTYLLEKSRVVFQADDERNYHIFYQLCAAAGLP
EFKELALTSAEDFFYTSQGGDTSIEGVDDAEDFEKTRQAFTLLGVKESHQMSIFKIIASILHLGSVAI
QAERDGDSCSISPQDVYLSNFCRLLGVEHSQMEHWLCHRKLVTTSETYVKTMSLQQVINARNALAKHI
YAQLFGWIVEHINKALHTSLKQHSFIGVLDIYGFETFEVNSFEQFCINYANEKLQQQFNSHVFKLEQE
EYMKEQIPWTLIDFYDNQPCIDLIEAKLGILDLLDEECKVPKGTDQNWAQKLYDRHSSSQHFQKPRMS
NTAFIIVHFADKVEYLSDGFLEKNRDTVYEEQINILKASKFPLVADLFHDDKDPVPATTPGKGSSSKI
SVRSARPPMKVSNKEHKKTVGHQFRTSLHLLMETLNATTPHYVRCIKPNDEKLPFHFDPKRAVQQLRA
CGVLETIRISAAGYPSRWAYHDFFNRYRVLVKKRELANTDKKAICRSVLENLIKDPDKFQFGRTKIFF
RAGQVAYLEKLRADKFRTATIMIQKTVRGWLQKVKYHRLKGATLTLQRYCRGHLARRLAEHLRRIRAA
VVLQKHYRMQRARQAYQRVRRAAVVIQAFTRAMFVRRTYRQVLMEHKATTIQKHVRGWMARRHFQRLR
DAAIVIQCAFRMLKARRELKALRIEARSAEHLKRLNVGMENKVVQLQRKIDEQNKEFKTLSEQLSVTT
STYTMEVERLKKELVHYQQSPGEDTSLRLQEEVESLRTELQRAHSERKILEDAHSREKDELRKRVADL
EQENALLKDEKEQLNNQILCQSKDEFAQNSVKENLMKKELEEERSRYQNLVKEYSQLEQRYDNLRDEM
TIIKQTPGHRRNPSNQSSLESDSNYPSISTSEIGDTEDALQQVEEIGLEKAAMDMTVFLKLQKRVREL
EQERKKLQVQLEKREQQDSKKVQAEPPQTDIDLDPNADLAYNSLKRQELESENKKLKNDLNELRKAVA
DQATQNNSSHGSPDSYSLLLNQLKLAHEELEVRKEEVLILRTQIVSADQRRLAGRNAEPNINARSSWP
NSEKHVDQEDAIEAYHGVCQTNSKTEDWGYLNEDGELGLAYQGLKQVARLLEAQLQAQSLEHEEEVEH
LKAQLEALKEEMDKQQQTFCQTLLLSPEAQVEFGVQQEISRLTNENLDLKELVEKLEKNERKLKKQLK
IYMKKAQDLEAAQALAQSERKRHELNRQVTVQRKEKDFQGMLEYHKEDEALLIRNLVTDLKPQMLSGT
VPCLPAYILYMCIRHADYTNDDLKVHSLLTSTINGIKKVLKKHNDDFEMTSFWLSNTCRLLHCLKQYS
GDEGFMTQNTAKQNEHCLKNFDLTEYRQVLSDLSIQIYQQLIKIAEGVLQPMIVSAMLENESIQGLSG
VKPTGYRKRSSSMADGDNSYCLEAIIRQMNAFHTVMCDQGLDPEIILQVFKQLFYMINAVTLNNLLLR
KDVCSWSTGMQLRYNISQLEEWLRGRNLHQSGAVQTMEPLIQAAQLLQLKKKTQEDAEAICSLCTSLS
TQQIVKILNLYTPLNEFEERVTVAFIRTIQAQLQERNDPQQLLLDAKHMFPVLFPFNPSSLTMDSIHI
PACLNLEFLNEV

motor IQ/IQ coiled-coil GTD

Exon A Exon C Exon D Exon E

6.2 Overview of cloning vectors

6.2.1 pcDNA3 (Invitrogen, ThermoFisher)

The eukaryotic expression vector pcDNA3 was used to generate Myc-epitope-tagged Spir and myosin V proteins for ectopic expression in HEK293 and HeLa cells. Gene expression is regulated by the strong CMV promoter. An ampicillin resistance gene is present for bacterial selection.

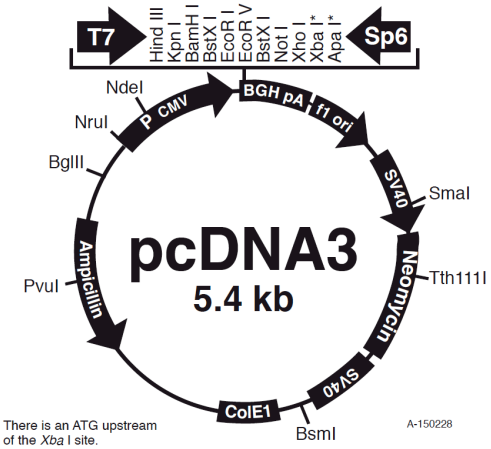

Copyright by Invitrogen, ThermoFisher

6.2.2 pAcGFP-C1 (TakaraBio/Clontech)

The eukaryotic expression vector pAcGFP-C1 was used to generate N-terminal AcGFP-tagged Spir and myosin V proteins for ectopic expression in HEK293 and HeLa cells. Gene expression is regulated by the strong CMV promoter. A kanamycin resistance gene is present for bacterial selection. The AcGFP cassette was substituted by an mStrawberry cassette (released with *Age*I / *Xho*I) to generate pmStrawberry-C1 expression vectors.

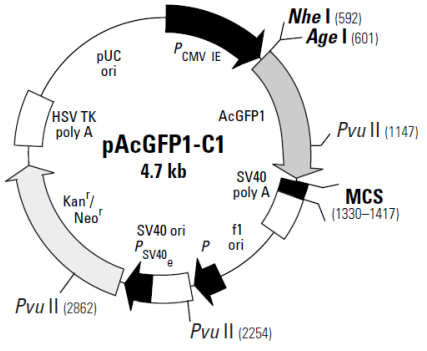

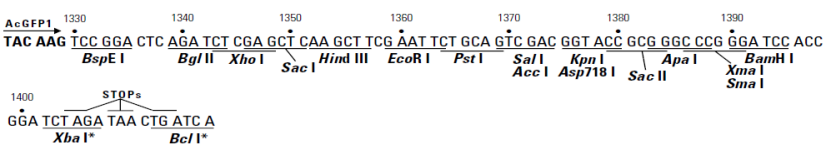

Copyright by Invitrogen, ThermoFisher

6.2.3 peGFP-C2 (Takara/Clontech)

The eukaryotic expression vector peGFP-C2 was used to generate N-terminal eGFP-tagged Spir and myosin V proteins for ectopic expression in HEK293 and HeLa cells. Gene expression is regulated by the strong CMV promoter. A kanamycin resistance gene is present for bacterial selection. The eGFP cassette was substituted by an mStrawberry cassette (released with *Age*I / *Xho*I) to generate pmStrawberry-C2 expression vectors.

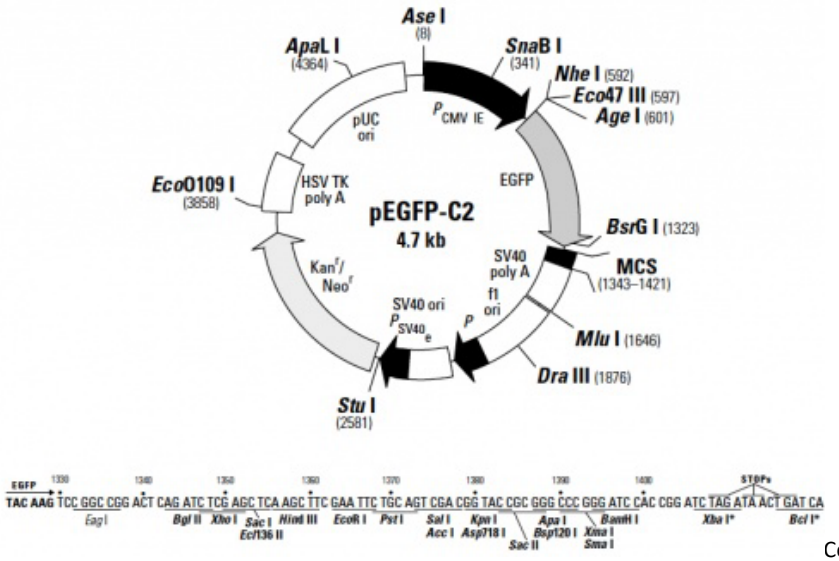

Copyright by Invitrogen, ThermoFisher

6.2.4 pGEX-4T-1-NTEV (based on pGEX-4T-1, GE Healthcare Lifesciences)

The bacterial expression vector pGEX-4T-1-NTEV used here was modified by introducing a TEV (Tobacco Etch Virus) nuclear-inclusion-a endopeptidase site downstream of the GST coding sequence for cleavage of the GST tag following protein purification. This vector was used to generate N-terminal GST-tagged Rab11a and myosin V proteins for expression of recombinant proteins in *E.coli* and subsequent protein purification. Gene expression is regulated by the tac promoter, a ubiquitous *E.coli* promoter. An ampicillin resistance gene is present for bacterial selection.

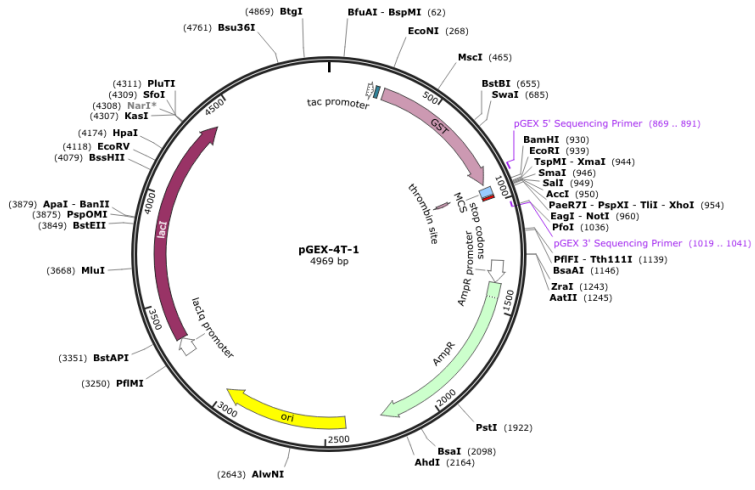

Copyright by GSL Biotech LLC (SnapGene)

6.2.5 pGEX-4T-3 (GE Healthcare Lifesciences)

The bacterial expression vector pGEX-4T-3 was used to generate an N-terminal GST-tagged Spir-2 protein for expression of recombinant proteins in *E.coli* and subsequent protein purification. Gene expression is regulated by the tac promoter, a ubiquitous *E.coli* promoter. An ampicillin resistance gene is present for bacterial selection.

6.2.6 pProEX-HTb

The bacterial expression vector pProEX-HTb used here was modified by inserting the coding sequence of the mCherry red fluorescent protein at the beginning of the multiple cloning site (*Bam*HI / *Xho*I). This vector was used to generate N-terminal His_6-mCherry-tagged Spir-2 peptides for expression of recombinant proteins in *E.coli* and subsequent protein purification. Gene expression is regulated by the trc promoter, a ubiquitous *E.coli* promoter. A TEV site is present downstream of the His_6 amino acid sequence for cleavage of the His_6 tag following protein purification. An ampicillin resistance gene allows for bacterial selection.

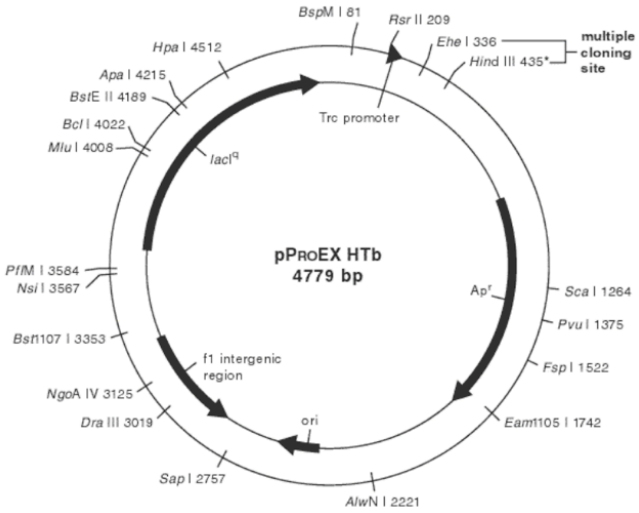

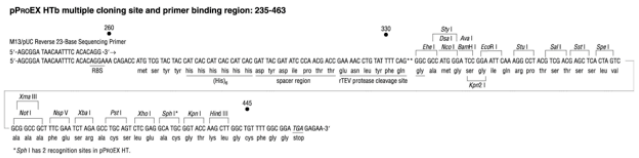

6.3 Expression vectors used in this thesis

6.3.1 Eukaryotic expression vectors

Construct name	Expression vector	Boundaries (restriction sites)	Purpose
Myc-Spir1-FL	pcDNA3-Myc-hs-Spir-1	aa 2 - 756 (*Bam*HI / *Sac*I)	Co-IP
Myc-Spir2-FL	pcDNA3-Myc-hs-Spir-2	aa 2 - 714 (*Bam*HI / *Hind*III)	Co-IP, Immunostaining
Myc-Spir2-KWM	pcDNA3-Myc-hs-Spir-2-KIND-WH2-GTBM	aa 2 - 437 (*Bam*HI / *Xho*I)	Co-IP, Immunostaining
Myc-Spir2-2-423	pcDNA3-Myc-hs-Spir-2-2-423	aa 2 - 423 (*Bam*HI / *Xho*I)	Co-IP
Myc-Spir2-KW	pcDNA3-Myc-hs-Spir-2-KIND-WH2	aa 2 - 410 (*Bam*HI / *Xho*I)	Co-IP, Immunostaining
Myc-Spir2-MSF	pcDNA3-Myc-hs-Spir-2-GTBM-SB-FYVE	aa 361/398 - 714 (*Bam*HI / *Xho*I)	Co-IP, Immunostaining
Myc-Spir2-411-714	pcDNA3-Myc-hs-Spir-2-411-714	aa 411 - 714 (*Bam*HI / *Xho*I)	Co-IP
Myc-Spir2-SF	pcDNA3-Myc-hs-Spir-2-SB-FYVE	aa 438 - 714 (*Bam*HI / *Xho*I)	Co-IP, Immunostaining
Strawberry-Spir2-MSF	pmStrawberry-C1-hs-Spir-2-GTBM-SB-FYVE	aa 361 - 714 (*Eco*RI / *Kpn*I)	Transient expression, FLIM-FRET
Strawberry-Spir2-MSF-LALA	pmStrawberry-C1-hs-Spir-2-GTBM-SB-FYVE-L408A,L409A	aa 361 - 714 (*Eco*RI / *Kpn*I)	Transient expression, FLIM-FRET
Strawberry-Spir2-SF	pmStrawberry-C2-hs-Spir-2-SB-FYVE	aa 438 - 714 (*Xho*I / *Bam*HI)	Transient expression, FLIM-FRET
GFP-MyoVa-D-FL (*)	provided by Bruno Goud	Lindsay et al., 2013	GST-Pulldown, Transient expression
GFP-MyoVa-D-QR (*)	provided by Bruno Goud	Lindsay et al., 2013	GST-Pulldown, Transient expression
GFP-MyoVa-F-QR (*)	provided by Bruno Goud	Lindsay et al., 2013	Transient expression
GFP-MyoVa-CC-GTD (#)	peGFP-C2-mm-MyoVa-CC-GTD	aa 1260 - 1880 (*Eco*RI / *Sal*I)	Transient expression

GFP-MyoVa-GTD	pAcGFP-C1-mm-MyoVa-GTD	aa 1467 - 1880 (*Hind*III / *Sal*I)	Co-IP, Transient expression, FLIM-FRET
Strawberry-MyoVa-GTD	pmStrawberry-C1-mm-MyoVa-GTD	aa 1467 - 1880 (*Hind*III / *Sal*I)	Transient expression, FLIM-FRET
GFP-MyoVb-CC-GTD	pAcGFP-C1-hs-MyoVb-CC-GTD	aa 904 - 1848 (*Hind*III / *Sal*I)	Co-IP
Strawberry-MyoVb-CC-GTD	pmStrawberry-C2-hs-MyoVb-CC-GTD	aa 909 – 1848 (*Hind*III / *Xba*I)	Transient expression
GFP-MyoVb-GTD	pAcGFP-C1-hs-MyoVb-GTD	aa 1467 - 1848 (*Hind*III / *Sal*I)	Co-IP, Transient expression
GFP-Rab11a	peGFP-C3-cl-Rab11a	1 – 216 (*Xho*I / *Hind*III)	Transient expression
Strawberry-Rab11a	pmStrawberry-C1-mm-Rab11a	aa 2 - 216 (*Eco*RI / *Bam*HI)	Transient expression
Strawberry-FMN2-FH2-FSI	pmStrawberry-C2-mm-FMN-2-FH2-FSI	aa 1135 - 1578 (*Bam*HI / *Xho*I)	GST-Pulldown
GFP	pAcGFP-C1		Co-IP, FLIM-FRET
GFP-linker-Strawberry	pAcGFP-C1-linker(A-S-G-A-G)-mStrawberry	aa 1 - 236 (*Bsp*EI / *Bgl*II)	FLIM-FRET

Table 16 | Overview on eukaryotic expression vectors. (*), these expression vectors were generated and kindly provided by the lab of Bruno Goud, Institut Curie, Paris, France; (#), this expression vector was generated and kindly provided by the lab of Alistair Hume, University of Nottingham, Nottingham, UK; *aa*, amino acid.

6.3.2 Bacterial expression vectors

Construct name	Expression vector	Boundaries (restriction sites)	Purification	Purpose
GST-Spir2-MSF	pGEX-4T-3-hs-Spir-2-GTBM-SB-FYVE	aa 361 - 714 (*Bam*HI / *Xho*I)	GSH Sepharose 4B, Superdex 200	GST-Pulldown
His_6-mCherry-Spir2-linker	pProEX-HTb-mCherry -hs-Spir-2-linker	aa 361 - 519 (*Xho*I / *Hind*III)	Ni-NTA Agarose, Superdex 200	GST-Pulldown, Binding studies
His_6-mCherry-Spir2-linker-LALA	pProEX-HTb-mCherry -hs-Spir-2-linker-L408A,L409A	aa 361-519 (mutagenesis)	Ni-NTA Agarose, Superdex 200	GST-Pulldown
Spir2-linker peptide	purchased from GenScript	aa 401-427		Crystallisation, Fluorescence anisotropy
GST-MyoVa-GTD	pGEX-4T-1-NTEV-mm-MyoVa-GTD	aa 1467 - 1880 (*Hind*III / *Sal*I)	GSH Sepharose 4B, Superdex 200	GST-Pulldown, Binding assays
MyoVa-GTD (*)	pProEX-HTb-hs-MyoVa-GTD	aa 1461 - 1853 (*Bam*HI / *Xho*I)	HisTrap, TEV, Superdex 200	Crystallisation, GST-Pulldown
GST-MyoVb-GTD	pGEX-4T-1-NTEV-hs-MyoVb-GTD	aa 1467 - 1848 (*Bam*HI / *Xho*I)	GSH Sepharose 4B, Superdex 200	GST-Pulldown, Binding assays
GST-Rab11a-Q70L	pGEX-4T-1-NTEV-cl-Rab11a-Q70L	aa 1 - 216 (*Eco*RI / *Eco*RI)	GSH Sepharose 4B, Superdex 200	GST-Pulldown
Rab11a-Q70L (*)	pET28-rTEV-hs-Rab11a-Q70L	aa 1 - 173 (*Nco*I / *Eco*RI)	HisTrap, TEV, Superdex 200	GST-Pulldown
GST-FMN2-eFSI	pGEX-4T-1-NTEV-mm-FMN2-eFSI	aa 1523 - 1578 (*Bam*HI / *Xho*I)	GSH Sepharose FF, Superdex 200	GST-Pulldown
His_6-mCherry	pProEX-HTb-mCherry	aa 1 - 236 (*Bam*HI / *Xho*I)	Ni-NTA Agarose, Superdex 200	GST-Pulldown
GST	pGEX-4T-1-NTEV		GSH Sepharose 4B, Superdex 200	GST-Pulldown

Table 17 | Overview on bacterial expression vectors. (*), these expression vectors were generated and kindly provided by the lab of Anne Houdusse, Institut Curie, Paris, France; *aa*, amino acid.

6.4 Buffers, solutions and media

Agar selection plates for bacterial culture	- 25 g LB_0 medium - 13 g select agar - fill up with H_20 to 1 l - autoclave for 20 min at 121°C - cool to approx. 42°C - add antibiotics
Agarose solution for gel electrophoresis	- dissolve desired amount of agarose in 0.5x TBE by boiling and shaking (1% - 2.5%)
Ampicillin solution (10%)	- 1 g Ampicillin sodium salt in 10 ml H_20 - filter sterile and store aliquots at 4°C
APS solution (10%)	- dissolve 10% Ammoniumpersulfat (w/v) in H_2O - store at 4°C
β-Mercaptoethanol solution (12.8 M)	- mix stock solution with H_2O to obtain 12.8 M
Coomassie staining solution	- 10% acetic acid - 40% ethanol - 0.6% (w/v) Coomassie brilliant blue G250 - 0.6% (w/v) Coomassie brilliant blue R250
Chloramphenicol solution	- dissolve 34 mg/ml in ethanol
DNA ladder (1 kb; 100 bp) for agarose gel electrophoresis	- 100 µl 6x DNA loading dye - 60 µl ladder (peqGOLD; 1 kb, 100 bp) - 440 µl H_20
	-
DNA loading dye (6x)	- 10 mM Tris-HCl, pH 7.6 - 0.03% bromophenol blue - 60% glycerol - 60 mM EDTA

FCSIII for cell culture	- inactivate at 56°C (waterbath) for 30 min - store 50 ml aliquots at -20°C
Full Medium for cell culture	- DMEM - 10% FCSIII - 2 mM L-Glutamine - 100 units/ml Penicillin - 100 µg/ml Streptomycin
HEPES buffer solution for use in cell culture (1M)	- dissolve in sterile H_2O - adjust pH to 7.5 - filter sterile, store 1 ml aliquots at -20°C
IPTG stock solution (0.1 M)	- dissolve in sterile H_20 - filter sterile, store 2 ml aliquots at -20°C
Kanamycin stock solution (25 mg/ml)	- dissolve Kanamycin monosulfate in H_20 - filter sterile and store 2 ml aliquots at -20°C
LB medium (Luria/Miller)	- dissolve 25 g/l in H_20 - autoclave for 20 min at 121°C
Mouse Brain Pulldown buffer	- 25 mM Tris-HCl, pH 7.4 - 150 mM NaCl - 5 mM $MgCl_2$ - 10% (v/v) glycerol - 0.1% (v/v) Nonidet P-40 - 0.1 M NaF - 1 mM Na_3VO_4 - add freshly: 1 mM PMSF, complete Mini Protease Inhibitor Cocktail

Mowiol solution	- dissolve 15 g Mowiol 4-88 in 70 ml H_2O - add 30 ml glycerol - add 2.5% (w/v) n-propylgallat - centrifuge at 17,300 x *g* for 15 min - store 1 ml aliquots at -20°C
Paraformaldehyde solution (3.7%)	- dissolve 7.4 g paraformaldehyde in 100 ml 1x PBS - add 2 drops 10 M NaOH - incubate at 60°C for at least 30 min - add 100 ml 1x PBS, adjust to pH 7.4 - store 10 ml aliquots at -20°C
PBS (2x) for protein purification	- 2300 mg/l = 16.2 mM Na_2HPO_4 - 400 mg/l = 5.4 mM KCl - 400 mg/l = 2.94 mM KH_2PO_4 - 16000 mg/l = 275 mM NaCl
PBS (10x)	- dissolve 95.5 g PBS powder in 1 l H_20
PBST (1x; 0.05% Tween20)	- add 0.05% Tween20 to 1x PBS
PMSF stock solution (0.1 M)	- dissolve in ethanol - store 2 ml aliquots at -20°C
Ponceau S staining solution	- 5% acetic acid - 0.1% (w/v) Ponceau S
Pulldown buffer	- 25 mM Tris-HCl, pH 7.4 - 150 mM NaCl - 5 mM $MgCl_2$ - 0.1% NP-40 - 10% glycerol
SDS-PAGE-buffer (10x)	- 250 mM Tris - 1.9 M glycine

	- 1% SDS (w/v)
SDS protein sample buffer (5x) **Laemmli buffer**	- 100 mM Tris-HCl, pH 6.8 - 50% glycerol (v/v) - 15% SDS (w/v) - 25% β-Mercaptoethanol (v/v) - 0.025% bromophenol blue (w/v) - store 1 ml aliquots at -20°C
SPECS buffer	- 1x PBS - 50 mM NaCl
Stripping buffer	- 62.5 mM Tris-HCl, pH 6.7 - 2% SDS
TBE buffer (10x)	- 890 mM Tris - 890 mM boric acid - 20 mM EDTA, pH 8.0
Transfer buffer (10x)	- 250 mM Tris - 1.92 M glycine
Transfer Buffer (1x)	- 25 mM Tris - 192 mM glycine - 20% methanol
Tris-EDTA, pH 8.0 **for plasmid DNA storage**	- 20 mM Tris - 1 mM EDTA - adjust pH to 8.0 with HCl - autoclave
Triton X-100 (0.2%)	- 0.2% in 1x PBS
Tween20 (10%)	- dilute Tween20 in 1x PBS

Table 18 | Overview on buffers, solutions and media.

6.5 SDS polyacrylamide gels

Separating gel

	7.5%	10%	12%	15%
H_2O	5.7 ml	4.8 ml	4.1 ml	3.45 ml
3 M Tris pH 9.0	1.3 ml	1.3 ml	1.3 ml	1.3 ml
Acrylamide30	2.6 ml	3.5 ml	4.2 ml	4.85 ml
20% SDS	50 µl	50 µl	50 µl	50 µl
TEMED	10 µl	10 µl	10 µl	10 µl
10% APS	50 µl	50 µl	50 µl	50 µl

Table 19 | Preparation of SDS separation gels.

Stacking gel

H_2O	2.6 ml
1 M Tris pH 6.8	420 µl
Acrylamide30	550 µl
20% SDS	17 µl
TEMED	5 µl
10% APS	33 µl

Table 20 | Preparation of SDS stacking gels.

6.6 Primer

Primer name	Tm (°C)	Primer sequence (5' > 3')
Cloning primer		
part1-MyoVb-Beginn-5'	90.7	CAGTGCACAAGGGTCTGGATCCCTGACCCTGATGAGGTATGGCGCTCAG
***Hind*III-part2-MyoVb-Beginn-5'**	93.0	CCCAAGCTTTCGGTGGGCGAGCTCTACAGCCAGTGCACAAGGGTCTGGATCCCT
bis-MyoVb-tail-*Sac*II-3'	88.3	TCCCCGCGGTAATCCTGAGGGCCTTCAGCTCCCG
MyoVb-tail-*Sac*II-5'	93.4	TCCCCGCGGGCGAGGCCCGCTCAGCAGAGCATC
Hs-MyoVb-tail-Stop-*Bam*HI-3'	77.1	CGGGATCCCTAGACTTCATTGAGGAATTCCAGATT
***Hind*III-Myc-hs-MyoVb-tail-5'**	65.3	CCCAAGCTTGCCGCCGCCATGGAGCAGAAGCTGATCTCCGAGGAGGACCTGGAGGCCCGCTCAGCAGAGCATCTG
hsMyoVb-*Hind*III-aa904-5'	87.9	CCCAAGCTTCGGCCCTCAGGATTGAGGCCCGC
hsMyoVb- *Hind*III -aa1143-5'	81.0	CCCAAGCTTCGATGACGGTCTTCCTGAAGCTG
hsMyoVb- *Hind*III -aa1336-5'	85.5	CCCAAGCTTCGCTAAAGCAAGTTGCCAGGCTG

hsMyoVb- *Hind*III -aa1467-5'	83.9	CCCAAGCTTCGCAGGGCATGCTGGAGTACCAC
hsMyoVb-Stop-*Sal*I-3'	76.0	CGGTCGACCTAGACTTCATTGAGGAATTCCAG
***Bam*HI-MyoVb-tail-1467-5'**	82.5	CGGGATCCCAGGGCATGCTGGAGTACCAC
MyoVb-tail-1467-Stop-*Xho*I-3'	78.9	CCGCTCGAGTCAGACTTCATTGAGGAATTCCAG
***Hind*III-mm-MyoVa-1467-5'**	74.8	CCCAAGCTTCGAAAGAAAAGGATTTCCAAGGAATG
mm-MyoVa-Stop-*Sal*I-3'	82.9	GCGTCGACTCAGACCCGTGCGATGAAGCCCAG
***Bam*HI-MyoVa-tail-1467-5'**	73.4	CGGGATCCAAAGAAAAGGATTTCCAAGGAATG
MyoVa-tail-1467-Stop-*Xho*I-3'	84.2	CCGCTCGAGTCAGACCCGTGCGATGAAGCCCAG
***Bam*HI-Myc-hs-Spir2-1-5'**	68.9	CGGGATCCGCCGCCGCCATGGAGCAGAAGCTGATCTCCGA GGAGGACCTGGACGCGGGTCGGCGCGCGGGAG
Hs-Spir2-424-Stop-*Xho*I-3'	91.5	CCGCTCGAGTCACTTGAGCAGCACGCGGGGCCG
Hs-Spir2-437-Stop-*Xho*I-3'	77.0	CCGCTCGAGTCAAGATGTATTCATCTCTTCCATTTC
Hs-Spir2-442-Stop-*Xho*I-3'	77.3	CCGCTCGAGTCAAGACTCTTCTTCCTCAGATGTATTC
Hs-Spir2-451-Stop-*Xho*I-3'	87.0	CCGCTCGAGTCACCGTTTCAGCGTCACCTCCCC
***Bam*HI-Myc-hs-Spir2-412-5'**	69.5	CGGGATCCGCCGCCGCCATGGAGCAGAAGCTGATCTCCGA GGAGGACCTGGGCAGCGCCCAGCGCCCGCGG
***Bam*HI-Myc-hs-Spir2-425-5'**	99.3	CGGGATCCGCCGCCGCCATGGAGCAGAAGCTGATCTCCGA GGAGGACCTGGCGCCTACCTTGGCTGAAATG
***Bam*HI-Myc-hs-Spir2-452-5'**	99.6	CGGGATCCGCCGCCGCCATGGAGCAGAAGCTGATCTCCGA GGAGGACCTGGACCGCTCCTTCTCAGAGCATG
Hs-Spir2-Stop-*Xho*I-3'	80.5	CCGCTCGAGTCACTTGAAGTCAAGAGTCCTGGTG
***Xho*I-hsSpir2-452-5'**	85.9	CCGCTCGAGCGACCGCTCCTTCTCAGAGCATG
***Xho*I-Straw-Spir2-452-5'**	85.1	CCGCTCGAGCTGACCGCTCCTTCTCAGAGCATG
hsSpir2-Stop-*Bam*HI-3'	75.7	CGGGATCCTCACTTGAAGTCAAGAGTCCTG
Hs-Spir2-375-*Xho*I-5'	93.1	CCGCTCGAGGGCGAGGGCTGGGCTGCCCGC
***Hind*III-hs-Spir2-533-3'**	82.8	CCCAAGCTTCTAATCGGGGGTCATGGAGGCCTC
QuikChange PCR primer		
QC-MyoVb-*Sac*II-5'	90.1	GAGCTGAAGGCCCTCAGGATTGAGGCCCGCTCAGCAGAG CATC
QC-MyoVb-*Sac*II-3'	90.1	GATGCTCTGCTGAGCGGGCCTCAATCCTGAGGGCCTTCAG CTC
QC-MyoVb-full-frame-5'	88.2	CTCAGATCTCGAGCTCAAGCTTCGTCGGTGGGCGAGCTCT ACAGC
QC-MyoVb-full-frame-3'	88.2	GCTGTAGAGCTCGCCCACCGACGAAGCTTGAGCTCGAGAT CTGAG

HsMyoVb-Q1748R-5'	84.9	CAAGCAGCCCAGCTCCTGCGCTTAAAGAAGAAAACCCAGG
HsMyoVb-Q1748R-3'	84.9	CCTGGGTTTTCTTCTTTAAGCGCAGGAGCTGGGCTGCTTG
Hs-Spir2-Stop-533-5'	88.1	GAGGCCTCCATGACCCCCTAGGCCTAACACCTGTGGCTGG AGTTC
Hs-Spir2-Stop-533-3'	88.1	GAACTCCAGCCACAGGTGTTAGGCCTAGGGGGTCATGGA GGCCTC
Hs-Spir2-MyoLinkAAK-5'	78.0	CGCCCGCGGCCCCGCGTGGCGGCCAAGGCGCCTACCTTGG C
Hs-Spir2-MyoLinkAAK-3'	78.0	GCCAAGGTAGGCGCCTTGGCCGCCACGCGGGGCCGCGGG CG
Sequencing primer		
M5B-660bp-5'		GGCAAGTACATCCAGATTGGC
M5B-1165bp-5'		GTCAAGACCATGTCCCTGCAG
M5B-1678bp-5'		CTCTCTGATGGTTTTCTGGAG
M5B-2182bp-5'		GTCCTGGAGAACCTCATCAAG
M5B-2611bp-5'		CAGAAGCACGTGCGGGGCTGG
Hs-MyoVbfl-3253-5'		CGGGATGAAATGACCATCATAAAG
Hs-MyoVbfl-3912-5'		GAGGCCTATCACGGGGTCTGC
Hs-MyoVbfl-4606-5'		CTGAAAAAGCACAATGATGAC
Hs-MyoVbfl-5133-5'		CTCAGGTACAATATAAGTCAG

Table 21 | Overview on primers used in this thesis. *Tm*, melting temperature.

6.7 Antibodies

6.7.1 Primary antibodies

Antibody	Species/ clonality	Purpose	Company	Order number
Living Colors® A.v. Peptide Antibody	rabbit polyclonal	Western blot	TakaraBio/ Clontech	632376
Living Colors® DsRed Polyclonal Antibody	rabbit polyclonal	Western blot	TakaraBio/ Clontech	632496
anti-c-Myc (9E10)	mouse monoclonal	Western blot Immunostain	Santa Cruz Biotechnology	sc-40
anti-Myosin Va	rabbit polyclonal	Western blot	Cell Signaling Techology	#3402
anti-Rab11 (D4F5 XP)	rabbit monoclonal	Western blot	Cell Signaling Technology	#5589
anti-Spir-1 (SA2133)	rabbit polyclonal	Western blot	(Schumacher et al., 2004)	-

Table 22 | Overview on primary antibodies.

6.7.2 Secondary antibodies

Antibody	Species	Purpose	Company	Order Number
Amersham ECL anti-mouse IgG, HRP-linked	sheep	Western blot	GE Healthcare Life Sciences	NA931-1ML
Amersham ECL anti-rabbit IgG, HRP-linked	donkey	Western blot	GE Healthcare Life Sciences	NA934-1ML
anti-mouse-CY5	donkey	Immunostain	Dianova	715-175-151
anti-mouse-TRITC	donkey	Immunostain	Dianova	715-025-151

Table 23 | Overview on secondary antibodies.

6.8 Chemicals and reagents

6.8.1 Restriction endonucleases

Restriction endonuclease	Concentration	Company	Order number
***Bam*HI-HF**	20,000 units/ml	NEB	R3136S
***Bgl*II**	10,000 units/ml	NEB	R0144L
***Bsp*EI**	10,000 units/ml	NEB	R0540S
***Eco*RI-HF**	20,000 units/ml	NEB	R3101L
***Hind*III-HF**	20,000 units/ml	NEB	R3104S
***Kpn*I-HF**	20,000 units/ml	NEB	R3142L
***Sac*II**	20,000 units/ml	NEB	R0157S
***Sal*I**	20,000 units/ml	NEB	R0138S
***Xho*I**	20,000 units/ml	NEB	R0146L

Table 24 | Overview on restriction endonucleases.

6.8.2 DNA polymerases

DNA polymerase	Concentration/volume	Company	Order number
AccuPrime™ Pfx DNA Polymerase	2.5 units/µl	ThermoFisher	12344-024
Taq DNA Polymerase	5000 units/ml	NEB	M0273L
Pfu DNA Polymerase	500 U	Promega	M7745

Table 25 | Overview on DNA polymerases.

6.8.3 Enzymes

Enzyme	Concentration/volume	Company	Order number
Alkaline Phosphatase, Calf Intestinal (CIP)	10,000 units/ml	NEB	M0290L
T4 DNA Ligase	400,000 units/ml	NEB	M0202L

Table 26 | Overview on further enzymes.

6.8.4 Chemicals

Article	Quantity	Company	Order number
1,4-Dithioerythritol (DTE)	5 g	Sigma-Aldrich	D8255-5G
Acetic acid, Rotipuran, 100%, p.a.	1 l	Carl Roth	3738.1
Albumin standard (2.0 mg/ml)	10 x 1 ml	ThermoFisher	23209
Ammoniumpersulfat	100 g	Sigma-Aldrich	A3678
Ampicillin sodium salt	25 g	Sigma-Aldrich	A9518-25G
β-Mercaptoethanol	100 ml	Carl Roth	4227.3
Boric acid	1 kg	Sigma-Aldrich	B0252-1KG
Brillant Blue G 250	10 g	Carl Roth	9598.1
Brillant Blue R 250	10 g	Carl Roth	3862.1
Bromophenol blue sodium salt	10 g	Carl Roth	A512.1
Chloramphenicol	25 g	Sigma-Aldrich	C0378-25G
Coomassie Plus Protein Assay Reagent for Bradford assays	950 ml	ThermoFisher	1856210
cOmplete Mini, EDTA-free	25 tabs	Roche	11836170001
DL-Dithiothreitol (DTT)	5 g	Sigma-Aldrich	D0632-5G
dNTP solution set	25 µM each	NEB	N0446S
Ethanol >99.8 %, p.a.	2.5 l	Carl Roth	9065.2
Ethanol >99.8 % + 1 % MEK	2.5 l	Carl Roth	K928.1
Ethidiumbromide solution, 0.5%	15 ml	Carl Roth	HP46.1
Glycerine-solution for microscopy		Leica	11513872
Glutathione Sepharose 4B	10 ml	GE Healthcare Life Sciences	17-0756-01
Glycine, 99%	5 kg	Carl Roth	3790.3
Hydrochloric acid, Rotipuran, 25%	1 l	Carl Roth	6331.1
Immersion liquid, Type F		Leica	11513859
Imidazole	500 g	Sigma-Aldrich	56750-500G
Isopropyl-β-D-1-thiogalactopyranoside (IPTG)	5 g	Sigma-Aldrich	I6758-5G
Isopropanol, >99.5%	2.5 l	Carl Roth	9866.5
Kanamycin B sulfate salt	250 mg	Sigma-Aldrich	B5264-250MG
LB-Medium (Luria/Miller; 10 g/l NaCl)	5 kg	Carl Roth	X968.4
L-Glutathione reduced, >98%	25 g	Sigma-Aldrich	G4251-25G

Luminata™ Forte Western HRP Substrate	100 ml	Merck-Millipore	WBLUF0100
Magnesium chloride hexahydrate	100 g	Sigma-Aldrich	M2670-100G
Methanol, LiChrosolv	2.5 l	Merck-Millipore	1.06007.2500
Milk powder	500 g	Carl Roth	T145.2
MOWIOL 4-88 Reagent	100 g	Calbiochem	475904
N-propyl-gallate	100 g	Sigma-Aldrich	P3130
Ni-NTA Agarose	25 ml	Qiagen	1018244
Nonidet P-40 BioChemica (NP-40)	500 ml	AppliChem	A1694,0500
Paraformaldehyde	250 g	Carl Roth	0335.1
PBS-Buffer powder	10 l	AppliChem	A0965,9010
peqGOLD 100bp DNA Ladder	50 µg	PeqLab	25-2010
peqGOLD 1kb DNA Ladder	5 x 50 µg	PeqLab	25-2030
Phenylmethylsulfonylfluorid, PMSF	5 g	Sigma-Aldrich	P-7626-5G
Ponceau S, practical grade	50 g	Sigma-Aldrich	P3504-50G
Protein G-Agarose	5 ml	Roche	11243233001
Protran® Nitrocellulose Transfer Membrane BA85, 0.45 µm		Whatman	10401196
Precision Plus Protein Dual Color Standards	500 µl	Bio-Rad	161-0374
RNAse away		Molecular Bioproducts	7000
Rotiphorese Gel 30, Acrylamid/Bis-Acrylamid solution	1 l	Carl Roth	3029.1
Rubidium chloride, >99%, p.a.	10 g	Carl Roth	4471.1
Select agar	250 g	Sigma-Aldrich	A5054-250G
Sodium chloride, >98%	1 kg	Sigma-Aldrich	S3014-1KG
Sodium dodecyl sulfate (SDS)	500 g	Sigma-Aldrich	L4390-500G
Sodium fluoride	100 g	Fluka	71519
Sodium hydroxide pellets		Merck	106462
Sodium orthovanadate	10 g	Sigma-Aldrich	450243-10G
TEMED	100 ml	Sigma-Aldrich	T9281
Triton X-100, for molecular biology	100 ml	Sigma-Aldrich	T8787-100ML
Trizma base	5 kg	Sigma	T1503-5KG
Tween 20, BioChemica	500 ml	AppliChem	A1389,0500
UltraPure™ Agarose	100 g	ThermoFisher	16500100

Table 27 | Overview on chemicals.

6.9 Cell culture media, reagents and supplements

Article	Quantity	Company	Order number
D-MEM (HG) W/O NA PYR (CE)	500 ml	ThermoFisher	41965-062
Dimethyl sulfoxide (DMSO), Hybri-Max	5 x 10 ml	Sigma-Aldrich	D2650
HyClone FetalClone III Serum (FCS III) Lot: AVL90602	500 ml	GE Healthcare Life Sciences	SH30109.03
L-Glutamine; 200 mM	100 ml	ThermoFisher	25030024
Lipofectamine reagent	1 ml	ThermoFisher	18324012
Dulbecco's Phosphate Buffered Saline (PBS)	500 ml	Sigma-Aldrich	D8537
Penicillin/Streptomycin solution	100 ml	ThermoFisher	15140122
Poly-L-Lysine	50 ml	Sigma-Aldrich	P4707
Trypan Blue solution (0.4%, sterile-filtered, suitable for cell culture)	100 ml	Sigma-Aldrich	T8154-100ML
Trypsin-EDTA (0.05%)	100 ml	ThermoFisher	25300054
Water, sterile filtered, BioReagent, suitable for cell culture	1 l	Sigma-Aldrich	W3500-1L

Table 28 | Overview on cell culture media, reagents and supplements.

6.10 Kits

Kit	Company	Order number
NucleoSpin® Gel and PCR Clean-up	Macherey-Nagel	REF 740609.50
QIAGEN® OneStep RT-PCR Kit	Qiagen	210210
QIAGEN® Plasmid Maxi Kit (25)	Qiagen	12163
QIAprep® Spin Miniprep Kit (250)	Qiagen	27106
QuikChange® Site-Directed Mutagenesis Kit	Stratagene	200518

Table 29 | Overview on kits.

6.11 Equipment

Article	Company	Order number
ÄKTApurifier	GE Healthcare Life Sciences	
Cell counting chamber (Neubauer, depth: 0.1 mm; 0.0025 mm^2)	Marienfeld-Superior	0640010
Centrifuge, 5417 R, refrigerated	Eppendorf	
Centrifuge, 5424	Eppendorf	
Centrifuge, Multifuge 1 s-r, refrigerated	Heraeus	75004331
Centrifuge, refrigerated, BC Avanti J-26 XP	Beckman Coulter	JXS 10 G30
Centrifuge bottle, polycarbonate, 50 ml	Beckman Coulter	357000
Centrifuge bottle, polypropylene, 1000 ml	Beckman Coulter	366752
E-Box 3026 WL-26M (UV-Transilluminator)	PeqLab	
Forma Orbital Shaker, 37°C	Thermo Scientific	
Forma Orbital Shaker, refrigerated	Thermo Scientific	
GeneQuant 1300	GE Healthcare Life Sciences	28-9182-13
ImageQuant LAS 4000	GE Healthcare Life Sciences	28-9558-10
JA-25.50 rotor for Avanti J-26 XP	Beckman Coulter	S/N 10E 2140
JLA-8.1000 rotor for Avanti J-26 XP	Beckman Coulter	969329
High Load™ 16/60 Superdex 200 pg	GE Healthcare Life Sciences	28989335
Leica AF6000 LX Life Cell Imaging System	Leica	
Mastercycler ep gradient S	Eppendorf	5345 000.510
Mini Trans-Blot® Cell	Bio-Rad	170-3930
PowerPac™ 300	Bio-Rad	165-5051
PowerPac™ Basic Power Supply	Bio-Rad	164-5050
Spectrofluorometer, Fluoromax-4	Horiba, Jobin Yvon	
TissueRuptor	Qiagen	9001272
Water bath	Memmert	

Table 30 | Equipment overview.

6.12 Disposable materials

Article	Company	Order number
Amicon Ultra, 30K, Centrifugal filters	Millipore	UFC803024
Amicon Ultra-4, 50K, Centrifugal filters	Millipore	UFC805024
Autoclave indicator tape (120°C)	A. Hartenstein	STKD
Blotting papers, Grade 3 MM Chr	Whatman	3030.917
Cell culture dish (100 x 20 mm)	Greiner Bio-One	664160
Cell culture plate (6-well)	Greiner Bio-One	657160
Cellstar tubes, canonical (15 ml)	Greiner Bio-One	188 271
Cellstar tubes, canonical (50 ml)	Greiner Bio-One	227 261
CryoTube Vials (1 ml)	Nunc	366656
Microscope cover glasses, 15 mm	A. Hartenstein	DKR2
Microscope slides, Menzel-Gläser, Superfrost Plus	Thermo Scientific	J1800AMNZ
Needles, BD Microlance 3, 20G x 1.5“	BD Biosciences	301300
Parafilm® “M” Laboratory Film	Pechiney Plastic Packaging	PM-996
Pasteur pipettes	A. Hartenstein	PP07
PCR SoftTubes (0.2 ml)	Biozym	710920
Petri dishes (94 x 16 mm)	A. Hartenstein	PP90
Pipette tips, blue (100-1000 µl)	Axygen	T-1000-B
Pipette tips, white (0.5-10 µl)	Axygen	T-300
Pipette tips, yellow (2-200 µl)	Sarstedt	70.760.002
Reaction tubes (1.5 ml)	A. Hartenstein	RK1G
Reaction tubes (2.0 ml)	A. Hartenstein	RK2G
Syringe (2 ml)	BD Biosciences	237
Syringe (10 ml)	BD Biosciences	274
Syringe with needle, 1 ml 26G x 3/8“, Luer	BD Biosciences	300015
T25 cell culture flask (25 cm^2, 50 ml)	Sarstedt	83.1810.002
T75 cell culture flask (75 cm^2, 250 ml)	Sarstedt	83.1813.002
Transfection tubes (5 ml, 75 x 12 mm)	Sarstedt	55.476.013
Ventilation cap tubes (14 ml)	Sarstedt	62.515.006
Videoprinter paper	VWR	PEQRCD80E1091
WillCo-Dish (Glass-bottom dish; 40 mm)	WillCo Wells B.V.	GWSt-5040

Table 31 | Overview on disposables.

7 List of abbreviations

A

aa · *Amino acid*
AAA · *ATPases Associated with Diverse Activities*
ABD · *F-actin binding domain*
AcGFP · *Aequorea coerulescens GFP*
ADF · *Actin depolymerising factor*
ADP · *Adenosine diphosphate*
AMPA · *α-amino-3-hydroxy-5-methyl-4-isoxazolepropionic acid*
Arf · *ADP-ribosylation factor*
Arp2/3 · *Actin-related protein 2/3*
ARPC · *Arp complex protein*
ATP · *Adenosine triphosphate*

B

bp · *Base pair*
Br · *Brachydanio rerio*
BSA · *Bovine serum albumine*

C

Caax · *Cysteine-aliphatic-aliphatic-arbitrary*
cAMP · *Cyclic adenosine monophosphate*
Capu · *Cappucino*
cDNA · *Complementary DNA*
CIP · *Calf intestinal alkaline phosphatase*
CMV · *Cytomegalovirus*
Cobl · *Cordon-bleu*
Co-IP · *Co-immunoprecipitation*
Crag · *Calmodulin-binding protein related to a Rab3 GDP/GTP exchange protein*
CRISPR · *Clustered Regularly Interspaced Short Palindromic Repeats*
CV · *Column volume*
Cy5 · *Cyanine dye 5*

D

DENN · *Differentially expressed in normal and neoplastic cells*
DFV · *Discoidal/fusiform-shaped vesicle*
DLC2 · *Dynein light chain 2*
DLIC · *Dynein light intermediate chain*
DMEM · *Dulbecco's modified eagle's medium*
Dm-MyoV · *Drosophila myosin V*
DMSO · *Dimethylsulfoxide*
dNTP · 2´-Desoxyribonucleosid-5´-triphosphate
dRab11 · *Drosophila Rab11*
DTE · *1,4-Dithioerythritol*

E

EB · *Elution buffer*
ECM · *Extracellular matrix*
EDTA · *Ethylenediaminetetraacetate*
EE · *Early endosome*
EEA1 · *Early endosome antigen 1*
EFBD · *exon-F binding domain*
EGF · *Epidermal growth factor*
eGFP · *Enhanced GFP*
EHD1 · *Eps-15-homology domain-containing protein 1*
EHD3 · *Eps-15-homology domain-containing protein 3*
ER · *Endoplasmatic reticulum*
ERM · *Ezrin-radixin-moesin*
Evi5 · *ecotropic viral integration site 5 protein*

F

F-actin · *Filamentous actin*
FCCS · *Fluorescence cross-correlation spectroscopy*
FCS · *Fluorescence correlation spectroscopy*
FCSIII · *Fetal calf serum III*
FH · *Formin-homology domain*

FL · *Full-length*

FLIM-FRET · *Fluorescence lifetime microscopy-Förster resonance energy transfer*

FMN · *Formin family formin*

FMN-2 · *Formin-2*

FSI · *Formin/Spir interaction sequence*

FYVE · *Fab1, YOTB/ZK632.12, Vac1, EEA1*

G

G-actin · *Globular actin*

GAP · *GTPase activating protein*

GDF · *GDI displacement factor*

GDI · *Guanine nucleotide dissociation inhibitor*

GDP · *Guanosine diphosphate*

GEF · *Guanine nucleotide exchange factor*

GFP · *Green fluorescent protein*

Gg · *Gallus gallus*

GluA1 · *Glutamate ionotropic receptor AMPA type subunit 1*

GLUT4 · *Glucose transporter type 4*

GS · Griscelli syndrome

GST · *Glutathione-S-transferase*

GTBM · *Globular tail domain binding motif*

GTD · *Globular tail domain*

GTP · *Guanosine triphosphate*

H

HCl · *Hydrochloric acid*

HEK293 · *Human embryonic kidney 293 cells*

HeLa · *Human cervix carcinoma cells*

HIV · *Human immunodeficiency virus*

HPLC · *High pressure liquid chromatography*

HRP · *Horse-radish-peroxidase*

Hs · *Homo sapiens*

I

IC · *Intermediate compartment*

Ile · *Isoleucine*

INF2 · *Inverted formin 2*

IPTG · *Isopropyl-β-D-thiogalactopyranoside*

IQ motif · *Isoleucine glutamine motif*

J

JMY · *Junction-mediating and regulatory protein*

JNK · *Jun N-terminal kinase*

K

KCl · *Potassium chloride*

kDa · *Kilodalton*

KH_2PO_4 · *Potassium dihydrogen phosphate*

KIF · *Kinesin superfamily*

KIND · *Kinase non-catalytic C-lobe domain*

KW · *KIND-WH2*

KWM · *KIND-WH2-GTBM*

L

LALA · *L408,409A*

LB_0 · *Lysogeny broth*

LE/MVB · *Late endosome/multi-vesicular body*

Lmod · *Leiomodin*

LTP · *Long-term potentiation*

M

mA · *Milliampere*

MaxiPrep · *Plasmid-Maxi-Purification*

MDa · *Megadalton*

mDia1 · *Mammalian Dia 1*

$MgCl_2$ · *Magnesium chloride*

MIN · *Multifunctional Integrase*

MiniPrep · *Plasmid-Mini-Purification*

MLPH · *Melanophilin*

mM · *Millimolar*

Mm · *Mus musculus*

MMP · *Matrix metalloproteinase*

mRNA · *Messenger RNA*

MSF · *GTBM-SB-FYVE*

MT-MMP · *Membrane-type matrix metalloproteinase*

MTOC · *Microtubule organising centre*

Myo1E · *Myosin 1E*

Myo1p · *Myosin 1 (Yeast)*

Myo5p · *Myosin 5 (Yeast)*

myoB · *Myosin IB (Dictyostelium)*

myoC · *Myosin IC (Dictyostelium)*

MyoIb · *Myosin Ib*

MyoVa · *Myosin Va*

MyoVb · *Myosin Vb*

MyoVc · *Myosin Vc*

MyRIP · *Myosin and Rab interacting protein*

N

Na_2HPO_4 · *Sodium hydrogen phosphate*

Na_3VO_4 · *Sodium orthovanadate*

NaCl · *Sodium chloride*

NaF · *Sodium fluoride*

Ncd · *Nonclaret disjunctional*

NEB · *New England Biolabs*

NPF · *Nucleation promoting factor*

NT3 · *Wash Buffer*

NTA · *Nitrilotetraacetat*

NTI · *Binding Buffer*

O

oN · *Over night*

P

PAGE · *Polyacrylamide gelelectrophoresis*

PBS · *Phosphate buffered saline*

PBST · *PBS/Tween20*

PCC · *Pearson Correlation Coefficient*

PCR · *Polymerase chain reaction*

PEM-5 · *Posterior end mark-5*

Phe · *Phenylalanine*

P_i · *Inorganic phosphate*

PIP3 · *Phosphatidylinositol-3,4,5-trisphosphate*

PMSF · *Phenylmethylsulfonylfluoride*

PSD · *Postsynaptic densities*

R

Rab · *Ras-like in brain*

Rab11-FIP · *Rab11 family-interacting protein*

Ran · *Ras-like nuclear*

Ras · *Rat sarcoma*

RCP · *Rab coupling protein*

RE · *Recycling endosome*

REI-1 · *RAB-11-interacting protein-1*

REP · *Rab escort protein*

Rho · *Ras homology*

Rip11 · *Rab11-interacting protein*

RT · *Room temperature*

RT-PCR · *Reverse transcriptase PCR*

S

SB · *Spir-box*

SDS · *Sodium dodecyl sulfate*

SEC · *Size exclusion chromatography*

SEM · *Standard error of mean*

SF · *SB-FYVE*

SHD · *Synaptotagmin homology domains*

She3 · *Swi5-dependent HO expression 3 protein*

Slac-2a · *Slp Homolog Lacking C2 Domains A*

Slac-2c · *Slp Homolog Lacking C2 Domains C*

SNARE · *Soluble NSF Attachment Protein Receptor*

Spir2-KW · *Spir-2-KIND-WH2*

Spir2-KWM · *Spir-2-KIND-WH2-GTBM*

Spir2-MSF · *Spir-2-GTBM-SB-FYVE*

T

T_A · *Annealing temperature*

TBC · *Tre2/Bub2/Cdc16*

TBE · *Tris-borate-EDTA*

t_E · *Elongation time*

TEV · *Tobacco Etch Virus*

TGN · *Trans-Golgi network*

TH1 · *Tail homology 1 domain*

TIRF · *Total internal refelction*

TLR4 · *Toll-like receptor 4*

Tm · *Melting temperature*

TRITC · *5(6)-Tetramethylrhodaminisothiocyanat*

Tyrp1 · *Tyrosinase-related protein 1*

Tyrp2 · *Tyrosinase-related protein 2*

V

Val · *Valine*

Vangl2 · *Vang-like protein 2*

Vrp1p · *Verprolin 1 (Yeast)*

VSV · *Vesicular stomatitis virus*

W

WASP · *Wiskott-Aldrich syndrome protein*

WAVE · *WASP-family verprolin homology*

WH2 · *Wiskott-Aldrich syndrome protein homology 2*

Wsp1p · *Wiskott-Aldrich syndrome protein 1 (Yeast)*

X

Xt · *Xenopus tropicalis*

8 List of figures

9 List of tables

10 Acknowledgements

The realisation of this PhD thesis over the last three years would not have been possible without the support and encouragement of several people I would like to sincerely acknowledge in the following and concluding lines of this work.

First of all I want to express my honest gratitude to my supervisor, Prof. Dr. Eugen Kerkhoff, for giving me the opportunity to do my PhD in his lab. I very much appreciated all the discussions about ongoing work and the valuable advices for future experiments. I very well remember all those Western-blot-Fridays when I finally faced the outcome of a week loaded with co-IPs or pulldowns, you also sitting in front of the screen, and no matter which bands we saw or not saw, you always had an optimistic view on it. I thank you for your enormous help by teaching me to use the microscopes in order to obtain high quality microscopic images. I enjoyed the efficient and close, although sometimes exhausting, way to collaborate in finalising our paper to get it accepted at the end. At some point I felt the pressure you built up was a bit too high or not appropriate, but it finally paved the way to get the right results. I would conclusively also like to thank you for the opportunities you provided to join the Summer School in 2014 and all of the meetings over the years.

I furthermore express my gratefulness to my thesis committee, including Prof. Dr. Eugen Kerkhoff, Prof. Dr. Stephan Schneuwly and PD Dr. Michael Kessels for their enthusiastic discussions, helpful advices and for offering me new directions for the future work, not only as part of my research reports, but during the whole thesis time.
Of course, I also want to very much thank my examination committee, namely Prof. Dr. Eugen Kerkhoff, Prof. Dr. Stephan Schneuwly and Prof. Dr. Veronica Egger for their willingness to assume my examiners, PD Dr. Oliver Bosch for his readiness to take the position of the chairperson, and Prof. Dr. Dr. Michael Krahn for his attendance as substitute examiner.

I want to express my gratitude to my collaborators, Prof. Dr. Anne Houdusse, Dr. Olena Pylypenko, Dr. Thomas Weidemann and Dr. Martin Kollmar, whos experimental and illustrating contributions and valuable advices have been irreplaceable to advance this thesis, and who have a major contribution to the publication of this work.
In line with that I want to thank Prof. Dr. Alistair Hume and Prof. Dr. Bruno Goud for their precious ideas to promote this work and for providing a set of expression vectors that very much helped to get the experiments done in a reasonable time.

A special thank is addressed to my colleagues and former colleagues at D4: Anette, Arabel, Birgit, Corinna, Dagmar, Eva-Maria, Ina, Judith, Julia, Sylvia and Verena. I very much appreciated you being my colleagues and I very much enjoyed the time together, regardless if discussing methodical problems, philosophising about the prettinesss of Western blot bands, or sitting together in the kitchen, talking (or rather listening in my case) about everything else, and eating the one or another cake. Arabel, I thank you for all the crucial discussions in life, about football and Formula 1, and Birgit, I thank you for helping me out whenever I had an organisational problem or whenever I needed something for the lab, and for all the Friday evenings during the last months that did not felt that lonely having you around.

Verena, I thank you for all the useful discussions about the work in the lab, about preparing and writing the thesis and for providing me a different view on science and all the aspects around. I very much enjoyed cooperating with you in the last summer, and I think we prepared some nice experiments together. Finally, I can tell that you became a true friend!

I also would like to thank Vladi, who often enough supported me with all kinds of materials, and who shared his knowledge about methods and software, and of whom I knew I could always go to when I needed something.

I thank Carina Michel, an excellent Master student in the lab, for her support and the kind working environment during the nine months we worked together. I might not imagine how it would have worked out at these days if not you, but another student would have been in the lab.

A special thank is attributed to Tanja, for organising everything around the lab work, starting with all the meetings and Summer Schools, and ending with taking care on all the finances. You have been a great support in every problem I had to face outside science, and you always had a solution for everything. But in the end, I mostly appreciated you being around when I had to talk away anything that burdened me.

I sincerely thank my mother, who always believed in me, not only in regard of this thesis, but in every aspect over the last 28 years, starting from my school time, continuing along my studies and lasting until now. I know, I am not always the best son in the world one could imagine, but I try it over and over. I also know that I spent too much time working than in sharing time with you, as long as it is possible. I promise I will try to change that.

The final words of this work are devoted to someone, who became a special person for me and, as far as I can tell, the best friend in live one could ever imagine; Annette.

Annette, I mean it when I tell that you teached me in principle everything I needed to know about the experiments I perfomed throughout this thesis; only one reason for that I very much missed you over the one year you have been busy with tremendously more important things. Without your support, help and advice, I believe, I would not have been able to succeed in finalising this thesis.

But far from that, I am not sure how I can express my gratefulness for you as appropriate as you deserve it.

It is not just that I think I am not really able to describe how fortunate and proud I am that I got the chance to share the lab with you, and how much I enjoyed it being your colleague.

It is not just the blind faith in every respect that developed over the last four years by now, and that I can always rely on you for having a solution for any kind of problem.

And it is not just our regular coffee breaks which at some point simply made my day.

It is rather that I believe and hope that I have won a friend for life, a friend I can fully trust in every aspect, a friend to whom I can confine anything I feel I need to share, regardless of what it is, and a friend who always takes the time to find the right words and to support me in every way you can, simply creating a better feeling in every weak minute, hour and week I had.

It is that I believe you not only guided me to become a better scientist, but more important, to become a better person.

It is my feeling that until I met you I didn't even know what it means to have a good friend.

It is not less than that.

Ich danke dir für alles!